NASA CONTRACTOR REPORT

NASA CR-2727

ANALYSIS OF STRUCTURAL DYNAMIC DATA FROM SKYLAB

Volume I - Technical Discussion

Leonard Demchak and Harry Harcrow

Prepared by
MARTIN MARIETTA CORPORATION
Denver, Co. 80201
for George C. Marshall Space Flight Center

NATIONAL AERONAUTICS AND SPACE ADMINISTRATION • WASHINGTON, D. C. • AUGUST 1976

TECHNICAL REPOF

1. REPORT NO.	2. GOVERNMENT ACCESSION NO.	3. RECI
NASA CR-2727		

4. TITLE AND SUBTITLE	5. REPORT DATE
Analysis of Structural Dynamic Data from Skylab Volume I - Technical Discussion	August 1976
	6. PERFORMING ORGANIZATION CODE M-175
7. AUTHOR(S) Leonard Demchak and Harry Harcrow	8. PERFORMING ORGANIZATION REPORT #
9. PERFORMING ORGANIZATION NAME AND ADDRESS Martin Marietta Corporation P. O. Box 179 Denver, Colorado 80201	10. WORK UNIT NO.
	11. CONTRACT OR GRANT NO. NAS8-31224
12. SPONSORING AGENCY NAME AND ADDRESS National Aeronautics and Space Administration Washington, D. C. 20546	13. TYPE OF REPORT & PERIOD COVERED Contractor Report Final
	14. SPONSORING AGENCY CODE

15. SUPPLEMENTARY NOTES

16. ABSTRACT

This report presents the results of a study to analyze data and document dynamic program highlights of the Skylab Program. Included are structural model sources, illustration of the analytical models, utilization of models and the resultant derived data, data supplied to organization and subsequent utilization, and specifications of model cycles.

This analysis is published in two volumes:

Volume I - Technical Discussion - NASA CR-2727

Volume II - Skylab Analytical and Test Modal Data - NASA CR-2728

17. KEY WORDS	18. DISTRIBUTION STATEMENT
	STAR Category 15

19. SECURITY CLASSIF. (of this report)	20. SECURITY CLASSIF. (of this page)	21. NO. OF PAGES	22. PRICE
Unclassified	Unclassified	220	$7.25

For sale by the National Technical Information Service, Springfield, Virginia 22161

CONTENTS

List of Tables

List of Figures

INTRODUCTION

The Skylab cluster is the most complex spacecraft structure that has ever been analyzed, assembled, tested and flown. Skylab was an extension of the Apollo Applications Program (AAP) and was intended to provide an experimental man rated laboratory in space utilizing primary components and systems developed under the Apollo program. This report represents a compendium of Skylab structural dynamics analytical and test programs. These programs are assessed to identify lessons learned from the structural dynamic prediction effort and to provide guidelines for future analysts and program managers of complex spacecraft systems. It is a synopsis of the structural dynamic effort performed under the Skylab Integration contract and specifically covers the development, utilization and correlation of Skylab Dynamic Orbital Models.

The Apollo Applications Program was initiated in 1965, and continued to 1969, when the program was officially titled Skylab. Early configurations included the LEM docking systems, MDA with five docking parts, boom systems and consideration of rotating space station using S-IVb, CSM, LEM and S-II stages, to create artificial gravity environments. The prime consideration always was the development of an orbiting space laboratory with self contained power to permit extended man exploration of his planet and surrounding environment. Specifically, the developed space station was to be designed utilizing, where possible, existing "off the shelf" structural hardware from the Apollo program.

Skylab, therefore, represented an evolved structural design utilizing existing space hardware except for specific manned laboratory and experimental requirements. These included development of the Multiple Docking Adapter (MDA), deployment assembly for a redesigned (inverted) lunar decent vehicle (ATM) required to house the space telescopes, necessary solar array assemblies to provide power and modification of the third stage, SIVb, of the Saturn V to provide for an Orbital Workshop (OWS).

The development of such an orbiting, manrated laboratory, required development of significant dynamic methodologies to predict expected response and load performances during orbital operation. These principally concerned the generation of advanced state of the art technologies associated with:

- o Docking response studies.
- o Modeling of complex structure.
- o Vibration analyses of large degree of freedom systems.
- o Acoustic, vibration and shock criteria.
- o Testing of orbital structural assemblies.

As a summary of the detailed technical effort included during the development phases of Skylab, we represent three cycles of developed structural models. These cycles represented:

- o Initial or preliminary Skylab design model.
- o Models developed and used to verify dynamic test.
- o Final analytical structural models, correlated with dynamic test and used to verify flight readiness and launch support activities.

The NASA Skylab structural test program consisted of both static and dynamic test. These included structural tests on components, subsystems and major assemblies and were performed at contractor, NASA JSC and NASA MSFC test facilities. Static test included influence coefficient, static load and tension test. These tests produced data required in the early design phase and necessary in the development of analytical structural models. Solar array and assembly deployment, performance and forced response structural testing were completed but are beyond the scope of this study and are not included within the report. Extensive structural dynamic payload vibroacoustic tests were performed on both launch and orbital payload assemblies, i.e., forward of vehicle station 3200. The dynamic tests were performed to verify/correlate vibration environments and derived structural analytical data. Of principal concern, for this report, is the orbital payload assembly acoustic and modal survey tests. Analytical model test data correlation studies resulted in a more detailed zonal vibration criteria and minor modification in the deployment assembly analytical model. Significant testing philosophies, procedures and instrumentation requirements for future complex structural test were developed during this test program. In fact, a large amount of test data relating to structural and modal damping, automatic test procedures, vibration criteria resolution, and test instrumentation requirements were obtained and as yet remains unused.

Program changes during the last year of the Skylab project resulted in reduced structural flight instrumentation which

greatly hampered detail evaluation of the Skylab mission except for some phases of ignition, liftoff and launch times. However, utilization of the limited data available did provide some flight correlation data with an insight in what data are required for future systems. Provided as a summary to this report is a relatively detail critical review of the Skylab program, decisions made and definitive recommendations for future dynamic programs of this nature.

Interspaced within the report are structural model sources, illustration of the analytical models, utilization of models and the resultant derived data, data supplied to organizations and subsequent utilization, and specifications of model cycles.

1. STRUCTURAL MODEL DEVELOPMENT

The Skylab program was an outgrowth of the Apollo Application's Program (AAP), initiated in 1965. Actually, the Skylab was a final configuration designation which had evolved from numerous trade studies during the AAP program.

These studies resulted in the preliminary design of the Apollo Telescope Mount (ATM) and Orbital Workshop (OWS) Solar Arrays, Multiple Docking Adapter (MDA), origination of the docking program, ATM and its telescope configuration, Gimbal Ring Assembly, Space Structure Transition Section (STS), Airlock Module (AM) with the AM trusses and a preliminary OWS floor configuration. This configuration, presented in Figure 1.1 was referred to as the "wet workshop".

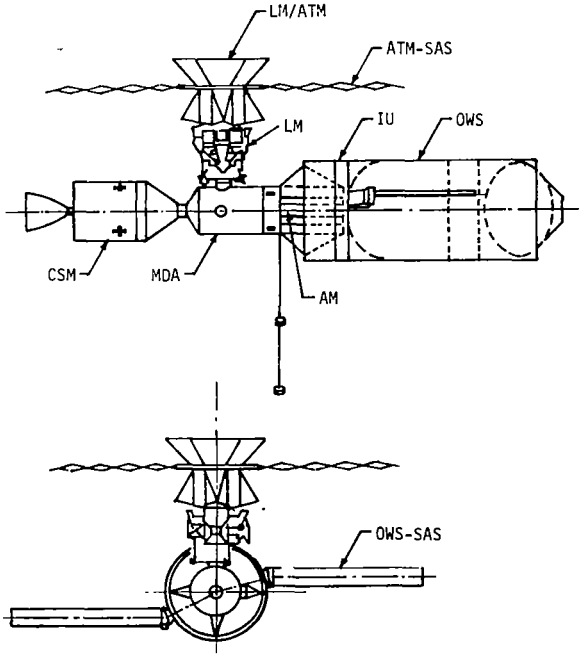

Figure 1.1 - AAP Wet Workshop Configuration

The Skylab program was officially inaugurated in 1969 with one configuration, but two concepts. These concepts were identified as wet or dry Orbital Workshops, which referred to a live or spent third stage, S-IVb, Saturn V workshop.

The decision was made to replace the Lunar Module (LM) and its docking port with the Apollo Telescope Mount (ATM) and Deployment Arm (DA), which simplified the mission by deleting the LM docking event.

The Skylab orbital cluster consists of the Orbital Workshop (OWS), Instrument Unit (IU), Fixed Airlock Shroud (FAS), Airlock Module (AM), Structural Transition Section (STS), DA truss, Multiple Docking Adapter (MDA), deployed ATM and deployed SASs of the ATM and OWS. When the Command and Service Module (CSM) docked to the axial port of the MDA, (Figure 1.2), it resulted in the Axial Configuration. The rescue mission required the use of another CSM docked to the MDA radial port; this was referred to as the Radial Configuration (Figure 1.3).

Late in 1969, the dry workshop was officially adapted as the Skylab configuration. This section documents the development and design of the structural models associated with the Skylab Dry Workshop configuration.

1.1 Skylab Vibration Analyses Chronology

The wet workshop mathematical models were represented primarily with equivalent beam stiffnesses. This "stick" model consisted of a mass spring representation of the modules which made up the configuration of Figure 1.1. Only the ATM rack structural model was a finite element representation of the stiffness of the actual structure. The formulation of such a model involved the idealization of an actual structural member or assembly of members into a series of discrete or or finite elements. These elements were considered to be connected at node points to form a network or model from which stiffness characteristics could be obtained for the structure, using a digital computer program. The Martin Marietta system of structural analysis programs utilized the direct stiffness method. A stiffness matrix was formed for each discrete element (axial member, beam, plate, etc.) and the element stiffness matrices were merged to form the overall stiffness matrix for the entire assembly represented by the model. To obtain good representative stiffness characteristics of this complex structure, the original model was formed in more detail than that used in the dynamic model. The large stiffness matrix was then reduced or collapsed to one of more manageable proportions. The effect of all intermediate, or collapsed, stiffnesses was retained in the final stiffness matrix.

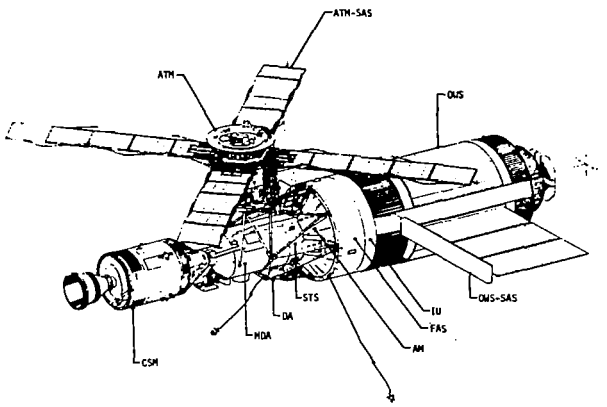

Figure 1.2 - Skylab CSM Axial Docking Configuration

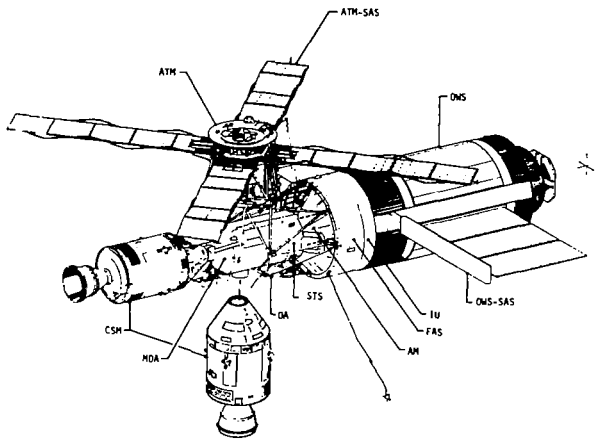

Figure 1.3 - CSM Radial Docking Configuration

The main cluster configuration was defined as shown in Figures 1.4 and 1.5. During the initial phases of the Skylab cluster structural configuration redefinition from a docked ATM and "wet workshop" to the deployed ATM and "dry workshop" structural analytical models of the principal Skylab systems were in a state of change.

The mathematical models became larger and more complicated as the Skylab structural design cycle progressed. Table 1.1 illustrates the DOF and subsequent mode increase.

In 1970, the NASA associate contractors provided better mass and stiffness matrices for the components which comprised Skylab configurations than those used in the original stick model wet workshop. In the new models, only the OWS, ATM solar panels, and MDA were represented with

beam elements (EI, AE, KAG, GJ). All other components of the model were represented with free-free and fixed-free mass and stiffness matrices. The total degrees of freedom (DOF) which made up the model, prior to any reduction, approached 20,000 DOF.

The technique used to compute the modes was modal coupling (Reference 1), with the modes of the various components being computed separately. These uncoupled modes were mathematically coupled and transformed to form a set of coupled modes. During this coupling process, a frequency cutoff criterion was defined for the coupled mode set. The frequency limit then determines the number of component modes required in the coupled analysis.

It is known that some component modes are more important than others in modal coupling. The obvious place to look for the important component modes was in the ATM and OWS solar arrays, since these two components accounted for approximately 80 percent of the total number of modes required. The method for selecting the important component modes involved selecting the solar array modes which had the largest effect on the main beam response and discarding all others in the vibration analysis. To calculate accurate loads on the solar arrays, all panel modes had to be used. The method employed was to calculate the accelerations at the solar panel attachment point on the model with the truncated panel modes and to use derived accelerations to base drive the solar array cantilevered modes.

In 1971, it was recognized that the vibration analyses used for the loads analyses were not necessarily sufficient for control system analyses. The concept of uniform frequency cutoff was used for the controls model. The concept was to retain all modes of each component to a specific frequency determined by the size limitation of the computer program, which at that time was 115 DOF. The modal selection technique did not guarantee maximum control moment gyro (CMG) or rate gyro motion. Of course, this limited the frequency definition in the controls model to slightly less than 5.0 cps. As one might suspect, this was not adequate for loads calculations. Here again, the modal selection technique was employed to increase the frequency definition of the loads model above 10 cps.

In 1972, the decision was made to assess the accuracy of the loads versus the controls modes, to assess the validity of solar array modal selection techniques, and to determine an acceptable frequency fidelity for vibration analyses. It was concluded that all future vibration analyses would contain individual component frequencies equal to or greater than 15.0 cps. The solar arrays used consecutive uncoupled modes up to 5.0 cps and used modal selection techniques for defining important modes up to 15.0 cps. A single model for both loads and controls analysis, determined in accordance with the aforementioned criteria, was considered more accurate than previous vibration analyses based on consecutive modes and frequency cutoff for a limited number of coupled modes. The mathematical models were now so complex that the final modal coupling run using over 200 DOF requring a CDC 350K core storage capacity.

Table 1.1 - Model Complexity History

Config.	Main Beam Freq.-cps	OWS - SAS		ATM - SAS		Total DOF	Coupled Freq.	Model Modes	Report ED-2002-	Date
		Freq.	Modes	Freq.	Modes					
Axial	27.2	10.5	22	2.8	4	100	19.0	85	790-1	4-15-69
Axial	28.8	19.5	7	32.0	12	115	28.4	100	790-2	7-24-70
Axial	21.5	20.0	14	20.5	11	114	23.6	105	790-3	9-23-70
Axial	20.3	18.3	12	20.3	12	115	20.3	97	790-4	1-14-71
Axial	19.5	18.3	12	20.3	12	115	19.6	96	790-5	4-12-71
Axial	13.2	13.6	10	9.5	10	115	13.7	103	790-6	7-16-71
Axial	15.7	13.6	10	14.0	11	133	15.5	118	790-7	2-15-72
Axial	16.1	15.1	21	14.0	17	180	15.0	157	1444	5-22-72
Axial	15.3	17.0	25	15.8	19	212	15.3	168	1564	12-20-72
Radial	24.5	10.5	22	2.8	4	100	19.1	91	790-1	4-15-69
Radial	18.5	26.5	8	31.8	11	112	18.5	90	790-2	7-24-70
Radial	18.5	16.6	10	17.7	10	112	18.6	96	790-3	9-23-70
Radial	16.7	15.3	10	14.0	11	115	18.6	98	790-4	1-14-71
Radial	16.2	15.3	10	14.0	11	115	15.4	96	790-5	4-12-71
Radial	9.2	8.6	8	7.9	11	115	9.8	97	790-6	7-16-71
Radial	15.4	13.6	9	7.9	11	144	15.4	122	790-7	2-15-72
Radial	15.4	15.9	10	7.9	11	146	16.0	129	1444	2-15-72
Radial	16.1	17.0	25	15.8	19	221	15.1	173	1564	12-20-72

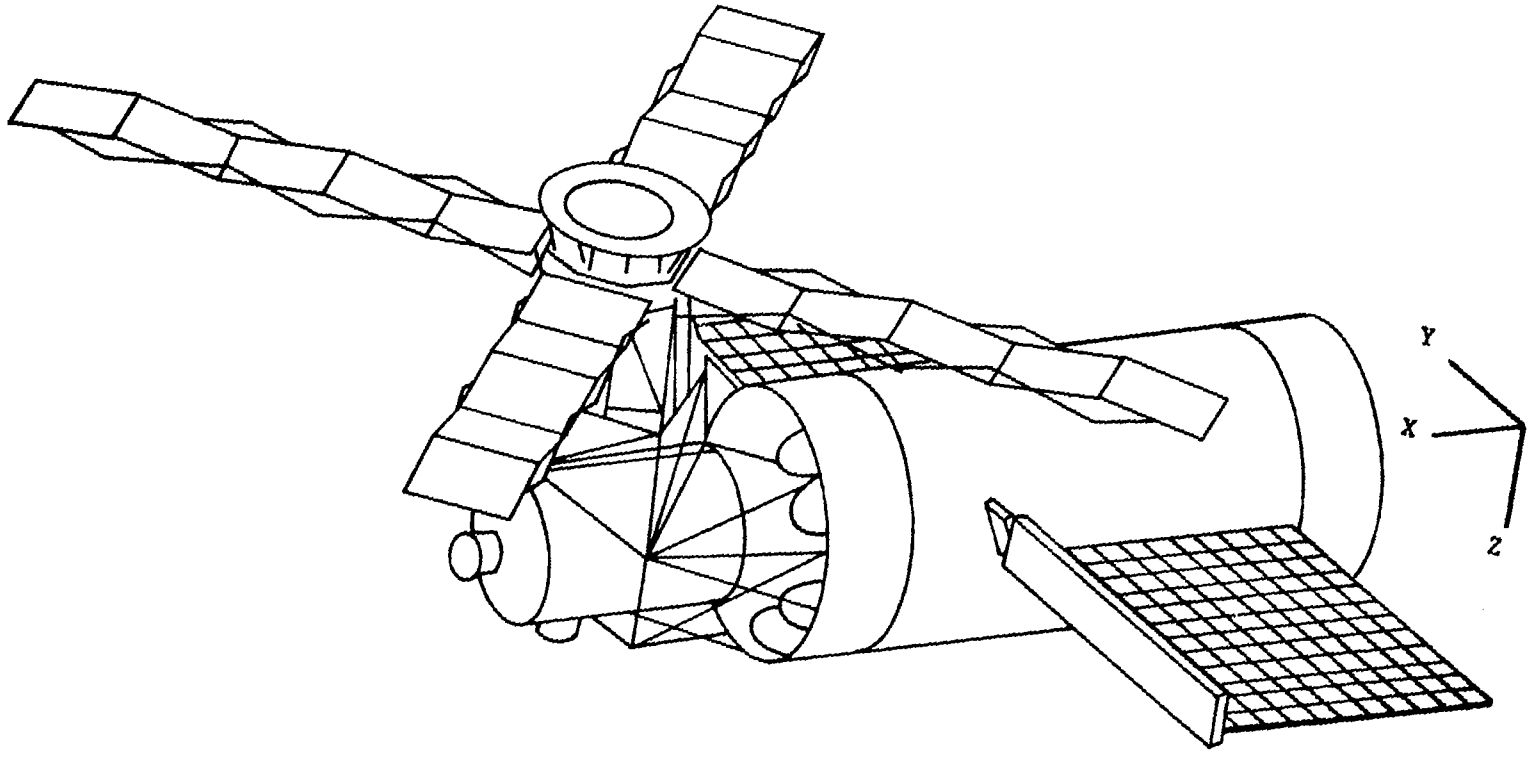

Figure 1.4 Skylab Configuration 3.1

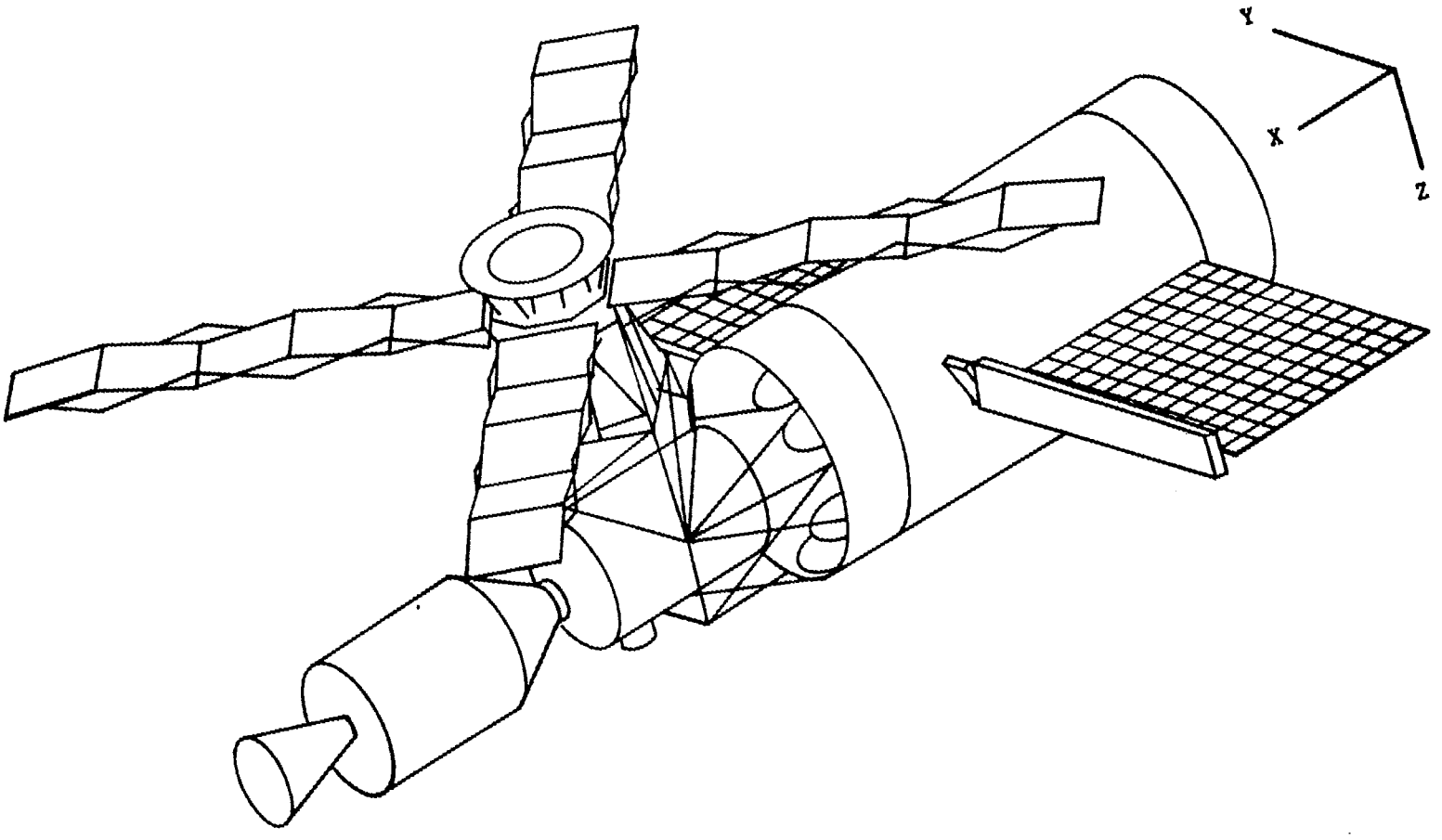

figuration 1.2

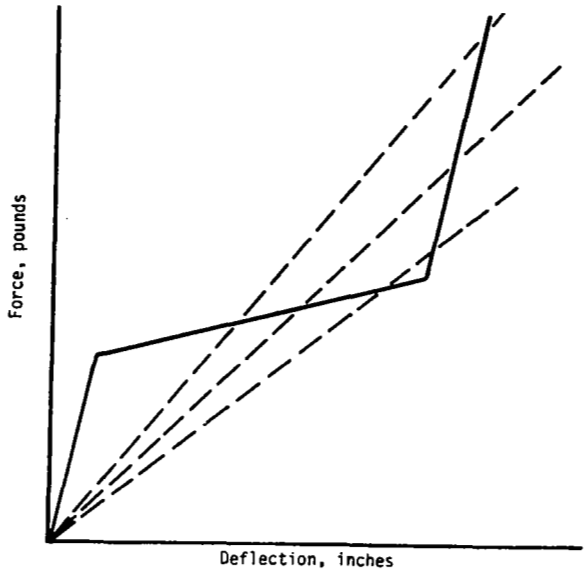

Figure 1.6 - Nonlinear Force-Deflection Relationship

1.2 Evolution of Structural Models

Throughout the 3 year development program, hardware changes and raised mass and stiffness definition of the structure, required updating of the Skylab mathematical models. Three time periods have been chosen as representative of the program to illustrate Skylab model evolution. The first or initial model was documented in July 1970, and was the first formulation of the "Skylab" cluster. The second or pretest model, represented the Skylab configuration just prior to the Ground Vibration Survey (GVS). Additionally, pretest modes were derived using a dynamic test configuration as shown in Figure 1.7. The final or preflight model was documented in December 1972. It represented the final flight model and contained stiffness scaling factors derived during GVS correlation studies. This model was used for final flight readiness reviews, flight anomalies studies and flight evaluation. This report does not document the Skylab anomalies studies.

Prime Skylab mission configurations are shown in Figures 1.4 and 1.5. Structural model evolution is shown as a pictorial representation in Figures 1.8 through 1.13. These figures represent, in a similar manner, the mathematical modeling associated with the vibration studies (see Section 1-1). These component systems/assemblies will be used to illustrate the detailed model development of Skylab.

An interesting learning experience came to the surface in the field of mathematical modeling. The Skylab models were developed from approximately 11 modules. In the modal coupling procedure, several modulus were tied together to form a main beam. The remaining modulus were modally coupled to the main beam. For this example, the main beam consisted of the FAS, IU and OWS modules. The finite element models for these structures were developed by NASA associate contractors. Historically, interface loads had been required at the FAS/IU and IU/OWS, which made it desirable to have a centerline point at each of these interfaces. There is a limitation to the number of degrees of freedom which can be retained in a dynamics model. Another reason to maintain a centerline node point is to make the main beam module compatible with the sizes of the other modules. However, the centerline coordinates were not modeled in the original model. To derive a centerline node point, the radial degrees of freedom were first reduced out to allow radial motion to occur in a typical breathing mode manner. A geometric transformation relating IU ring motion of all tangential and longitudinal coordinates in terms of motion at the IU centerline reduced further the number of IU ring interface coordinates. Coupling which occurred between the radial and tangential degrees of freedom in effect constrained the IU ring motion radially. A visual analogy of this phenomenon is to imagine that the IU centerline point represents the motion of a radially slotted rigid plate. This caused the OWS-SAS loads to be conservative to the point of exceeding published design limits. In order to alleviate this situation, all IU coordinates were collapsed out of the main beam model. This allowed the main beam stiffness model to reflect the OWS-SAS attach point flexibility as defined in the original IU finite element model, thus alleviating the problem with the OWS-SAS loads.

A facet of modeling which had to be considered on Skylab was providing an adequate vibration analysis where it was known that a component of the configuration exhibited nonlinear behavior. This was true particularly in the ATM where the gimbal ring assembly (GRA) is suspended within the rack on a nonlinear spring. The spring rate is high for small deflections up to the point where the preload in the spring is relieved and becomes soft thereafter, until the GRA bottoms out on the rack stop. A simple illustration of this problem is demonstrated with the load-deflection curve of Figure 1.6. For a control system vibration analysis, where vehicle forces are small, it is reasonable to use a GRA spring constant based on the force deflection range which passes through the origin. The docking and latching forcing functions cause GRA responses and corresponding deflections which operate in the nonlinear range. The cost and schedule impact of performing a nonlinear analysis dictated the use of an iterative process in the vibration analysis using the spring constants and frequencies determined from the dashed lines of Figure 1.6. Luckily, a few iterations of the GRA frequency produced a model which provided loads consistent with the desired force-deflection relationship.

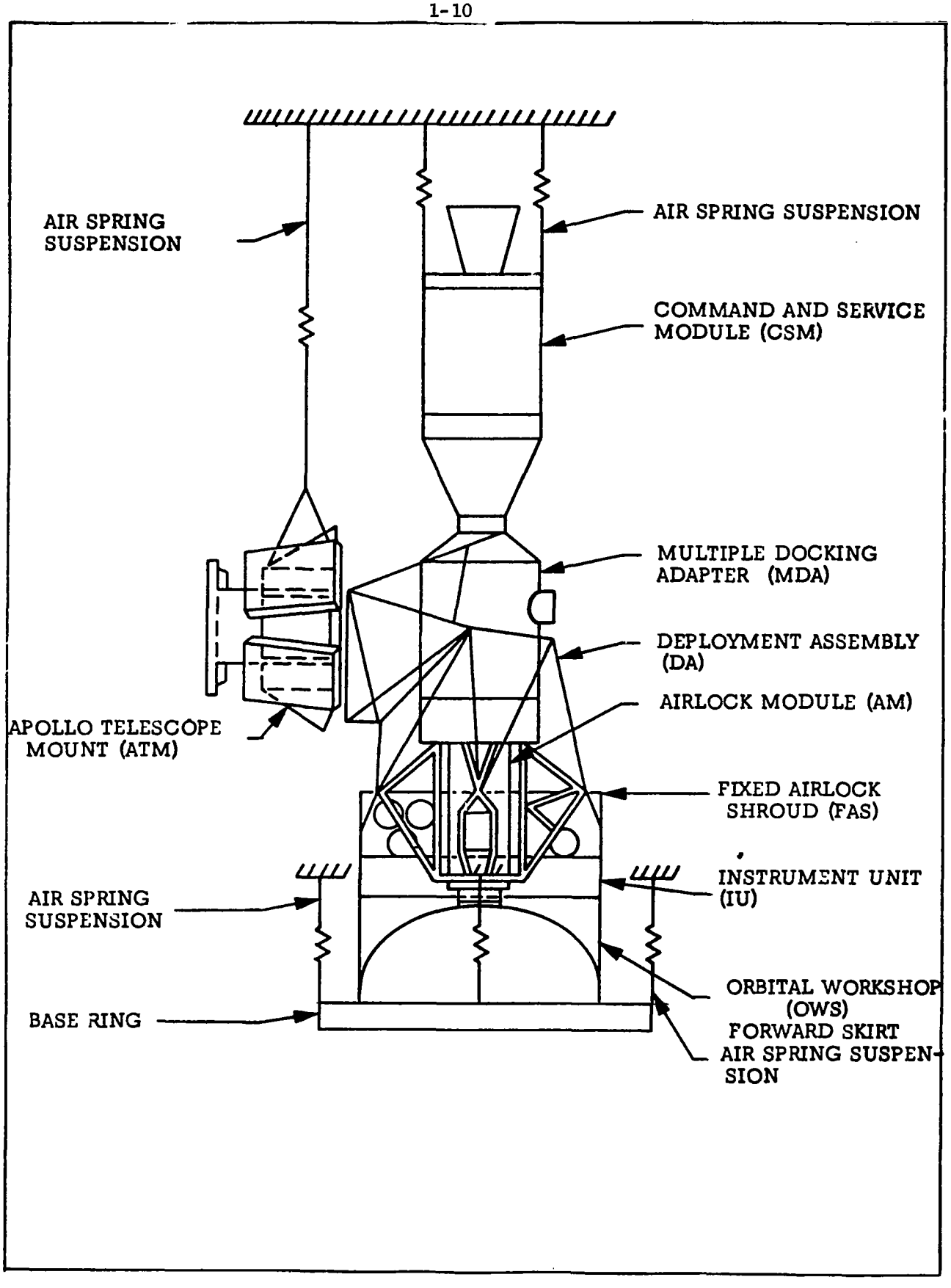

Figure 1.7 Skylab A Orbital Configuration (Configuration 6) Test Setup Modal Survey Tests

1.2.1 Orbital Workshop Assembly - The orbital workshop assembly analytical model evolved from an Apollo launch configuration beam stiffness model used in the initial Skylab analyses. Principal changes to this model related to more detailed representations of the Solar Array System, the backup structure which reflected motion of the arrays to a center line model, and interface points for compatibility to the STS/AM/AM-TRUSS subassembly.

The model was composed of three major subassemblies. These were the OWS structural model, OWS Solar Array System, and the FAS/IU assembly. (See Figures 1.8, 1.9 and 1.9a)

1.2.1.1 OWS Structural Model - The initial model was represented by a six mass point, 6 DOF, centerline model. This model actually represented the stiffness associated with a spent third stage, S IVb, of the Apollo launch vehicle. The resulting 36 by 36 free-free mass and stiffness matrices were collapsed to 28 by 28 matrices. The primary concern associated with this assembly was upgrading the stiffness matrix to reflect a dry workshop configuration.

Both the pretest and flight models of this assembly were represented by a six centerline point model resulting in 36 by 36 mass and stiffness matrices. The final model did reflect revised stiffness data associated with the aft skirt section, but its effect to the overall modal characteristics were minor. However, changes in the mass data during the three modeling periods were significant.

1.2.1.2 OWS Solar Array System - Detailed models were utilized from the start to define the solar array system. The initial model reflected a 25 grid point model resulting in overall 96 by 96 mass and stiffness matrices. Modeling problems developed not because of limited size of the model but to inadequate definition of its response. Specifically, these included irregular tip deflections, no effect of radial motion (later defined as backup structure), and no separate representation for near or far side arrays although their orientation was different (see Figure 1.9a). The pretest and flight models, although similar in size (93 by 93 and 99 by 99), were significant improvements. These models contained separate stiffness matrices for each array, inclusion of structural effects from the centerline model to the OWS skin, and effects of the beam fairing interface with the deployed arrays.

1.2.1.3 FAS/IU/OWS Forward Skirt - This assembly had been principally designed during the APP development cycle. Remaining concerns to this assembly was associated with interface responses, load paths, and attachment points with adjacent assemblies. The effects of AM truss design even with truss realignment and bottle arrangement did not significantly influence the systems response. The primary design driver was the design and development of the ATM deployment assembly (DA). Recall that, at the Skylab configuration designation, one substructure remained for major design. This was the ATM DA (see DA section).

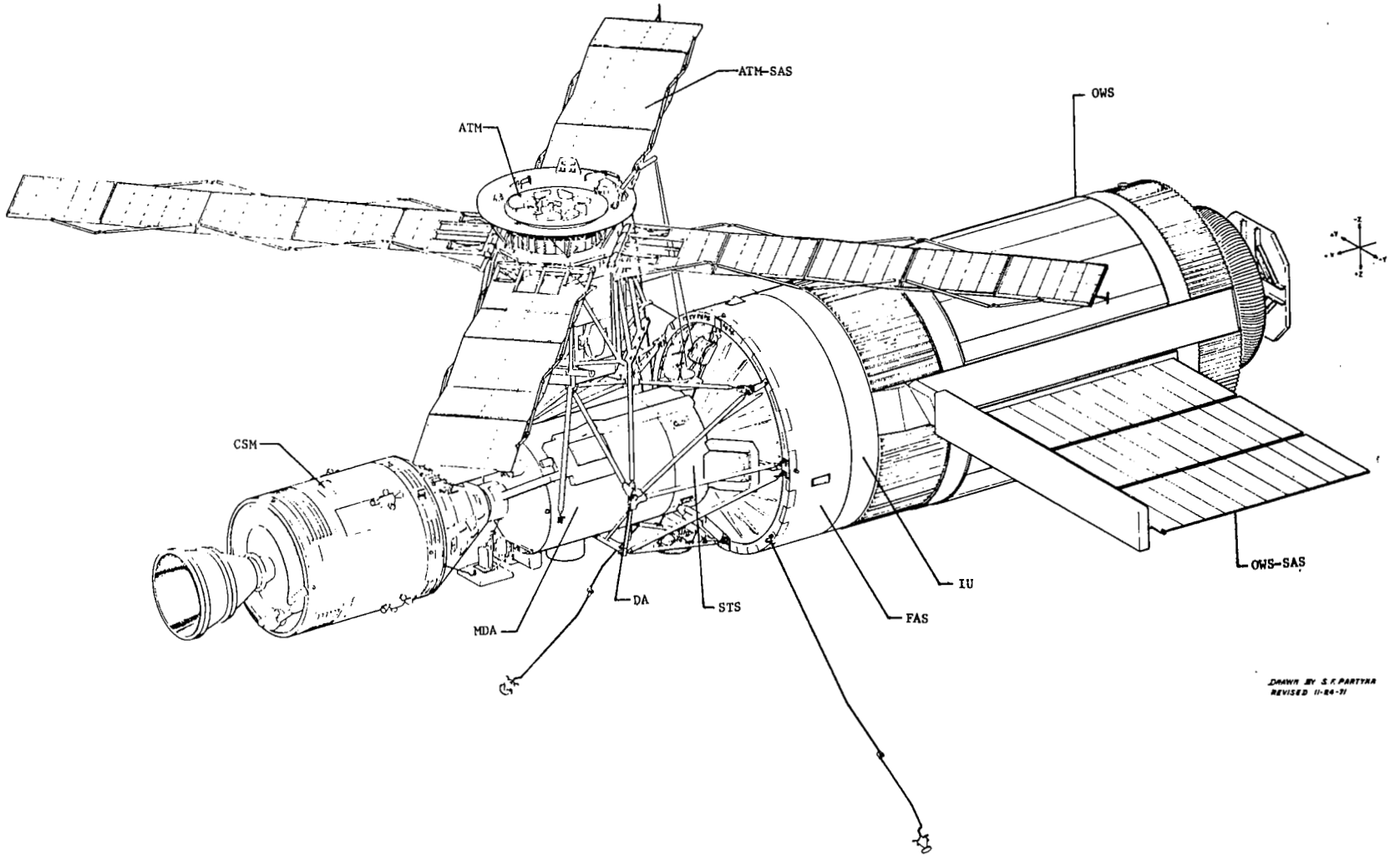

Figure 1.8. Skylab Component Systems

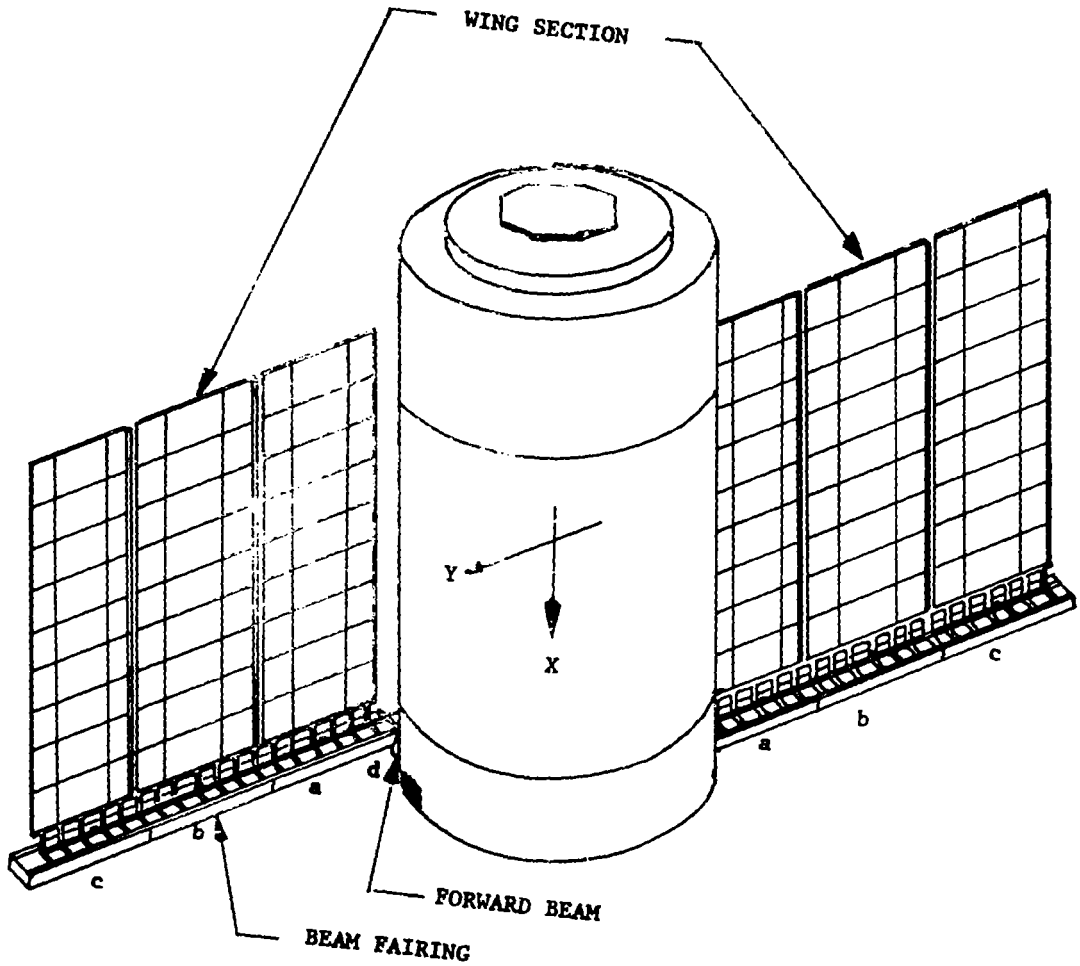

Figure 1.9 FAS/IU/OWS

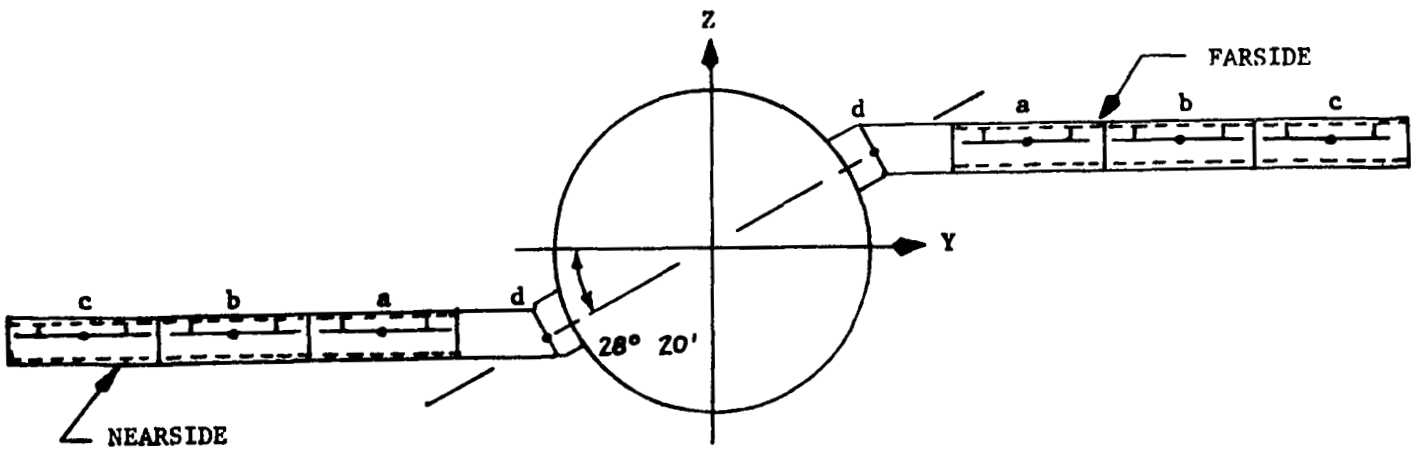

LOOKING AFT
(POSITIVE X = FORWARD)

Figure 1.9a OWS Solar Array System

The initial FAS/IU model was structured as a finite element model, using preliminary load path data of the "L-Beam" DA and considering only the mass affects of bottle attachment. Later models included structural flexibilities associated with the ECS and O_2 bottles. The pretest model contained grid points in the assembly so that direct attachment to the DA and AM was possible. The final model additionally included flexibilities associated with the OWS forward skirt. This was due to refinement of OWS Solar Array attachment points and upgrading load allowables on the beam fairing OWS skirt interface.

1.2.2 Multiple Docking Adapter Assembly - The multiple docking assembly analytical structural model evolved from the AAP program study. Actually, it was initially composed of five docking parts and a payload shroud configuration. With the dry workshop designation, the assembly was refined to the MDA cylinder portion, STS/AM/AM-truss and two docking ports. Depending upon which orbital configurations were analyzed, the CSM was considered. (See Figures 1.8, 1.10, 1.10a and 1.10b)

1.2.2.1 AM/STS Structure - During the AAP development phase of the Skylab program, this assembly was treated as a beam model. At the initiation of the dry workshop concept, redesign of the trusses provided truss rearrangement for EVA missions from the Air Lock Module (AM). Actually, this was utilized to free the pinned OWS Solar Array system and deployment of the parasol configuration during mission operations.

Analytical modeling changes of this structural system occurred in only two models. These were the initial and final models. The initial model was represented as a finite element, beam truss model with two nitrogen (N_2) bottles attached rigidly to the trusses. The final model included effects of the AM/OWS-dome bellows torsional spring flexibility and arc assembly interface attachment for the N_2 bottles. This model was combined with the MDA structural assembly to yield the MDA/STS/AM modal coupling partition.

1.2.2.2 Axial and Radial MDA Port Structure - The initial model was completed by considering three degrees of freedom at each latch point and considering the port models, axial or radial, independent of the MDA centerline beam model. Significant revision was made for the pretest model due to completion of the MDA static influence coefficient test and a more definitive model of the MDA. Port stiffness matrices were defined from a model defined by elastic ports and an elastic MDA. By removing the flexibilities associated with the MDA, the port stiffnesses were obtained. The final model was revised only for the radial port to reflect the 37.75 degree rotation of the CSM about its longitudinal axis in order to place it into the proper radial-dock orientation.

1.2.2.3 MDA Structure - Although the MDA was considered as a centerline beam model in all three modeling phases the pretest and final models were derived from a finite element model which was collapsed to a centerline model of the MDA. The MDA was combined with the STS/AM-truss model to yield the modal coupling partition.

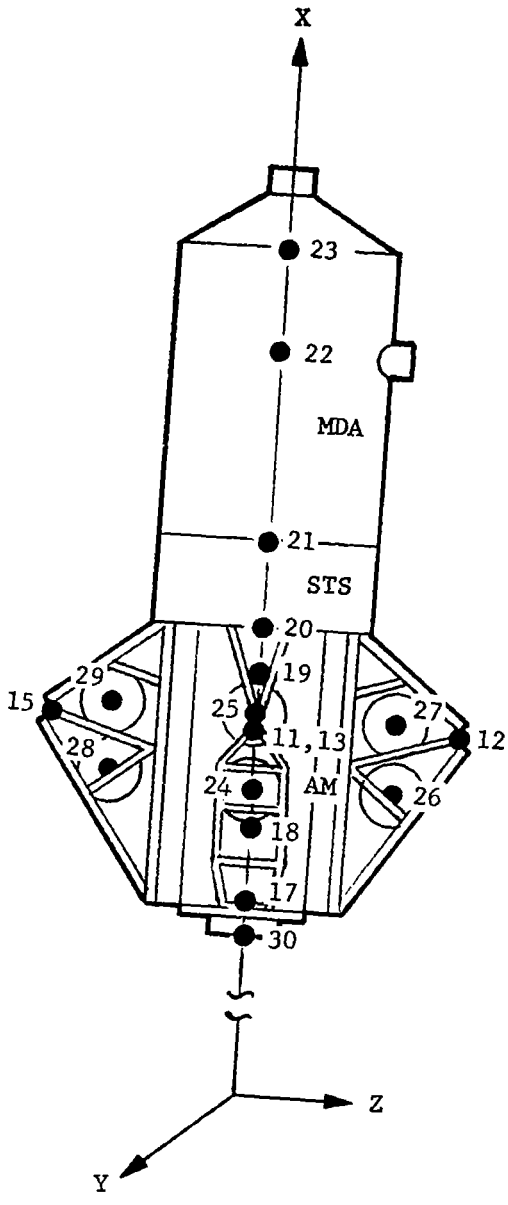

Figure 1.10 MDA/STS/AM Model

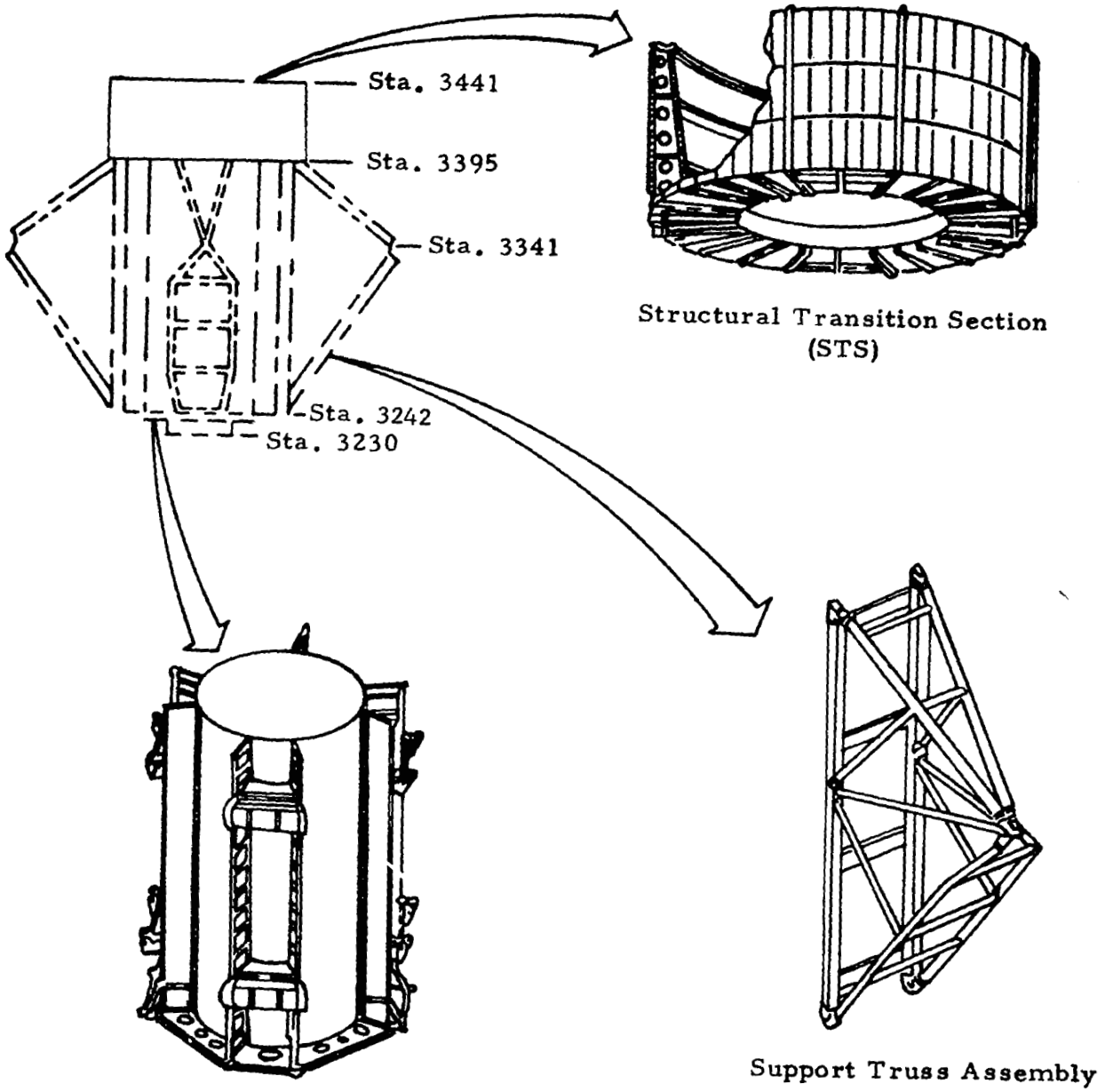

Figure 1.10a Airlock Module

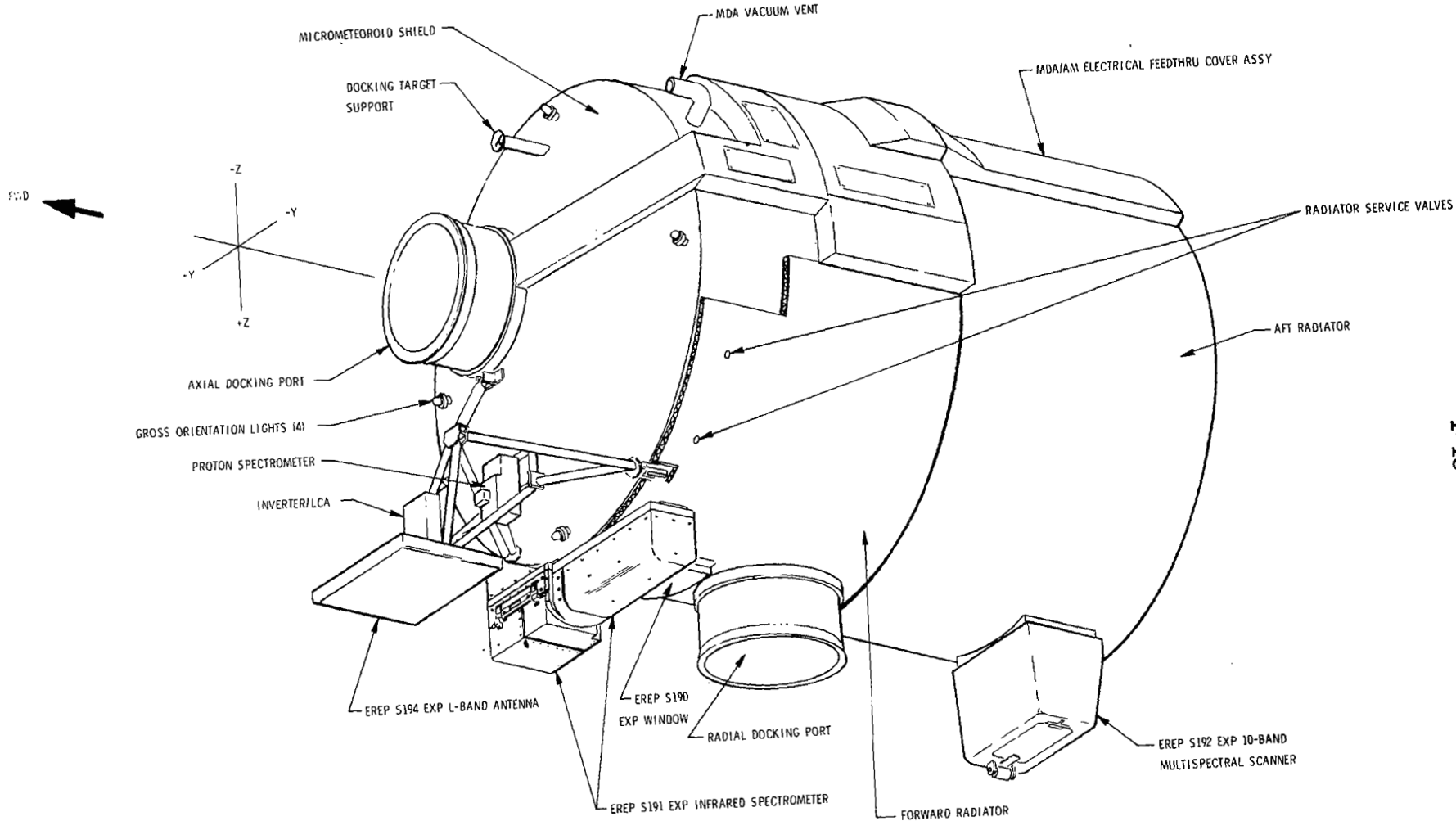

Figure 1.10b MDA

1.2.2.4 CSM Structure - An Apollo CSM model was used throughout the analysis phase and remained significantly unchanged until after the test (see Figures 1.8, 1.11 and 1.11a). Due to dynamic test correlation studies the CSM stiffness was modified by increasing the torsional stiffness between the Command Module (CM) and Service Module (SM) by a factor of 3.19.

1.2.3 Apollo Telescope Mount Assembly - The ATM evolved from a simple assembly to be deployed from a SM service bay, to the most complex structural component of the Skylab program. (See Figures 1.8, 1.12, 1.12a, b, c, d, e, f and g)

1.2.3.1 ATM Solar Array System - Several models of the ATM-SAS had been developed during the AAP program. These had been modeled, tested and revised. Therefore, the array system was completed prior to the Skylab designation. Changes made to this structural assembly dealt with revising mass properties and incorporating, in the pretest and final models, accurate definition of backup structure flexibilities.

1.2.3.2 ATM Rack, Spar Canister and Gimbal Ring Assembly Structure - This system created the most concern and revision of any of the major structural assemblies of the orbital assembly. These concerns were due to:

a. inadequacy of original lock system for the Spar Canister, requiring an additional lock assembly, launch lock, that did not totally eliminate interface responses;

b. error in mass modeling with the failure to consider total effects of the ATM wire bundles which did not reflect actual CG offset problems;

c. redesign of the EVA removable rack launch strut;

d. numerous problems associated with ATM forced response test and effects of Spar modeling.

This structural system was the most complex of the structural systems and, therefore, was modeled in detail initially. The initial model was represented by 484 grid points using finite beam and shell elements. A flow chart for developing the ATM rack, as shown in Figure 1.12b is represented in Figure 1.12c. The ATM gimbal system was modeled as a substructure then coupled to the rack model (Figure 1.12d). The Spar/Canister was assumed to be a rigid subcomponent.

The model was not significantly changed during the pretest period. The final model resulted in a revised interpretation of the roller-spring stiffness data. Of principal concern during the analysis, was the nonlinearities of the roller-spring rates that affected the controls response.

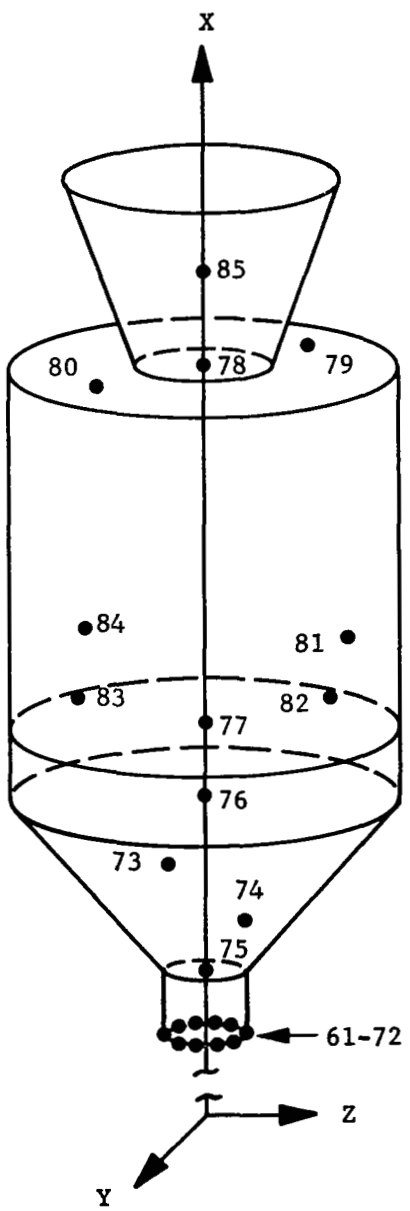

Figure 1.11 Axially Docked CSM

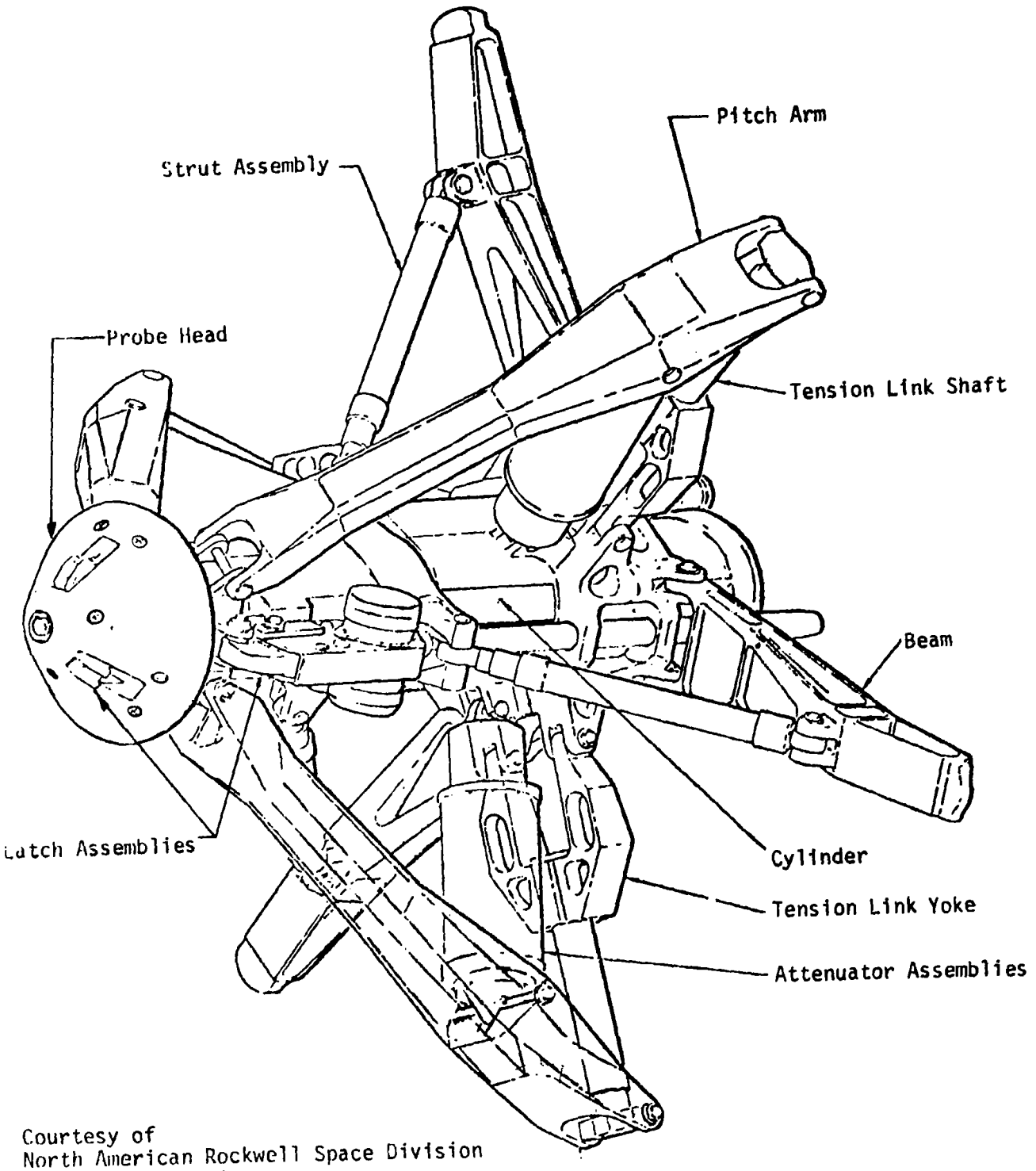

Courtesy of
North American Rockwell Space Division
Downey, California

Figure 1.11a Apollo Docking Probe Assembly

The roller-spring rates were updated by assembly bench tests to obtain deflection-load curves which were linearized (see Figure 1.12e). The radial stiffness of the two type B ATM rack roller-springs were changed from 113 lb/in to 37500 lb/in. Thus, all four (type A and B) of the rack roller-springs, which connected the rack to the GRA had radial stiffness of 37500 lb/in. This was the only change to the basic rack stiffness data. The Spar/Canister was considered flexible instead of rigid and was modeled as depicted in Figure 1.12f.

1.2.3.3 DA Structure - At the Skylab configuration designation, only one substructure was left for major design. This was the ATM Deployment Assembly (DA). Modeling problems existed in the definition of first primary bending frequency, attach point designation, and load path definition. Due in part to the major configuration change, removal of LEM docking, three radial MDA docking ports, and conversion to the dry workshop concepts, requirements were established for immediate assessment of control and load impacts due to the DA. This precipitated numerous orbital cluster vibration analyses using varying models of the DA. However, since we have previously defined three modeling phases for Skylab, we will not discuss the "L-Beam" and other preliminary DA models.

The initial model assumed structural members to be thin walled aluminum tubes and was a truss-beam stiffness model (see Figure 1.12g). The model was revised by the dynamic test correlation results. This was accomplished by scaling down the stiffness matrix by a factor of 0.6. Actually, as a result of the dynamic test, remodeling should have been performed primarily at the interface connection points. However, detailed models were not available from the prime contractor so the scaling was applied to the entire DA. Later, in comparison of flight results, this correction had to be revised and stands as the only significant modeling error made in the Skylab Orbital Dynamic Analyses.

1.3 Conclusions

Initially, model changes were brought about by the solidification of the Skylab design. Beam models were replaced by more accurate finite element representations of the substructures. Locations and size of instrumentation packages were decided upon, thereby requiring more detailed descriptions of the modal mass distributions.

Further model changes were required to obtain finer descriptions of areas of interest, such as the ATM and OWS Solar Arrays. This increased the number of degrees of freedom in critical areas requiring reduction in the number of DOF in other substructures in order to stay within computer size limitations. Modal coupling and modal selection techniques were developed (see Methodology section, 2.1) to help solve this problem. The GVS brought to the surface model inadequacies. Model correlation techniques determined that CSM torsional springs and DA

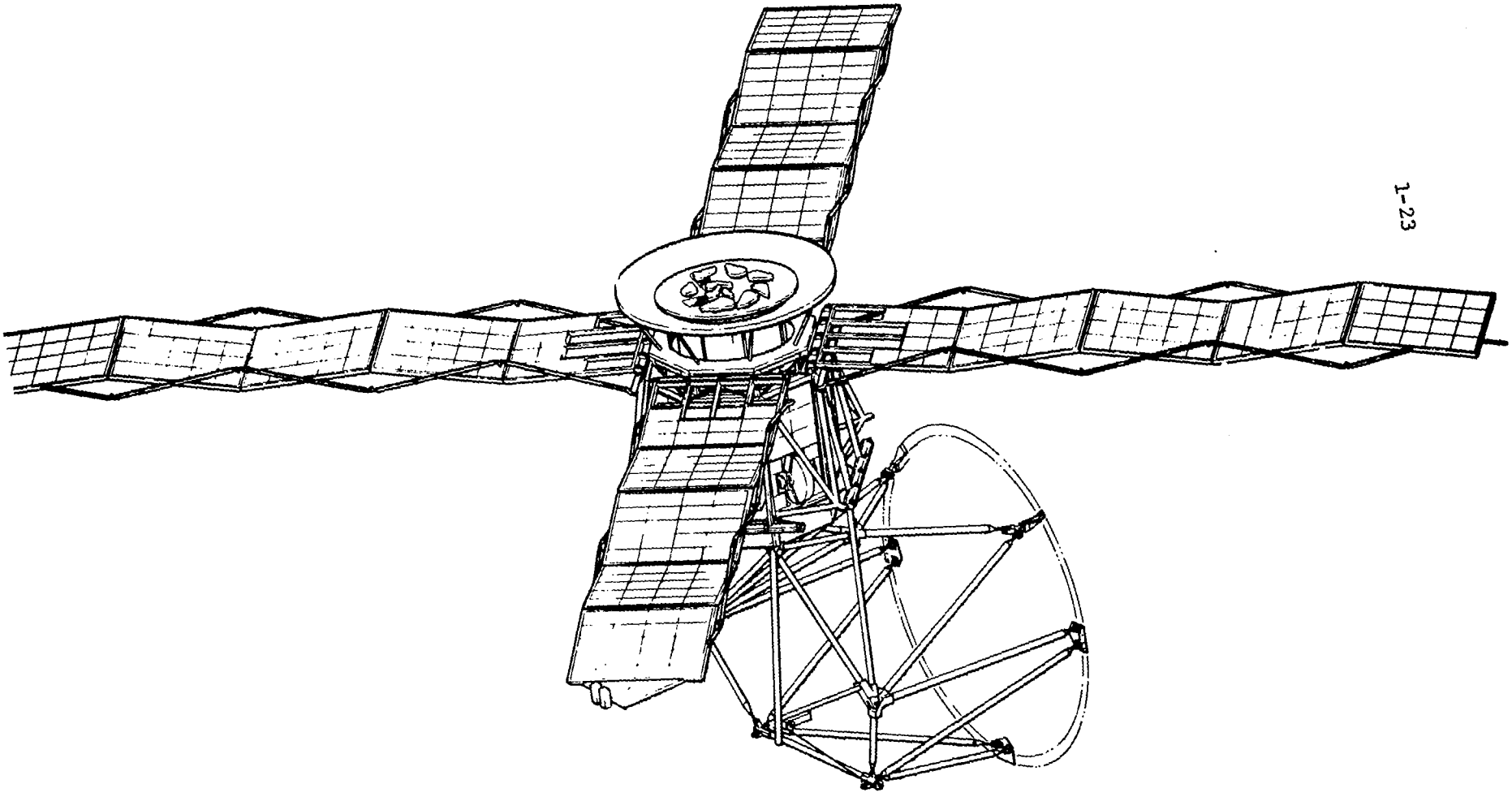

Figure 1.12 Deployed ATM

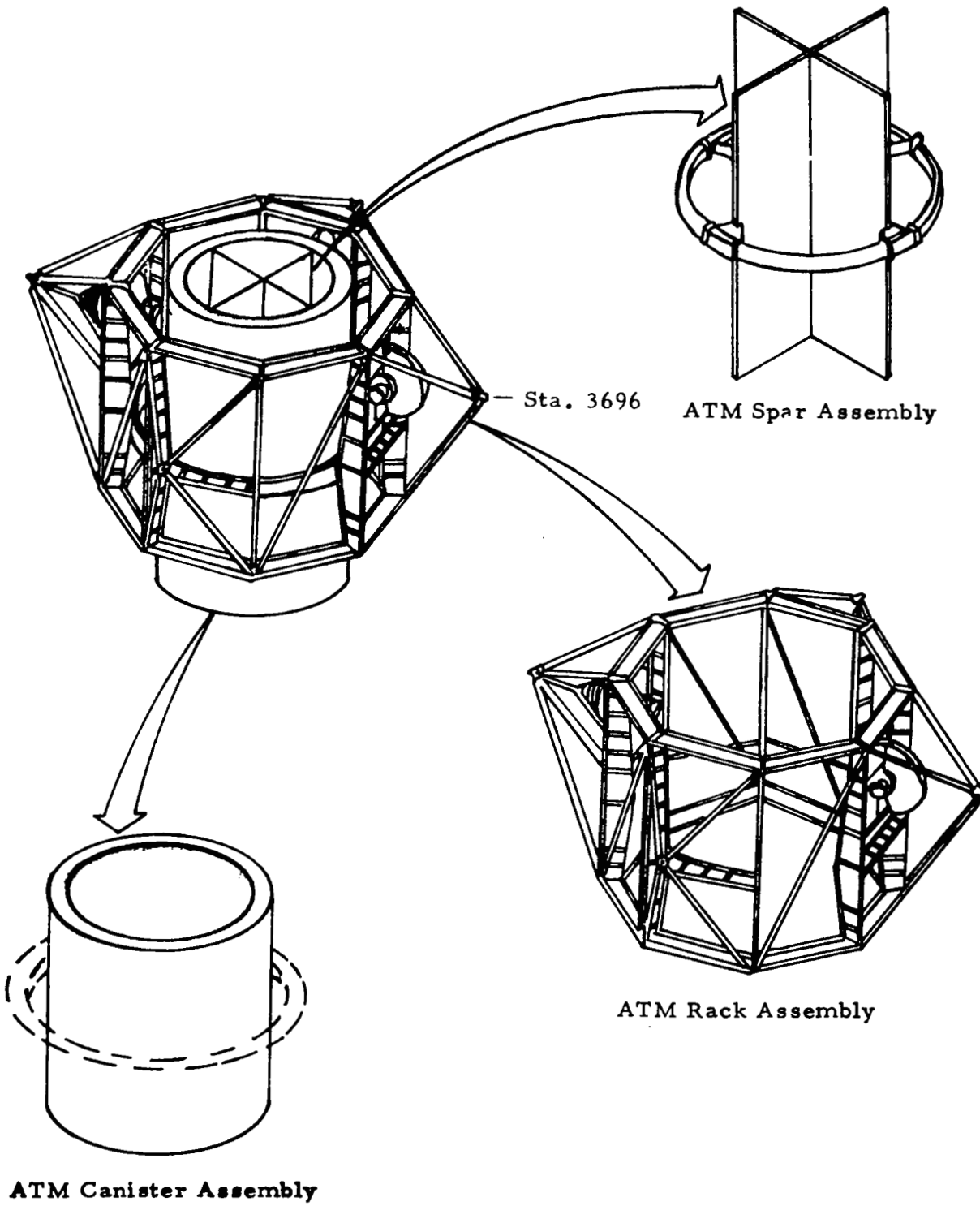

Figure 1.12a APOLLO Telescope Mount

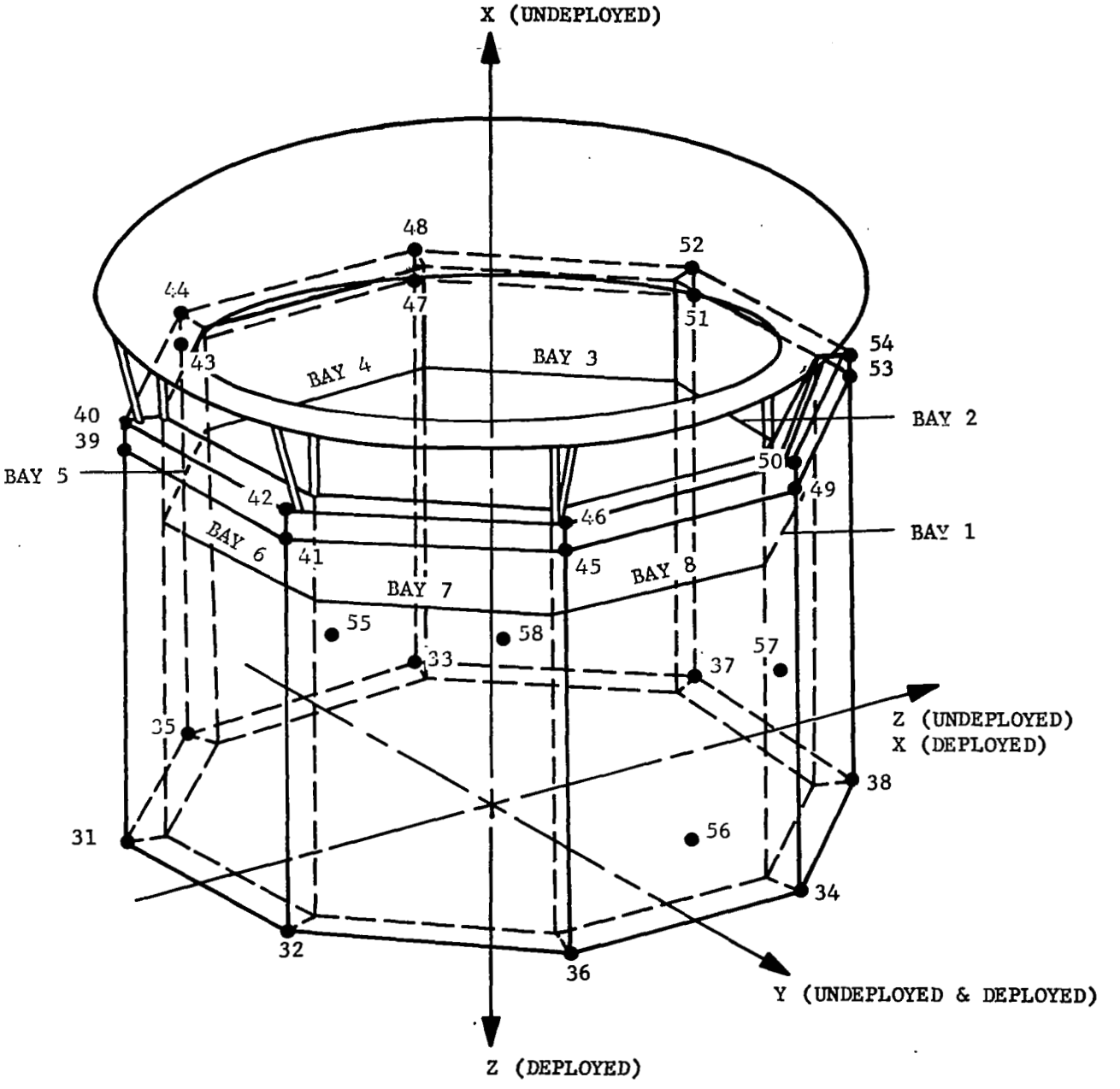

Figure 1.12b ATM Rack Model

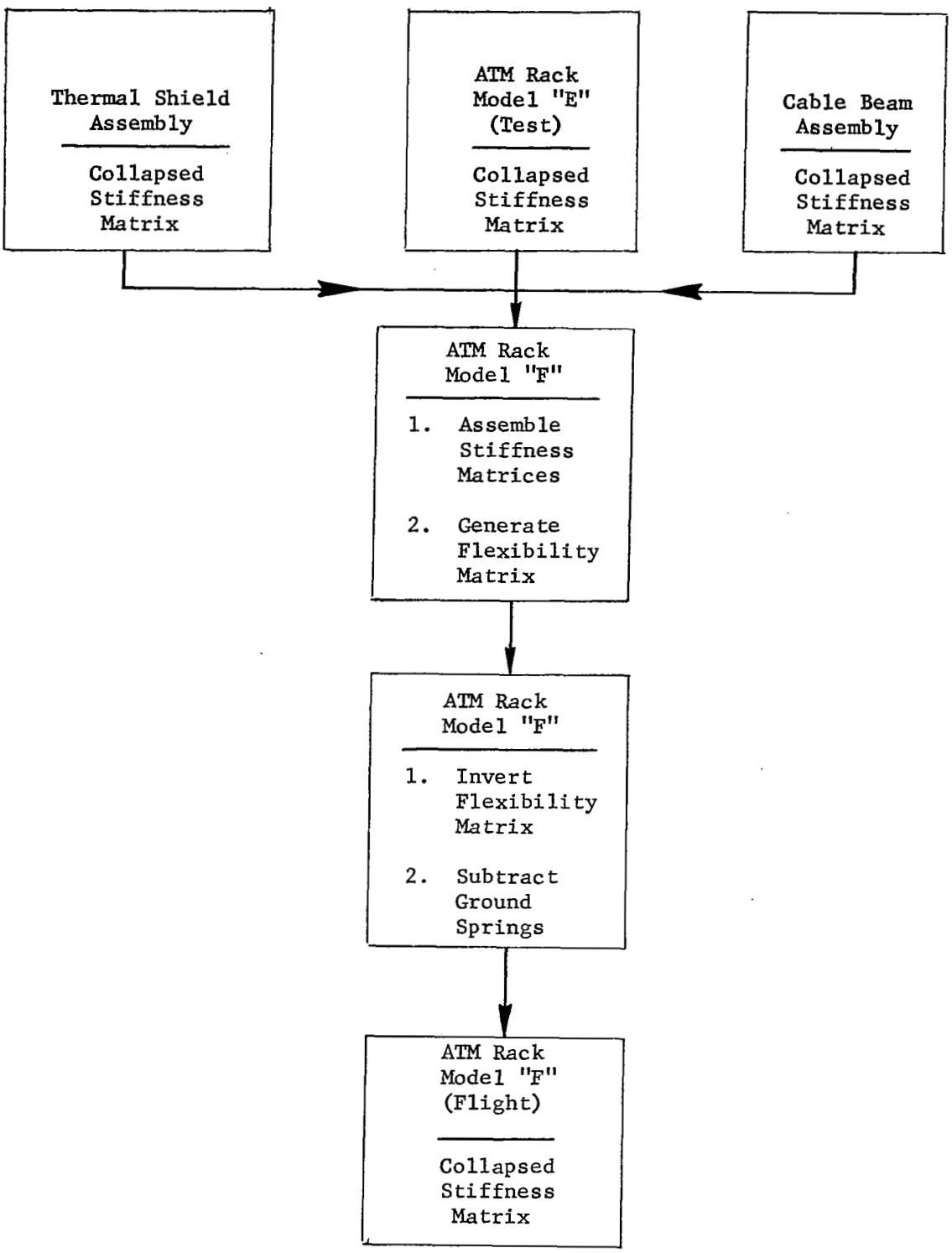

FIGURE 1.12c - FLOW CHART FOR DEVELOPING ATM RACK FLIGHT LOADS MODEL

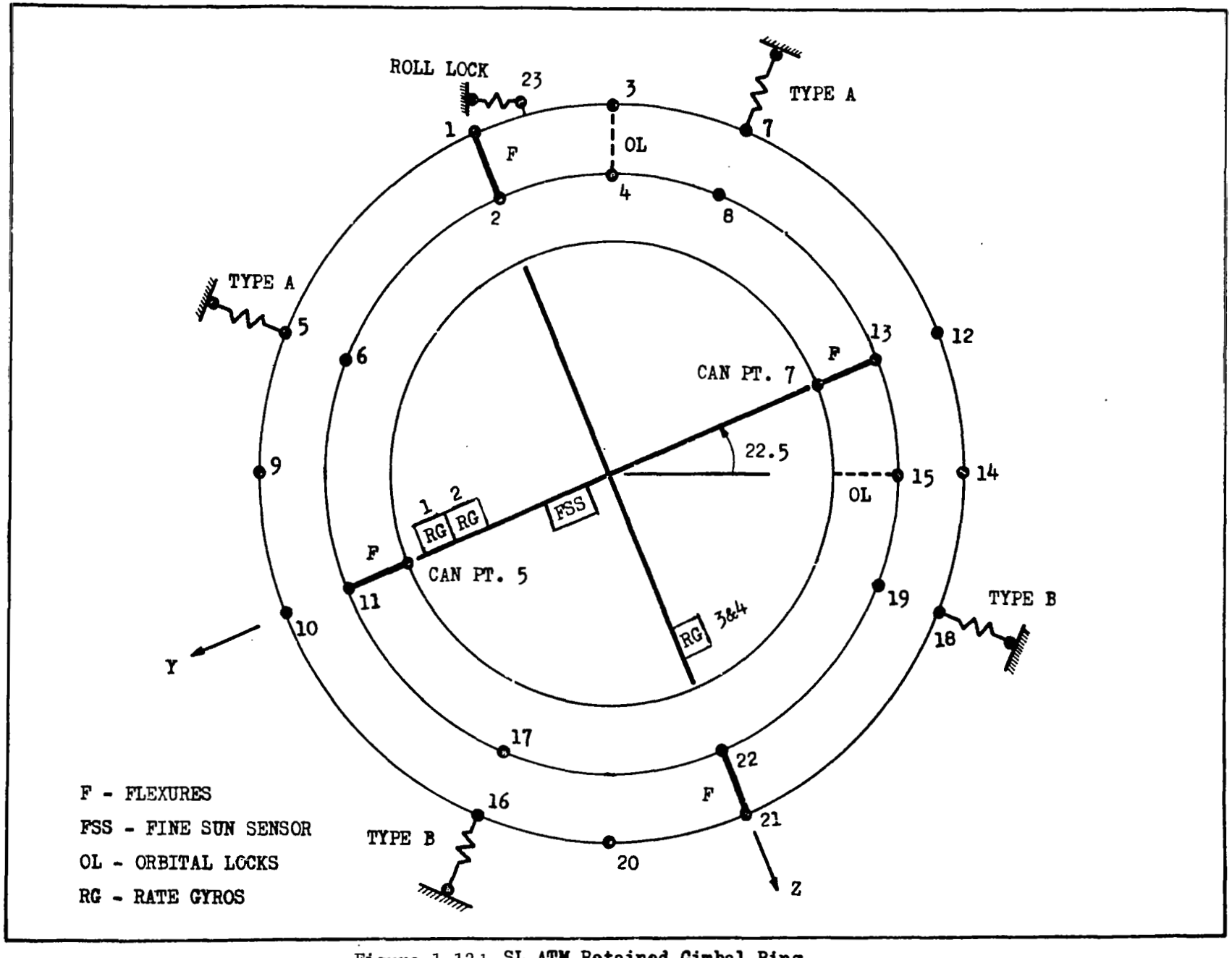

Figure 1.12d SL ATM Retained Gimbal Ring Assemble Structrral Model

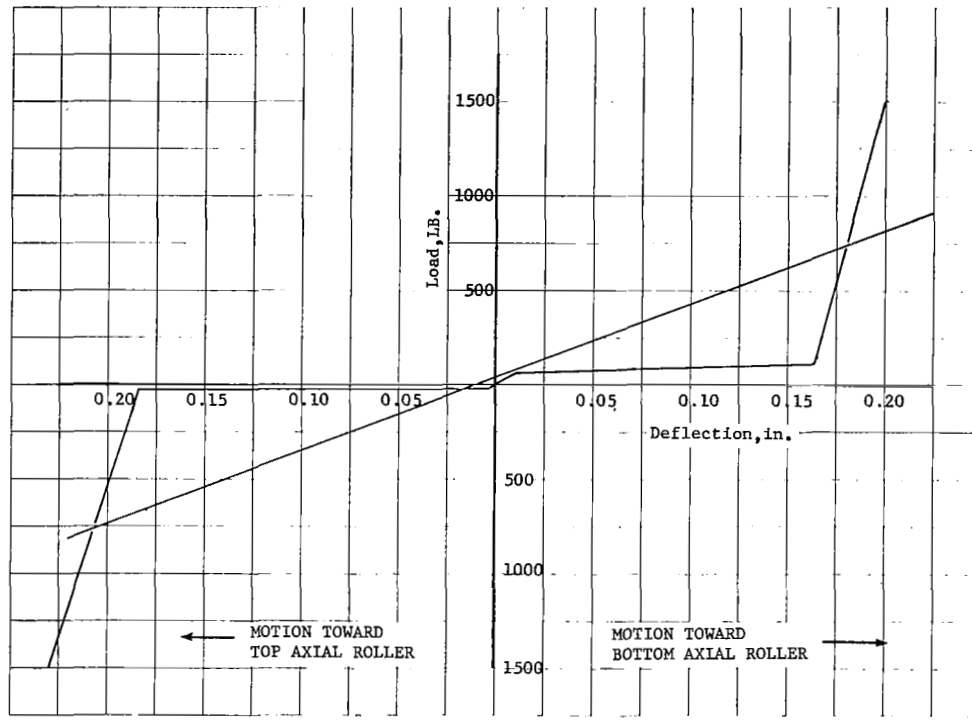

Axial Roller Effective Spring

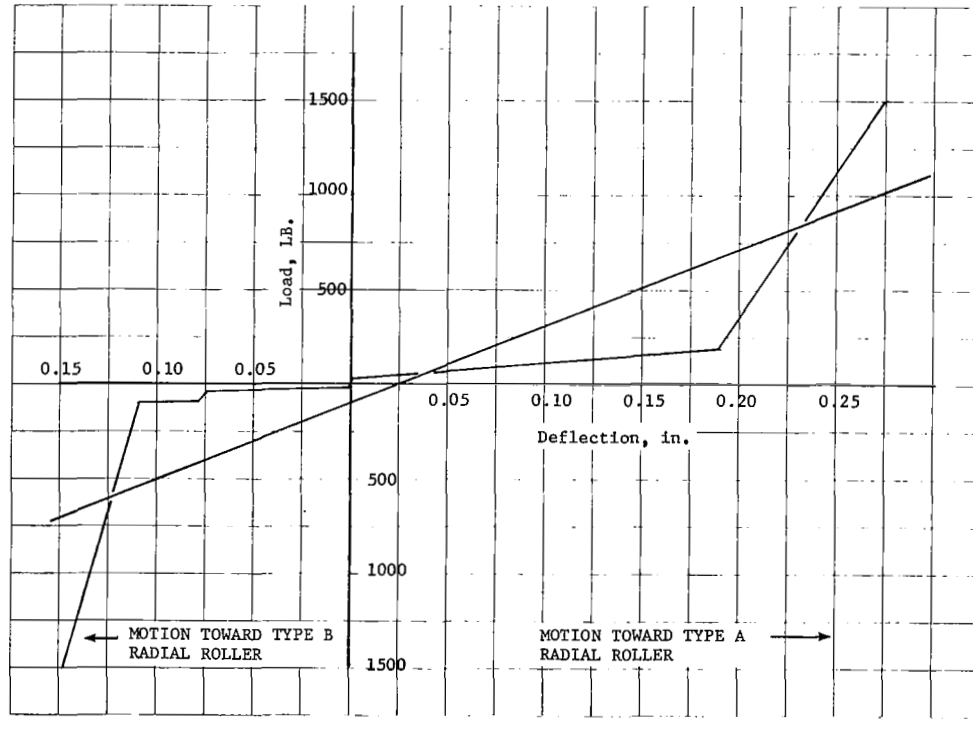

Radial Roller Effective Spring

Figure I.12e GRA Roller Effective Spring Rates

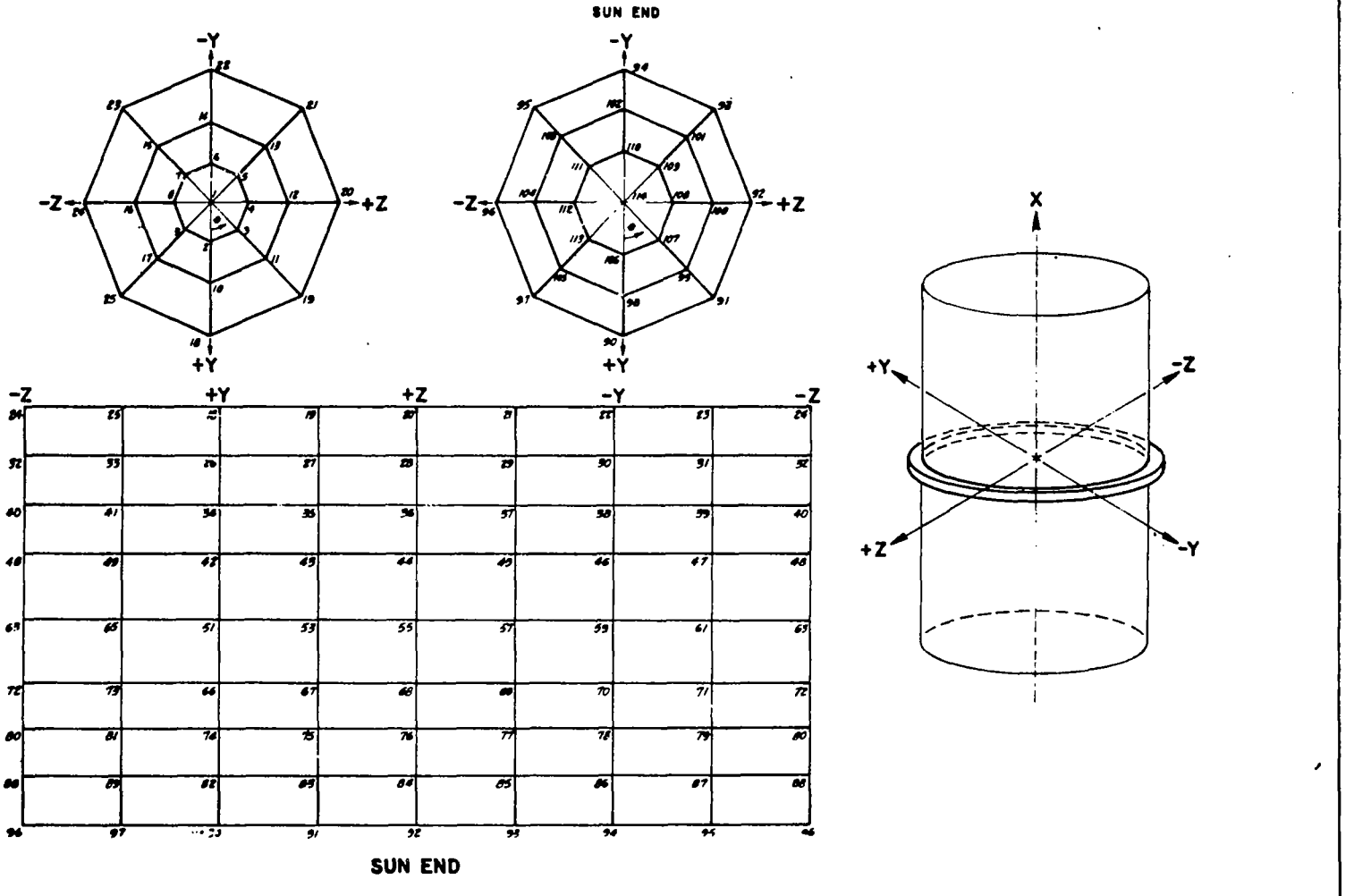

Figure 1.12f SL ATM Canister Structural Model

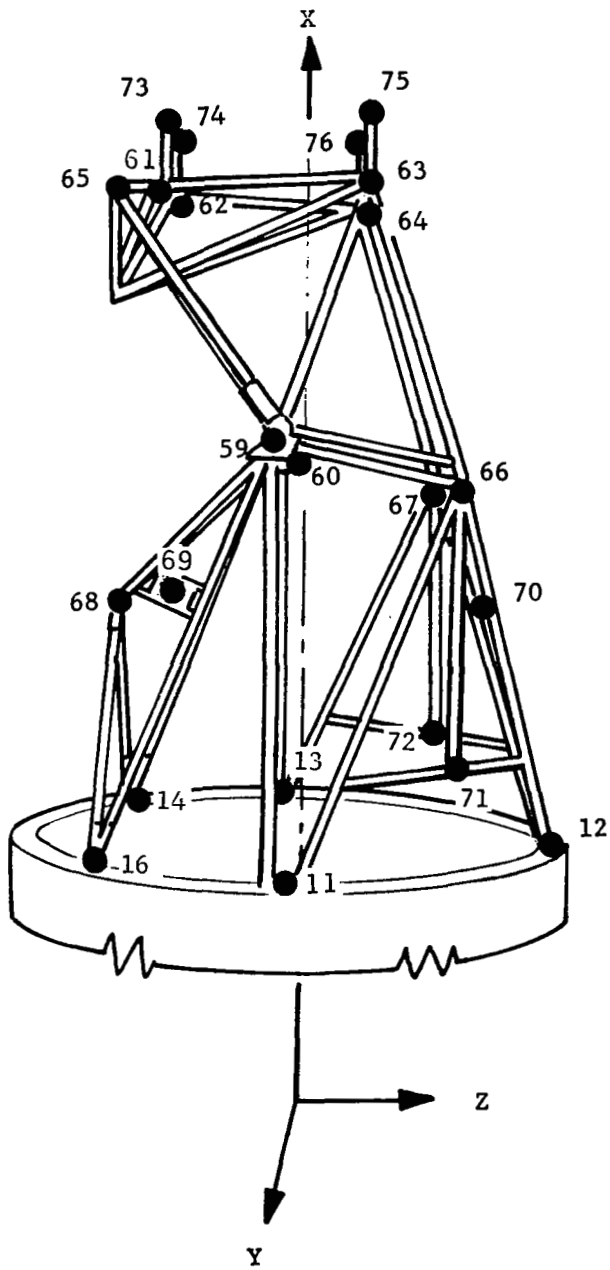

Figure 1.12g Undeployed DA Model

stiffness scaling factors had to be added to the models. Finally, the requirement of tolerance studies of the structure, generated additional modeling in the form of perturbed stiffness and mass matrices. At the time, this required reruns of the modal coupling and new solutions of the eigenproblems. Figure 1.13 provides a graphic summary of the model evolution presented here.

1.3.1 Recommendations -

a. Early definition of a final configuration can eliminate costly remodeling.

b. Prior to final configuration definition, inexpensive beam and stick models, with small numbers of DOF's, should be used wherever possible.

c. The final configuration model interface areas should be modeled as fine as possible. Modal coupling and modal selection techniques should then be used to reduce the number of DOF's to within the computer size limitations. This would have eliminated the model discrepancies discovered during flight.

d. After the design configuration is finalized, model perturbations can be handled using an eigensolution sensitivity approach (see Methodology Section, 2.3). This technique provides an economical eigensolution for a perturbed model by circumventing the necessity for regeneration of the complete model. Major design changes, mass redistributions, test derived scaling factors and tolerance studies can be handled effectively by this technique.

e. If a GVS is to be performed on a test article, the GVS should be performed as early as possible to permit a thorough model evaluation.

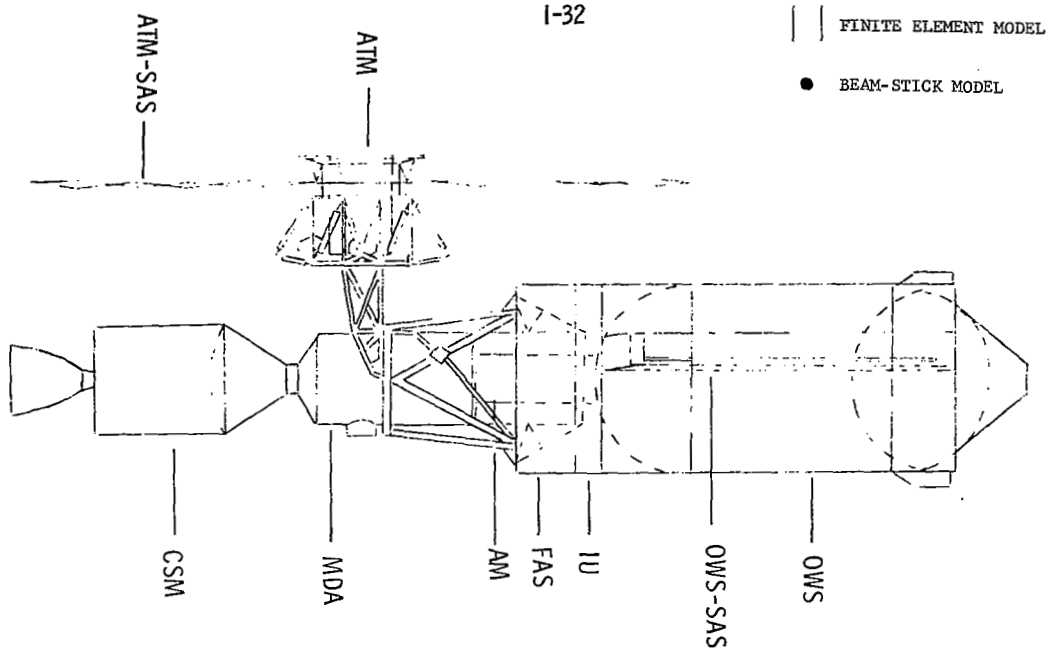

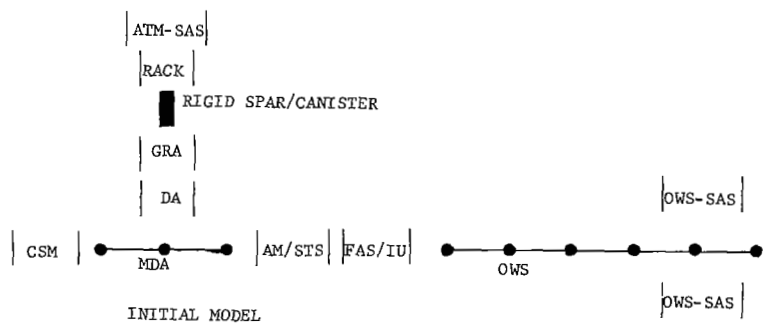

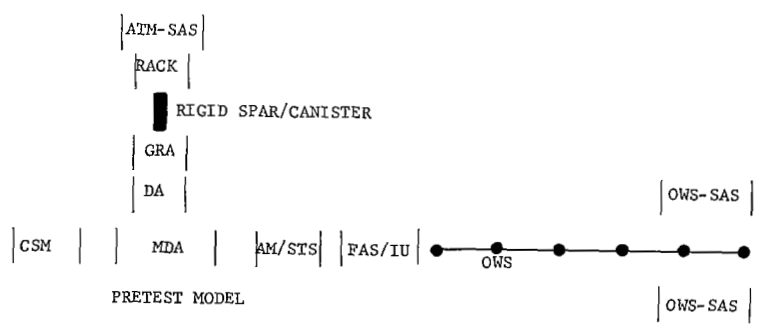

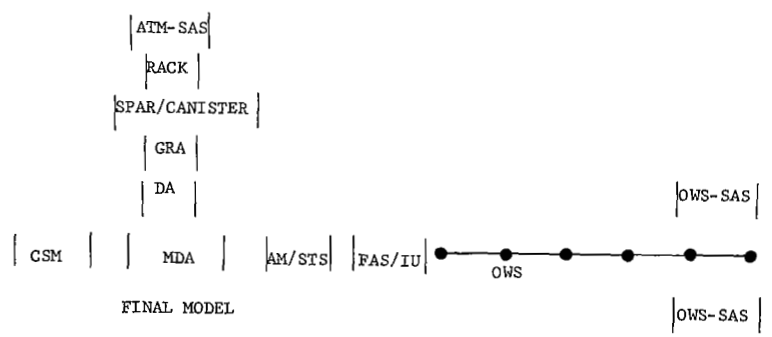

Figure I.13 Graphic Summary of Model Evolution

2.0 SKYLAB ANALYTICAL METHODOLOGIES

The Apollo Applications Program (AAP) which evolved into the Skylab program presented numerous dynamic problems which required significant analytical developments to cope with the complexity and sophistication of a manned orbital laboratory. Principal concern in the structural dynamic areas were 1) a large flexible structural system requiring detailed modeling to define accurately modal characteristics for load and control studies, 2) subsequent refinement in modal coupling and mode selection programs, 3) requirement for a sophisticated docking impact analysis due to structural load modal sensitivity, 4) control impulse definition, complicated with the interaction of control sensors at various locations of the orbital structural to natural model characteristics and a requirement for accurate definition of propellant and impulse requirements, and 5) structural model correlation and revision due to differences in analytical and dynamic test results.

Technical requirements and resulting analytical methodologies were originated early in the program and expanded throughout the Skylab program. During the program and in the years hence, these analytical tools have been refined and expanded into other areas/projects of application. Figures 2.1 through 2.3 define the chronological development of the principal Skylab structural dynamic methodologies. Principal methodologies developed under the Skylab program were:

a. Skylab modal characteristics,
b. docking response of flexible bodies,
c. structural model correlation with dynamic test.

2.1 Skylab Modal Characteristics

Skylab represented the most complex structural assembly that had been considered to date by any scientific organization and as such presented distinct analytical problems to the analysts. Actually, the growth of modal characteristics began under the original AAP studies and their concepts will be included.

2.1.1 Early Assessment - Initial problems facing the analyst on the AAP and subsequently the Skylab programs were size problems associated with existing or revised computer programs. These problems included:

a. MDA finite element models required to find a model to define six degree of freedom response at skin stations;

b. incapability of structural models from associate contractors to define structural response adequately;

c. models too course to effectively answer control system design requirements;

d. difficulty in determining modal tolerances on a totally three dimensional structural system;

In an attempt to retain sufficient accuracy of models and at the same time a rational approach to structural model size limitations, a "beamology" approach to mathematical modeling evolved. Primary consideration was given to detailed modeling of the interfaces and either direct mass point centerline models or detailed structural model of systems which were later collapsed/reduced to centerline point models for a compatible mass matrix on these centerline models were determined.

Even with these considerations, the size and complexity of the structural elements which comprised the Skylab configuration did not lend themselves to efficient "direct" vibration analyses. This was primarily due to computer size limitations associated with long computer run times. Some program run times were beyond the mean time to failure of the individual computer systems. This problem was partially resolved by applying a component mode substitution method (modal coupling). This method considers the structural system to be an assemblage of subsystem components. The vibration modes for each component are determined separately then a reduced or truncated set of these modes are used to synthesis the total system.

The next section describes the chronology associated with the development of this technique with parallel methodology development.

2.1.2 Methodology Development - Of most concern in the early development of system modal characteristics was the requirement to obtain some modal fidelity limits on the model. The Skylab was such a complex model that many modes were present that had to be accurately defined to complete design study requirements. Initially, this was resolved by assuming isolated structural systems, i.e., due to structural damping major systems did not significantly couple, therefore, these complex systems could be analyzed as "uncoupled systems". Such systems were assumed to be ATM docking ports, and OWS Solar Array System. As these assumptions were not valid, the development of adequate methodologies followed.

It is not the intent of this report to republish all previously developed and published methodology. However, to assure the completeness of the report, Figure 2.1 illustrates the Skylab modal characteristic methodology development.

2.2 Skylab Docking Response

The docking problems of spacecraft, in the past years, has been focused on the docking requirements of the Apollo and Skylab missions. However, missions of the future, in particular Space Shuttle, will require

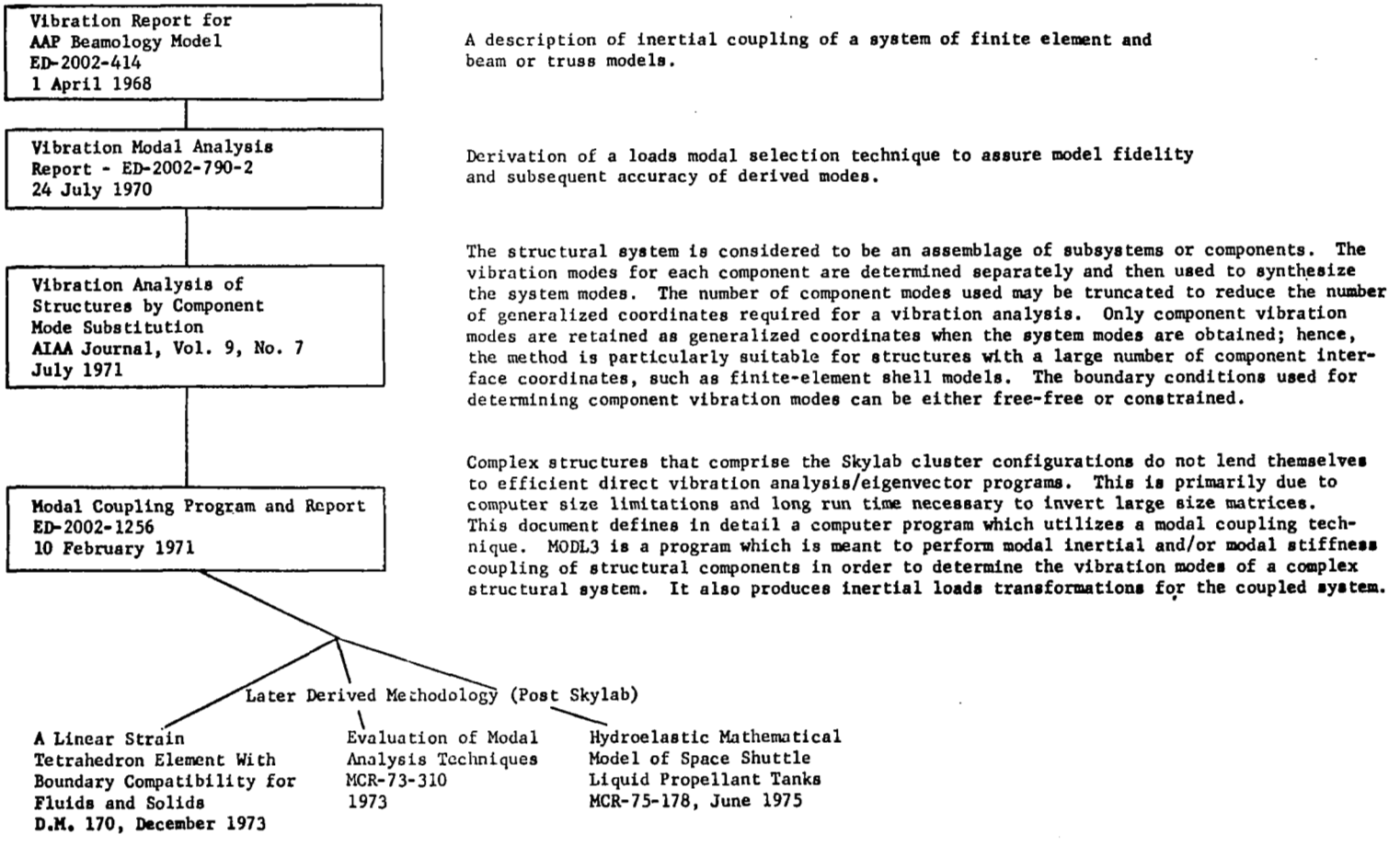

Figure 2-1. Chronology of Modal Analysis Methodology

docking of space vehicles with space station satellites and necessitate extensive docking analyses. The docking maneuver and its associated responses will affect the design of these large, flexible structures. Additionally, definition of successful capture boundaries, spacecraft attitude control requirements, propellant utilization studies, and man/machine interaction or the degree of automation are required.

One of the first studies dealing with docking dynamics presented a generic analysis of rigid body docking dynamics from initial physical contact of two spacecraft to final latching. The docking interval was specified in three phases - initial contact, continuous maneuver and latching - and assumed that the first and third phases occurred over a finite time interval. The study presented an analysis that revealed gross effects of significant docking parameters, including attitude misalignment, initial relative vehicle rates and docking rate.

A two-dimensional analysis of the dynamics of the probe and drogue docking concept was presented (Reference 2) in 1966. The mathematical simulation of the docking maneuver assumed the docking vehicles were rigid bodies, but included a provision whereby the probe vehicle might be modeled as a rigid structure with spring and dashpot attached masses. Probe rotation was constrained by a resisting moment, and probe axial deformation was assumed to act in accordance with a prescribed energy absorber. The restriction that the probe-tip must remain in contact with the drogue surface was not introduced, and it was assumed that, when the probe was not in contact, it returned to its equilibrium position in a prescribed manner. This assumption precluded the necessity for an iterative solution if nonlinear shock attenuators were included. Latching was assumed to have occurred when (and if) the probe tip reached a designated position in the drogue socket. All postlatch analyses were conducted with the probe tip assumed pinned in the socket.

In 1967, analyses were completed of the docking maneuver that considered an Apollo docking mechanism (Reference 3). The primary goal of this analysis was to determine the nature of the loading on the two docking vehicles caused by the docking mechanism and to evaluate the internal elastic loads induced in the vehicle. The general approach to the development of the analytical method was to solve the two-body dynamics problem in which rigid bodies are subjected to loading from a model of the docking mechanism. These load histories were then used in a generalized modal response analysis to determine the resulting elastic response of the docking vehicles.

Additional studies were completed (Reference 4) based on impulse-momentum relationships and considered friction between probe and drogue, energy losses due to permanent deformation, attitude control of the chase vehicle, and thrusting of the chase vehicle following initial contact. All motion was considered to take place in a plane, and the probe tip was constrained to lie on or within the drogue cone walls. Given the spacecraft mass properties and a set of initial conditions,

the simulation was able to predict whether a docking maneuver would be successful (capture) or fail (miss). The simulation also provided an estimate of the contact loads that would occur during the attempt. This simulation was used to obtain results for docking maneuvers of the Skylab spacecraft.

Skylab analysts completed an analytical study of the docking dynamics of two space vehicles that were more general than the efforts of previous investigators. The equations of motion, coupled with pertinent constraint equations and equations of momentum-impulse, were developed without regard to any particular docking mechanism concept. Their equations resulted from applying Hamilton's principle of least action (Reference 5) as if the system under analysis were a conservative system subjected to auxiliary, holonomic constraint conditions. They modified the resulting equations to account for the possibility of unconservative forces and nonholonomic constraint conditions through application of the principle of virtual work. They showed that if the mass properties (inertial forces) of the docking mechanism were negligible, the requirement for momentum-impulse equations disappeared.

The Skylab docking event assumed the role as the most significant orbital dynamic load problem. As such, it precipitated a direct physical mating, docking response, test computer hybrid study at NASA JSC which established initial boundaries, rates and latch forces. In excess of 6000 physical dockings were simulated and basic formulation of the docking problem was accomplished.

The modeling of the drogue/probe assembly (see Figure 1.11a) and resulting sliding motion coupled with control sensitivities, were initially considered as the most significant problem area. Therefore, docking problems were considered in two ways, one the changing of modal properties of the system during the docking event due to engagement, and two, being large nonlinearities being excited, eg., propellant slosh. The complexity of the docking problem was felt to be predominantly in the description of the probe neck as it contacted the drogue. It is interesting to note that at this time capture was not considered the significant event and, therefore, overall cluster response due to docking was considered small due to structural damping.

The initial loads methodology for the docking event considered general step and ramp buildup forces and utilized a modal acceleration method for resolving the transient responses.

As a result of the hybrid computer test results and films of orbital mating of the CSM/LEM, more detailed studies were initiated to resolve impact of latch forces to Skylab design.

The results of a study of the response of flexible space vehicles to docking impact have been detailed in Reference 6. This study resulted

in a comprehensive analytical development and digital computer program to investigate the docking dynamic characteristics of elastic space vehicles. The analysis considered influence of one or more attitude control systems acting during the maneuver. The resulting mathematical model was programmed for numerical evaluation; primary program output consisted of time history plots of significant program variables, including vehicle velocities, probe deformation characteristics, probe/drogue interface forces and moments, and control system parameters.

Note that this analysis and that of Reference 6 were the first in which the elastic properties of the two docking vehicles were considered. The analysis also considered the effects of sliding friction between probe and drogue, internal binding friction caused by probe deformation, and the possibility of nonlinear stiffness and damping characteristics.

The development of a complete Skylab dynamic docking maneuver analysis program, from impact through the latching sequence was a significant state of the art development.

Recent studies utilizing those derived programs include general docking methods, propellant responses, spinning body dynamics and response of flexible, rotating components.

Figure 2.2 schematically depicts the docking study evolution.

2.3 Model Correlation to Vibration Testing

Analytical modeling of complex test articles seldom agree with dynamic test results. Design changes, data tolerance effects, mathematical techniques and engineering judgement impose uncertain constraints on the analytical model.

This section describes a rational methodology to correct the model discrepancies discovered by dynamic tests which was developed on the Skylab program. The problem is approached by formulating the eigenproblem in terms of perturbed nominal model finite element data and nominal modal coordinates. The extent of coupling produced by elemental stiffness and/or mass matrices between the nominal modes determines the respective distributions of modal strain energy and modal kinetic energy among the model elements. The extent of this coupling is limited by orthogonality of the nominal model eigenvectors with respect to the unperturbed finite element data. This property is utilized to decrease the size of the eigenproblem required to calculate modal perturbations produced by a given element perturbation. Thus, the sensitivity of a particular mode to perturbation of a specific model elements can be determined economically. The model sensitivity information is used to define a set of test data that is most applicable for adjusting the analytical model to correlate with dynamic test results.

The chronology of the development of this technique is depicted in Figure 2.3. It should be noted that at the time of this report, additional development is proceeding in this area.

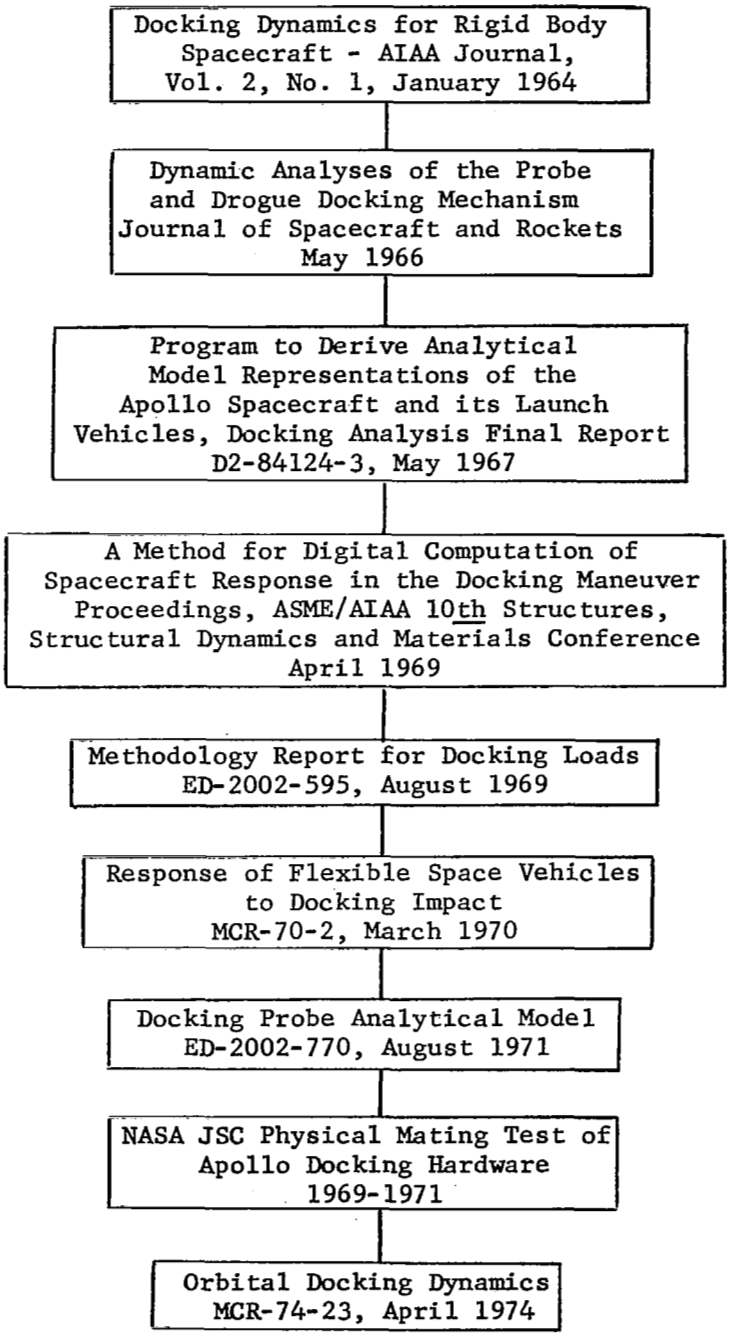

FIGURE 2.2 - CHRONOLOGY OF DOCKING RESPONSE METHODOLOGY

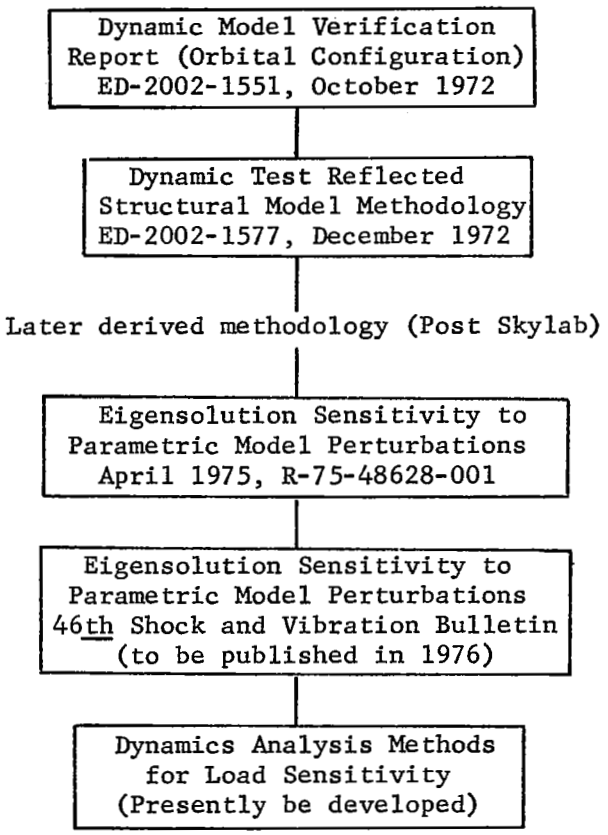

FIGURE 2.3 - CHRONOLOGY OF EIGENSOLUTION SENSITIVITY TO PARAMETRIC MODEL PERTURBATIONS

3.0 ORBITAL CLUSTER INTERIOR ACOUSTICS

The purpose of the Skylab Interior Acoustics contract was to coordinate with the National Aeronautics and Space Administration/Marshall Space Flight Center (NASA/MSFC) and equipment contractors to assure compliance with the acoustic requirements established by the Medical Research and Operations Directorate. The following are examples of tasks which were performed and are summarized in this section.

a. Identify and locate noise sources in the Skylab. Determine the frequency of use and duration of operation of noise sources as a function of mission profile time.

b. Update analyses as required to evaluate the effects of additive noise sources at crew work stations and rest stations. These analyses shall reflect nominal continuous levels and maximum levels resulting from equipment/experiment operation during the mission profile.

c. Coordinate with MSFC and MSC to establish measurement requirements, locations and time/line schedule for obtaining noise level measurements during the Skylab mission.

d. Analyze interior noise level measurements obtained during the missions and correlate results with predicted levels.

Prior to a presentation of the acoustic data measured during the SL-2, 3 and 4 missions, a discussion and description of the Skylab noise sources, the Skylab compartment characteristics and the acoustic methodology utilized, are presented.

3.1 Acoustic Acceptance Criteria

3.1.1 Skylab Internal Noise Levels - The Medical Research and Operations Directorate at JSC, recognizing that the acoustic environment could influence the astronaut's performance and ability to communicate, published a criteria for the Skylab internal noise levels as shown in Figure 3.1.The criteria was applicable to any noise source or combinations of noise sources operating continuously in the Skylab interior. Of particular concern was the desire to insure adequate, uninterrupted sleep periods for the astronauts.

The development of the criteria was based, in part, on experience gained during the Apollo program, where crew members had objected to the noise output of the post-landing-ventilation (PLV) fans. These fans were planned for extensive application throughout the Skylab ventilation control system. Consequently, MSFC conducted an extensive development program to provide mufflers for these fans to reduce noise levels to acceptable limits.

3.1.2 Speech Interference Levels - The preferred frequency speech interference level (PSIL) was selected to assess the speech-interfering aspects of the Skylab interior noise sources. The PSIL is defined as the arithmetic average of the sound pressure levels in each of the three octave sound bands with center frequencies of 500, 1000 and 2000 Hz.

The PSIL associated with the Skylab interior noise criteria in Figure 3.1 was 56.7 dB. For this PSIL value, face to face communications at 14.7 psia ambient pressure are possible using "a normal noise" when a speaker and listener are less than five feet from each other (see Reference 7).

Another rating system, the modified speech interference level (MSIL), includes the higher frequency noise. MSIL is defined as the arithmetic average of the sound pressure levels in each of the four octave bands with center frequencies of 500, 1000, 2000 and 4000 Hz. The MSIL associated with the Skylab interior noise criteria is 56.25 dB. PSIL and MSIL values in each Skylab section due to operation of the individual noise sources at 5.0 psia ambient pressure are presented in Table 3.1.

3.2 Definition of Environment

3.2.1 Noise Sources and Locations - Skylab equipment and experiments were reviewed to determine noise sources. Tables 3.2 and 3.3 present a listing of the Skylab equipment and experiments; noise sources are indicated with an arrow or asterisk in these two tables. Originally, the noise sources were grouped according to the contractor subdivisions. It was determined that grouping the noise sources according to acoustic space would provide more meaningful results. The three acoustic spaces chosen were the MDA, AM/STS and OWS. The noise source, number, location, frequency of operation and table number for its sound power level are presented for each compartment in tables 3.4, 3.5 and 3.6. Figures 3.2 through 3.10 indicate the locations of each of these noise sources. The sound power levels for each compartment are delineated in Tables 3.7 through 3.13.

A-weighted sound levels (dBA) were calculated for the noise sources at an atmospheric pressure of 5.0 psia. Octave band sound pressure levels were converted to the equivalent A-weighted sound level by applying the relative response for the A-weighted network to the estimated octave band levels and obtaining the overall level from the resulting octave band levels. These equivalent A-weighted sound levels are presented in Table 3.14.

3.2.2 Compartment Characteristics - The volumes and surface areas of the MDA, STS, AM and OWS were calculated. In addition to these, equipment volumes, surface areas and common wall areas between each compartment were calculated. The results of these calculations are presented in Table 3.15, Skylab Acoustical Compartment Characteristics.

Reverberation times for the flight configuration were estimated from the Skylab mockup. Figures 3.11 through 3.13 present the reverberation times for the MDA/STS, AM and OWS at pressures of 5.0 psia and 14.7 psia.

3.2.3 Acoustic Methodology - Sound pressure level estimates for each compartment, due to noise sources in the same compartment, were calculated using the following equation for a reverberant sound field:

$$SPL = PWL - 10\,Log_{10}V + 10\,Log_{10}\,(P/PReF) + 10\,Log_{10}\,T60 + 19.6\ dB \quad (1)$$

where

V = volume of section containing noise source ft^3,

P = ambient pressure in the enclosure, psia,

P_{ref} = reference ambient pressure = 14.7 psia,

T60 = reverberation time of enclosure, sec

To obtain estimates of the sound pressure levels in the compartment due to noise sources in other compartments, the following expression was used from Reference 7:

$$PWL_2 = PWL_1 + 10\,Log_{10}\,(SW/R_1) - TL \quad (2)$$

where

PWL_1 = noise source PWL located in Room 1,

PWL_2 = PWL of noise source applicable to Room 2,

SW = area of common wall between Rooms 1 and 2,

R_1 = room constant of Room 1 = $S\,\bar{\alpha}\,/(1 - \bar{\alpha}) = .049V_2/T60$

TL = transmission loss of common wall = 0 for an open passage

Combining equations (1) and (2) yields the PWL of the noise source applicable to Room 2 in terms of the SPL in Room 1.

$$PWL_2 = SPL_1 + 10\,Log_{10}\,(SW/4) - 10\,Log_{10}\,(P/PRef) - TL \quad (3)$$

From equation (2), the following definition of T60 is applicable.

$$T60 = .049V/S\bar{\alpha} \quad (4)$$

where

$\bar{\alpha}$ = average absorption coefficient.

Now, $\bar{\alpha} = \frac{\sum_{o}^{n} S_i \alpha_i}{\sum_{o}^{n} S_i}$ (Reference 7)

where

S_i = surface area of the ith wall

α_i = absorption coefficient of the ith wall

3.3 Flight Measurement Results

3.3.1 Noise Measurements During Skylab Mission (Experiment M487) - The objectives of experiment M487 were to measure, evaluate and report the habitability features of the crew quarters and working areas of the crews in engineering terms useful to the design of future manned spacecraft. A portion of this experiment included the measurement of sound pressure levels on Skylab using a portable sound level meter (Bruel + Kjaen, type 2203) and octave filter set (Bruel + Kjaen, type 1613). Eight measurement locations were selected and are shown in Figures 3.14 through 3.17. These are the aft OWS area (4 locations), the forward OWS area (1 location), the STS/AM area (2 locations) and the MDA area (1 location). The sound level meter, used to obtain these data, was oriented as follows:

a. OWS Wardroom - parallel to CDR food tray, microphone pointed towards OWS (location #1);

b. OWS Experiment Compartment - parallel to floor at LBNP, microphone pointed towards sleep station (location #2);

c. OWS Waste Management Compartment (WMC) - on floor, microphone pointed towards +X (location #3);

d. OWS Sleep Compartment - in PLT compartment, on floor, microphone pointed towards +X (location #4);

e. OWS Forward Compartment - parallel to floor located at locker ring area, microphone pointed towards +Y (location #5);

f. AM - parallel, with microphone pointed towards +X in middle of compartment (location #6);

g. MDA - at Experiment M512 station, microphone pointed towards -X (location #7);

h. STS - microphone pointed at Mole Sieve A (location #8).

3.3.2 Flight Environmental Conditions for SL-2, SL-3 and SL-4 - The following ventilation system fan operational mode existed during the period the acoustic data were obtained on the SL-2 mission:

a. CSM portable fan in MDA was off;
b. cabin fans 1 and 2 in MDA were on low;
c. OWS interconnect fan (STS duct fan) on hi;
d. cabin heat exchange module (STS heat exchange fans (3)) on hi;
e. OWS heat exchanger fans (4) in MDA were on hi;
f. OWS duct fans (8) in OWS were on hi.

For the SL-3 and SL-4 missions the following operation mode existed:

a. CSM portable fan in MDA on hi;
b. cabin fans 1 and 2 in MDA were on hi;
c. STS duct fan on hi;
d. STS heat exchanger fans (3) on hi;
e. OWS heat exchanger fans (4) in MDA were on hi;
f. OWS duct fans (12) in OWS were on hi.

In addition to the M487 acoustic measurements obtained during the SL-3 mission, acoustic noise source measurements were also obtained. These measurements were made in the immediate vicinity of eleven noise sources in the Skylab interior. Specific information applicable to sound level meter (SLM) distance and orientation to each noise source was not received so a distance of 3 feet was assumed. The results of these measurements are presented in Table 3.16.

3.3.3 Comparisons of Predicted and Measured Skylab SPL's - A comparison of the Skylab measured SPL data from the SL-2, SL-3 and SL-4 missions with previously predicted SPL's is indicated in Figures 3.18 through 3.20.

Figure 3.18 compares the MDA/STS SPL's and indicate the MAX/MIN envelope of the Skylab flight data and the composite of predicted continuous noise source in the MDA/STS. A comparison of the data indicates the predicted SPL's begin to exceed the measured data by 3 to 6 dB, from 1000 to 4000 Hz. Below 1000 Hz, the data compare favorably.

A comparison of acoustic data applicable to the Airlock module is indicated in Figure 3.19. The predicted data fall within the measured SPL envelope at the lower frequencies and begin to exceed the envelope above 1000 Hz.

A comparison of acoustic data applicable to the OWS is indicated in Figure 3.20. The predicted data fall within the measured SPL envelope, especially in the mid-frequency range.

3.4 Acoustical Environment Mapping

A comparison of the Max/Min M487 SPL data obtained during the SL-2, SL-3 and SL-4 missions is indicated in Figure 3.21. The highest acoustic

levels were measured in the STS, influencing the MDA and AM SPL's to some extent. In general, the only areas to exceed the acoustic criteria by 2 to 3 dB were the STS, AM and OWS waste management compartment.

Preferred speech interference levels (PSIL's) and modified speech interference levels (MSIL's) were calculated based on the M487 SPL data. These PSIL and MSIL values are indicated in Tables 3.17 and 3.18, for eight locations in Skylab. These values do not exceed the acoustic criteria PSIL's and MSIL's in any area.

3.5 Skylab Crew Mission Acoustic Evaluation

A review of the Skylab crew comments applicable to the acoustic environments they were exposed to during the SL-2, SL-3 and SL-4 missions is discussed in the following paragraphs, and is based on data contained in Reference 8.

3.5.1 SL-2 Mission Acoustic Evaluation - Crew Acoustic evaluations are described as follows:

a. verbal communications - "within the MDA you could holler at someone in the workshop, however, could not holler from workshop to MDA";

b. SIA communications - "terrible for ground communications; have to keep certain SIA's turned down";

c. experiment M-509 - "when 509 thrusters fire, it is quite loud in OWS; I recommend everybody in OWS to wear ear protection (PLT)";

d. pre-sleep - "very quiet in sleep area; noisiest seems to be MDA/STS; can hardly hear fans running in OWS, but can hear refrigeration pumps, (CDR)";

e. post-sleep - "reported that both mouth sounds and snoring are as loud in zero G as they are at 1 G;

f. Crew Subjective Evaluation of Compartments:

Location	CDR	SPT	PLT
OWS Wardroom	excellent, extremely low	excellent	very good
OWS WMC	excellent	adequate	very good
OWS Sleep Area	low except for noise from WMC blower	too high when others are moving about, needs sound proofing	very good
OWS Exp. Compt.	low	ok	very good
OWS Fwd Dome	excellent	ok	very good
Airlock	low	N/A	all right
MDA/STS	fine	ok	satisfactory; gets high during EREP runs

3.5.2 SL-3 Mission Acoustic Evaluation - Crew acoustic evaluations are described as follows:

a. CDR - "can have duct fan heat exchangers turned off and can't tell any difference in noise level, they are so quiet";

b. PLT - "have to holler pretty loud to be heard from crew quarters up into the dome. Voices do not transmit up through the airlock at all. Have to use intercom to talk to anyone in MDA/STS. SIA's keep squealing all the time. Noise is definitely satisfactory";

c. CDR - "noise, very nice, very good";

d. Environmental Noise Factors Causing Interference: PLT - "just SIA's; OWS is comparatively quiet. No interference with ability to sleep". SPT - "never, no interference with sleep". CDR - "sometimes noises worry you, but after 3 or 4 days you get used to them".

e. Habitability Improvements:

PLT - "keep noise makers away from the sleep area, in the future. Portable fans run quiet, don't make any noise."

f. Subjective Evaluation of Compartments:

Location	CDR	SPT	PLT
OWS Wardroom	adequate noise level is ok, communications is good in here	very good, noise levels are satis-factory every-	very good, noise level is quite low, no objec-tionable noise
OWS WMC	ok	very good	very good
OWS Sleep Area	need to be able to de-crease noise level from rest of vehicle as it is hard to sleep when somebody else isn't asleep	looks reasona-bly good	very good
OWS Expt. Compt.	ok (adequate)	very good, satisfactory everywhere	very good, no objectionable noise
OWS Fwd Dome	ok (adequate)	very good	very good
Airlock	ok (adequate)	very good	very good
MDA/STS	ok (adequate)	very good	very good, higher in STS with fans on but its a very comfortable noise level

3.5.3 SL-4 Mission Acoustic Evaluation - Crew acoustic evaluations are described as follows:

a. Communications - CDR: "Squeal; verbal communications is possible in workshop area between compartments except WMC when door is closed and fan is on". SPT: "Squeal is ok if you are in same compartment, for verbal communications. If you try to go from one to another compartment, it is awful hard. There's too much noise or absorption of sound. If you are in experiment compartment, then you can call up to someone above you but it takes a fair amount of volume." PLT: "When on the same level (Z plane), there is no difficulty with verbal communications. Noise level increases as you go up and down (X axis). When separated by 10 to 15 feet along the X axis, it is extremely difficult to communicate by shouting."

b. Environment - CDR: "Surprised at how little noise there is in spacecraft. MDA/STS is only place there's quite a bit of noise in. In OWS, it is extremely quiet. All the different pumps and everything in MDA make all the noise. It's about the same or possibly higher (slightly) then noise level in the command module." SPT: "There's just a little too much noise to get sound sleep, more than I'd like to have." PLT: "It's good to have a little noise."

c. Environmental changes - CDR: "No change from noise pattern mentioned earlier. Surprisingly quieter than I expected. Noise in MDA/STS/AM is at a high level and it has affected our recordings. ATM C&D pumps are quite noisy and noise as it comes down through airlock is amplified by the dome for megaphone effects. Gets fairly noisy by the time it gets down to experiment compartment. Can turn pumps off at night so it won't interfere with sleep." SPT: "Noise is high in MDA and at ATM console. Find it gets to me when I am trying to concentrate or trying to use the speaker. Noise of pump in airlock used to get to me when working in MDA." PLT: "Can hear ergometer right now quite well and ATM pumps are quite loud. All the pumps are loud. Rate gyros are loud."

d. Subjective Evaluation of Compartments:

Location	CDR	SPT	PLT
OWS Wardroom	Very low in wardroom as it is in entire OWS unless you've got the EREP/ATM cooling loop running; then the dome takes the noise as it comes down the airlock and serves as a great big megaphone and sends it down slightly amplified.	Great, no problem	Really not that bad
OWS WMC	OK, but a little noisy with separators going. Not uncomfortable at all.	Great	Ok
OWS Sleep Area	Excellent, very quiet. Walls and doors pretty well damp out noise as well as light attenuators.	Fine	Noise propagates into sleep compartment when anyone else is doing something. Can't rest. There is no noise control in vehicle.
OWS Expt. Compt.	Fine	No comments	Very good
OWS Fwd Dome	Adequate. Just a little bit noisier than exp. compt. because closer to MDA/STS	No comments	Adequate. Ok, except it is reasonably high. There is sound focusing up in dome area because of spherical nature.
Airlock	No rating given. Extremely noisy. Coolant pumps are noisy.	ATM/EREP coolant pump noise problem is way too high. Should locate potential noise sources away from metal walls that can act like an acoustical can.	Fairly high

d. Subjective Evaluation of Compartments (Continued):

Location	CDR	SPT	PLT
MDA/STS	Unacceptable. Highly unacceptable, biggest offender is rate gyro	Way too high. Both pump and rate gyros make a racket. After a while, you can tune out the noise but can't think as clearly in there.	Fairly high

3.6 Articulation Index (AI) Analyses - The articulation index (A.I.) is a general criterion applicable for judging the effects of noise on communication. The AI predicts the intelligibility of speech (i.e., the percentage of words or sentences which are correctly understood) for a specified noise environment One method available to determine the AI, and utilized herein, is the weighted-octave-band (WOB) method, as described in Reference 9. The intelligibility criteria applicable to the AI is described as follows:

An A.I. of	Provides communications .....
0.7 to 1.0	Satisfactory to excellent
0.3 to 0.7	Slightly difficult to satisfactory; up to 98% of sentences are heard correctly.
0.0 to 0.3	Impossible to difficult; special vocabularies and radio-telephone voice procedures are required.

Articulation indices have been calculated for the SIA/ATM data (SL-4 mission), the MDA M-487 data (SL-3 mission), and the OWS Experiment M-487 data (SL-3 mission). The AI values compared the Skylab mission data to two speech spectrums, one applicable to a moderate voice and one to a raised voice. The AI values are indicated as follows:

Speech Reference	SIA/ATM	MDA	OWS Exp. Area
Moderate Voice	0.048	0.054	0.550
Raised Voice	0.150	0.186	0.723

These data indicate that communications in the OWS area shall be satisfactory to excellent, while communications in the SIA/ATM and MDA/STS areas might be quite difficult. These preliminary AI estimates tend to support the crew comments as described in paragraph 3.5.

3.7 Flight Anomalies

On Mission Day 33, the SL-4 crew noticed a "loud whine, not quite a squeal, but a whining noise", when they turned on the pumps. The pilot, on Mission Day 34, performed some acoustic measurements to investigate this noise source.

A tabulation of the SPL's measured during the coolant loop noise investigation is indicated in Table 3.19 and includes measured and calculated overall SPL's in terms of dBA, calculated overall SPL's and the measured octave band SPL's.

The AM SPL's compare closely with each other and are a maximum of 9 dB higher than the acoustic criteria at 1000 Hz. The STS/ATM SIA SPL's exceed the criteria at 500 Hz by 6 dB, and by 5 dB at 1000 Hz. The MDA CSM hatch SPL's exceed the criteria by 2 dB at 1000 Hz. The OWS experiment compartment SPL's are a minimum of 10 dB below the acoustic criteria.

3.8 Conclusions

3.7.1 M-487 Flight Data - The data measured in the OWS indicated this area to be the quietest region of the Skylab cluster. The OWS data were 5 to 10 dB below the acoustic criteria specification, excluding the WMC area, and generally enveloped the predicted SPL's. The STS measured data indicated this region to be the noisiest of the Skylab cluster, which tended to support previously predicted SPL's. The STS acoustic environment tended to influence the MDA and AM environments to a significant degree. Both STS measured and predicted SPL's exceeded the acoustic criteria specification. The MDA measured acoustic dataagreed closely with predicted SPL's, and did not exceed the criteria. The only MDA noise source of a problem nature was the rate gyros. Rate gyro acoustic data tended to exceed the MDA fan data by 5 to 10 dB.

3.7.2 Noise Source Data - The noise source data obtained in the OWS indicate that the refrigeration system SPL's are 5 to 10 dB higher than the VCS fan SPL's, but do not exceed the acoustic criteria. The

AM duct fan muffler noise source SPL's are quite high in the low frequency region, exceeding the criteria by as much as 11 dB at 250 Hz. The Mole Sieve compressor noise source data are quite noisy at 500 Hz, exceeding the criteria at 500 Hz. The MDA noise source data are dominated by the rate gyro SPL's, which exceed the criteria by as much as 7 dB at 500 Hz.

ATM Coolant Loop acoustic data was obtained during the SL-4 mission by the PLT crew member. Noticable increases in the SPL occurred in the Aft Airlock and Forward Airlock locations, where increases as high as 12 dB at 1000 Hz were measured with the pumps operating.

3.9 Recommendations

a. The acoustic environment in Skylab was not unlike that of earth living in that the crew was able to obtain "rest" periods from the higher level noise in the work area (MDA/STS). Future manned long term missions should address noise control in the early design stages. Consideration of absorption material and more efficient suppression of noisy equipment in confined spaces such as the AM and MDA/STS should be incorporated into future programs.

b. The intercom design must be improved to alleviate feedback problems and improve communications.

c. Sleep areas should be better isolated from the rest of the crew quarters in terms of noise and other extraneous disturbances.

d. Updated acoustic criteria should be defined, similar to that indicated in Figure 3.1.However, these criteria should be more detailed, and be broken down into sleep, work, normal communications intermittent, etc., criteria. In other words, one criteria cannot satisfactorily meet the requirements for all conditions, especially in a long-exposure orbital application.

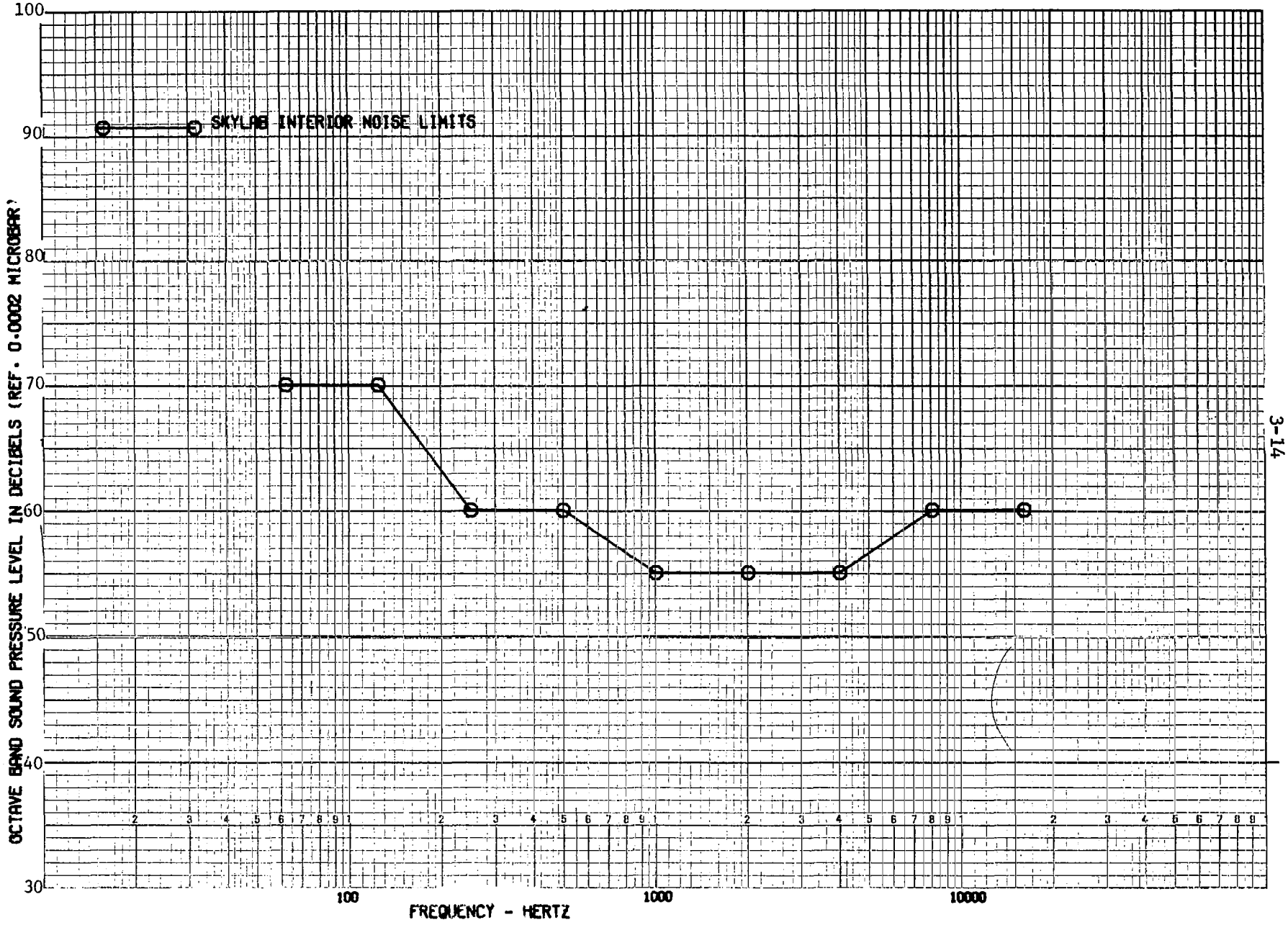

Figure 3.1 ACOUSTICAL NOISE LIMITS ACCEPTABLE FOR CONTINUOUS EXPOSURE

Table 3.1. Speech Interference Levels Due to Individual Noise Sources at 5.0 PSIA

Noise Source and Location	MDA/STS		AM		OWS	
	PSIL	MSIL	PSIL	MSIL	PSIL	MSIL
Fan Muffler Assemblies Located in MDA	52.2	52.5	49.0	49.2	32.2	32.4
Cabin Heat Exchanger Located in STS	52.2	48.0	49.0	44.7	32.3	27.9
Interconnect Fans Located in STS	46.0	43.4	42.8	40.1	26.1	23.3
Teleprinter (Print Speed) Located in STS	56.4	54.9	53.2	51.6	36.5	34.8
Mole Sieve Fans Located in STS	57.1*	54.7	53.8	51.4	37.2	34.6
Tape Recorder (Playback Mode) Located in STS	30.7	31.5	27.5	28.2	Not Avail.	Not Avail.
OWS Cooling Module Located in AM	44.0	40.7	50.5	47.3	33.8	30.5
Refrigeration System Located in OWS	31.4	28.5	37.8	31.9	45.1	42.5
Focal Collector Located in OWS	29.7	26.5	36.1	33.1	43.5	40.5

* Exceeds noise criteria of PSIL = 56.7 dB or MSIL = 56.25 dB

Table 3.1 (continued)

Noise Source and Location	MDA/STS		AM		OWS	
	PSIL	MSIL	PSIL	MSIL	PSIL	MSIL
Odor Fan Located in OWS	19.9	18.4	26.3	25.0	33.6	32.4
Suit Drying Station Located in OWS	26.2	24.6	32.6	31.2	40.0	38.6
Portable Fans (3) Located in OWS	30.3	29.6	44.1	42.9	44.1	43.6
Ergometer Located in OWS	51.1	47.0	57.5*	53.7	64.8*	61.0*
M509 Thrusters Located in OWS	80.5*	84.7*	86.9*	90.8*	94.3*	98.2*
T020 Thrusters Located in OWS	67.7*	71.9*	74.2*	78.6*	81.5*	86.0*

* Exceeds noise criteria of PSIL = 56.7 dB or MSIL = 56.25 dB

Table 3.2 Skylab Equipment and Experiment List

A. Command & Service Module

1. SPS Engine
2. Running Lights (8 places)
3. Scimitar Antenna
4. Docking Light
5. Pitch Control Engines
6. Crew Hatch
7. Pitch Control Engines
8. Rendezvous Window
9. EVA Hand Holds
10. EVA Light
11. Side Window
12. Roll Engines (2 places)
13. EPS Radiator Panels (6 places)
14. SM RCS Module (4 places)
15. ECS Radiator

B. Multiple Docking Adapter

1. Docking Target
2. Experiment M512 Facility
3. ECS Duct to Port 5
4. Vacuum Vent Panel
5. Frame Electrical Umbilical
6. Spare Fan Container
7. Spare Light Container
8. Film Vault No. 1
9. ECS Duct
10. Experiment S082A Cannister
11. Flight Data File
12. Speaker Intercom
13. ATM C&D Console
14. Film Vault No. 4
15. Film Vault No. 3
16. Experiment S009 Support Structure
17. DA Truss Motor (AM)
18. Area Fan (2 places)
19. Film Vault No. 2
20. DA Structure (AM)
21. CO_2 Absorbers and Shims
22. Docking Port No. 3
23. Experiment S065
24. Experiment S101 Resupply
25. Experiment S101
26. Running Light (4 places)
27. External Duct
28. Vacuum Vent Connection for Experiment M512

C. Airlock Module

1. Windows (4 places)
2. Molecular Sieves (2 places)
3. Discone Antennas (2 places)
4. Thermal Blanket
5. O_2 Tanks (6 places)
6. Cabin Press. Relief Valve
7. Suit Storage
8. Bio-Med Cable
9. Suit Storage
10. Undefined Storage Vol.
11. Camera Equip. Storage
12. STS C&D Panel
13. 70MM Film Storage
14. Forward Airlock Hatch
15. Tape Recorder
16. Spare Pressure Control Unit
17. EVA/IVA Umbilicals
18. AFT Compartment Control Panel
19. Heat Exchangers
20. Light Assy.
21. AFT Airlock Hatch
22. Lock Compartment EVA Panels
23. Running Lights (4 places)
24. N_2 Tanks (5 places)
25. EVA/IVA Umbilicals
26. O_2/N_2 Panel
27. Suit Cooling Module
28. Permanent Storage

D. Instrument Unit

None

E. Orbital Workshop

1. OWS Hatch
2. VCS Mixing Chamber & Filter
3. VCS Duct
4. Storage Lockers
5. VCS Duct
6. Thermal Shield
7. O_2 Press. Supply Line
8. Meteoroid Shield
9. Water Containers (10 places)
10. Food Storage (2 places)
11. Storage Lockers
12. O_2 Press. Regulators for H_2O Supply
13. Sleep Restraints
14. Intercom Box
15. Storage Lockers Front & Back
16. Sleep Restraint
17. Sleep Restraint
18. Experiment M131 Equip. Stowage Container
19. Storage Locker
20. Privacy Curtain
21. Experiment M131 Rotating Chair Control Console
22. Storage Locker
23. Drying Area
24. Trash Disposal Airlock
25. TV Outlet
26. Utility Outlets
27. Food Heater
28. Proposed Window
29. Intercom Box
30. Storage Lockers
31. Solar Array Assy.
32. Storage Cabinets
33. Ion Source Shield
34. Utility Outlet
35. Refrig./Freezer
36. Fire Extinguisher
37. Food, Water Heater & Chiller Table
38. Gravity Work Bench
39. Ergometer
40. Gas Analyzer
41. Intercom Box
42. Helmet Box
43. Experiment Support System
44. Lower Body Negative Press. Device
45. OWS Control & Display Console
46. Intercom Box
47. Rotating Chair
48. VCS Duct
49. Crotch Area
50. Meteoroid Shield
51. Thermal Shield
52. Running Light (4 places)
53. Waste Storage Tank
54. APCS Thrusters
55. Meteoroid Shield
56. Trash Disposal Separation Screen
57. APCS GN_2 Spheres (15 places)
58. Running Light (4 places)
59. Solar Array Panels
60. Acquisition Light
61. Interior Light
62. Food Storage Freezer
63. Limb Motion Sensor Assy. Container
64. Microbiological Specimen Freezer
65. Body Mass Measurement Device
66. Force Measuring Unit
67. Proposed VCS Duct
68. Spares Container
69. Astro Aids Container
70. Interior Lights
71. Scientific Airlock
72. Data System
73. Force Measuring Unit
74. VCS Fan Cluster
75. Food Container
76. Intercom Box
77. Suit Container
78. Emergency Access
79. UV Stellar Astronomy Container
80. N_2 Tanks (3 places)

E. Orbital Workshop (Continued)

81. Force Measuring Unit
82. Interior Lights
83. Main Access
84. Heat Filter Fan
85. Emergency Access
86. Portable Water Bottle
87. Interior Lights
88. VCS Fan Cluster
89. Food Container
90. Food Container
91. Coronagraph Container (Experiment T025)
92. Scientific Airlock
93. UV X-Ray SOL-Photo (Experiment S020)
94. Sample Array System Container
95. Water Microbiological Control Equip.
96. Utility Outlet
97. Photometer System Container (Experiment T027)
98. Foot Controlled Maneuvering Unit (Experiment T020)
99. Automatically Stabilized Maneuvering Unit (Experiment M509)
100. Intercom Box
101. Food Containers
102. Restraints Container (Experiment M508)
103. Work Task Board (Experiment M508)
104. Tools

F. Apollo Telescope Mount

1. Command Antenna
2. Telemetry Antenna
3. ATM Solar Array Wing No. 1
4. ATM Solar Array Wing No. 2
5. ATM Solar Array Wing No. 3
6. Command Antenna
7. ATM Solar Array Wing No. 4
8. Telemetry Antenna
9. Charger Battery Regulator Module (6 places)
10. Control Moment Gyro (3 places)
11. ATM Rack
12. CMG Investor No. 3
13. Canister
14. AS&E Aperture Door (Experiment S054)
15. NRL-A Film Retrieval Door (Experiment S082A)
16. Hα-2 Aperture Door
17. NRL-B Aperture Door (Experiment S082B)
18. NRL-B Aperture Door (Experiment S082B)
19. NRL-A Aperture Door (Experiment S082A)
20. HCO-A Aperture Door (Experiment S055A)
21. Fine Sun Sensor Aperture Door
22. Acquisition Sun Sensors
23. Hα-1 Aperture Door
24. HAO Aperture Door (Experiment S052)
25. GSFC Aperture Door (Experiment S056)

Table 3.3 Experiment ERD's Reviewed

EXPERIMENT NUMBER	DESCRIPTION
T020*	Foot Controlled Maneuvering Unit
T003	Inflight Aerosol Analysis
T027	Contamination Measurement
T013	Crew Vehicle Disturbances
T018	Precision Orbital Tracking
M512	Materials Processing in Space
M479	Zero Gravity Flammability
M074*	Specimen Mass Measurements
M131*	Human Vestibular Function
M133*	Sleep Monitoring Experiment
M151	Time and Motion Study
M172*	Body Mass Measurement
M113	Blood Volume and Red Cell Life Span
M111	Cytogenetic Studies of Blood
M112	Man's Immunity - Inviro Aspects
M114	Red Blood Cells
M091	Pre-and Post-Flight LBNP
M071	Mineral Balance
M073	Bioassay of Body Fluids
M093	Vectorcardiogram
M171*	Metabolic Activity
D021	Expandable Airlock Technology
D024	Thermal Control Coatings
S009	Nuclear Emulsion
S019	UV Stellar Astronomy (End Item Spec.)
S063	UV Airglow Horizon Photography
M092*	Inflight LBNP
M509*	Astronaut Maneuvering Equipment
S150	Galactic X-Ray Mapping
S149	Particle Collection
S020	X-Ray/UV Solar Photography
S190	Multispectral Photographic Facility
S191	Infrared Spectrometer
S192	10 Band Multispectral Sources
S193	Microwave Radiometer
T025	Coronagraph Contamination Measurement
ESS	Experiment Support System
EREP	Earth Resources Experiment
EXT TV	External Television
M415	Thermal Control Coatings
M487	Habitability/Crew Quarters
Proton Spec	Proton Spec
S073	Gegenschein/Zodiacal Light
S183	Ultra Violet Panorama
S194	L-Band Radiometer
S195	Earth Terrain Camera
T002	Manual Navigations Sightings

*Experiments Having Identified Noise Sources

Table 3.4 - Noise Sources Located in MDA

Noise Source	Number of Noise Sources	Location Shown in Figure	Frequency of Operation	Sound Power Level Estimates
MDA Fan Muffler Assembly	3	3.2,3.3	Continuous	Table 3.7
S009 Experiment: Nuclear Emulsion	1	3.3	Intermittent	N/A
Portable Vacuum Cleaner *	1	---	Intermittent	Table 3.11
S190 Experiment: Multispectral Photographic Facility	1	3.2	Intermittent	N/A
S191 Experiment: Infrared Spectrometer	1	3.2	Intermittent	N/A
S192 Experiment: 10 Band Multispectral Sources	1	3.3	Intermittent	N/A

* operates in AM/STS and OWS also

Table 3.5 - Noise Sources Located in AM/STS

Noise Source	Number of Noise Sources	Location Shown in Figure	Frequency of Operation	Sound Power Level Estimates
OWS Cooling Module	1 (4 fans)	3.5	Continuous	Table 3.10
Cabin Heat Exchanger (CHEM)	1	3.2,3.5	Continuous	Table 3.9
Interconnect Duct Fan/Muffler	1	3.3,3.4	Continuous	Table 3.9
Condensing Heat Exchanger Module	2	------	Continuous	Table 3.8
Teleprinter	1	3.3,3.4	Intermittent	Table 3.8
Tape Recorder	1	3.5	Intermittent	Table 3.8
Portable Vacuum Cleaner *	1	-----	Intermittent	Table 3.11

* portable vacuum cleaner also operates in MDA and OWS

Table 3.6 - Noise Sources Located in OWS

Noise Source	Number of Noise Sources	Location Shown in Figure	Frequency of Operation	Sound Power Level Estimates
Ventilation Control System (VCS) Fan Cluster	3	3.6,3.7,3.8	Continuous	Table 3.11
Refrigeration System	2	3.8,3.10	Continuous	Table 3.11
Portable Fans	3	---	Continuous or Intermittent	Table 3.11
Odor Fan	1	3.6,3.8	Intermittent	Table 3.11
Fecal Collector	1	3.6,3.10	Intermittent	Table 3.11
Suit Drying Station	2	3.7,3.8	Intermittent	Table 3.11
Portable Vacuum Cleaner *	1	---	Intermittent	Table 3.11
Experiment M509: Nozzles-Astronaut Maneuvering Unit	1	3.6,3.7	Intermittent	Table 3.12
Experiment T020: Nozzles-Foot Controlled Maneuvering Unit	1	3.6,3.7	Intermittent	Table 3.13
Experiment M171: Ergometer	1	3.6,3.9	Intermittent	Table 3.10

* portable vacuum cleaner may be operated in AM/STS and MDA

Table 3.6 - Noise Sources Located in OWS (continued)

Noise Source	Number of Noise Sources	Location Shown in Figure	Frequency of Operation	Sound Power Level Estimates
Experiment M131: Revolving Chair	1	3.6,3.9	Intermittent	N/A
Experiment M074: Specimen Mass Measurements	1	3.6,3.10	Intermittent	N/A
Experiment M172: Body Mass Measurements	1	3.8	Intermittent	N/A

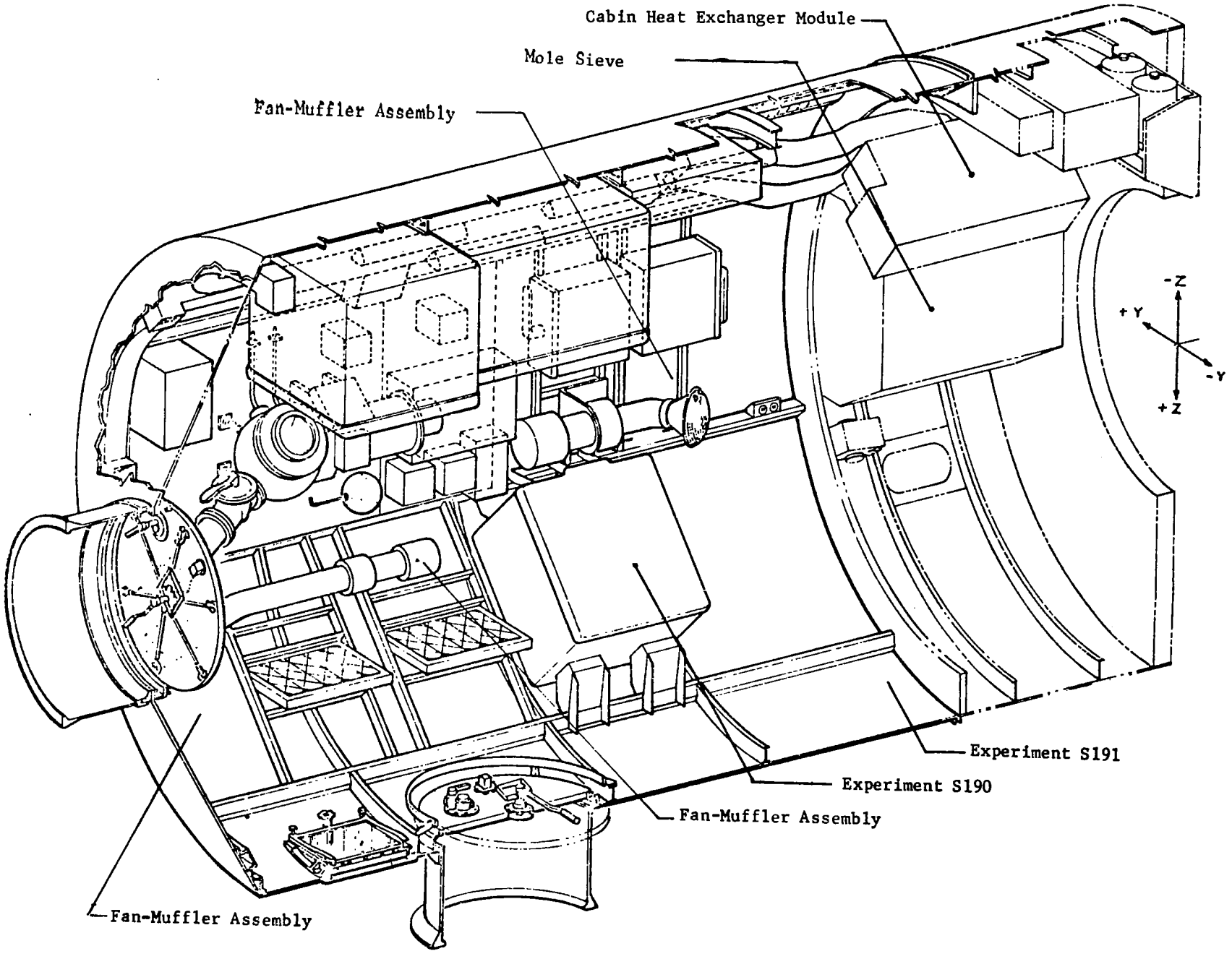

Figure 3.2 Location of MDA and STS Noise Sources

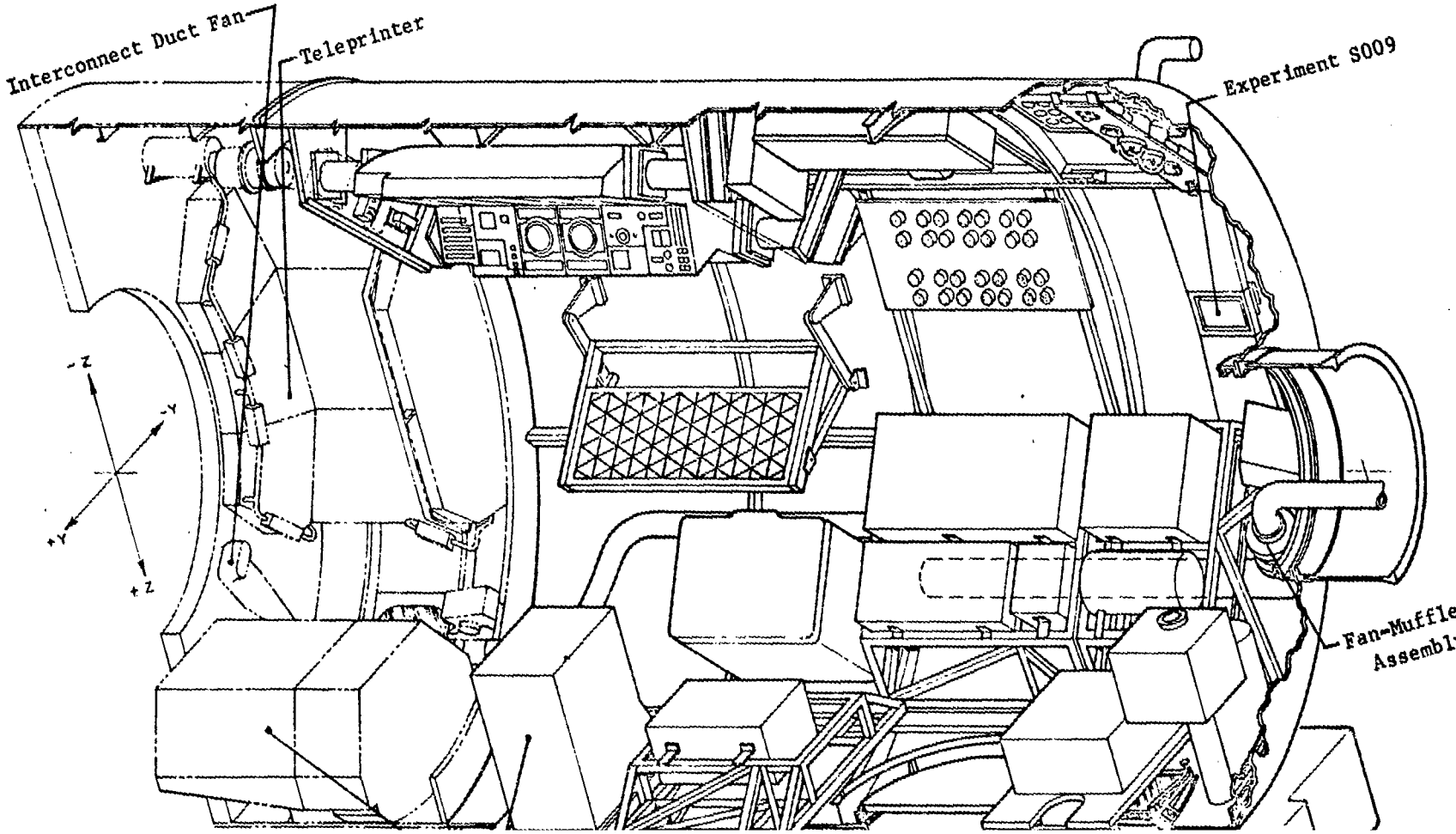
Interconnect Duct Fan
Teleprinter
Experiment S009
Fan-Muffler Assembly
-Z
-Y
+Y
+Z

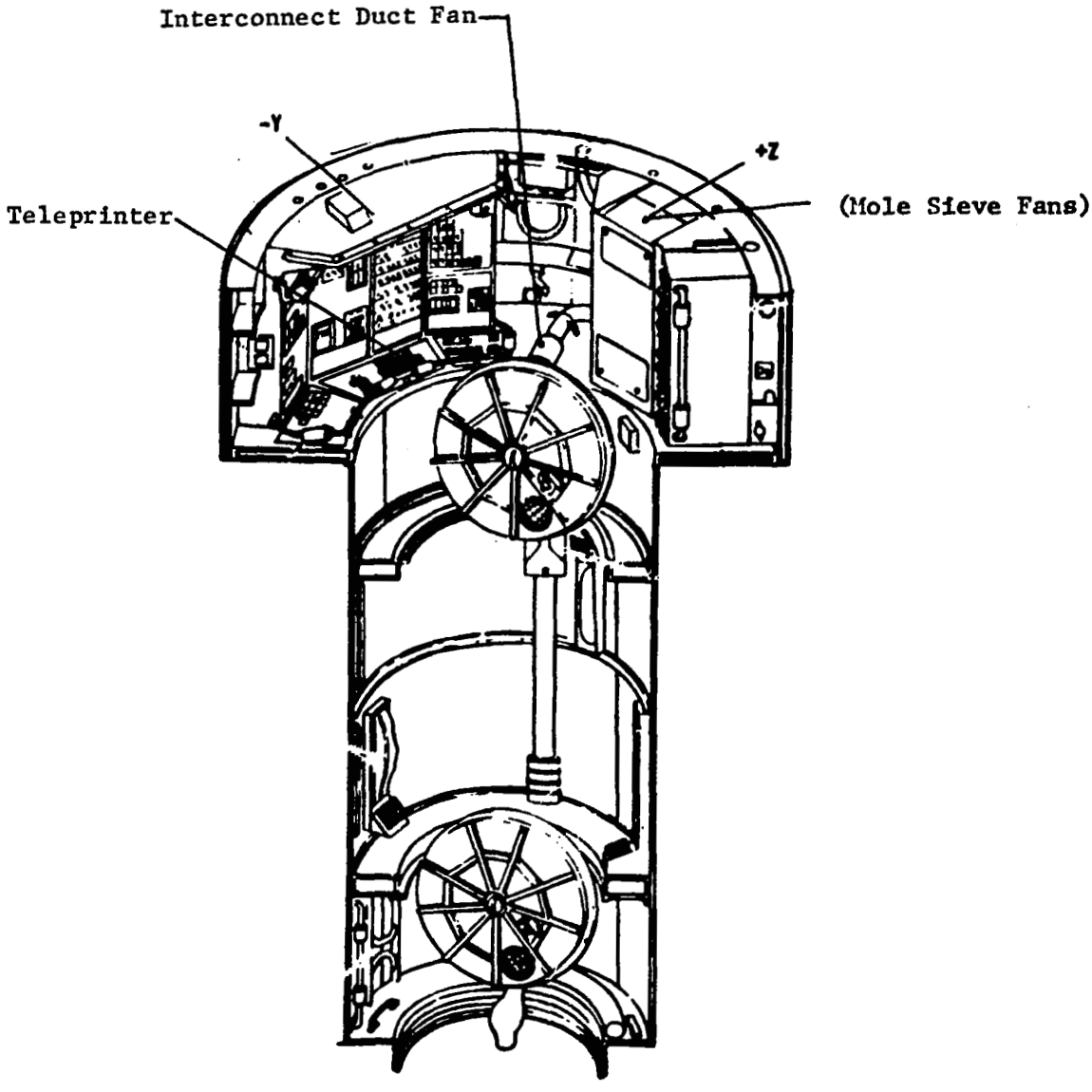

Figure 3.4 Location of AM/STS Noise Sources

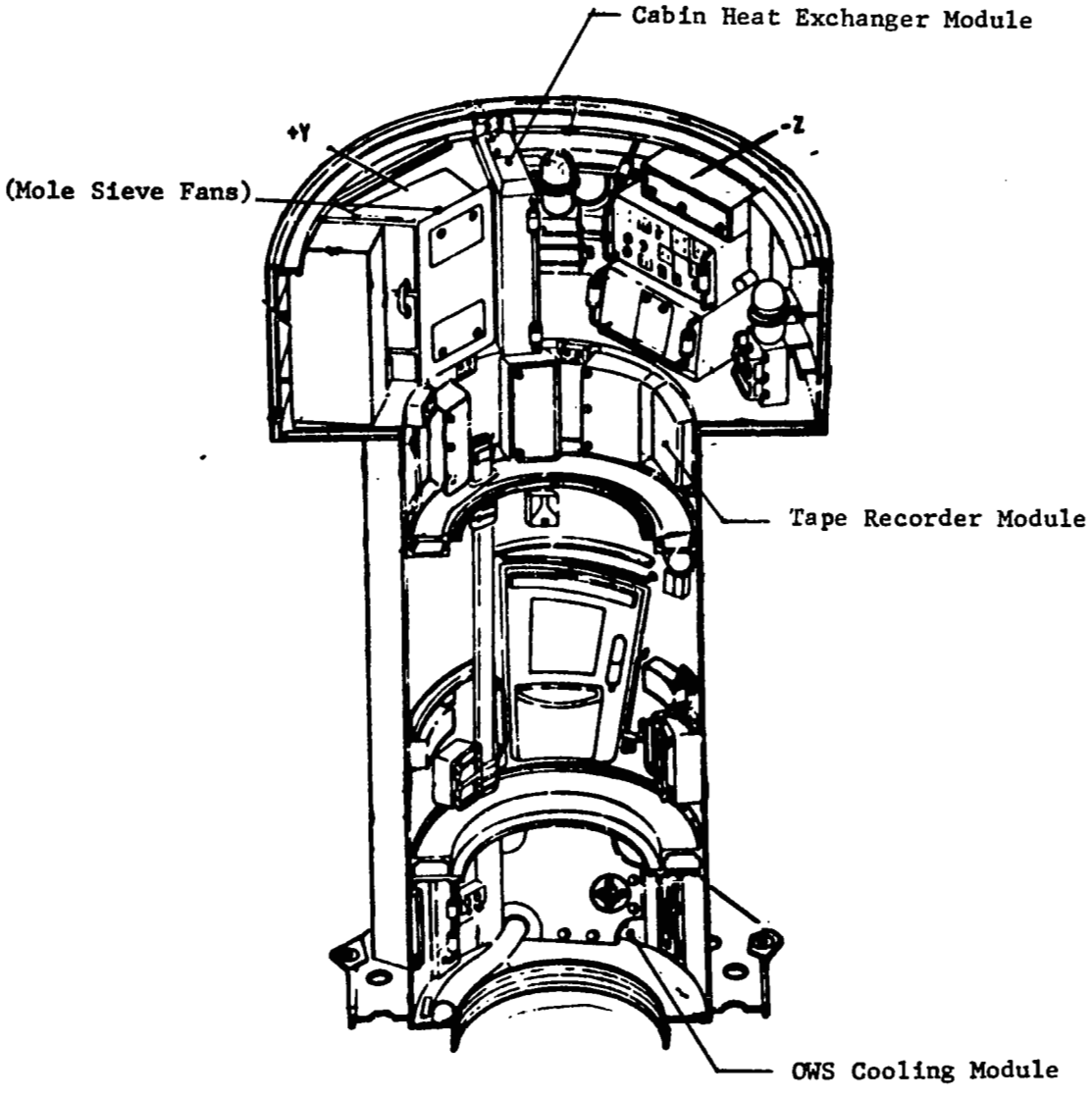

Figure 3.5 Location of AM/STS Noise Sources

SATURN WORKSHOP

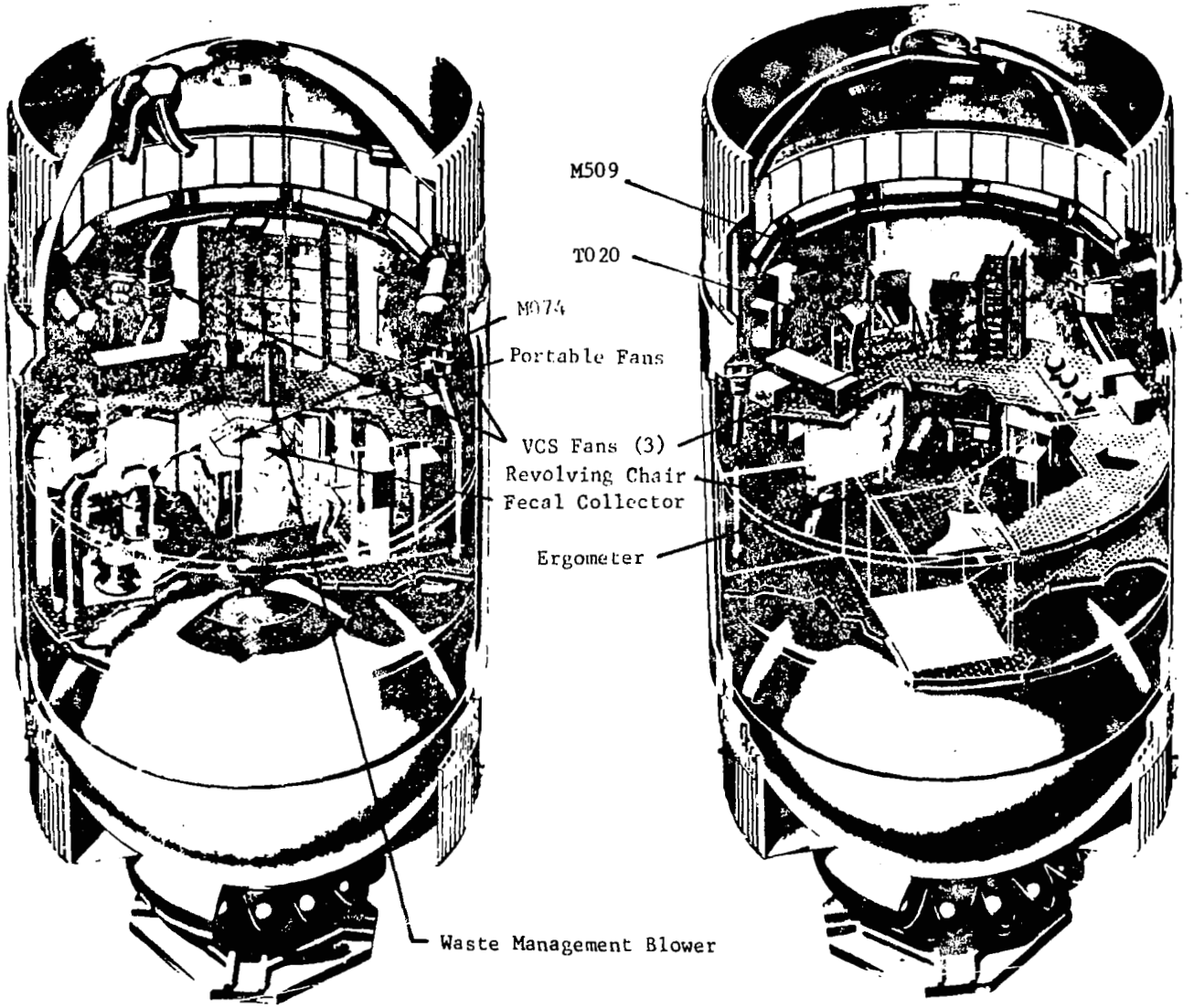

Figure 3.6 Location of OWS Noise Sources

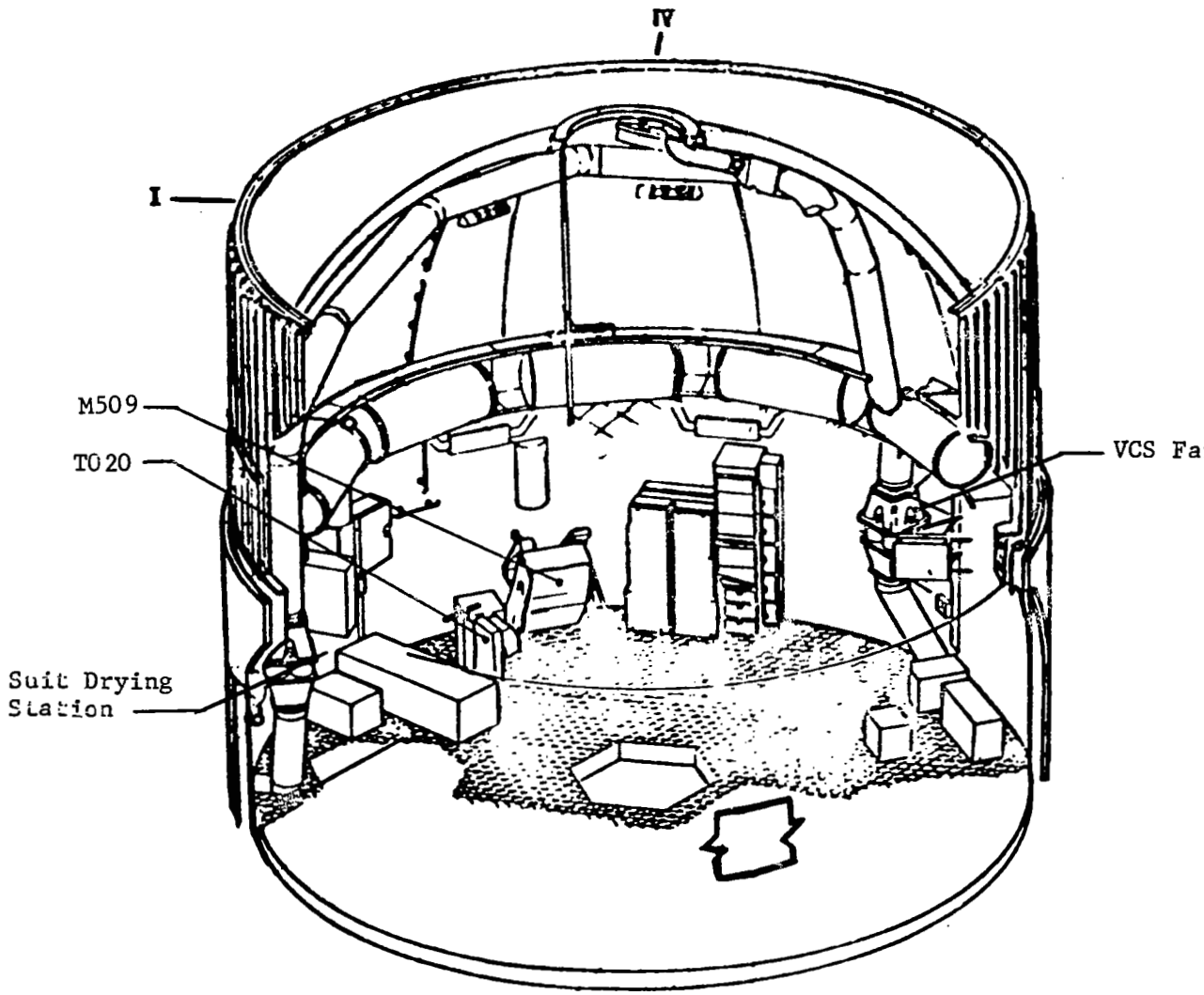

Figure 3.7 Location of Noise Sources in OWS Forward Compartment

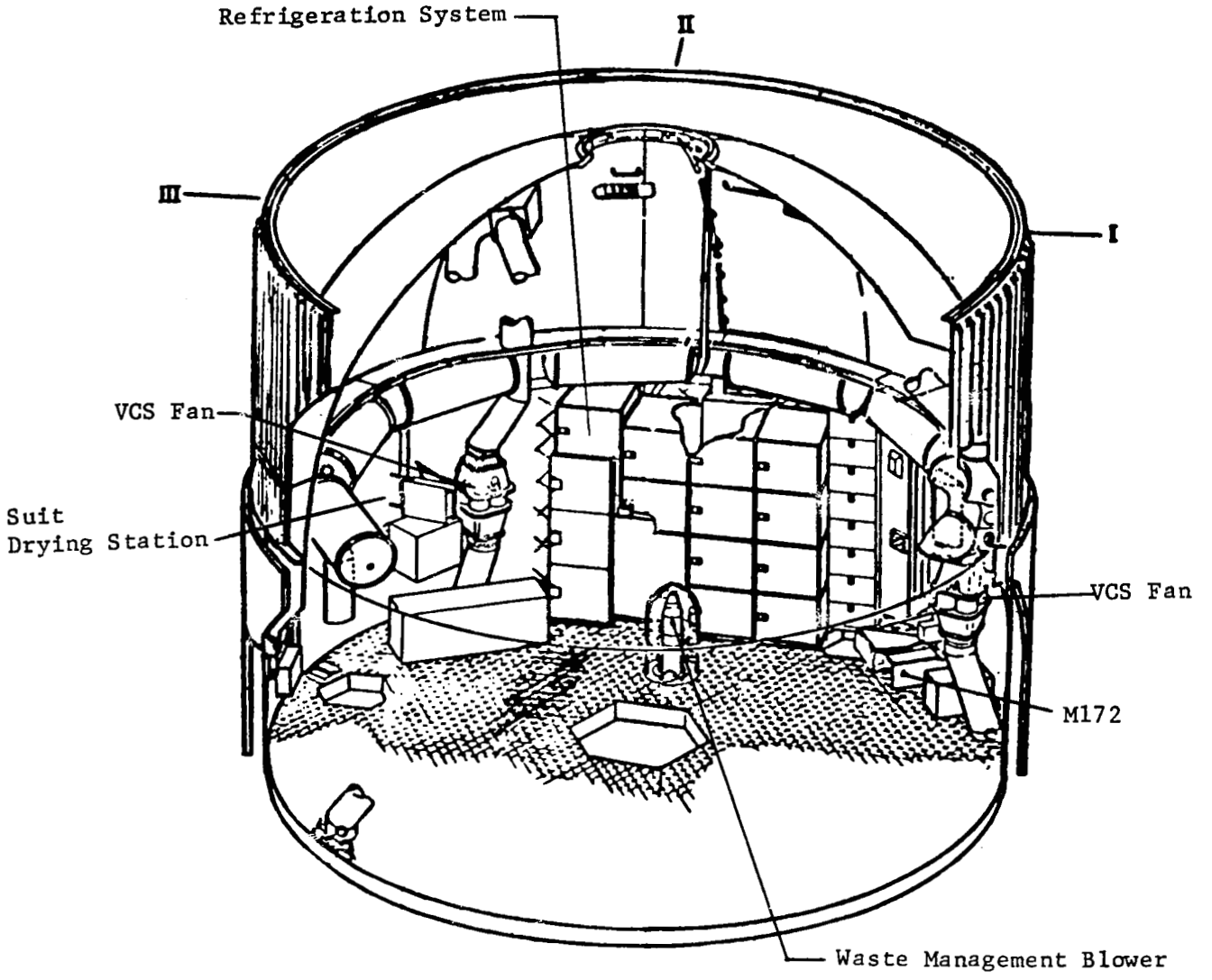

Figure 3.8 Location of Noise Sources in OWS Forward Compartment

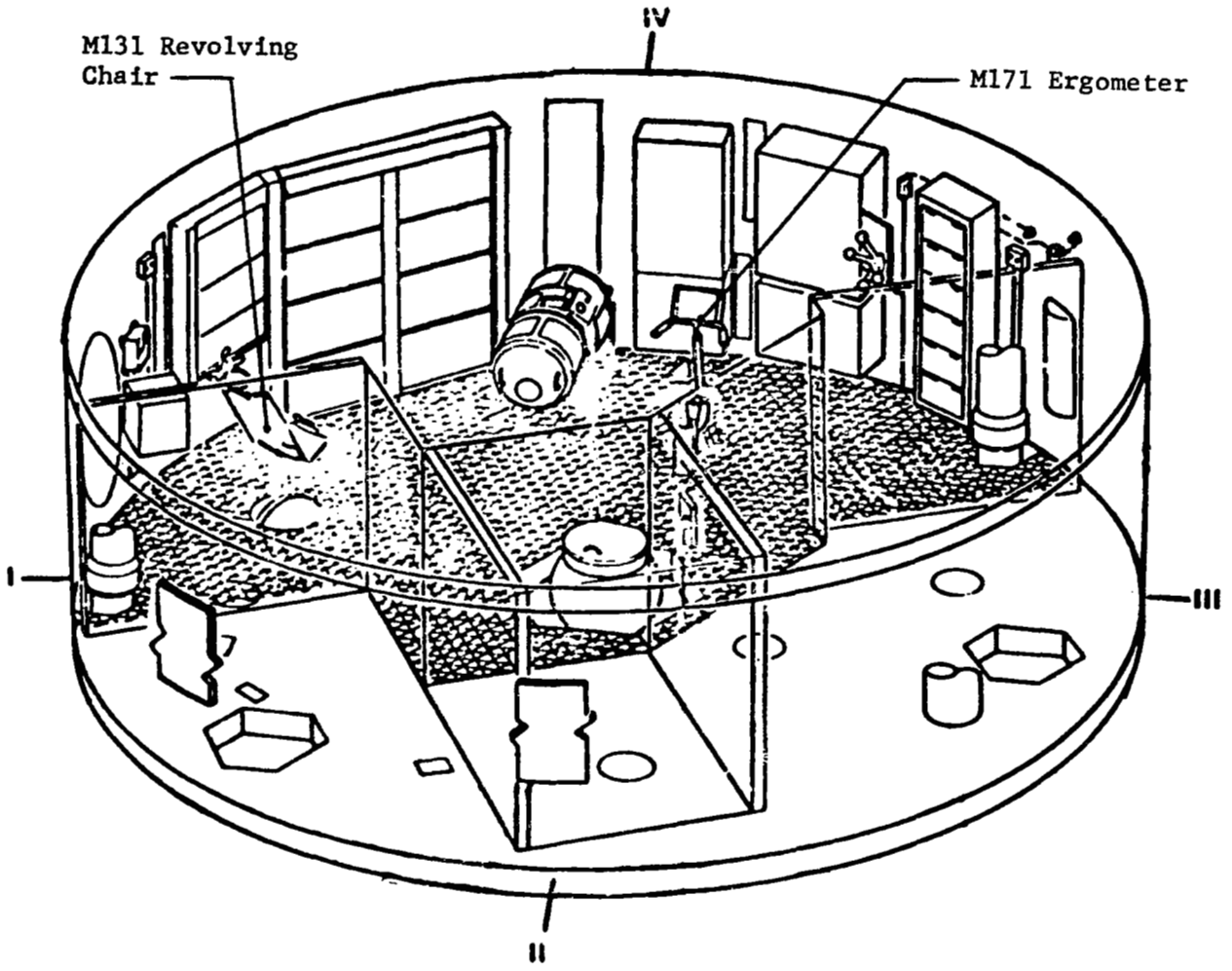

Figure 3.9 Location of Noise Sources in Experiment Compartment

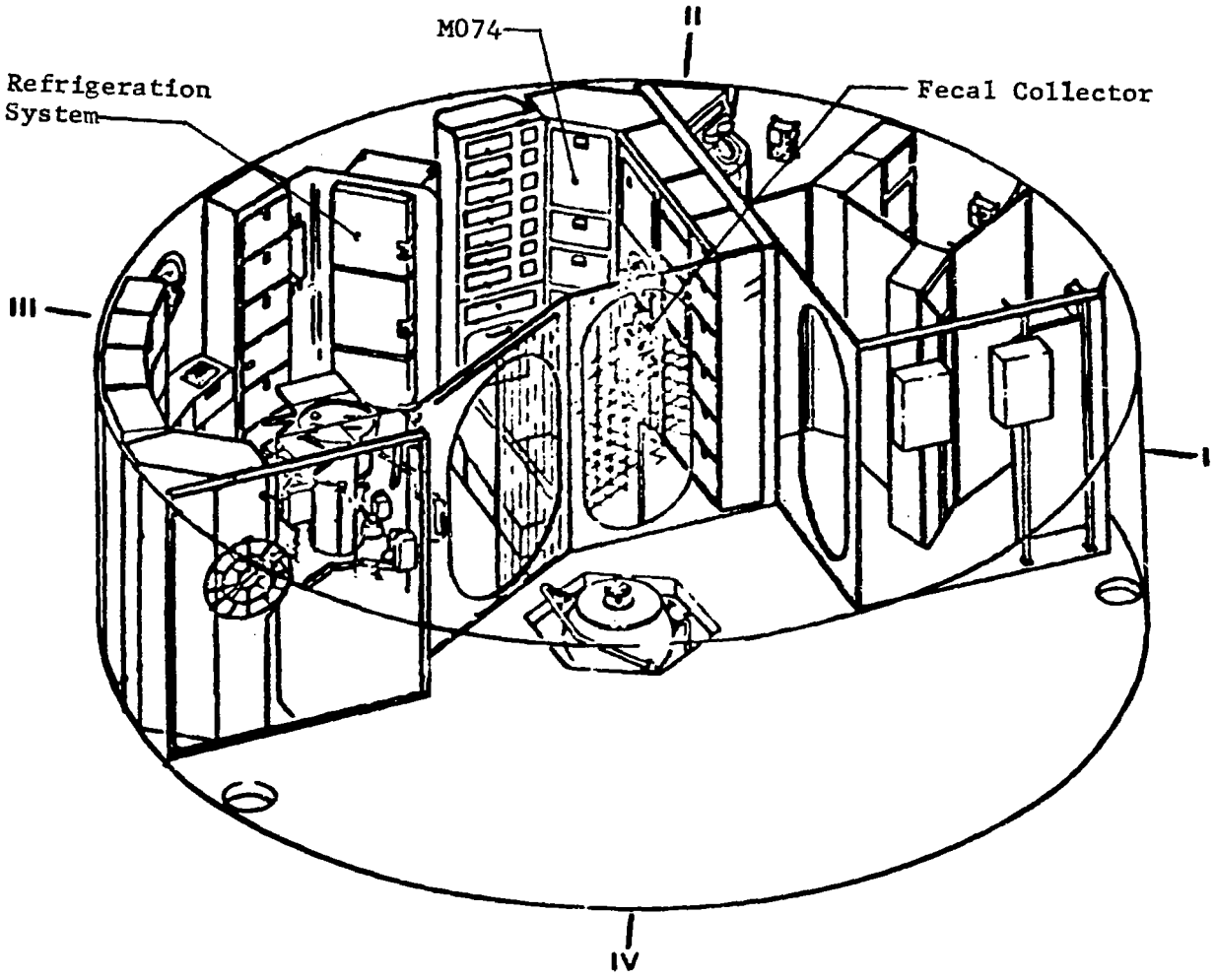

Figure 3.10 Location of Noise Sources in OWS Wardroom Compartment

Table 3.7 **MDA Noise Source Power Levels**

OCTAVE BAND FREQUENCY (HERTZ)	FAN MUFFLER ASSEMBLY CRITERIA (3 FANS) PWL (DB)
62.5	64.8
125	69.8
250	74.8
500	69.8
1000	69.8
2000	72.8
4000	72.8
8000	69.8

Table 3.8 **MDA/STS Noise Source Power Levels**
14.7 PSIA Atmosphere

OCTAVE BAND FREQUENCY (HERTZ)	TELEPRINTER		CABIN HEAT EXCHANGER MODULE	
	PRINT SPEED (dB)	SLEW SPEED (dB)	ONE FAN (dB)	3 FANS (dB)
125	53.6	45.4	59.1	63.9
250	52.8	65.8	68.4	73.1
500	78.1	85.4	70.3	75.0
1000	78.3	86.0	68.5	73.3
2000	77.0	85.3	67.2	72.0
4000	76.5	84.2	56.1	60.9
8000	72.5	80.2	51.5	56.3

OCTAVE BAND FREQUENCY (HERTZ)	CONDENSING HEAT EXCHANGER	TAPE RECORDER	
	12.1 VOLT MODE (dB)	PLAYBACK MODE (dB)	RECORD MODE (dB)
125	--	41.4	42.2
250	(82.3)	47.9	46.2
500	76.5	50.7	40.0
1000	79.5	51.5	44.9
2000	76.6	46.2	44.6
4000	73.7	53.4	53.0
8000	75.7	51.7	50.5

Table 3.9 **MDA/STS Noise Source Power Levels**
5.0 PSIA Atmosphere

OCTAVE BAND FREQUENCY (HERTZ)	TELEPRINTER		CABIN HEAT EXCHANGER MODULE		INTERCONNECT DUCT FAN
	PRINT SPEED (dB)	SLEW SPEED (dB)	ONE FAN (dB)	THREE FANS (dB)	ONE FAN (dB)
125	49.3	--	64.3	69.0	
250	51.9	64.1	70.8	75.5	60.3
500	76.0	85.9	71.7	76.5	65.7
1000	75.7	84.3	68.5	73.2	66.4
2000	73.8	80.9	58.4	63.2	62.1
4000	69.9	76.8	50.0	54.8	55.1
8000	65.0	73.3	45.0	49.8	53.7

OCTAVE BAND FREQUENCY (HERTZ)	CONDENSING HEAT EXCHANGER	TAPE RECORDER	
	12.1 VOLT MODE (dB)	PLAYBACK MODE (dB)	RECORD MODE (dB)
125	--	41.4	42.2
250	70.2	47.9	46.2
500	72.5	50.7	40.0
1000	75.4	51.5	44.9
2000	70.5	46.2	44.6
4000	64.0	53.4	53.0
8000	69.7	51.7	50.5

Table 3.10 **AM Noise Source Power Levels in Decibels**

OCTAVE BAND FREQUENCY (HERTZ)	OWS COOLING MODULE (4 FANS)	
	14.7 PSIA	5.0 PSIA
125	60.5	--
250	70.0	72.7
500	66.3	67.7
1000	67.5	67.5
2000	64.7	62.8
4000	60.7	53.7
8000	55.3	48.2

Table 3.11 OWS Noise Source Power Levels (PWL's)
14.7 PSIA Atmosphere

OCTAVE BAND FREQUENCY (HERTZ)	PORTABLE FANS		*ODOR FAN	FECAL COLLECTOR BLWR, +1 SEPARATOR	VCS FAN CLUSTERS	
	1 FAN (dB)	3 FANS (dB)	(dB)	(dB)	1 CLUSTER (dB)	3 CLUSTERS (dB)
63	65.7	70.5	67.0	64.0	68.2	73.0
125	62.7	67.5	65.0	67.0	70.7	75.5
250	65.7	70.5	67.0	67.0	73.2	78.0
500	67.2	72.0	64.0	69.0	70.7	75.5
1000	65.2	70.0	58.5	76.0	66.2	71.0
2000	60.2	65.0	53.0	60.0	58.7	63.5
4000	62.7	67.5	54.0	57.0	55.2	60.0
8000	52.7	57.5	52.0	50.0	52.2	57.0

OCTAVE BAND FREQUENCY (HERTZ)	REFRIG. SYSTEM (dB)	SUIT DRYING STATION (dB)	PORTABLE VACUUM CLEANER (dB)	*SHOWER (PLUS UNKNOWNS) (dB)	M171 ERGOMETER (dB)
63	64.0	---	---	72.6	---
125	54.0	54.5	(72.0)	72.0	86.3
250	53.0	69.0	81.0	81.0	92.6
500	66.0	67.0	80.0	80.0	93.4
1000	55.0	69.5	77.0	87.0	93.1
2000	53.0	58.0	72.0	86.0	82.6
4000	44.0	60.0	72.0	83.4	75.1
8000	46.0	55.5	69.0	73.0	69.4

Table 3.12 **Experiment M509 Nozzles Sound Power Levels at 5.0 PSIA Ambient Pressure**

OCTAVE BAND CENTER FREQUENCY, HERTZ	OCTAVE BAND SOUND POWER LEVEL, dB				
	4.3 POUNDS THRUST NOZZLE	2.35 POUNDS THRUST NOZZLE	2.15 POUNDS THRUST NOZZLE	1.25 POUNDS THRUST NOZZLE	MULTI-NOZZLE CONFIGURATION-15.8 POUND THRUST
125	(88)	(81.4)	(81)	----	(90.6)
250	97.5	90.4	90	83.7	100.1
500	107.4	99.8	99.4	92.9	109.8
1000	116.2	109.4	109.0	102.6	118.9
2000	125.9	118.6	118.2	111.8	128.4
4000	131.8	126.5	126.1	121.3	135.4
8000	136.5	131.6	131.2	127.1	140.4

Table 3.13 **Experiment T020 Nozzles Sound Power Levels**

OCTAVE BAND CENTER FREQUENCY, HZ	OCTAVE BAND SOUND POWER LEVEL, dB					
	5.0 PSIA AMBIENT PRESSURE			14.7 PSIA AMBIENT PRESSURE		
	1.3 POUNDS THRUST	1.0 POUNDS THRUST	0.3 POUNDS THRUST	1.3 POUNDS THRUST	1.0 POUNDS THRUST	0.3 POUNDS THRUST
250	83.7	81.9	67.9	70.0	68.8	59.9
500	93.8	92.9	78.9	82.6	82.0	69.0
1000	102.1	102.3	88.0	92.5	91.8	77.5
2000	113.0	112.9	99.2	102.5	102.1	89.4
4000	121.5	120.8	108.5	112.1	111.4	99.7
8000	128.7	127.8	117.8	120.0	120.0	110.0
16000	135.0	133.3	123.4	125.5	127.0	116.8
31500	140.1*	138.9*	131.1*	133.5*	133.5*	120.0*

*One-third octave band data at 40,000 Hertz was extrapolated and used in 31500 Hertz octave band estimate.

Table 3.14 **Equivalent A-Weighted Sound Levels Caused by Individual Noise Sources at 5.0 PSIA**

NOISE SOURCE	NOISE SOURCE LOCATION	EQUIVALENT A-WEIGHTED SOUND LEVEL dBA		
		MDA/STS	AM	OWS
MDA Fans (3)	MDA	59.7	56.4	39.4
Cabin Heat Exchanger Module (3 Fans)	STS	58.2	55.0	38.5
OWS Int. Conn. Duct Fan	STS	50.8	47.6	30.9
Mole Sieve Fans (2)	STS	62.7	59.4	42.7
Teleprinter (Print)	STS	61.3	58.0	41.3
Tape Recorder (Plybk)	STS	39.0	35.3	18.5
OWS Cooling Module (4 Fans)	AM	49.9	55.8	39.2
VCS Fan Clusters (3)	OWS	37.7	44.1	51.5
Refrigeration System	OWS	20.5	27.0	34.5
Portable Fans (3)	OWS	36.0	42.9	52.0
Odor Fan	OWS	26.4	32.9	40.3
Fecal Collector	OWS	38.5	44.6	51.9
Suit Drying Station	OWS	33.3	39.5	46.8
Portable Vacuum Cleaner	OWS	43.3	49.7	57.1
Shower	OWS	52.5	59.1	66.4
Ergometer	OWS	57.1	63.4	70.8
M509 Nozzles (15.8#)	OWS	102.0	108.4	115.8
T020 Nozzles (2.6#)	OWS	91.9	99.1	106.5

Note: The A-weighted sound level associated with the Skylab Interior Noise Limits is 64.5 dBA.

Table 3.15 Skylab Acoustical Compartment Characteristics

Compartment/Equip.	Volume
MDA	1159 ft^3
STS	301 ft^3
AM	293.5 ft^3
OWS	8000 ft^3
MDA/STS Equip.	160 ft^3
MDA/STS Total	1300 ft^3

Compartment/Equip.	Surface Area
MDA	549 ft^2
STS	175.9 ft^2
AM	217 ft^2
OWS	4895 ft^2
MDA/STS Equip.	600 ft^2

Compartment Interface	Common Wall Surface Area
STS/AM	23 ft^2
AM/OWS	8.9 ft^2

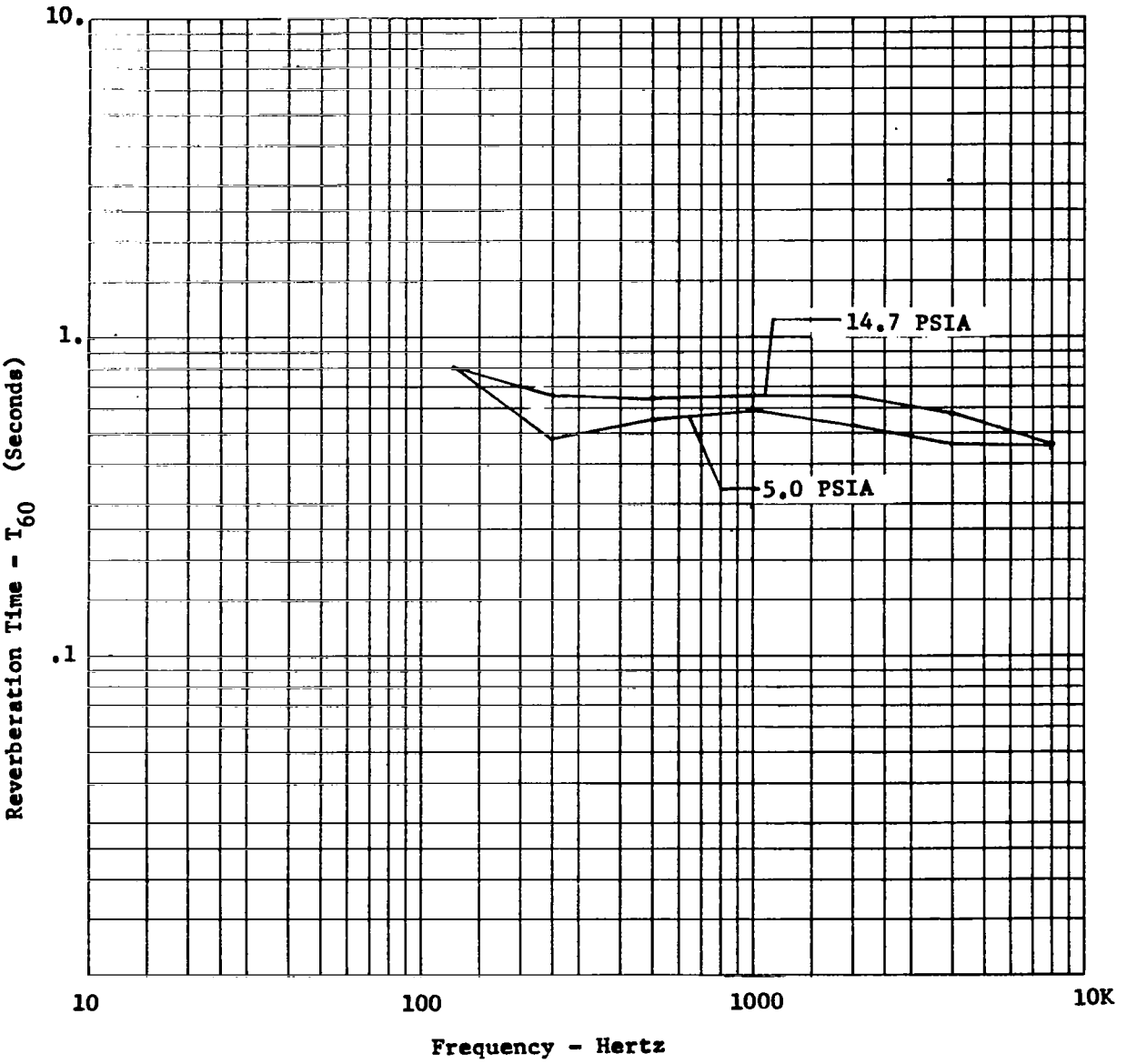

Figure 3.11 Estimated MDA/STS Reverberation Times at Atmospheric Pressures of 14.7 and 5.0 PSIA

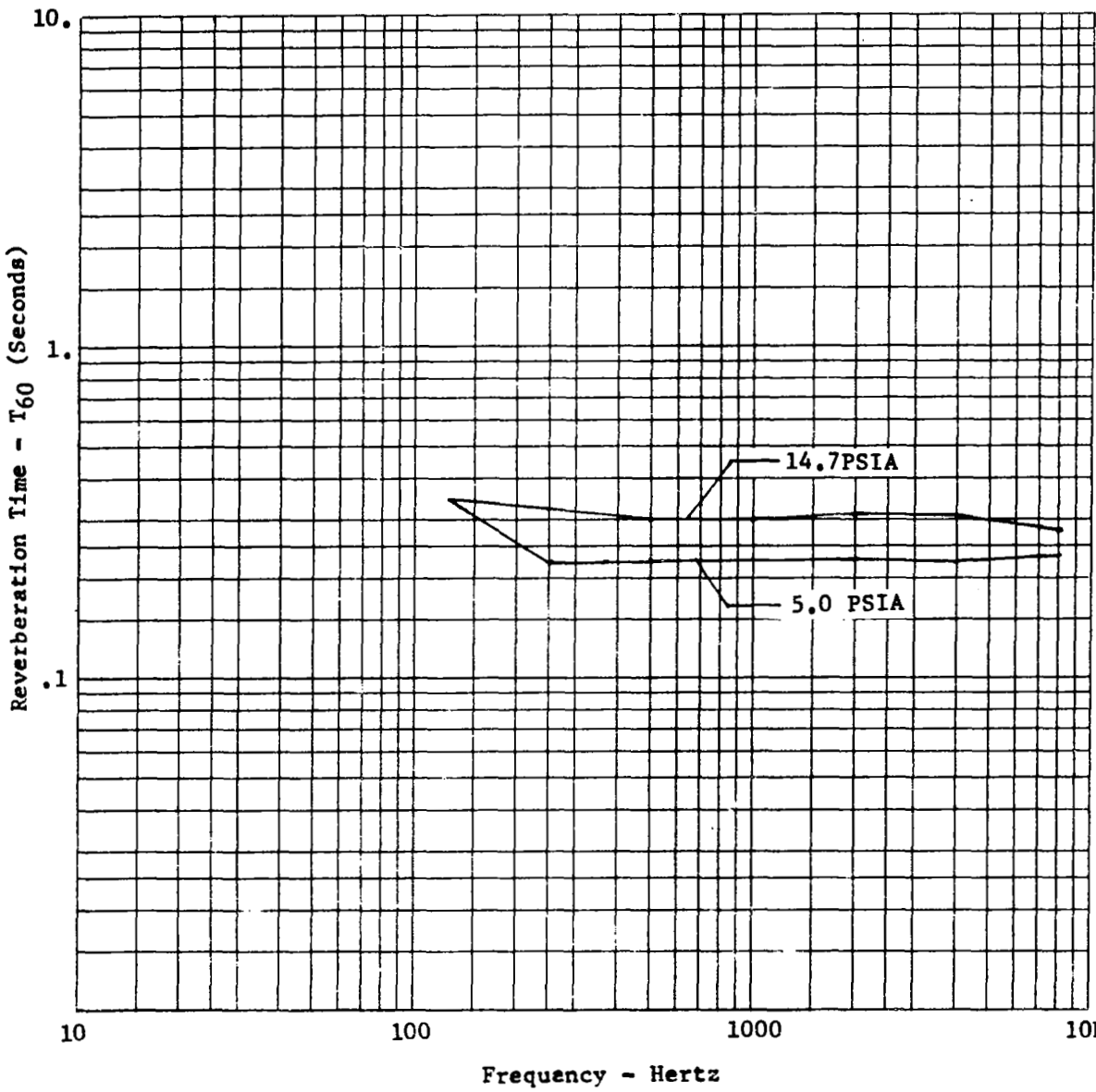

Figure 3.12 Estimated AM Reverberation Times at Atmospheric Pressures of 14.7 and 5.0 PSIA

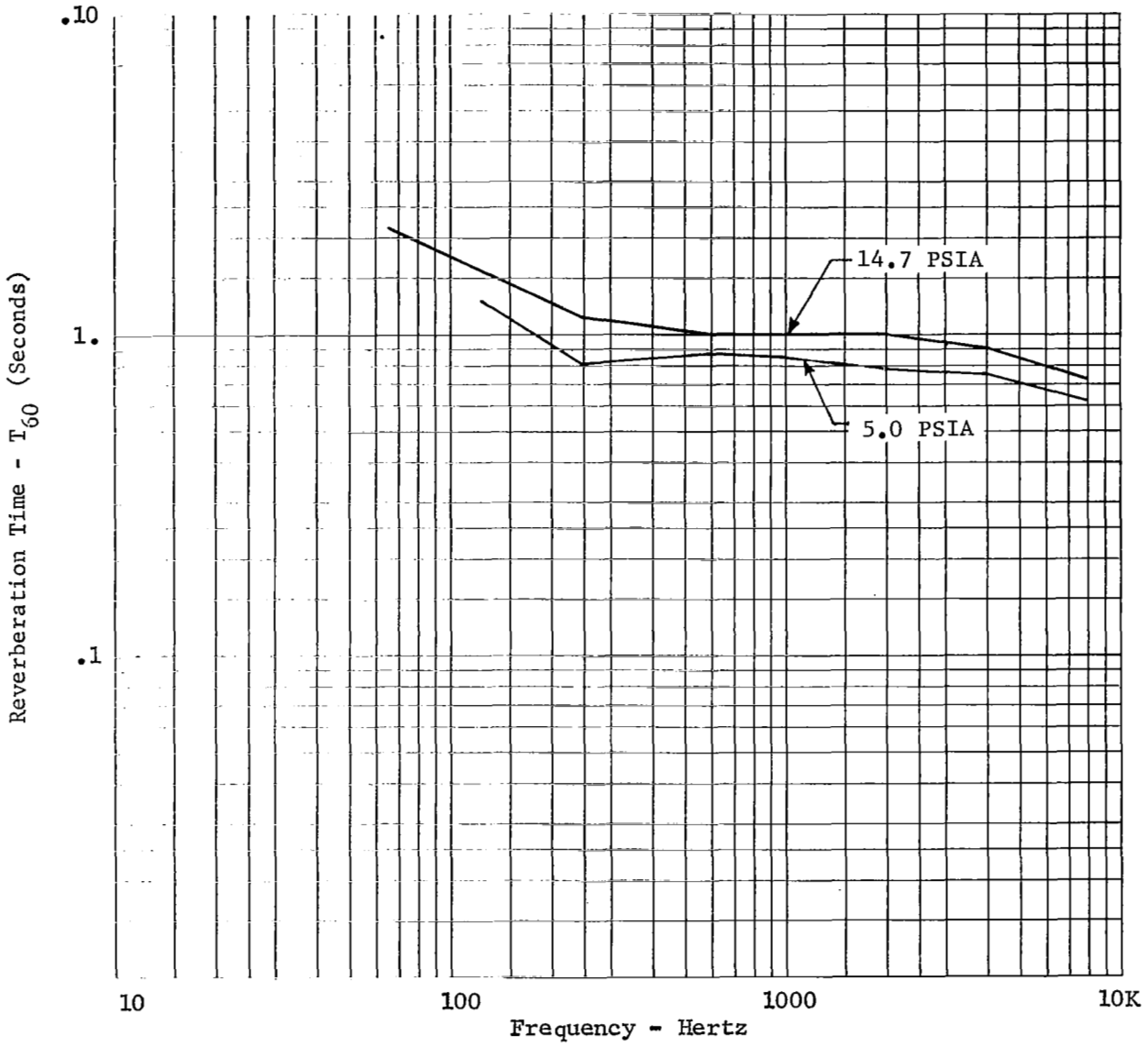

Figure 3.13 - Estimated OWS Reverberation Times at Atmospheric Pressure of 14.7 and 5.0 PSIA

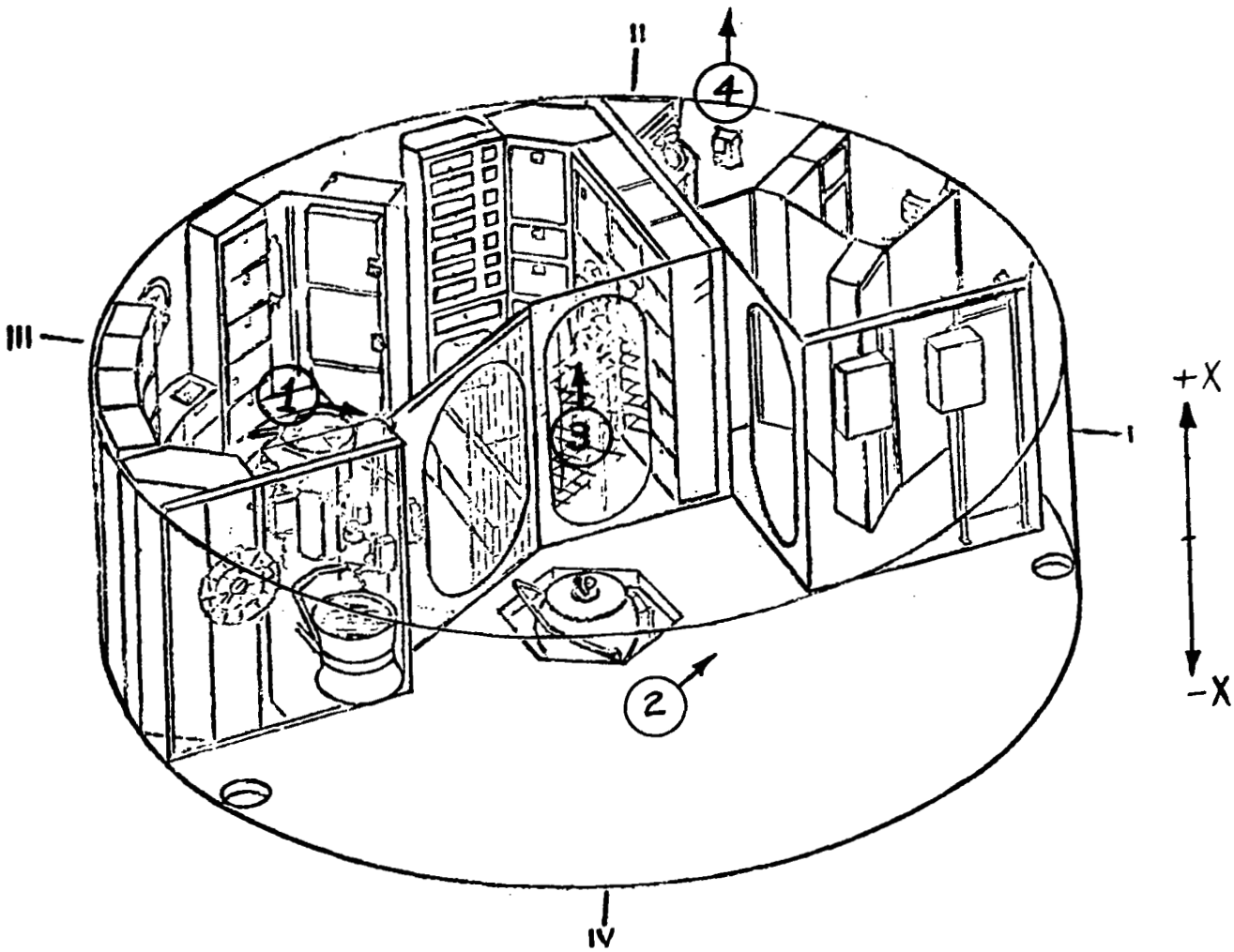

Figure 3.14 MEASUREMENT LOCATIONS IN THE OWS AFT COMPARTMENT

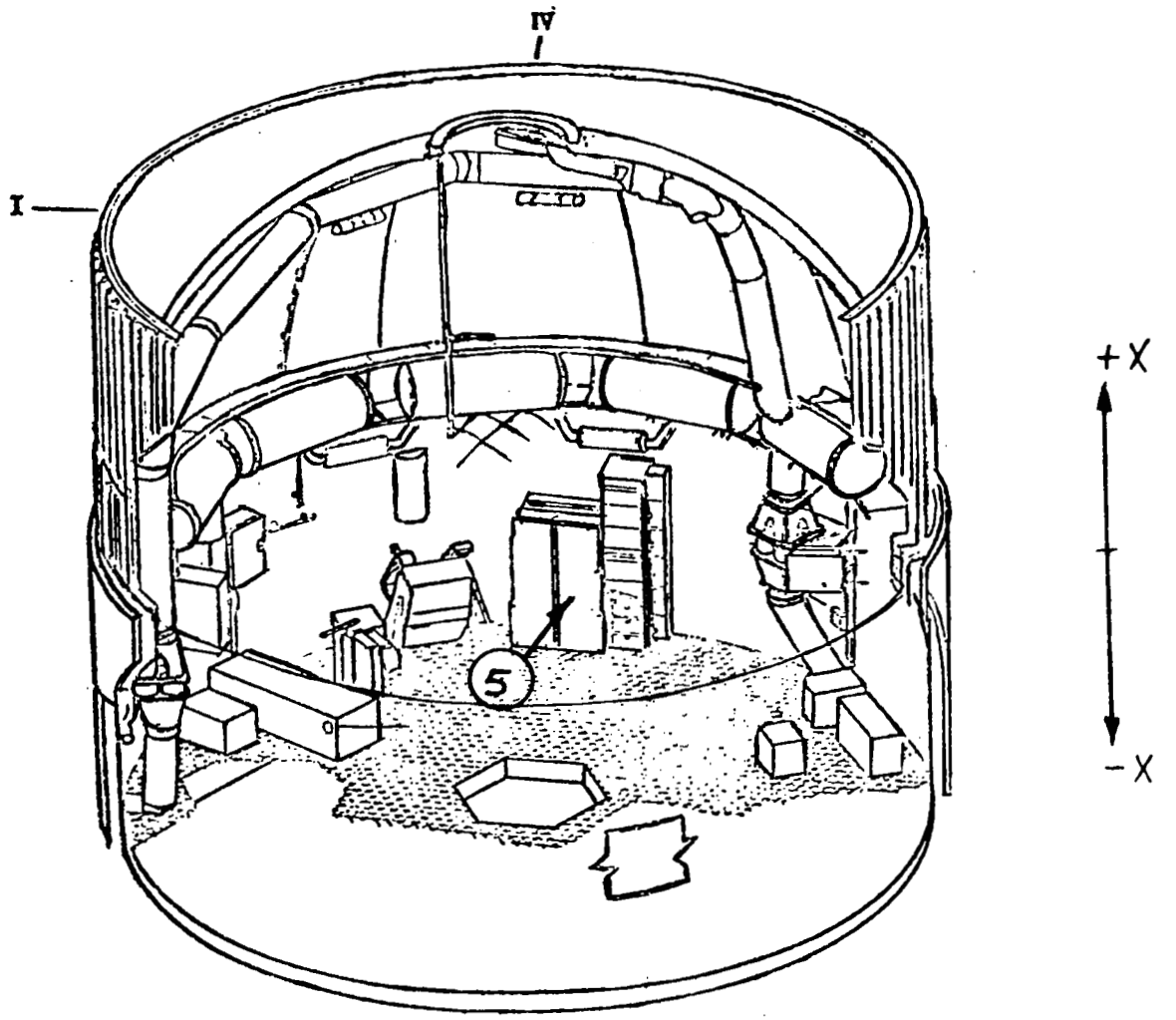

Figure 3.15 MEASUREMENT LOCATION IN THE OWS FORWARD COMPARTMENT

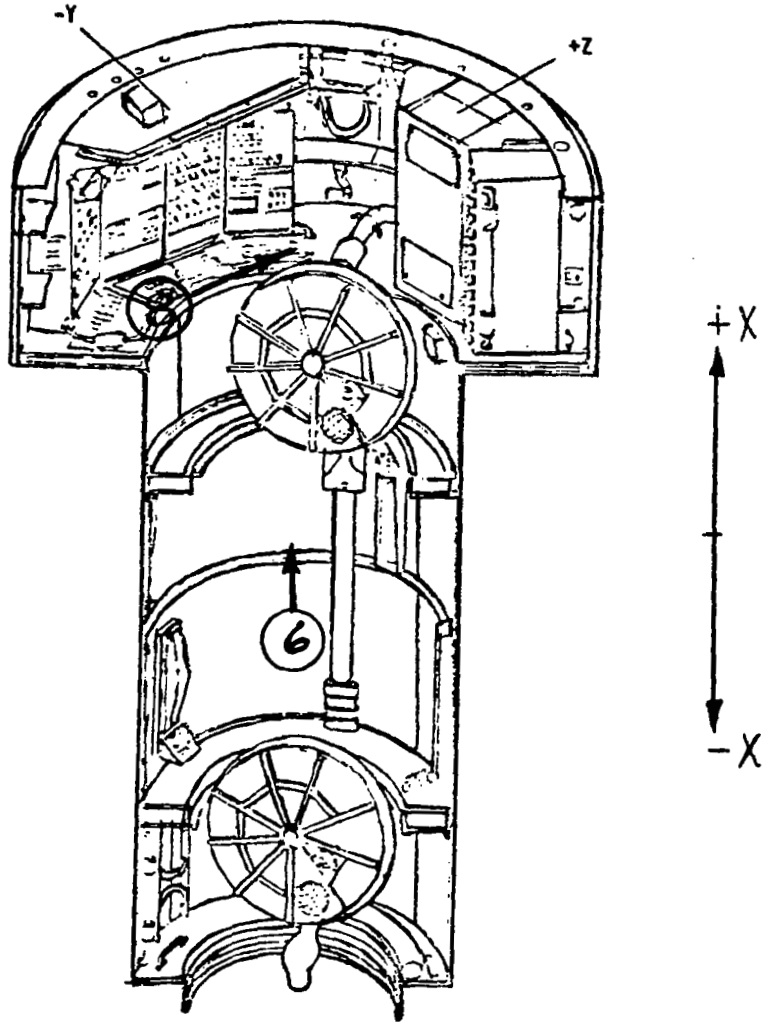

Figure 3.16 MEASUREMENT LOCATION IN THE STS/AM

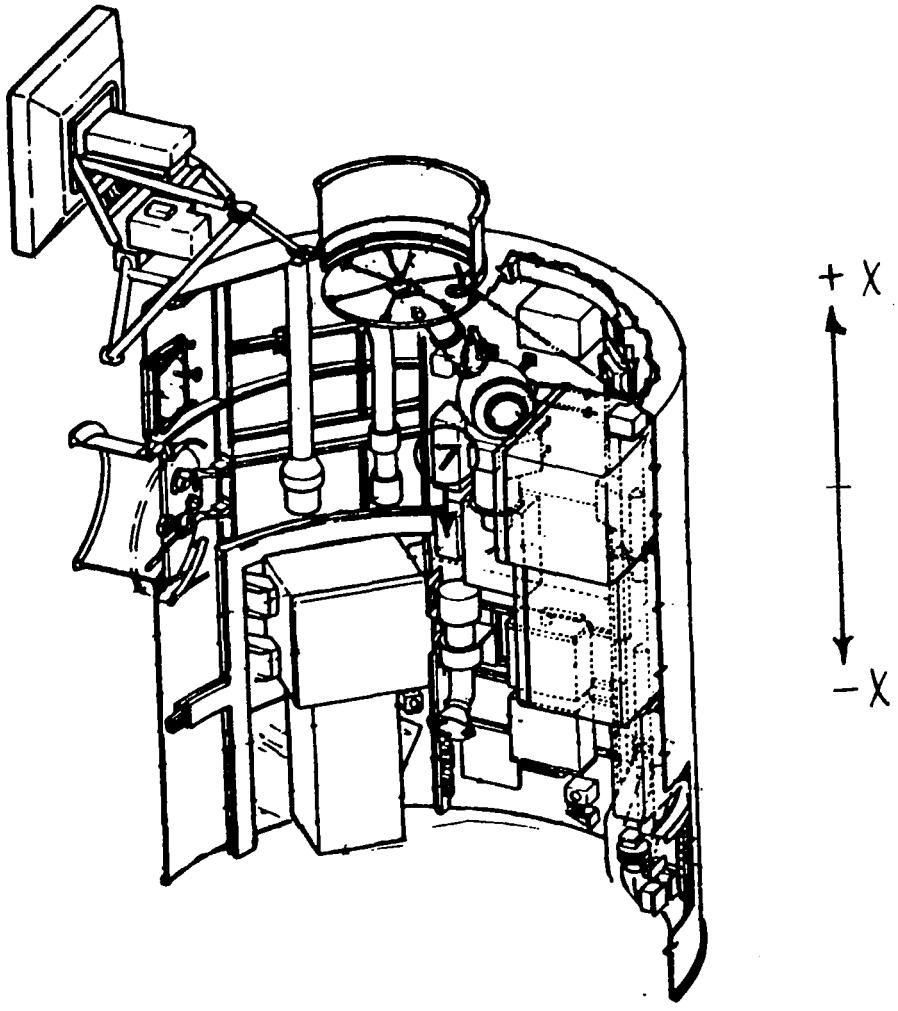

Figure 3.17 MEASUREMENT LOCATION IN THE MDA

Table 3.16 SKYLAB INTERIOR NOISE SOURCE SPL's MEASURED DURING SL-3 MISSION

Location/Description	Overall SPL in dBA		Overall SPL in dB (Calculated)	Octave Band Center Frequencies in Hertz							
				125	250	500	1000	2000	4000	8000	16000
	Meas'd.*	Calc.		(dB)	(dB)	(dB)	(dB)	(dB)	(dB)	(dB)	(dB)
MDA Rate Gyro	72.0	66.5	69.5	61.0	59.5	67.0	60.5	57.5	50.0	49.5	42.0
MDA Fan No. 1	66.0	58.3	62.2	58.0	56.0	55.0	54.0	51.0	45.0	41.0	29.0
MDA Fan No. 2	67.0	59.7	64.3	60.0	57.0	58.0	55.0	50.0	48.0	45.0	34.0
MDA CSM Fan	67.0	57.5	63.7	61.0	56.0	56.0	52.0	49.0	43.0	41.0	28.0
STS Circ. Fans	71.0	63.6	70.1	67.0	62.0	64.5	57.0	50.0	45.5	45.5	35.0
Mole Sieve Compressors	75.5	70.5	73.2	56.0	61.0	72.0	60.0	59.0	62.0	—	—
STS Panels	71.0	65.8	70.5	65.0	60.0	68.0	57.0	52.0	45.0	43.0	33.0
AM Duct Fan/Muffler	61.0	57.3	60.7	52.0	52.0	58.5	34.0	50.0	44.5	44.5	35.3
OWS Cool. Module (AM) (all 4 fans operating)	77.0	65.1	75.4	73.0	71.0	61.0	55.0	48.0	42.0	40.0	30.0
OWS Refrig. System	63.5	57.3	62.7	59.0	50.5	59.0	51.0	42.0	34.0	32.0	22.0
OWS VCS Duct Fans	56.5	49.0	52.5	45.0	46.0	48.0	45.0	39.0	29.0	32.0	24.0

* Data is questionable, since all values exceed calculated O.A. SPL's

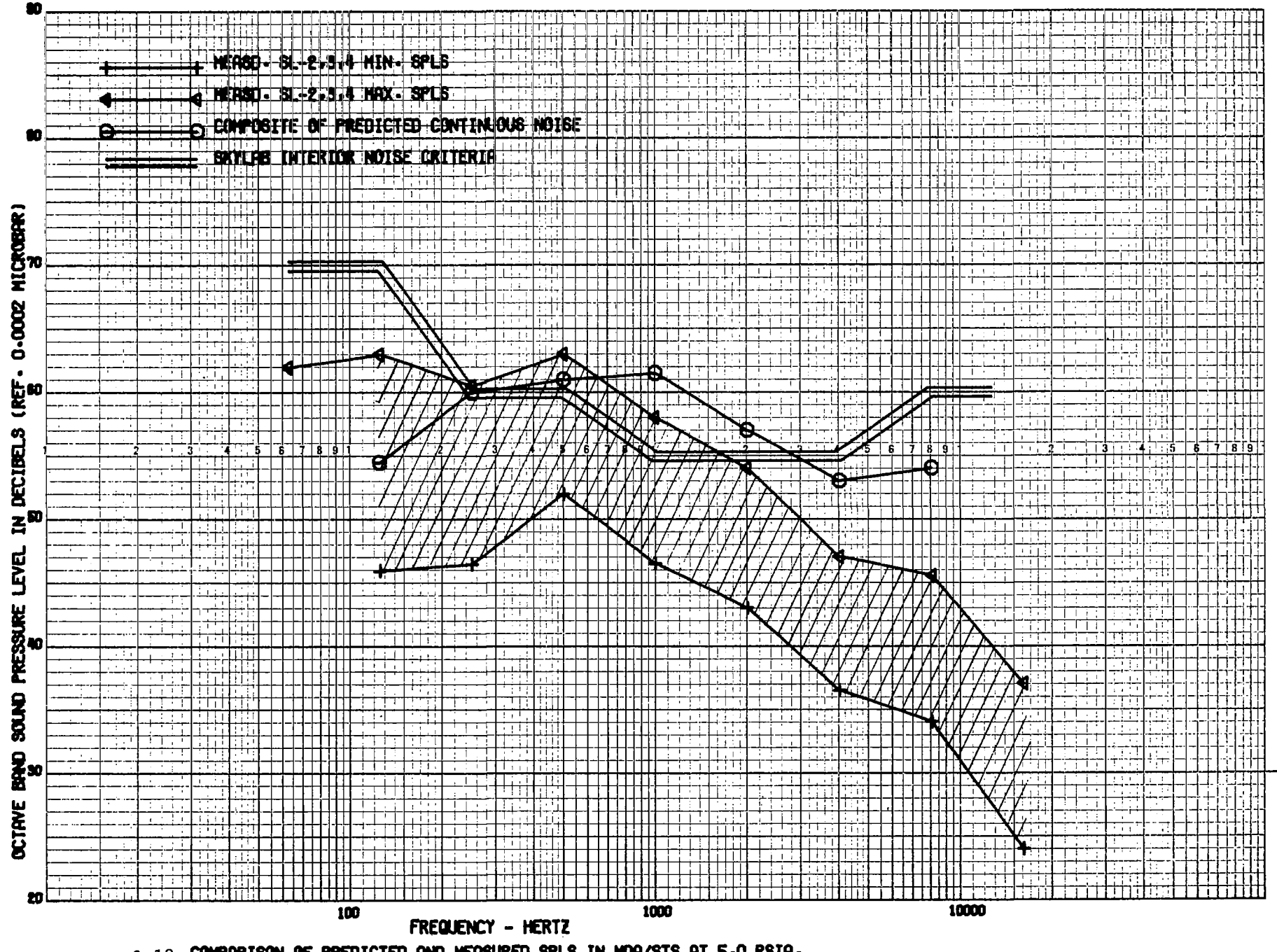

Figure 3.18 COMPARISON OF PREDICTED AND MEASURED SPLS IN MDA/STS AT 5.0 PSIA.

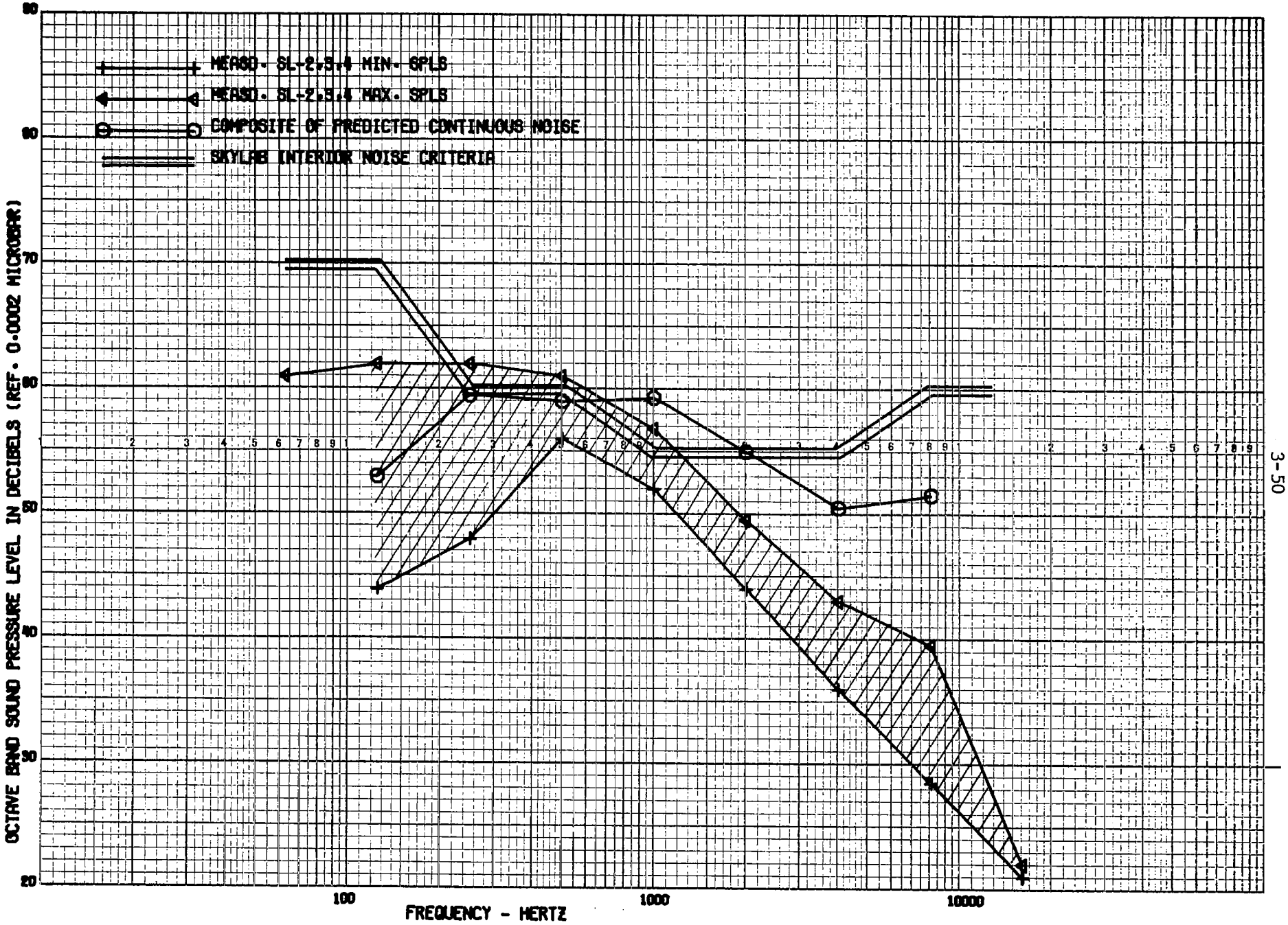

Figure 3.19 COMPARISON OF PREDICTED AND MEASURED SPLS IN AM AT 5.0 PSIA.

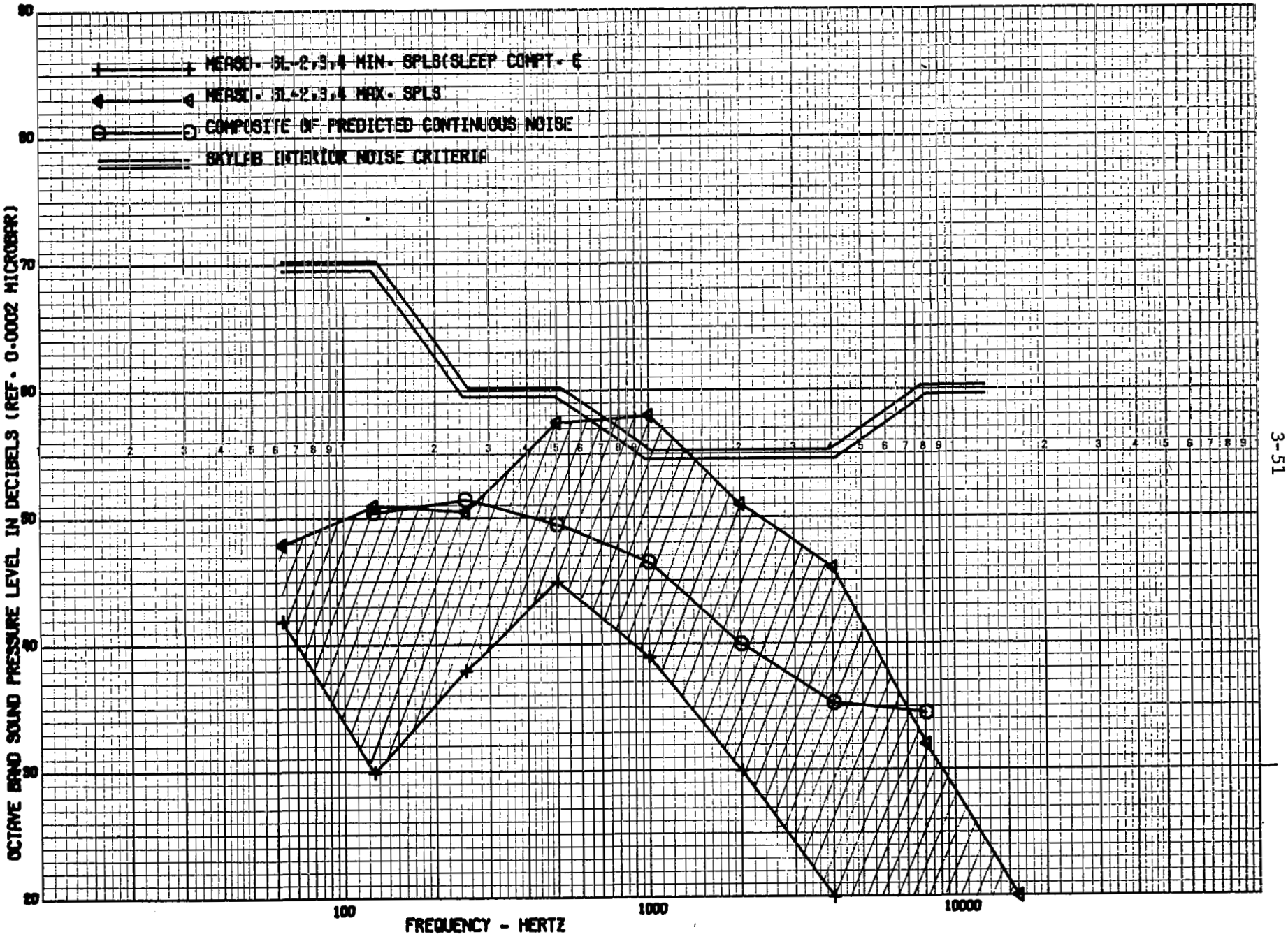

Figure 3.20 COMPARISON OF PREDICTED AND MEASURED SPLS IN OWS AT 5.0 PSIA.

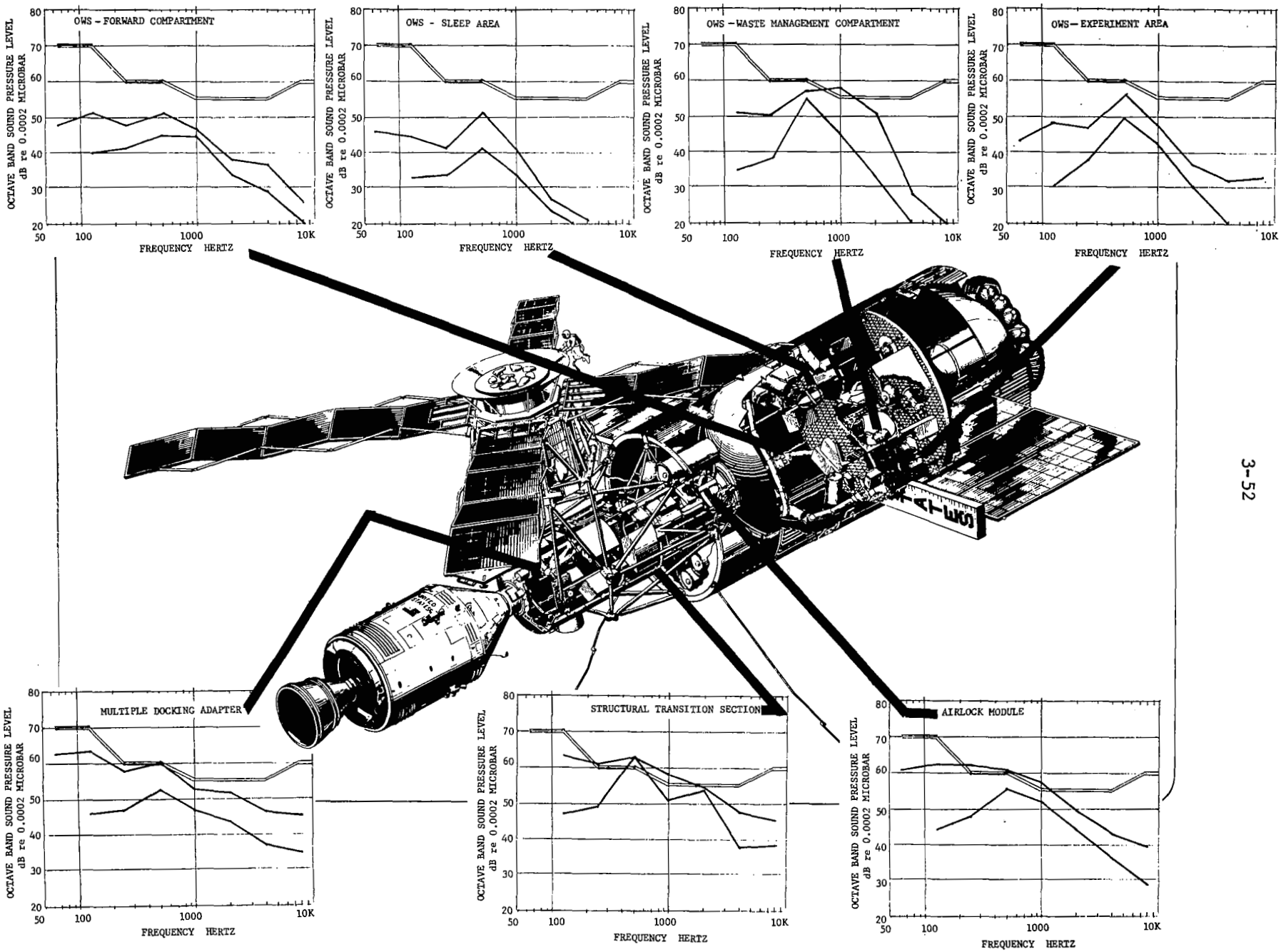

Figure 3.21 Comparison of Measured Acoustic Levels in Skylab.

Table 3.17 SPEECH INTERFERENCE LEVELS APPLICABLE TO SL-2, SL-3, AND SL-4 M-487 MEASURED FLIGHT DATA

Location	SL-2 (dB)	SL-3 (dB)	SL-4 (dB)	Noise Criteria (dB)
MDA	47.2	53.0	52.8	56.7
STS	55.8	58.3	--	56.7
AM	51.3	52.7	55.7	56.7
OWS Wdrm.	40.5	41.0	37.7	56.7
OWS Exp.	41.7	42.2	46.6	56.7
OWS WMC	43.8	55.5	--	56.7
OWS Sleep	38.3	34.3	33.0	56.7
OWS Fwd	40.7	44.5	44.0	56.7

Table 3.18 MODIFIED SPEECH INTERFERENCE LEVELS APPLICABLE TO SL-2, SL-3, AND SL-4 M-487 MEASURED FLIGHT DATA

Location	SL-2 (dB)	SL-3 (dB)	SL-4 (dB)	Noise Criteria (dB)
MDA	44.6	51.4	50.4	56.25
STS	51.3	55.5	--	56.25
AM	47.5	50.3	52.3	56.25
OWS Wdrm.	35.8	36.8	34.3	56.25
OWS Exp.	36.1	37.9	42.7	56.25
OWS WMC	37.9	48.4	--	56.25
OWS Sleep	33.3	31.0	28.6	56.25
OWS Fwd.	42.0	40.6	40.6	56.25

Table 3.19 SKYLAB INTERIOR SPL's MEASURED DURING COOLANT LOOP NOISE INVESTIGATION - SL-4.

Location/Description	Overall SPL in dBA		Overall SPL in dB (Calculated)	Octave Band Center Frequencies in Hertz							
				63	125	250	500	1000	2000	4000	8000
	Meas'd.	Calc.		(dB)	(dB)	(dB)	(dB)	(dB)	(dB)	(dB)	(dB)
ATM Pump On:											
Exp. Compt. (A)*	52.0	49.1	53.1	42.0	43.0	47.0	49.0	45.0	36.0	29.0	23.0
Exp. Compt. (B)*	55.0	47.8	52.4	41.0	44.0	46.0	49.0	41.0	35.0	31.0	26.0
CSM Hatch	59.5	60.2	65.2	55.0	59.5	60.0	57.0	57.0	49.0	45.0	40.0
ATM SIA	64.0	68.1	69.1	56.0	62.0	60.0	66.0	60.0	52.0	45.0	42.0
AM Aft Airlock	63.0	65.1	70.4	63.0	64.0	65.0	60.0	63.0	53.0	45.0	38.0
AM Fwd Airlock	68.0	66.0	70.1	65.0	61.0	60.0	63.0	64.0	52.0	50.0	41.0
ATM Pump Off:											
Exp. Compt.	55.0	47.6	51.9	41.0	44.0	45.0	48.0	43.0	34.0	28.0	22.0
CSM Hatch	60.0	55.6	61.7	52.0	60.0	—	—	52.0	50.0	45.0	41.0
ATM SIA	64.0	62.9	68.8	59.0	64.0	61.0	64.0	55.0	52.0	45.0	42.0
AM Aft Airlock	60.0	60.0	68.8	62.0	65.0	63.0	56.0	55.0	48.0	43.0	36.0
AM Fwd Airlock	60.0	60.0	68.1	65.0	60.0	59.0	61.0	52.0	49.0	43.0	40.0

*NOTE: EXPERIMENT COMPARTMENT (A) AND (B) SPL'S ARE APPLICABLE TO BEGINNING AND END OF MEASUREMENT ACQUISITION TIME PERIOD.

4.0 GENERAL TEST PROGRAM

The purpose of this section is to present the experience and knowledge gained from the Skylab Vibro-Acoustic Test Program. Included in this section are descriptions of test hardware, test setup, instrumentation requirements and data acquisition requirements. Each major test phase was evaluated and constructive criticism is supplied in a form that may be helpful in future test programs.

4.1 Vibro Acoustic Test Overview

The vibro acoustic test program which was performed on the Skylab Structural Model Vehicle included the Orbital Workshop Launch Configuration, Payload Launch Configuration and Payload Orbital Configuration Test Series. Separate Acoustic and Vibration Tests were conducted on these test configurations primarily to verify major structure and/or verify the analytical model.

4.1.1 Initial Testing Plan and Revisions - The initial test plan required acoustic and low frequency, vibration tests on the Orbital Workshop, as well as, Acoustic, Vehicle Dynamics, and modal survey vibration tests on the Payload Assembly (PA) Launch Configuration. A modal survey vibration test of the payload assembly orbital configuration was also required in the initial test plan. This test plan was later revised to include an Instrumentation Unit (IU) Acoustic Test and the ATM/CMG Acoustic Qualification Test for the Apollo Telescope mount.

4.1.2 Vibro Acoustic Test Objectives - The vibro acoustic test objectives were divided into three phases. Phase I being the Orbital Workship Tests; Phase II being the Payload Assembly Tests; and Phase III being the instrumentation unit and Apollo Telescope Mount Acoustic Tests. The objectives of the Phase I Tests were as follows:

a. Verify structural integrity of primary and secondary structure when exposed to dynamic environments.

b. Verify dynamic design and test criteria for components and subassemblies.

c. Obtain modal response data for analytical model verification.

The Payload Assembly Tests, Phase II Objectives were as follows:

a. Verify Structural Integrity of the Payload Assembly to the Dynamic Environment

b. Quality Flight Hardware Components

c. Obtain modal response data for an analytical model verification

d. Verify Dynamic Design and Test Criteria for components and sub-assemblies

The objectives of the Phase III tests were as follows:

a. Verify IU Dynamic Behavior

b. Verify Dynamic Design and Test Criteria for Components and Sub-assemblies

c. Verify Prototype FCC (IU) response characteristics

d. Full dynamic qualification of the ATM/CMG

4.1.3 - Generalization of Test Accomplishments - All the Test Objectives were accomplished for the Phase I, Orbital Workshop Tests. One component was qualified as a result of tests, with no requalification tests required.

The Phase IIA, Payload Assembly Launch Configuration Tests, accomplished all test objectives. This phase qualified four components with the requirement for six requalification tests. It also established the requirement for additional IU Acoustic Tests and additional ATM/CMG Acoustic Qualification Tests (Phase III).

The Phase II B, Payload Assembly Orbital Configuration Tests, accomplished all Test Objectives. Twenty-five unique test modes were acquired, which represent all identifiable major structural resonances in the zero to twenty hertz frequency range. These twenty-five test modes were determined to be comprised of nine major components. The quality of the test modes were excellent with only one mode exhibiting poor orthogonality characteristics.

All test objectives were accomplished for the Phase III, IU and Apollo Telescope Mount Acoustic Tests. The CMG was requalified due to tests and twenty-three requalification test were required for the IU components.

4.1.4 Test Anomolies and Criteria Summary - There were no test anomalies in the Phase I Tests. Six levels of environmental sub zones were raised, thirty-three were lowered and fourteen remained unchanged. Forty-seven additional environmental sub zones were added fc special component criteria.

In the Phase II A, Payload Assembly Tests a decision was reached to conduct additional IU Acoustic Tests due to a ST-124 exceedance and a FCC excedance.

The Dynamic criteria assement for the major components of the Launch Configuration Payload Assembly were as follows:

MDA

a. Delete sinusoidal evaluation criteria, all zones

b. Change weight specification for 2 environmental sub zones

c. Add 9 new environmental sub zones

AM (Including PS, DA, and FAS)

a. Raise 11 environmental sub zones

b. Add 3 new environmental sub zones

c. Special environmental criteria for 7 components

IU

a. Acoustic criteria increased by a factor of 2 db on the power spectral density (70-2000 HZ range)

ATM

a. Raise 2 environmental sub zones

4.2 Phase II A Payload Assembly Launch Configuration Tests

Acoustic and Vibration Tests were conducted on the Skylab Payload Assembly from 08 September through 08 October 1971. The Test Program for the Launch Configuration was comprised of the following major activities:

Payload Assembly - Lift-off Acoustic Environment
Payload Assembly - Boundary Layer Acoustic Environment
Acoustic Absorption Test
IU Acoustic Test
IU Modal Survey

4.2.1 Acoustic Tests

4.2.1.1 Test Requirements - The following conditions are summarized from the Acoustic Test Plan, S + E-ASTN-ADD-71-69

4.2.1.1.1 Test Objectives - The primary test objectives of the Payload Assembly Test Program were to:

a. Verify the structural integrity of the assembly

b. Verify the dynamic design and test criteria for components and sub-assemblies

c. Qualify flight hardware components

4.2.1.1.2 Specimen Configuration - The test specimen consists of an Instrument Unit, Fixed Airlock Shroud, Payload Shroud. Airlock Module, Multiple Docking Adapter, Apollo Telescope Mount, and Deployment Assembly. These items were assembled on an S-IV B OWS/Forward Skirt and Tank Dome Assembly as shown in Figure 4.1. Flight type components which were installed during the acoustic tests and denoted in figures 4.2, 4.3, and 4.4 are as follows:

a. PLV Fan Motor Assembly located in the Cabin Head Exchanger Module of the STS.

b. Film Vaults 3 and 4 located in the MDA.

c. H a 1 Camera located in Film Vault 4 of the MDA.

d. AS & E Camera located in Film Vault 3 of the MDA.

e. S056 Experiment Camera located in Film Vault 3 of the MDA.

f. PLV Fan Motor and Muffler Assembly located in the Cone Section of the MDA.

All other components and assemblies were either prototype or mass simulated models.

4.2.1.1.3 Facilities Description - All the tests described in this document were conducted in the acoustic test facility, building 49, Manned Spacecraft Center, Houston, Texas. The test specimen was located in a reverberation chamber with a volume of approximately 169,000 cubic feet as shown in the sketch in Figure 4.5.

4.2.1.1.5 Control and Data Systems - The acoustic test spectra were controlled by an automatic closed loop system capable of adjusting the test environment to within $\pm$ 2 db of prescribed values. Simulation limitations inherent in environmental acoustic testing were minimized by use of vibroascoustic transfer functions which were derived and used to adjust spectra so that selected test article responses in the OWS and IU would correlate with available flight data. Simplified block diagrams of the Acoustic Excitation/Control and Data Acquisition System are presented in Figures 4.6 and 4.7.

4.2.1.2 Test Summary - The Acoustic Testing, conducted in the NATF reverberent chamber, consisted of exposing the PA Test Article to both lift off and aerodynamic environments for a prescribed time. A Test Summary is presented in Table 4.1, which is a chronological listing of the Test Sequence, run number, description, Test reference, Test parameters, duration, data, overall SPL, data reference and remarks.

4.2.1.2.1 Test Procedure - The performance of each acoustic exposure, identified in Table 4-1 by run no.'s PA-A-002, 003, 006, 009, 010, 011, 012, 040, 041, 043, 044, and 045 was implemented by following the steps described in the detailed test procedure, DTP-SKY-7.

Acoustic absorption tests were performed by following the procedure outlined in reference (10). The tests are identified in Table 4-1 by run no.'s PA-A-013 through PA-A-038.

Table 4-1 run no.'s PA-A-046 and 047 sinewave sweeps were performed as required by reference 11.

4.2.1.2.2 Instrumentation - A total of 360 measurements, consisting of 285 accelerometers, 43 microphones, and 32 strain gages, were recorded during testing. The data acquisition system provided capabilities for recording 264 channels; therefore, a second run at each test condition with a repatch of 96 channels was required to obtain data from all 360 measurements.

No test was started with more than three data sensors in an inoperative condition. The test spectra were controlled to 10 surface mounted microphones.

The indicated total accounts for all instrumentation locations changes and additions as described in the Volume I Instrumentation Plan, ED-2002-1255, Revision A, dated 31 December 1976.

4.2.1.2.3 Data Summary - Data from the acoustic test can be found in references (12), and (13). Data not presented in these references are available from stored magnetic tapes. Measurement number versus run number and recorder channel number information are presented in Table II of the instrumentation plan noted in 4.2.1.2.2.

4.2.1.2.4 Test Description - The following contains summaries of Test Problem Areas and solutions to these problems. In addition, circumstances responsible for aborted test runs are tabulated by nature of error and frequency of occurrence.

PROBLEM: Lack of Acoustic Power in High Frequency bands (above 500 Hz)

CORRECTION: Air modulator/Horn Configurations were changed to to EPT-200 modulators, which have greater acoustic output in the upper frequency range.

PROBLEM: Data from PA-002 and PA-003 indicated that vibration inputs to the IU Components would exceed specification levels if the full lift-off spectrum was applied to the Test Article.

CORRECTION: An additional Low Level Test was run. A review of the data resulted in a decision to use an alternate lift-off spectrum which was based on the IU Data alone, since transfer functions computed from the S-IV B forward skirt measurements exhibited significant deviations from corresponding flight measurements.

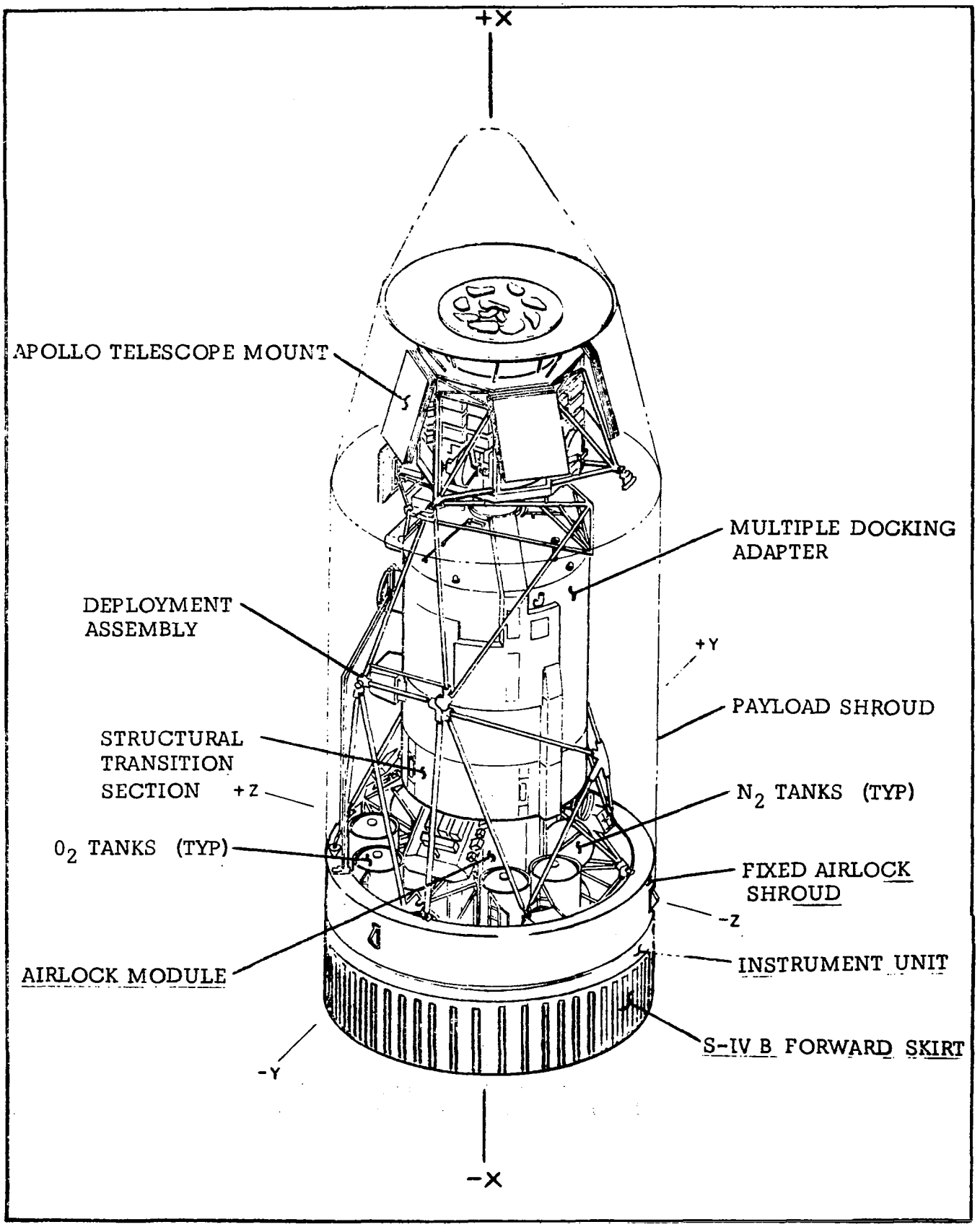

Figure 4.1 Payload Assembly Test Article Launch Configuration

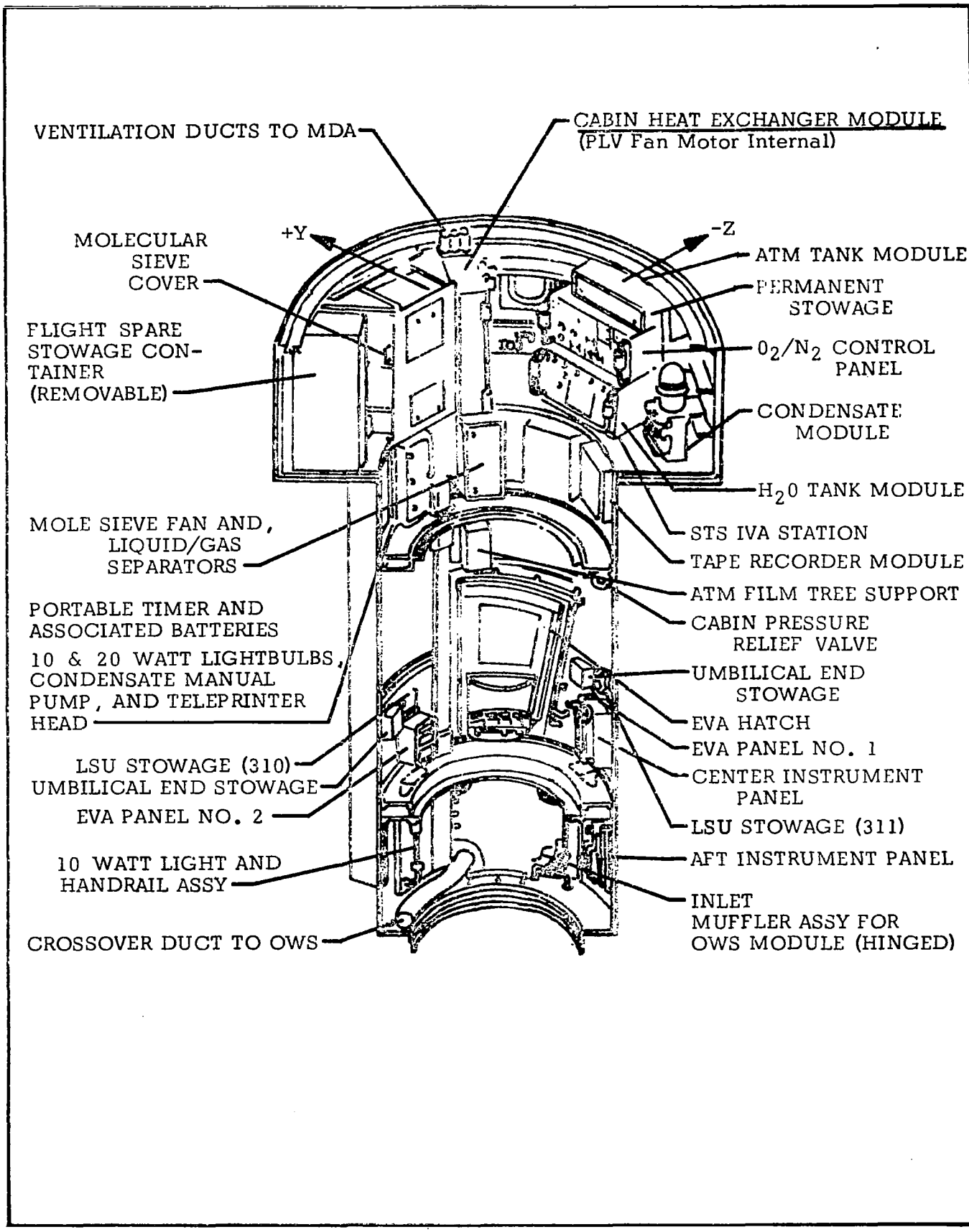

Figure 4.2 Payload Assembly Test - Airlock Module

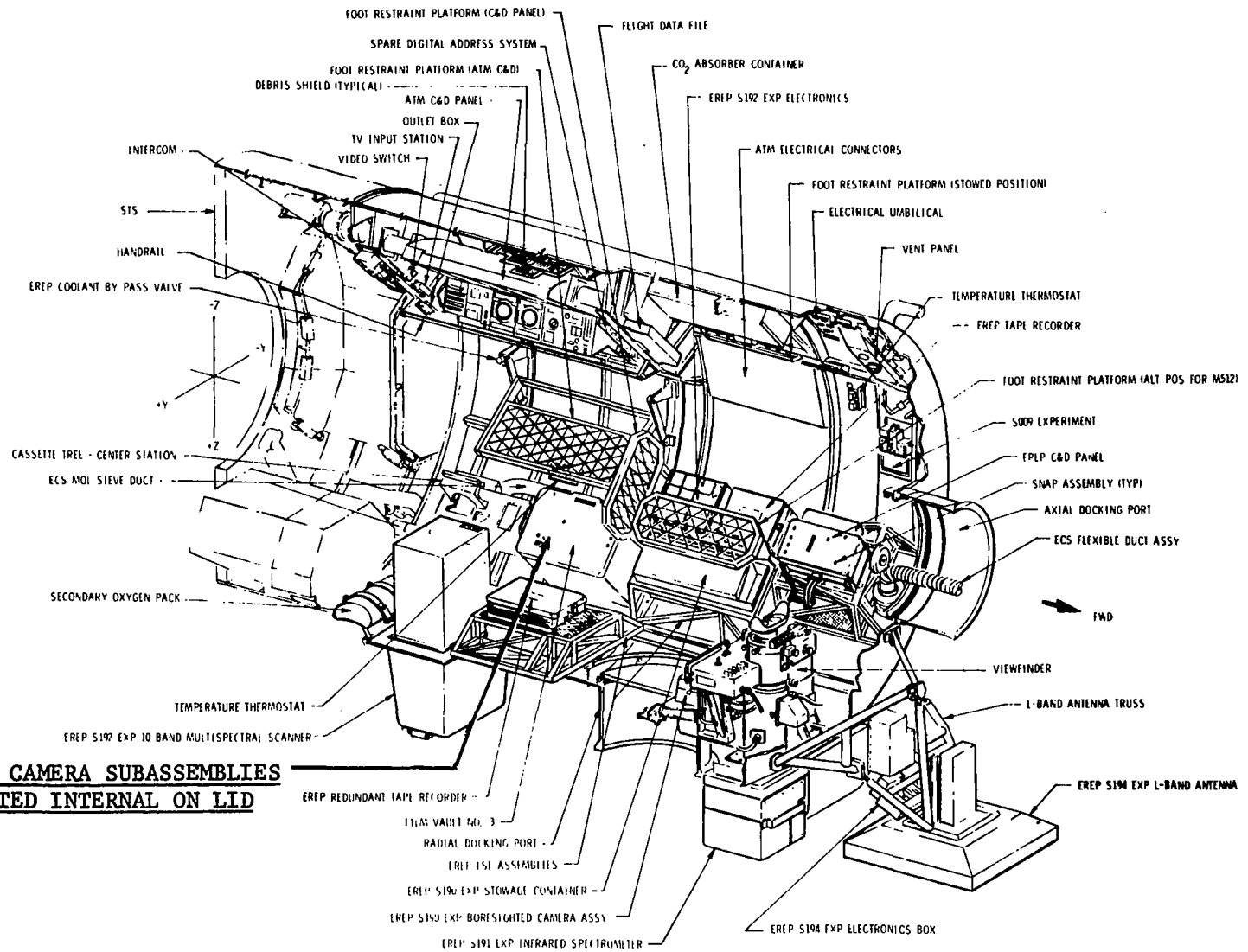

Figure 4.3 Payload Assembly Test-Multiple Docking Adapter, -Y Section

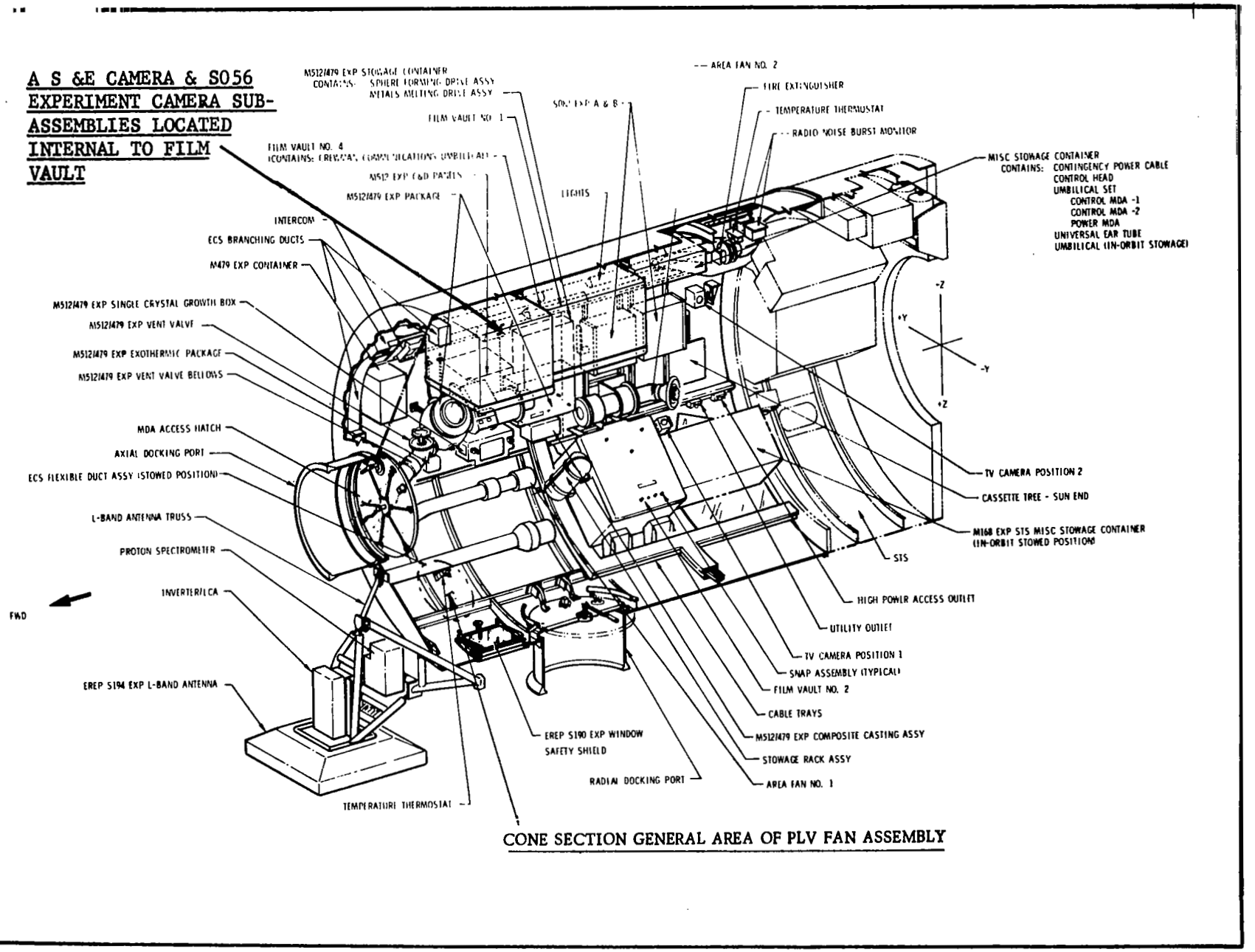

Figure 4.4 Payload Assembly Test-Multiple Docking Adapter, +Y Section

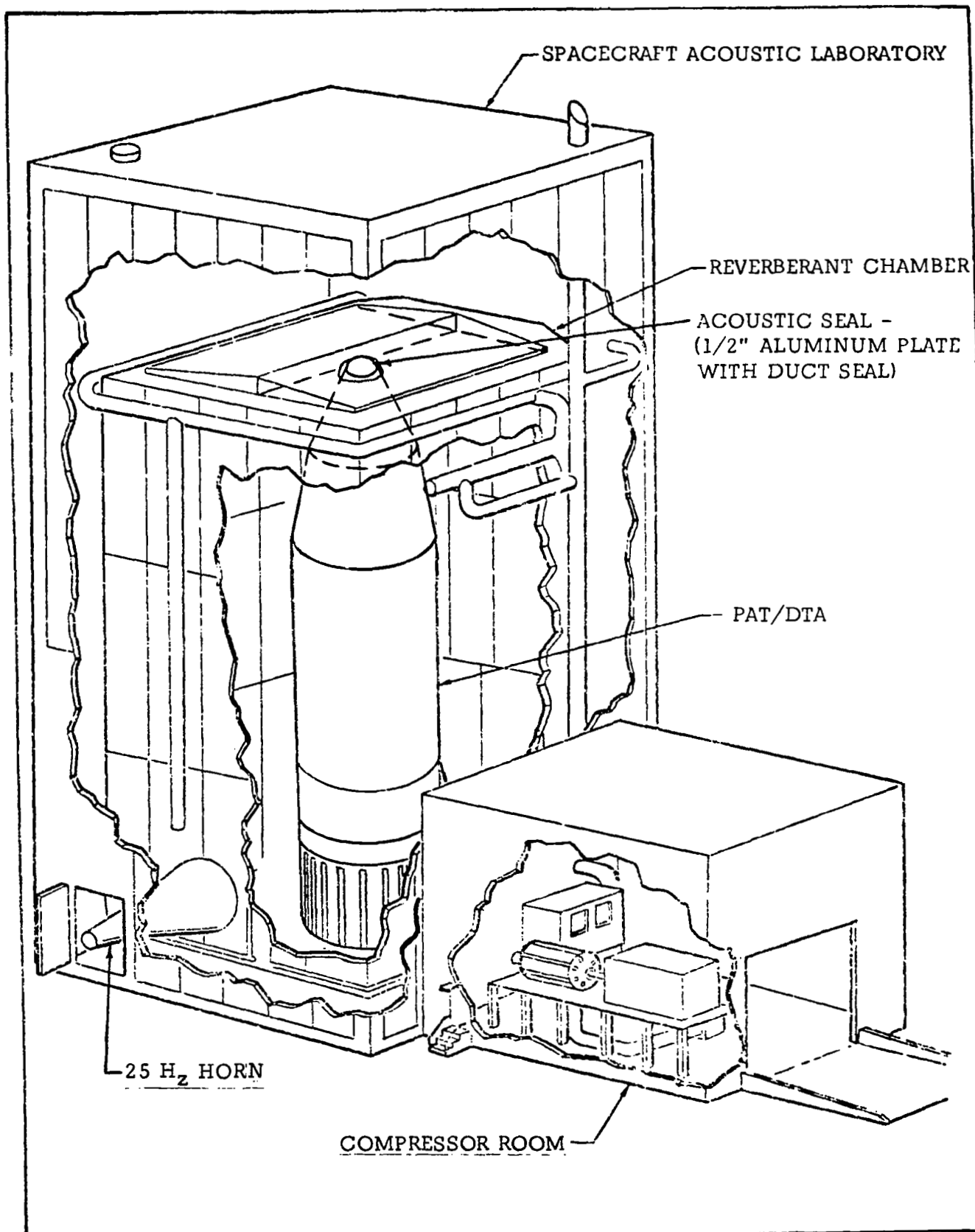

Figure 4.5 MSC Spacecraft Acoustic Laboratory Payload Assembly Test Configuration

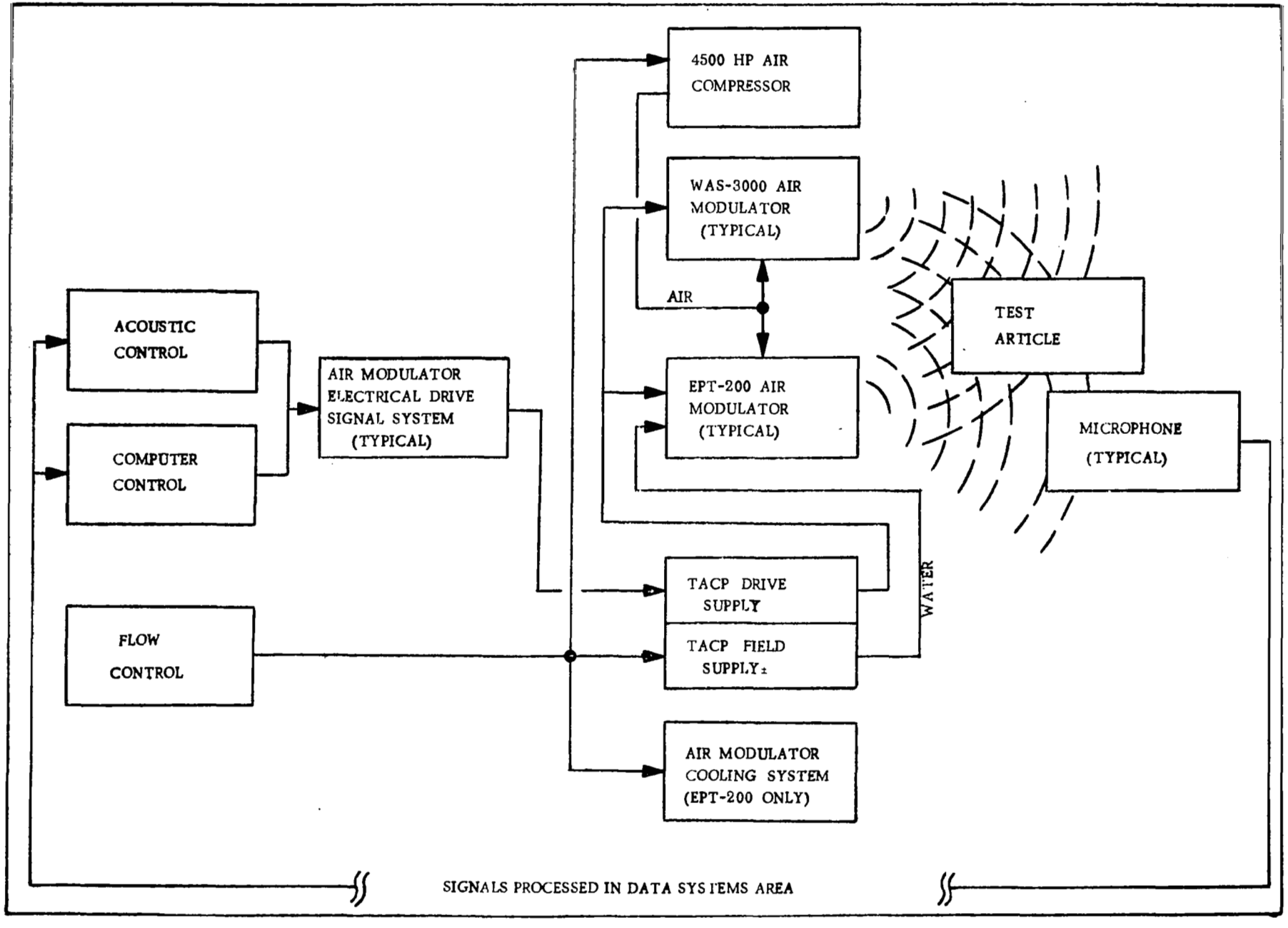

Figure 4.6 Acoustic System for PA Testing.

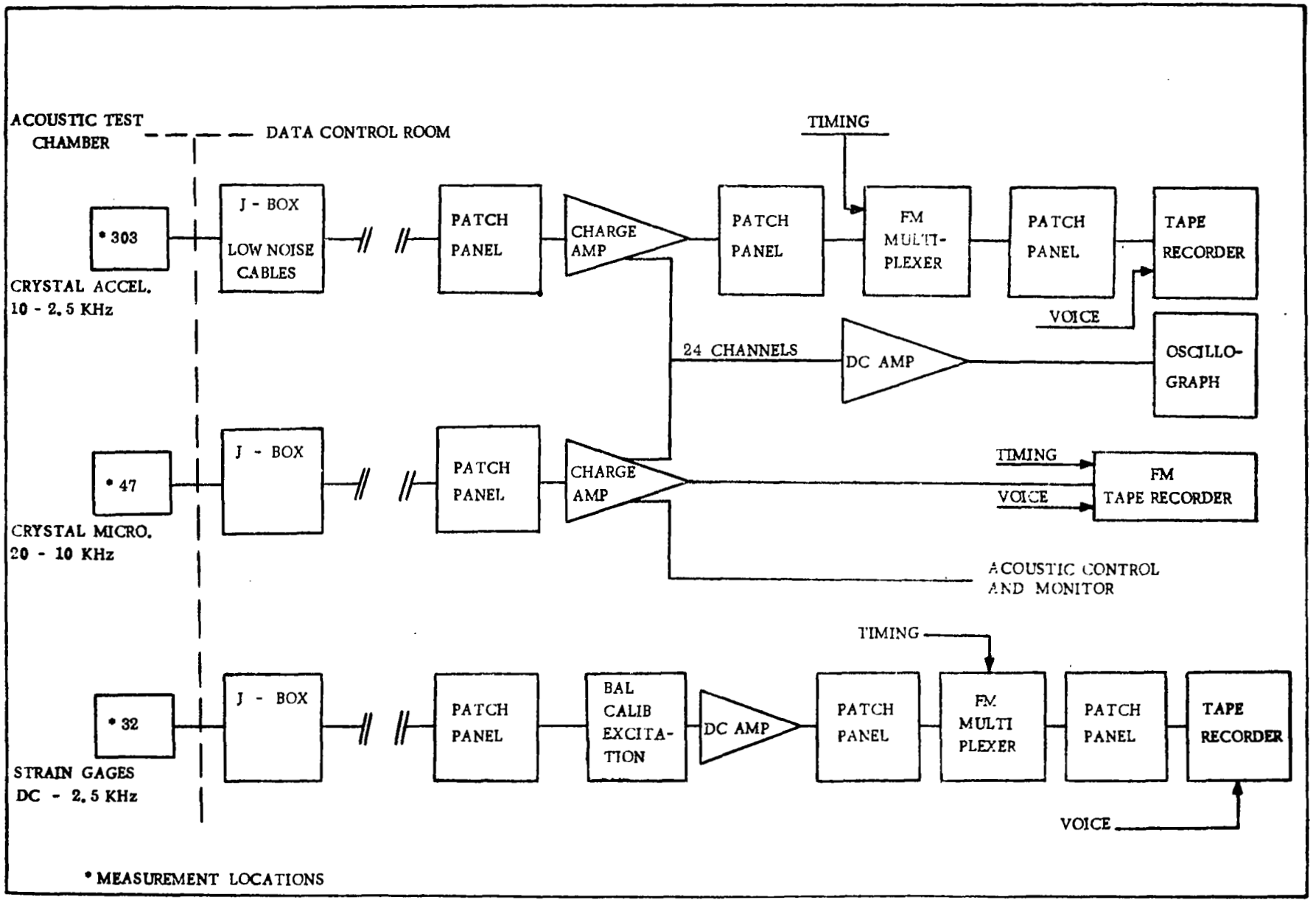

Figure 4.7 Data Acquisition System for PA Testing.

Table 4.1 Skylab Payload Assembly Acoustic/IU Modal Survey Test Summary

TEST SEQUENCE	TEST RUN NO.	TEST DESCRIPTION	TEST REFERENCE	TEST PARAMETERS	TEST DURATION	TEST DATE	OVERALL SPL(dB)	DATA REFERENCE	REMARKS
1. Acoustic Test	PA-A-001	Lift-off Spectrum	MSFC, Test Plan S&E-ASTN-ADD-71-69, Modified by TCBD, OMS/PA-47	-6dB Down From Lift-off Level	N/A	8/9/71	N/A	N/A	Test Aborted, Insufficient High Frequency Power, Modified Modulator Configuration and Continued Testing.
2.	PA-A-002				15 Seconds	8/9/71	145	Magnetic Tape	Test Completed Successfully, Re-patched Instrumentation, Re-rigged EVA Hatch, and Continued Testing.
3.	PA-A-003				15 Seconds	8/11/71	145	Magnetic Tape	*Test Completed Successfully, Re-Located Measurements SE-105-411L, SE-104-411R, SE-105-411T and SA-019-509, Continued Testing.
4.	PA-A-004		TCBD, OMS/PA-49		N/A	8/16/71	N/A	N/A	Test Aborted, Test Control Equipment Malfunction-Air Modulator Cooling System Corrected and Continued Testing.
5.	PA-A-005				N/A		N/A	N/A	Test Aborted, Test Control Equipment Malfunction-Computer, Corrected and Continued Testing.
6.	PA-A-006				15 Seconds		145	Magnetic Tape	Test Completed Successfully, Changed Mounting on SE-236-602R and SE-239-602R, Programmed Alternate Acoustic Lift-off Spectrum Loaded Into Computer and Continued Testing.
7.	PA-A-007	Alternate Lift-off Spectrum	MSFC, Test Plan S&E-ASTN-ADD-71-69, TCBD's OMS/PA-47 and 49	Full Level	N/A		N/A	N/A	Test Aborted, Test Control Equipment Malfunction-Computer, Corrected and Continued Testing.
8.	PA-A-008				15 Seconds		150	MSFC, DATA Book S&E-ASTN-ADD-71, Enclosure 3	Test Completed Successfully, Re-patched Instrumentation, and Continued Testing.
9.	PA-A-009					8/19/71	150	MSFC, Data Book S&E-ASTN-ADD-71, Enclosure 3	Test Completed Successfully, Re-configured for Boundary Layer Spectrum and Continued Testing.
10.	PA-A-010	Boundary Layer Spectrum	MSFC, Test Plan S&E-ASTN-ADD-71-69, and TCBD OMS/PA-47	-6dB Down From Boundary Layer Level			147	Magnetic Tape	*Test Completed Successfully, Re-Located Measurements SA-025-SE, SE-231-602L, SE-242-603L, SE-105-411L and SE-105-411T, and Continued Testing.
11.	PA-A-011			Full Level	60 Seconds	8/23/71	153	MSFC, Data Book S&E-ASTN-ADD-71, Enclosure 4	Test Completed Successfully, Re-patched Instrumentation, and Continued Testing.
12.	PA-A-012			Full Level	60 Seconds	8/25/71	153	MSFC, Data Book S&E-ASTN-ADD-71, Enclosure 4	Test Completed Successfully, Re-configured for Absorption Test and Continued Testing.
13. Acoustic Absorption Test	PA-A-013 thru PA-A-038	Tests Consisted of 1/3 Octave Band Acoustic Excitations	TCBD OMS/PA-52	120dB 1/3 Octave Intervals From 23.5 Hz to 5000 Hz	Decay Data	8/26/71 - 8/31/71	N/A	Magnetic Tape	*Test Completed, Re-located Measurements SA-015-509, SA-021-509, SA-022-509, SA-023-509, and SA-024-509, Re-programmed Computer with Special/IU Test Spectra and Continued Testing.
14. IU Acoustic Test	PA-A-039	Special IU Lift-off Spectrum	TCBD OMS/PA-56	Full Level	N/A	9/1/71	N/A	N/A	Test Aborted, Test Control Equipment Malfunction, Computer Corrected and Continued Testing.
15.	PA-A-040	Special IU Lift-off Spectrum			15 Seconds		147	MSFC, Data Book S&E-ASTN-ADD-71, Enclosure 5	Test Completed Successfully, Setup for Boundary Layer Condition and Continued Testing.
16.	PA-A-041	Special IU Boundary Layer Spectrum			15 Seconds		148	MSFC, Data Book S&E-ASTN-ADD-71, Enclosure 6	*Test Completed Successfully, Instrumented for Special IU Modal Survey and Continued Testing.
17. IU Modal Survey	PA-T-01 thru PA-T-47	Tests Consisted of Sine-wave Sweeps, Resonant Swells, & Decay's for Modal Data	MSFC Test Plan S&E-ASTN-ADD-71-125 & TCBD OMS/PA-56	Per Test Plan & Verbal Instruction	N/A	9/22/71 10/1/71	N/A	MSFC, Data Book S&E-ASTN-ADD-71, Enclosure 10	*Test Completed with Data Anomaly Between Mass PCC & Proto PCC Configurations, See Ref. 9 for Details, Re-instrumented IU for Additional Acoustic Tests and Continued Testing.
18. IU Acoustic Test Continued	PA-A-042	Special IU Lift-off Spectrum	TCBD OMS/PA-57	Full Level	N/A	10/7/71	N/A	N/A	Test Aborted, Test Control Equipment Malfunction, Corrected Problem and Continued Testing.
19.	PA-A-043				15 Seconds		148	MSFC, Data Book S&E-ASTN-ADD-71, Enclosure 7	Test Completed Successfully, Replaced 25 Hz Horn with Two 50 Hz Horns and Repeated Test.
20.	PA-A-044						147.5	MSFC, Data Book S&E-ASTN-ADD-71, Enclosure 8	Test Completed Successfully, Setup for Boundary Layer Condition and Continued Testing.
21.	PA-A-045	Special IU Boundary Layer Spectrum					148	MSFC, Data Book S&E-ASTN-ADD-71, Enclosure 9	Test Completed Successfully Setup for Sinewave Sweep and Continued Testing.
22.	PA-A-046 PA-A-047	Two Sinewave Sweeps		19.98 to 99 Hz .288 oct./min.	480 Seconds & 481 Seconds	10/8/71	148 & 150	Magnetic Tape	Test Completed Successfully.

*See Volume I Instrumentation Plan, SD-2002-1255, Revision A, December 31, 1971 for Location Changes.

Malfunctions responsible for aborted Test Runs.

NATURE OF ERROR	FREQUENCY OF OCCURRENCE
Was-300 modulator had insufficient Acoustic Power in upper frequency range.	1
Chattering of Air Modulator Cooling System Control relay	1
Test Control Computer Malfunction	3
Power output switch in "Dummy Load" Position resulting in no Acoustic Power Output	1
Microphone damaged when scaffolding was removed prior to testing	1

The total number of Test Malfunctions is small compared to the total number of tests these malfunctions had no major detrimental effect on the Total Test Program.

4.2.2 IU Modal Vibration Test - The Skylab Payload assembly acoustic test data showed that vibration responses of the Flight Control Computer (FCC) and the ST-124 package were significantly higher than vibration qualification criteria, as previously reported in "Skylab Payload Assembly Acoustic Testing." Marshall Space Flight Center's assessment of this problem led to the conclusion that any requalification program on the FCC would have a serious impact on the Skylab Program. In an effort to obtain a better understanding of the modal characteristics of the IU which were contributing to the excessive vibration of these components, a vibration test was conducted on the IU.

4.2.2.1 Test Requirements - All testing was conducted in accordance with MSFC Test Program Plan S +E - ASTN-ADD-(71-69), "PA Vibroacoustic Test Plan, Phase II". Minor modifications to the Program were incorporated through Test Control Board Directives (TCBD).

4.2.2.1.1 Test Objectives - The tests were conducted to define the mode shapes, resonance frequencies, and damping characteristics associated with the measured response of the Flight Control Computer (FCC) and the ST-124 stabilized platform mock-ups observed during the PA Acoustic Testing.

4.2.2.1.2 Test Specimen - The test configuration consisted of the Instrumentation Unit with a mass simulated FCC mock-up. Force controlled sweeps, resonant dwells and decays were performed. Following this activity, a prototype FCC was installed replacing the mass mock up, and subsequent tests were performed.

4.2.2.1.3 Test Facilities - Refer to Section 4.2.1.1.3 of this report for description.

4.2.2.1.4 Testing Apparatus - At each of the four exciter locations (Figure 4.8), a Ling A280 shaker was suspended from the facility crane by cables, thus forming a low-frequency pendulum (resonance below 2.0 Hz). The shaker was positioned with a mounting assembly and attached to the IU through a "stinger" with a load-cell force link. A typical shaker suspension system is shown in Figure 4.9. At three of the test locations, aluminum plates (which had been drilled and tapped for the force link) were bonded to the test article to provide shaker attachment points. At the fourth location, the force link was attached by drilling and tapping one of the ST-124 mounting bolts.

4.2.2.1.5 Control and Data Systems - The control system for the electrodynamic shaker consisted of a frequency synthesizer, its associated programing unit, and an amplitude-servo device for maintaining a constant input force over the frequency range. The electrical signal developed in these instruments was amplified by a solid state direct-coupled power amplifier to provide the necessary drive current for the shaker. A strain-gage load cell was installed between the shaker and the vehicle drive-point to provide force measurement for servo feedback. A block diagram of the control system is shown in Figure 4.10.

The readout system for phase tuning consisted of oscilloscopes with the force signal driving the horizontal axis and the reference accelerometer driving the vertical, thus providing a Lissajous ellipse. All accelerometer and force signals were filtered through a 10-Hz bandwidth tracking filter whose center frequency was tuned to the synthesizer drive signal frequency.

4.2.2.2 Test Summary - The PA/IU was subjected to low-force levels which were varied sinusoidally over a frequency range of 5 to 70 Hz at four different locations. Then resonant dwell tests were conducted based upon resonant frequencies observed and selected during the sine-sweep tests. In addition, the FCC mock-up was replaced with an FCC prototype, and subsequent tests were performed to determine the IU vibration characteristics with FCC prototype installed.

4.2.2.2.1 Test Procedure - Five sine-sweep tests were initally conducted over a frequency range from 5 to 70 Hz during which data from 61 fixed measurements were recorded. Following completion of the sine-sweep testing, the data were processed and plotted in the form of g(peak)/lb versus frequency and phase angle (relative to force) versus frequency. The data review team examined the processed data and selected frequencies for further investigation. At each frequency of interest, a survey of the vibration accelerations normal to the external surface was made by means of acceleration probes. Personnel manning the probes were directed to grid positions on the structure by test engineers located at a central instrumentation point. At each location of interest, acceleration values and phase (relative to either force or a reference accelerometer) were measured and logged. In addition, numerous frequencies

were selected, tuned, and acceleration data recorded for post-test examination.

Damping characteristics were determined by abruptly terminating power to the thruster and recording the vibration decay as measured by all accelerometers.

4.2.2.2.2 Instrumentation Summary - A total of 64 fixed servo accelerometers were recorded during the subject vibration tests, and a force transducer was used to control the force input to the specimen. Details concerning specific instrumentation locations are described in the Volume I Instrumentation Plan, ED-2002-1255 Revision A, dated 31 December 1971.

4.2.2.2.3 Data Summary - Tabulated data from the modal survey dwell tests are presented in reference (14). Data not presented are available from stored magnetic tapes. Information regarding recorded data is presented in Appendix E, Table II of the Instrumentation Plan, noted 4.2.2.2.2.

4.2.2.2.4 Test Description - Although, no major equipment problem were encountered, several test reruns were required for the following reasons.

CAUSE OF RERUN	FREQUENCY OF OCCURRENCE
Power supply 60 Hz noise; data unreadable	1
Poorly defined mode	1
Repeat for better log decremint data	6

ANOMALIES: The response of the FCC Prototype was significantly lower than the response of the mass mock-up for a given input force above 40 Hz. In particular, no significant 55-Hz responses were measured after installation of the prototype FCC. Acoustic test data previously obtained indicate that a 55-Hz mode contributed significantly to the FCC problem (FCC vibration levels greater than qualification levels). As a result of this disclosure, more testing was authorized to determine the effect of prototype installation on the IU response to random acoustic excitation.

4.2.3 Alternate Test Approach + Recommendation - Instrumentation recording limitating caused test turnaround delays.

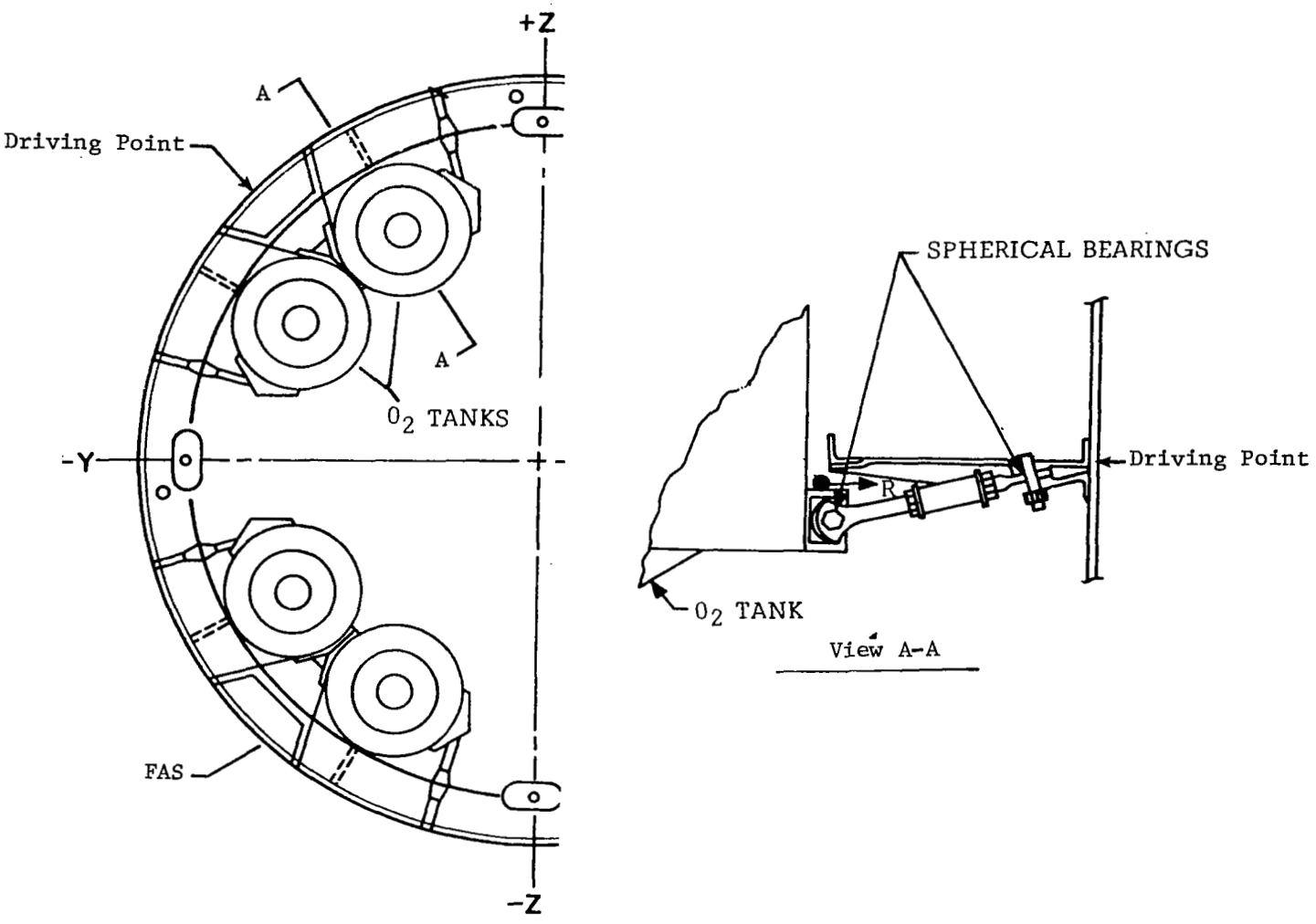

Figure 4.8 Thruster Driving Locations

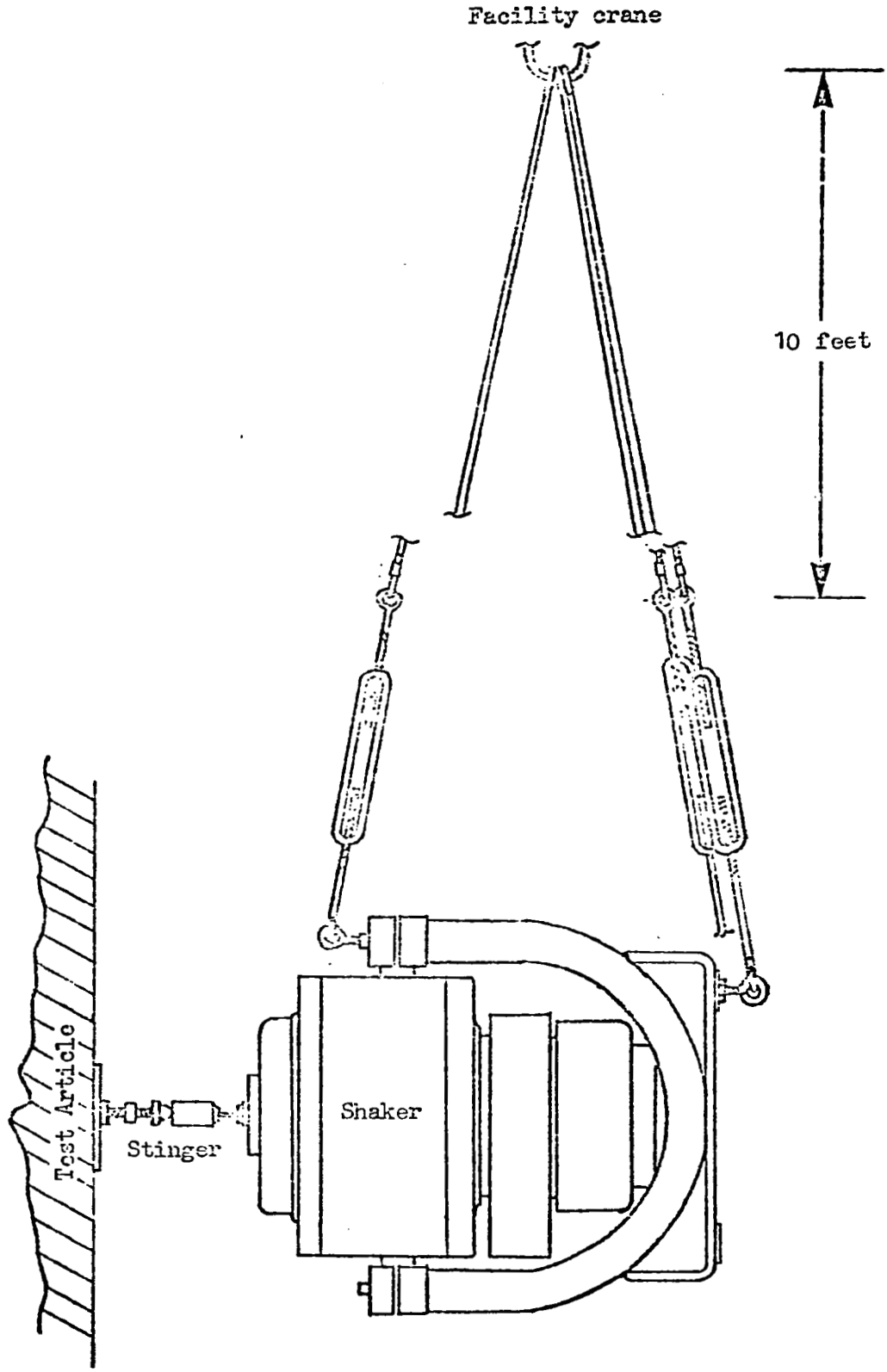

Figure 4.9 Shaker Suspension System

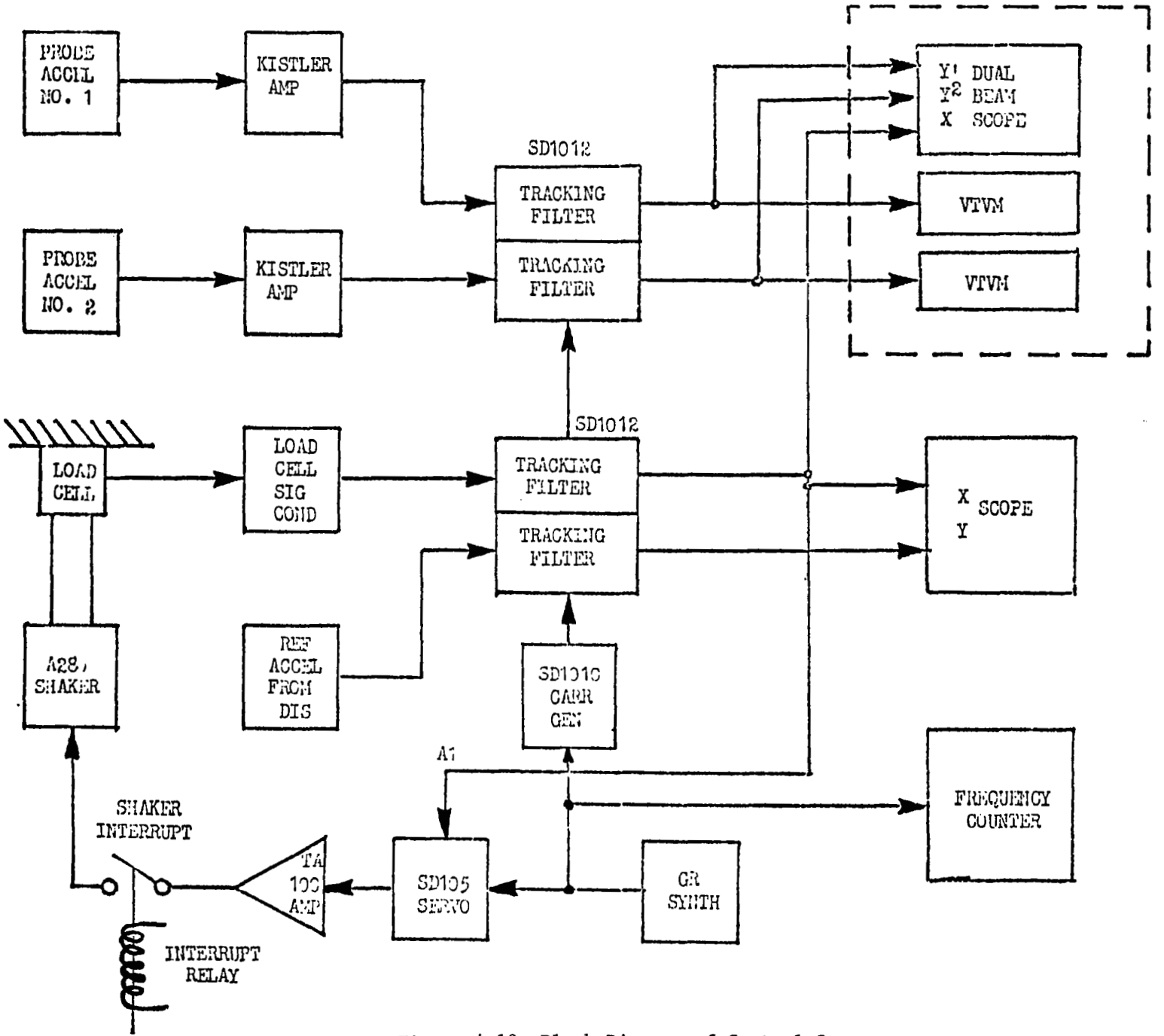

Figure 4.10 Block Diagram of Control System

CORRECTION: Scope instrumentation requirements within facility capability. This would require a pre-test analysis as a basis for identifying minimum requirements.

4.3 Phase II B - Payload Orbital Configuration Modal Survey - This modal survey was performed during the period extending from 23 May through 23 June 1972 at the Manned Spacecraft Center in Houston, Texas under the direction of Marshall Space Flight Center, Huntsville, Alabama. Data was acquired from this test which identified 23 elastic and 2 rigid body modes.

4.3.1 Test Requirements - The following reported conditions are standard modal survey test requirements.

4.3.1.1 Test Objectives - The Skylab modal survey test was performed to obtain the characteristic vibrational frequencies, mode shapes, damping coefficients, and generalized mass of the normal modes. Data derived from the test was used to evaluate the analytical results obtained with a mathematical structural model; and to further refine design load modeling techniques.

4.3.1.2 Test Specimen Configuration - Test configuration hardware consisted of the instrumentation unit (IU), fixed airlock shroud (FAS), the structural transition section (STS), the airlock module (AM), the multiple docking adapter (MDA), the ATM deployment assembly (DA), the Apollo telescope mount (ATM), and the command and service module (CSM). The aforementioned subassemblies were stacked upon the S-IVB configuration orbital workshop (OWS) forward skirt/tank dome assembly (see Figure 4.11). The ATM included semi-deployed solar arrays, two of which contained mass simulated panels.

Flight type components which were installed during the test were as follows:

a. PLV Fan Motor Assembly located in the Cabin Heat Exchanger Module of the STS;

b. Film Vaults 3 and 4 located in the MDA;

c. PLV Fan Motor and Muffler Assembly located in the cone section of the MDA.

All other components were either prototype or mass simulated models.

4.3.1.3 Test Facilities - The tests described were conducted in the Spacecraft Vibration Laboratory (SVL) of the Vibration and Acoustic Test Facility (VATF), building 49, MSC, Houston, Texas.

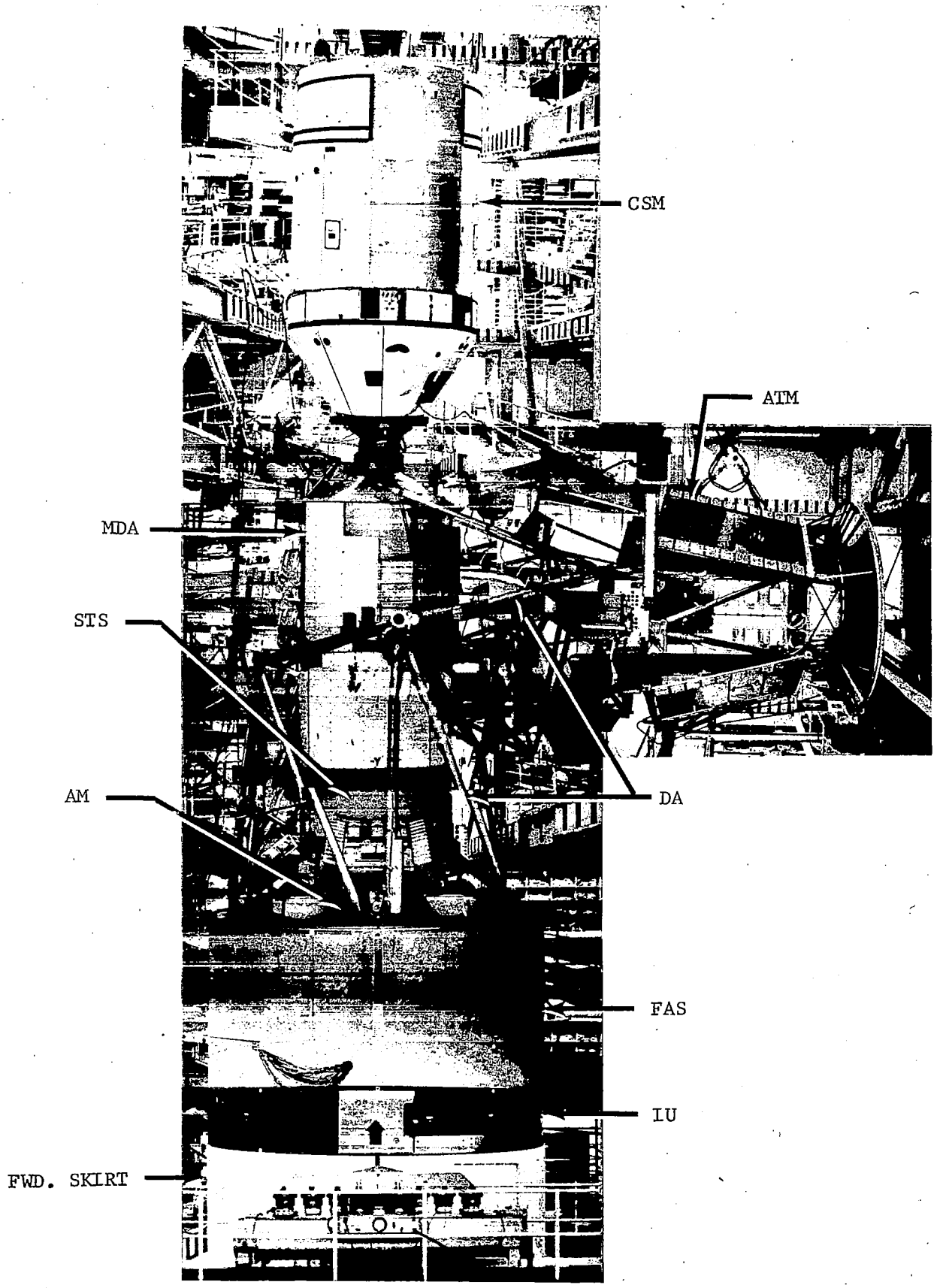

Figure 4.11 MODAL SURVEY TEST SETUP

4.3.1.3.1 Test Suspension System - The PA described in paragraph 4.3.1.2 was stacked in the orbital configuration on the 12,000 pound base ring fixture. The CSM and ATM were supported from above by one airspring each. Three additional airsprings attached to the outer periphery of the base support ring fixture by means of single attach point load cell links spaced 120 degrees apart. Suspension spring rates and damping characteristics were controlled by the regulation of air pressure to the plenum chambers of the five pneumatic springs. Air pressure was maintained to provide suspension resonance and damping characteristics at values where minimum interference with specimen modal resonance properties were realized, and the constraints of static stability were still observed. Protection against possible catastrophic failure of the suspension system was provided by automatic interlock system and by positioning eight static support stands in sufficient dimensional proximity to prevent any possible destructive translational or rotational motions reacting upon the test system.

4.3.1.3.2 Shaker Positioning - The excitation of predicted analytical modes demanded the placement and activation of the vibration exciters at precise geometrical positions and in exact force/phase combinations. In some cases, mechanical accessibility prevented realization of dimensional positioning. Twenty-one shakers were attached to the test specimen. Of these 21 shakers, 12 were controlled simultaneously. During this test series, the shakers at 18 locations were subsequently utilized for modal tuning.

The shakers employed in this test were rated at 150 force pounds and were Unholtz-Dickie Model 28 exciters. Of the 21 exciters emplaced, 14 were hard mounted to major building structural members, and seven were suspended upon spring yoke support systems. The exciters were connected to the structure by stringers designed to resonate at frequencies well above the upper frequency limits of test. No stringer or suspension problems were encountered during conduct of this test series.

4.3.1.4 Control and Data Systems - All test control and data operations were automated. The GAC 18/30 digital computer and its associated peripherals performed all facets of test control, data acquisition/reduction, and data display under the supervision of Automatic Modal Tuning and Analysis System (AMTAS) software for all phases of the test program with the exception of the wide band sweeps. Data emanating from the wide band sweeps were recorded on analog tapes for subsequent digital processing and graphic presentation.

Throughout the narrow band modal tuning and modal dwells, AMTAS operated in the automatic digital mode.

4.3.2 Test Summary - In order to accomplish the stated test objectives, the program was conducted in five distinct phases. These were:

a. An Automatic Modal Tuning and Analysis System (AMTAS) checkout and end-to-end calibration was conducted prior to initiation of the wide band sinusoidal sweeps. This assured the operational readiness and accuracy of the AMTAS system prior to commencement of actual testing.

b. Wide band sinusoidal sweeps were conducted using both single and paired shakers. For structurally mounted shakers, the frequency interval extended from 0.8 to 20 Hz. When pendulum mounted shakers were employed, the lower frequency limit was determined by the shaker suspension system isolation frequency. Single and paired shakers connected at each of 13 separate vehicle excitation stations were stepped over the test frequency range in increments of 0.1 Hz. The dwell duration at each 0.1 Hz frequency increment was adjusted to assure a minimum of 12 cycles per increment. The outputs of 62 preselected servo accelerometers were recorded on analog magnetic tape. These magnetic tapes were subseqeuntly processed by the Computation and Analysis Division (CAD) yielding Cospectrum, Quadrature spectrum, Cross spectrum, and phase angle plots and alphanumeric tabulations for each of 12 sweeps. Examination of these records afforded an insight into the number and regions of significant resonances, the presence of modal coupling, and the most efficient locations for the excitation of specific modes.

c. The rigid body modes of the specimen and suspension system were checked. Due to the physical asymmetry of the structure/support system, a high degree of modal coupling was observed. Only two rigid body (suspension) modes were acquired due to schedule limitations. These data are essential in determination of the effects of suspension constraints upon the modal damping.

d. Narrow band modal tuning was accomplished using multiple shaker installations at each frequency where resonant conditions were indicated by the wide band coincident-quadrature response plots. Coincident-quadrature plots were digitally produced for one force and three selected accelerometers. Force distributions and phasing relationships were adjusted among the various excitation stations to achieve fine tuning of the mode. Achievement of final tuning was determined by examination of both Lissajous patterns and the Coincident-Quadrature plots.

e. After fine tuning was accomplished, modal decay traces for 16 preselected accelerometers were recorded on oscillographs. In addition, 12 selected decay accelerometers were recorded on analog magnetic tape. If these modal decays proved free from beating, the narrow band force distributions were reestablished for purposes of data acquisition.

4.3.2.1 Test Procedure - A test procedure was generated by the test agency which reflected the requirements of the test plan and provided the procedural steps to accomplish wide band sweeps, fine tuning, narrow band sweeps, etc.

4.3.2.2 Instrumentation Summary - The types, quantity, location and identification of all dynamic instrumentation required during the test are presented in Martin Marietta Corporation (MMC) document ED-2002-1532, Volume III, dated 30 September 1972. In summary, transducers which were required for this test were of the following types and quantities.

Type	Quantity
Servo Accelerometers	200
Force Transducers	21
Strain Gages	20
Rate Gyros	9
Total	250

4.3.2.3 Data Summary - Coincidence-quadrature (CO/QUAD) plots and tabulations were obtained for all wide band sweep tests and CO/QUAD plots were obtained for narrow band sweep tests. CO/QUAD tabulations and two dimentional mode shape plots were obtained for all dwell tests and time amplitude traces were obtained for all decay tests. Refer to the following sections for further details.

4.3.2.3.1 Test Techniques Wide Band Modal Tuning Sweeps - The computer provided, through the Synchon interface, the required frequency and sweep rate parameters. Force control and abort exceedance supervision employed digital methods. The outputs of 62 preselected servo accelerometers were reocrded using the vidar multiplex system. This system multiplexed six channels of data onto each analog magnetic tape track using carriers of different center frequencies. The center frequencies and deviations for each channel were as shown below:

Data Channel 1	62.5 KHz + 10 KHz
Data Channel 2	100 KHz $\pm$ 10 KHz
Data Channel 3	137.5 KHz $\pm$ 10 KHz
Data Channel 4	175 KHz $\pm$ 10 KHz
Data Channel 5	212.5 KHz $\pm$ 10 KHz
Data Channel 6	250 KHz $\pm$ 10 KHz
Reference Channel	287.5 KHz $\pm$ 10 KHz

The 62 accelerometers were recorded on 11 data tracks. An IRIG "B" time code was recorded on Channel 6 of track 13. The tape recording speed was 60 inches per second (ips). A full scale 25 Hz calibration signal was recorded on each data channel preceding each data acquisition run. These tapes were delivered to CAD for processing. The final data emanated in the form of cospectrum, quadrature spectrum, cross spectrum, and phase angle plots and alphanumeric tabulations.

Normal turaround time from sweep test to processed data was 24 hours. These data were examined and analyzed in order to determine optimum frequencies and effective excitation stations for subsequent narrow band modal tuning and modal dwell tests.

4.3.2.3.2 Test Techniques Narrow Band Modal Tuning - Wide band sweep data were examined for selection of a resonant frequency, and an optimum shaker configuration (based upon observed efficiency in the wide band sweeps). The largest quadrature value governed the selection of the reference exciter and its associated input accelerometer. The reference exciter was brought up to a preselected force value. The forcing function was then tuned over a narrow frequency band in order to obtain the desired 90 degree phase shift between force and the local input acceleration as indicated by a Lissajous figure display. When the master shaker force-acceleration relationship had been optimized, a second shaker was energized. This procedure was repeated until all shakers of the preselected array had been activated. Frequency tuning, and adjustments of force and phase relationships among the various shakers were repeated until the optimum force-acceleration relationships were obtained for all of the Lissajous patterns (up to twelve were displayed on three oscilloscopes). Concurrent with the Lissajous pattern tuning procedures, three computer controlled Houston Instrument (HI) Model DP-1 digital plotters described the accelerometer co-quad response curves for three preselected accelerometers in real time. Iterative adjustments of force, phase, and frequency among all of the shakers were continued until a maximum quadrature combined with the best co-quad relationship was obtained.

The multiple shakers were swept across a two or three hertz band centering about the resonant frequency. Co-quad plots were produced for various combinations of forces and accelerometers to assure optimum modal tuning.

When the force distribution was judged to indicate a condition of modal resonance, the forcing array was abruptly terminated. The decaying output signals of 16 preselected accelerometers were recorded on oscillograph records. Twelve of the 16 accelerometers were recorded on analog magnetic tape for later data processing at MMC.

If examination of the modal decays revealed freedom from frequency beating, the forcing distribution was reinstated and the AMTAS data acquisition function initiated. Once activated, AMTAS collected all pertinent data, stored these data on disk and produced these data on punched cards. AMTAS computed raw co-quad data for 200 servo-accelerometer positions, and provided these on tabular printout. Raw data were transformed to the model node points, normalized, and the generalized mass was computed and listed. Normalized deflections were computed and planar deflection plots digitally produced for all of the 200 accelerometer locations. Modal orthogonalities were computed and listed.

Examination of the decays, deflection plots, and orthogonality listing provided an assessment of the degree of modal purity attained. Based upon this evaluation, a decision to retune or move on to another frequency was effected.

4.3.2.3.3 Specimen Protection - The AMTAS exhibited an extensive capability to protect the vehicle from excessive force or motion conditions. A 16 channel force and 32 channel accelerometer summing detector monitored active exciter forces and 24 critical accelerometer locations. Exceedance of predetermined force or acceleration levels during test resulted in automatic reduction of input forces. In addition, 20 strain gages located at critical load points on the DA and MDA docking tunnel were continually sampled to detect excessive stress. When any strain gage channel exceeded preselected strain limits, automatic abort occurred. In addition, 14 of the 20 strain gages were recorded on an oscillograph during modal dwells, thus providing a basis to identify the magnitude and location of any over stress induced during test. Vertical overtravel in excess of 1.5 inches in any of the five test article suspension air springs also triggered an automatic abort.

4.3.2.4 Test Description - The following test description gives a detailed accounting of other test activities, problems and solutions.

4.3.2.4.1 AMTAS Checkout - Prior to test, and at frequent intervals throughout the test program, the AMTAS system was exercised to reveal any inconsistencies of a hardware or software nature. Hardware and software anomalies revealed during these system checks and corrected were:

a. Problem: Narrow band digitally controlled/acquired sweep co-quad plots displayed spikes at 0.1 Hertz intervals.
Correction: Loose connection within a module of the synthesizer controller was identified and corrected, resultant co-quad plots were free from 0.1 Hertz repetive spikes.

b. Problem: On the 1.43 Hertz run planar plots, several singularities inconsistent with the data trend appeared.
Correction: Sequence numbers 56, 62, 109 and 116 were checked for orientation of axes of sensitivity and calibration. Sequence number 109 (SE 536-900-X) on the service module (SM) forward bulkhead was found to be reading 20% higher. This accelerometer was replaced.

c. Problem: The unity co-quad plots indicated a polarity reversal for sequence number 138.
Correction: The punched card data deck was inspected. It was determined that a negative instead of plus sign had been punched on the sequence number 138 card. The card was repunched with the correct sign.

d. Problem: A number of dwells were aborted due to exceedance of the various strain gage limits.
Correction: A DC offset was detected in the signal conditioning equipment which caused erroneous triggering of the force acceleration summing detector. The signal conditioning devices were corrected.

4.3.2.4.2 Other Observed Test Malfunctions - As is natural in a program of this size, both human and machine malfunctions will occur. The following circumstances were responsible for aborted test runs during this problem.

Nature of Error	Frequency of Occurrence
Computer Core Dump Caused by Software or Peripheral Error	3
AMTAS Control (AMC) Error	2
Tektronix Beehive Mod MI Alpha Crt Malfunction	12
Data Channel Dropout	2
Air Spring Assembly Electrical Failure	1
Strain Gage Malfunction	1
Wrong Accelerometer Selected	2
Transducer Malfunction on ATM Air Spring Assembly	1
DC Offset in NEFF Amplifier	1
Mispatched False Accelerometer Limits	1
Plotter Scaling Factor Incorrect	4
Incorrect Accelerometer Identification Numbers on Plotters	3
Data not Retrievable from Core	2
Incorrect Computer Inputs	5
Frequency Synthesizer Failure	2
Stinger Resonance 04H	1
Master Attenuator Operator and Functional Malfunction	4
Synchon Errors or Malfunctions (Selection of Incorrect Channels)	1
Loose Ground Wire on Shaker 04H Overtravel Switch	1
Program Update Problem - Computer Software	1
Line Printer Failure	1
Scanner Channel Interpretation Malfunctions	3

In consideration of the scope and complexity of the overall project, both human errors and equipment malfunctions represented a very miniscule fraction of the overall testing process.

4.3.3 Alternate Test Approach - The following test outline for future test application is submitted for review and represents some refinement from the Skylab test. Each test activity is preceeded by a statement of the purpose of the test, which is then followed by the necessary data requirements.

Purpose: To determine the force and phase distribution necessary to fine tune preselected modes.

Activity: Wide band sweeps should be conducted without restricting the number of simultaneous shakers or requiring constant force input. The following information is required from pretest analysis for each wide band sweep

(1) frequency range

(2) number of shakers, location and phasing requirements

(3) selected mode frequencies

(4) mode shapes

(5) maximum input force distribution and reference force

(6) minimum instrumentation requirements for selected mode shape identification

Minimum Data Requirements: (1) CO/QUAD plots and tabulations

(2) force amplitude plots and tabulations

Notes:

1. If linearity data is required, additional wide band sweeps should be conducted using constant amplitude control.

2. If selected modes are not identified by this technique, it may be necessary to change shaker locations and/or select additional shakers to suppress coupled modes.

FINE TUNING MODES

Purpose: To fine tune selected modes; and to acquire data identifying each test mode for correlation with the analytical model.

Activity: Perform fine tuning by quadrature peaking and acquire dwell, narrow band sweep, and decay data for each mode. The following information is required from wide band sweep data for each mode prior to tuning

(1) shaker force distribution and phase

(2) mode frequency

(3) decay measurements

(4) general mode shape

The following verifications should be made for each mode acquired.

(1) linearity check

(2) force amplitude and frequency drift

Minimum Data Requirements:

(1) dwell CO/QUAD tabulations

(2) decay data

(3) narrow band CO/QUAD plots and tabulations for each mode required

Notes:

1. If mode verification is negative it may be necessary to retune the mode, using constant amplitude control and/or frequency control.

4.3.3.1 Test Comparisons and Conclusions - The foregoing test outline represents an attempt to refine test requirements, without affecting data quality. These refinements could result in reduced cost and minimum schedule impact on similar test programs.

Specific differences in the foregoing outline and the Skylab payload tests are as follows:

1. more emphasis is placed on the analytical model in the form of pre-test requirements;

2. wide band sweeps of individual shakers can be replaced with multiple shaker wide band sweeps;

3. fine tuning time can be reduced since wide band data would be more representative of actual tuning conditions and also, requires less data interpretation than the single shaker data approach;

4. the need for a totally automated control and data acquisition/reduction system can be optional;

5. data reduction requirements can be kept to a minimum.

4.4 PHASE III ADDITIONAL IU ACOUSTIC TESTS

Due to differences in the response of the FCC mass mock up when compared with the FCC Prototype, MSFC authorized additional Acoustic testing on the IU. This section will discuss the objectives, summarize the tests and make some conclusion based on the test results. Descriptions of test requirements, test facilities; Control and Data Systems, and Instrumentation summary will be omitted since they have not changed from the previous IU Acoustic Tests. Test descriptions have also been previously summarized and appear in Table 4.1 as PA-042 through PA-047.

4.4.1 Test Objectives - The following objectives were decided upon for these tests:

a. determine the effect of the 25 Hz horn upon IU vibration responses;

b. determine if the substitution of a prototype FCC in the IU for a mass mock-up FCC significantly changed vibration response levels measured during the previous acoustic testing. In addition, conduct sine-sweep tests to assess the modal density of the reverberant chamber.

4.4.2 Test Summary - Three random acoustic runs were conducted during this investigation. The first run was conducted for the purpose of obtaining IU response data with a prototype FCC installed in this IU. Data from this run, along with previously obtained data, allowed a comparison of the FCC-prototype response data to the mass mock-up response data. Run PA-A-043 subjected the test article to an environment representing the local IU liftoff environment. Control instrumentation and horn/modulator selection and programing duplicated that used during the previous IU liftoff acoustic test (PA-A-040).

The second run was conducted for the purpose of obtaining a set of IU response data with the 25 Hz horn deactivated. After deactivating the 25 Hz horn, two 50 Hz horns were programmed to produce the low frequency environment normally produced by the 25 Hz horn. PA-A-044 also subjected the test article to the IU liftoff environment. Comparison of the data obtained during this run to data obtained during PA-A-043 enabled data analysts to assess any effect of the 25 Hz horn upon FCC and other IU responses.

The third run (PA-A-045) was conducted to obtain IU responses to the aerodynamic environment. The horn/modulator selection and programming duplicated that used during the previous IU aerodynamic noise run (PA-A-041) with the minor exception that 2-W-100 replaced 1-W-100 in the horn selection.

Although slightly higher low-frequency sound levels were produced in this run series (PA-A-043 through PA-A-045) than obtained in the previous comparable run series (PA-A-040 and PA-A-041), the differences are within prescribed tolerances and allowable limits. However, response data comparisons from these two run series required careful adjustments to eliminate variations resulting from these differences.

In order to assess the reverberation chamber characteristics with the test article in place, two sine-sweep runs were conducted. A special closed-loop system (very similar to that used for modal vibration excitation) was used to control the SPL at the throat of the 25-Hz horn to a constant level. An initial sweep was made to obtain instrument ranging information. The sinusoidal sound pressure at the 25-Hz horn throat was varied over a frequency range of 19.98 to 99 Hz, and data from all microphones and accelerometers were recorded on run PA-A-047. Subsequently, data processing was performed to obtain plots of g's (peak) versus frequency or sound pressure in psi (peak) versus frequency.

4.4.3 Conclusions on Additional IU Testing -

a. Assessment of the sines weep Acoustic Data did not indicate the presence of any unusual reverberant chamber characteristics

b. FCC response data obtained after the installation of the Prototype FCC showed a significant decrease in response at 55 Hz with lesser changes at other frequences below 100 Hz.

c. Data assessment indicated that no significant change in ST-124 responses were produced by the Prototype FCC installation or horn selection (25-Hz versus 50-Hz horns)

5. DYNAMIC STRUCTURAL MODEL VERIFICATION

5.1 Pre-Test Modal Vibration Analysis

This section presents the results of the final pre-test modal analysis for the Configuration 6 (Orbit) modal survey test. Configuration 6 is defined as consisting of the OWS Forward Skirt and Dome, IU, FAS, MDA, STS, AM, CSM, deployed DA, deployed ATM with folded ATM solar arrays and laboratory suspension systems with associated test fixtures. The modal data presented herein represent the best available mass and stiffness representation of the Configuration 6 Dynamic Test Article (DTA). These data were generated primarily for the purpose of providing a final mass matrix for use in on-site orthogonality checks during modal survey testing. In addition, these modal data will also be used in on-site mode shape comparisons during testing. Figure 5.1 shows the components of this configuration.

5.1.1 Base Ring and Base Ring Suspension System Structural Models - The Base Ring Suspension System model is based on geometry and weight data provided informally by NASA/MSC. Three air springs are located at 120 degree intervals around the Base Ring. Axial spring rates for each air spring are based on a natural frequency of 0.5 Hz and the suspended weight. The weight suspended by the three Base Ring air springs does not include the ATM or the CSM since they are each supported by their own independent air suspension systems. Portions of the deployed DA weight were allocated to two suspension systems, per informal discussions with NASA/MSC. Seventy percent of the deployed DA weight was allocated to the Base Ring Suspension System and the remaining 30 percent was allocated to the ATM Suspension System. The total suspended weight acting at the Base Ring Suspension System was 78,458 pounds, divided among three springs. The lateral pendulum springs were calculated using this weight and a pendulum length of 104 inches. The final spring rates were assembled into three 3x3 grounded stiffness matrices, which were then rigidly transformed to the aft OWS Forward Skirt centerline collocation point at station 3100, using a radius from the centerline to the Base Ring suspension points of 154.73 inches. Finally, a negative spring constant of -16.8118×10^6 inch-pound/radian was added directly to the θ_y and θ_z degrees of freedom at station 3100 to account for the inverted pendulum effect of the weight supported by the Base Ring Suspension System. This negative spring constant was calculated using an estimated CG location at station 3314.28 for the supported weight.

5.1.2 OWS Forward Skirt, Dome and IU Structural Models - The OWS Forward Skirt Structural Model (see Figure 5.2) is based on the OWS stiffness distribution taken from the NASA memorandum, "Change to AAP-1 Structural Characteristics," J. H. Farrow, 31 August 1970, No. S&E-ASTN-ADS-70-33. The OWS Forward Skirt is modeled using three centerline

collocation points resulting in an 18x18 free-free stiffness matrix. The OWS Forward Skirt mass model was supplied by the MMC Weights Group and consisted of three 6x6 matrices and combined to form an 18x18 mass matrix. The IU Structural model is based on the IU stiffness distribution supplied by NASA-MSFC in May 1970. The IU is modeled using two centerline collocation points resulting in a 12x12 free-free stiffness matrix. The IU mass model was supplied by the MMC Weights Group in the form of two 6x6 mass matrices which were combined to form a 12x12 IU mass matrix. All mass data reflects DTA weights and c.g.'s provided by NASA/MSFC.

5.1.3 FAS Structural Model - The basic FAS mass and stiffness data used in this analysis was provided by McDonnell-Douglas Corporation in Transmittal Memorandum 646-E236-061471. In order to be compatible with the IU model, an equivalent centerline collocation point was generated at the IU interface by rigidly transforming the skin-line points provided in the original mass and stiffness at the IU interface. The skin-line points at the Payload Shroud interface on the FAS were reduced out for this vibration analysis because they will not experience any dynamic loads other than their own mass loading.

5.1.4 AM/STS/Truss Structural Model - Updated mass and stiffness data were provided by McDonnell-Douglas. The AM/OWS dome bellows torsional spring was added and the stiffness matrix relieved to yield a 61x61 free-free stiffness matrix. Corresponding mass data appears in ED-2002-1326. The model consists of 4 AM tunnel centerline nodes and the MDA/STS interface at 6 degrees of freedom each, plus 6 truss N_2 bottles and the 4 Truss/FAS interface points at 3 degrees of freedom each. The bellows/OWS-dome interface is represented as one torsional degree of freedom at MMC Station 2320.0 (see Figure 5.3).

5.1.5 MDA Structural Model - The MMC Stress Group supplied a 144x144 constrained flexibility matrix for the MDA. After inverting the flexibility matrix to obtain a stiffness matrix, the stiffness matrix was collapsed to a 48x48 stiffness matrix. The 48x48 matrix was reduced to a 12x12 matrix by use of rigid body transformations to obtain a centerline model of the MDA. The 12x12 matrix represents two grid points (MMC stations 3605 and 3545) with six degrees of freedom each. The 12x12 matrix was then relieved with respect to MMC station 3441.765, resulting in an 18x18 free-free stiffness matrix.

The MDA mass reflects actual DTA weight and CG as determined by the MMC Weights Group. The mass properties for the STS/AM were updated to reflect data provided in an informal memo from Paul Heaton, MDAC-East, to Wayne Ivey, NASA/MSFC, dated 30 December 1971.

5.1.6 Axial Port Structural Model - The axial port structural model is massless and consists of a 42x42 free-free stiffness matrix which was added to the CSM to interface with the MDA stiffness model.

5.1.7 Axially Docked CSM Structural Model - MMC received a 92x92 stiffness matrix of the total CSM from North American (see Figure 5.4). However, the DTA uses a CSM which has been modified in two respects: 1) the flight SM engine and bell was removed and replaced with a spaced stack of steel plates which approximately duplicates the weight and CG of the SM engine and engine bell; 2) the DTA SM is a stripped down version of the flight hardware. Extensive ballast was added to the SM and Command Module in order to match the flight CSM total mass, CG and roll inertia. It is not known whether the yaw and pitch inertias of the DTA CSM are significantly different from the CSM Structural Model used for this analysis. It is also not known whether the DTA ballast was attached so as to increase the overall stiffness of the SM. Since time and funds did not allow generating a new DTA CSM mass and stiffness model, the flight CSM mass and stiffness model was used with one change. The stack of spaced steel plates used on the DTA to represent the SM engine and bell are much stiffer than the equivalent flight engine hardware. Therefore, a rigid transformation was made to lump the SM engine mass and stiffness formerly collocated at station 3929.16 to the aft structural collocation point on the SM structure, located at station 3921.50 (see Figure 5.4).

5.1.8 ATM Spar/Canister Structural Model - The ATM Spar/Canister stiffness model was generated by the MMC Stress Group (see Figure 5.5). The mass model was generated by the MMC Weight Group based on DTA weight data supplied by NASA/MSFC in document S&E-ASTN-SAE(71-48).

5.1.9 ATM Gimbal Ring Assembly GRA Structural Model - The ATM GRA stiffness is included in the ATM Rack stiffness model, described in a later section. The mass matrix for the GRA structural model was calculated by the MMC Weights group to reflect actual DTA weight and CG. This 6x6 CG mass matrix was transformed in a least-squared best fit manner to the 12 translation degrees of freedom assigned to the four launch lock nodes on the ATM Spar/Canister mass model.

5.1.10 ATM Solar Arrays, Stowed (ATM-SAS) Structural Model - The ATM-SAS structural model was updated from a reduced 52x52 stiffness matrix supplied by Sperry Rand Space Support Division in transmittal memorandum SP-232-0579. A corresponding 52x52 diagonal mass matrix was also supplied. The ATM-SAS model included the ATM-SAS backup structure.

One vibration analysis of the ATM-SAS structural model was performed, in the ATM-SAS local coordinates. Then the resulting mode shapes and inertia loading matrices were transformed by geometrical transformations to the four bays of the ATM Rack. Thus, the DTA vibration model assumes that the four ATM-SAS panels are identical. However, the DTA has one flight version panel, one prototype flight panel, and two mass simulated ATM-SAS panels. By definition, the ATM-SAS vibration analysis structural model should represent the flight and prototype ATS-SAS panels used on the DTA. However, the two mass simulated panels used on the DTA ATM will naturally exhibit a different dynamic response than predicted by this vibration analysis.

5.1.11 Deployed ATM Rack Structural Model - The deployed ATM Structural Model is based on a 160x160 free-free stiffness matrix provided by the MMC Stress Group in January 1971. This stiffness matrix was collapsed to a 96x96 free-free stiffness matrix. The rollers and locks stiffnesses were added and the entire Gimbal Ring Assembly stiffness matrix was reduced to six degrees-of-freedom at the center. The spar/canister is considered to be rigid. The four undeployed solar arrays were also considered to be rigid. The ATM mass model was provided by the MMC Weights Group and formed into a 96x96 mass matrix. The masses for the four undeployed solar arrays were rigidly transformed to the six collocation points on the appropriate ATM bays resulting in four 18x18 solar array mass matrices which were added to the 96x96 ATM mass matrix. The ATM Rack mass model was updated by the MMC Weights Group to reflect actual DTA weight and CG data.

5.1.12 Deployed DA Structural Model - The deployed DA structural model is based on a 63x63 mass and stiffness matrix provided by McDonnell-Douglas Corporation Transmittal Memorandum 646-E236-070771.

5.1.13 ATM Suspension System Structural Models - Configuration 6 is suspended by air springs in the axial direction at five locations. Three of these are located at 120 degree intervals around the Base Ring. The CSM is suspended from the aft SM structure while the ATM is suspended at Bay 2. The point of suspension on the ATM was considered to be directly over the ATM center of gravity. Axial spring rates for each of the five suspension locations are based on a natural frequency of 0.5 Hertz and the suspended weight. In addition to the axial springs, restoring forces due to pendulum action were simulated by adding lateral springs in both lateral axes at the points of suspension. For small deflections, the lateral spring rates are equal to the suspended weight divided by the pendulum length of each individual suspension point. The final spring rates were assembled into five 3x3 grounded stiffness matrices. The stiffnesses for the three Base Ring suspension points were rigidly transformed to the aft OWS Forward Skirt centerline collocation point at station 3100.0. The ATM suspension stiffness was transformed in a least-squares manner and added to the ATM stiffnesses at the four corners of Bay 2. The CSM suspension system was added to the CSM stiffness at centerline station 3921.5. Since adequate suspension system data were not available at the time of this analysis, the pendulum length of each suspension point was assumed to 180 inches and the radii from the centerline to the Base Ring suspension points were assumed to be 150 inches. Suspension System Structural Model was updated. The ATM updated weights and geometry data were supplied informally by NASA/MSC. The ATM suspension system was modeled as a double pendulum similar to the basic concept used for the CSM suspension system. The upper pendulum consists of only a single pendulum bar which is 134.6 inches long and weighs 90 pounds. The lower end of the bar interfaces at a tie point node located at X = 3668.10, Y = 0.0, Z = -219.20, which is above the CG of the combined ATM Rack, Spar Canister, GRA and the four ATM-SAS panels.

From the ATM Suspension System tie point, four turnbuckles (2 short and 2 long) and associated shackles and adapter plates carry the suspension

system load to the four corners of the ATM Bay 2. Local 2x2 stiffness matrices for each of the four turnbuckles were calculated assuming that each was a steel bar with an area of 0.50 square inches. Direction cosine transformations were then used to add each local turnbuckle stiffness matrix to those degrees-of-freedom of the ATM Rack stiffness matrix corresponding to the appropriate corners of Bay 2.

The upper end of the pendulum bar is pinned to the ATM air spring beam and air cylinders. The ATM air spring beam and cylinders are only allowed to move vertically and have an approximate moving weight of 500 pounds. The remainder of the ATM suspension hardware is involved in the lateral pendulum spring calculations, with 491.3 pounds lumped at the tie point node at station 3668.10 and another 121.35 pounds is spread out to the four corners of Bay 2 on the ATM Rack.

The 0.5 Hz ATM vertical air spring is based on a vertical moving weight of 25,390.8 pounds, which includes 1185.9 pounds to represent 30 percent of the weight of the deployed DA, since only 70 percent is supported by the Base Ring Suspension System. The upper pendulum lateral springs, acting at the tie point node, are based on the 491.3 pounds upper pendulum weight, lumped at the tie point, plus 24,399.5 pounds for the lower pendulum.

The lower pendulum springs, acting at the combined CG of the ATM/30 percent DA/lower part of ATM Suspension System, are based on 24,399.5 pounds and a lower pendulum length (tie point to CG) of 122.77 inches. There is no substantial ATM rack structure at the combined CG location (X = 3545.33, Y = 0.0, Z = -219.20) so the lateral lower pendulum springs were transformed in a rigid body manner to the lateral degrees-of-freedom at the four corners of Bay 2 and of Bay 6.

A check vibration analysis was also made of the free-free ATM rack, mass loaded with the ATM Spar/Canister, GRA and four ATM Solar Arrays, and grounded by the ATM suspension system mass and stiffness models. The resulting first six rigid body modes are tabulated in Table 5.1.

5.1.14 CSM Suspension System Structural Model - The CSM Suspension System Structural Model was updated. The basic suspension system model was changed from a single pendulum analysis with a massless suspension system to a more realistic double pendulum analysis which included the weight and inertia added by the CSM Suspension System. Weight and geometry data were supplied informally by NASA/MSC. The CSM Suspension System consists of two 100 pound rigid bars 95.8 inches long which are each pinned to 100 pound fittings on the SM aft end. These fittings act at station 3939.2 and are considered to be located at $\pm Y$ = 75.0, Z = 0.0. The upper end of each of the rigid bars is pinned to a 150 inch long crossbeam which rests on the CSM plenum chamber air cylinders. The beam plus the moving air cylinders weigh approximately 600 pounds, with each of the six air cylinders weighing 23 pounds. A single 0.5 Hz axial air spring acts at the center of the crossbeam, with a total suspended weight of 30,772 pounds, of which 29,772 is the CSM. Because the

six air cylinders are interconnected to a common plenum chamber, there is no air spring restraint due to the crossbeam rocking about the θ_z axis. The mass and inertia effects of the crossbeam and air cylinders was accounted for by lumping the beam and air cylinders to mass collocation points at the center of each air cylinder plus the center and ends of the crossbeam. The vertical links and SM fittings were collocated at the ends of the crossbeam and at the pivot point of the fittings. Finally, a rigid body transformation was written to transform all of the suspension system mass collocation points to the aft end of the CSM, at station 3921.50.

Lateral upper pendulum springs, based on a pendulum length of 95.8 inches, were assumed to act at each outboard suspension fitting of the CSM. The ends of the crossbeam were assumed fixed in the Z direction. Each upper lateral pendulum spring carried one half of the CSM weight plus a SM suspension system fitting plus a load cell plus one-half of the vertical support bar.

The lower lateral pendulum was considered to extend from the suspension fitting pivot, at station 3939.2, to the CG of the CSM, at station 3791.64, for a lower pendulum length of 147.56 inches. The lower pendulum weight was the CSM weight. The lateral lower pendulum springs were rigidly transformed to act at the two closest SM centerline structural nodes, located at stations 3921.5 and 3766.50. A similar rigid body transformation was used to transform the upper lateral pendulum springs, acting at the outboard SM suspension fittings, to the centerline SM node at station 3921.5.

A check vibration analysis was made of the free-free CSM grounded by the air spring and the double pendulum springs. The first six modes and frequencies of this check run correspond to a rigid CSM restrained by its suspension system. These frequencies for the CSM suspension system are listed and identified in Table 5.2.

5.1.15 Discussion of Pretest Model - The vibration analysis reflects, as closely as possible, the properties of the actual DTA. However, some deficiencies in the model are known to exist and are noted as follows:

a. The flight CSM structural model, modified in this analysis to reflect use of a simulated SM engine and engine bell, would be a reasonable simulation of the actual DTA if flight type equipment and bracketry is used throughout the DTA CSM. However, unless sufficient care is exercised in the locations and method of attachment of all ballast used in the DTA CSM, the detailed dynamic response of the vibration analysis model and the DTA can be expected to differ, primarily at higher frequencies.

b. This vibration analysis assumed that all four ATM-SAS panels are identical and are representative of flight hardware.

However, the DTA uses two ATM-SAS panels which are mass simulated but not stiffness simulated. Again the local response of the DTA and the analytical models can be expected to differ womewhat, especially at higher frequencies.

c. The ATM Rack stiffness matrix includes the stiffness effects of all four outriggers. However, the outrigger on Bay 2 on the DTA is removed to make room for the ATM Suspension System hardware. The stiffness effect of the removed outrigger was not subtracted from the ATM Rack stiffness matrix because the necessary free-free stiffness matrix for a single outrigger was not provided. In addition, the stiffening effect of the outriggers in the Orbit Configuration are probably not significant compared to the main structure of the ATM Rack.

The total vibration model contains 630 net discrete degrees of freedom. Briefly, the coupled modes analysis was performed as follows: The CSM and CSM suspension system were modally coupled to the MDA/STS/AM which in turn was modally coupled to the "Main Beam" consisting of the Base Ring Suspension System, Base Ring, OWS Forward Skirt, IU and FAS. In addition, the ATM Spar/Canister and the four ATM Solar Arrays were modally coupled to the ATM Rack and GRA. The ATM Rack was modally coupled to the Deployment Assembly which, in turn, was modally coupled to the "Main Beam" at the FAS interface. (It should be noted that the FAS O_2 tanks stiffness or mass were not changed as a result of the Launch Configuration modal test which showed that these tanks respond analytically at higher frequencies than the test article).

The final coupled modes analysis contained 208 modal degrees of freedom based on the following component modes and cut-off frequencies:

Component	No. Modes	Cut-Off Frequency, Hz.
Main Beam	39	44.80
MDA/STS/AM	29	43.80
CSM	16	49.00
DA	19	41.96
ATM Rack/GRA	31	44.97
ATM SAS, Bay 1	13	38.53
ATM SAS, Bay 3	13	38.53
ATM SAS, Bay 5	13	38.53
ATM SAS, Bay 7	13	38.53
ATM Spar/Canister	22	43.84

The above component cut-off frequencies insure accurate coupled modes for the test range of 0 to 20 Hz. Degrees-of-freedom and location coordinates for the ten modally coupled branches are shown in Table 5.3. A description of the first 78 modes of the analytical model is provided in Table 5.4. The generalized mass contribution (GMC) for the total analytical model is presented in Table 5.5.

Prior to commencing the study to correlate the analytical and test modes, the coupled analytical modes were reduced to the 193 degrees of freedom shown in Table 5.3. The resulting analytical modes were then re-normalized in the same fashion and with the same mass matrix as the test modes. The re-normalized analytical modes were plotted (two-dimensional) and GMCs were determined. Table 5.4 contains brief descriptions of the first seventy-eight coupled analytical modes. The column headed "Generalized Mass" in Table 5.4 provides an indication of the adequacy of the representation of the original model by the reduced modes and reduced mass matrix. That is, if the representation were entirely adequate, the generalized masses would be unity for each mode. As can be seen, modes involving the ATM components are not well represented by the reduced system. This is attributable to a basic lack of ATM instrumentation, resulting in an insufficient number of DOF's in the ATM components.

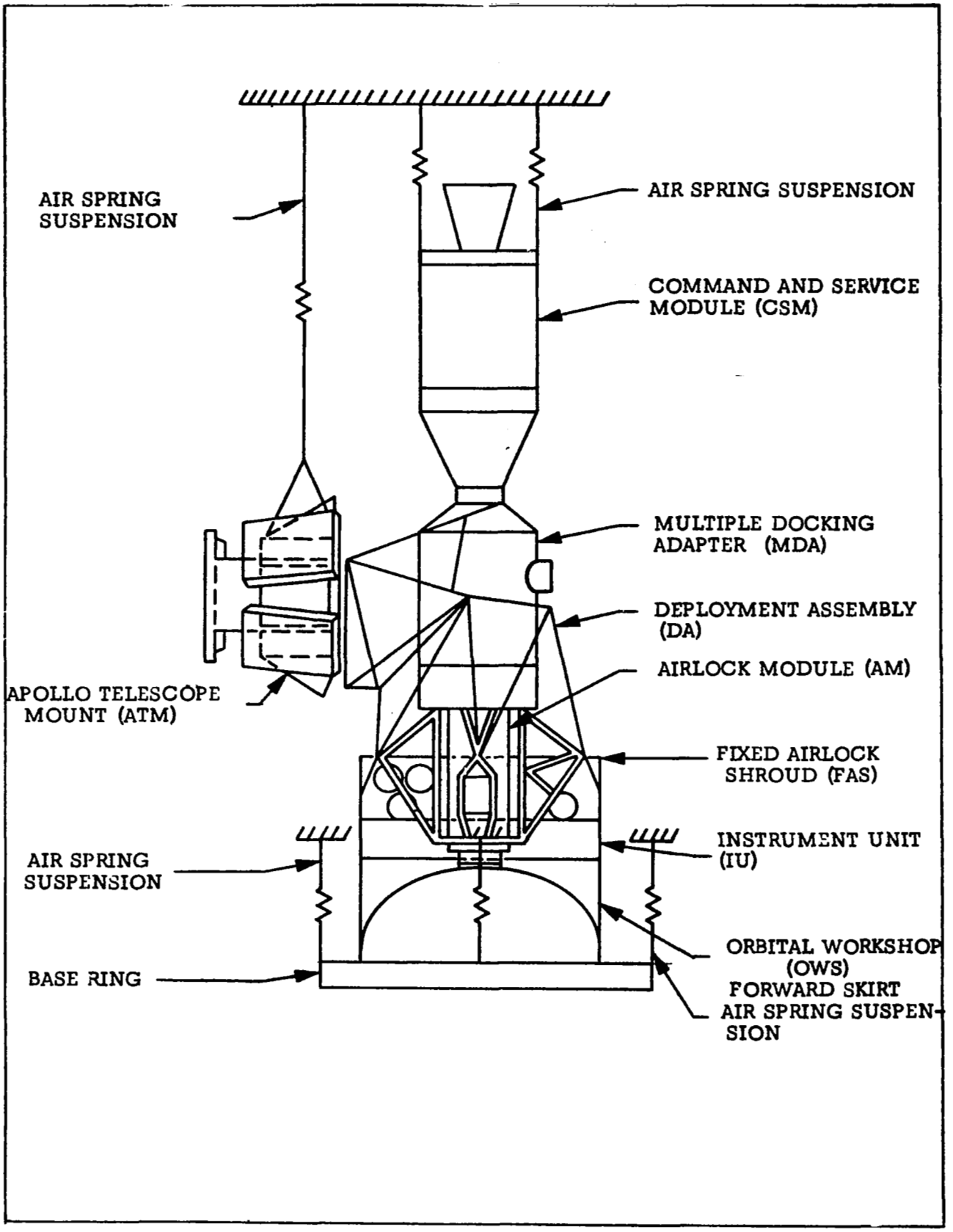

Figure 5.1 **Skylab A Orbital Configuration (Configuration 6) Test Setup Modal Survey Tests**

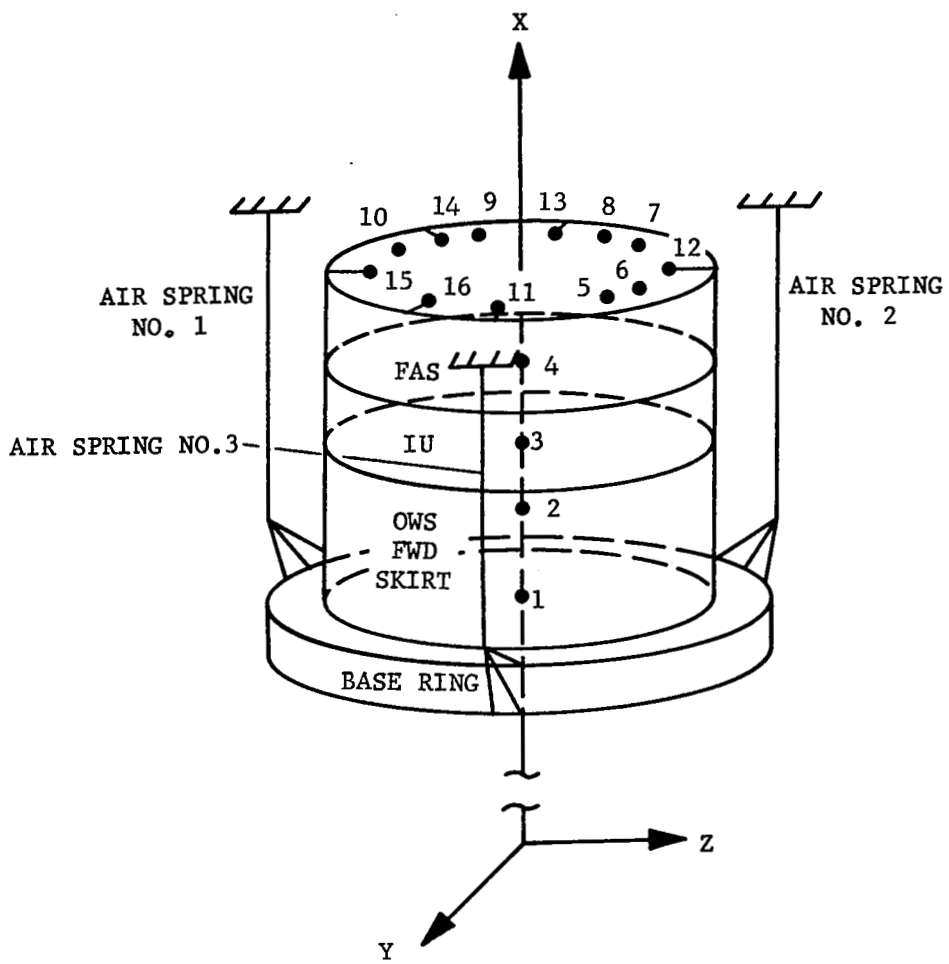

Figure 5.2 Base Ring/OWS Forward Skirt/IU/FAS Model for Configuration 6

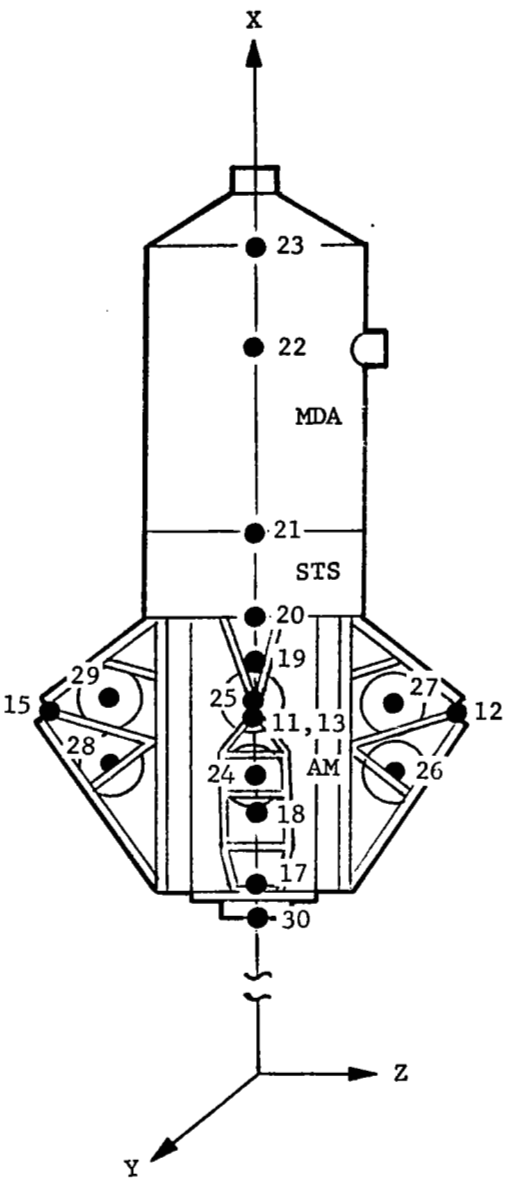

Figure 5.3 MDA/STS/AM Model

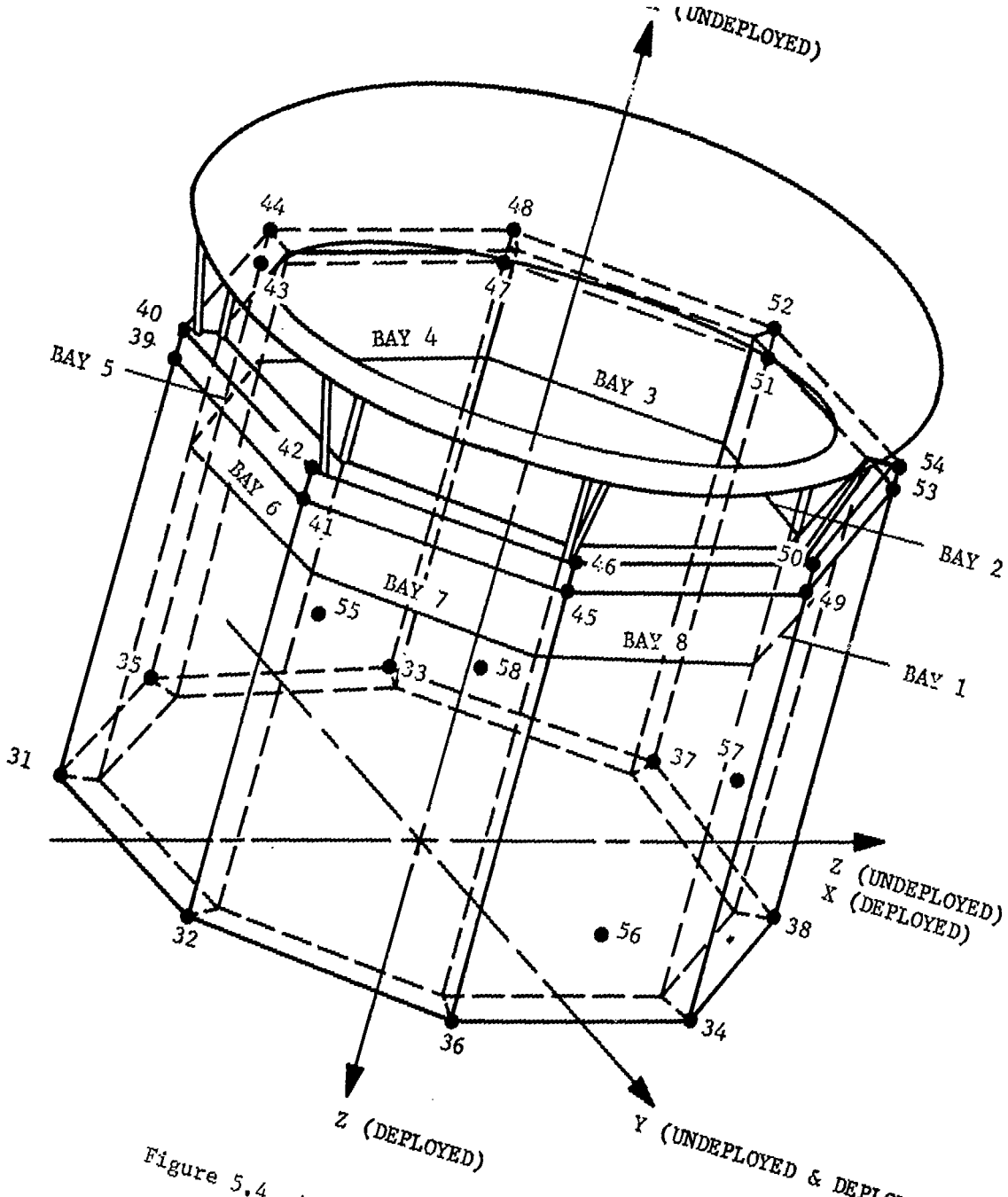

Figure 5.4 ATM Rack Model

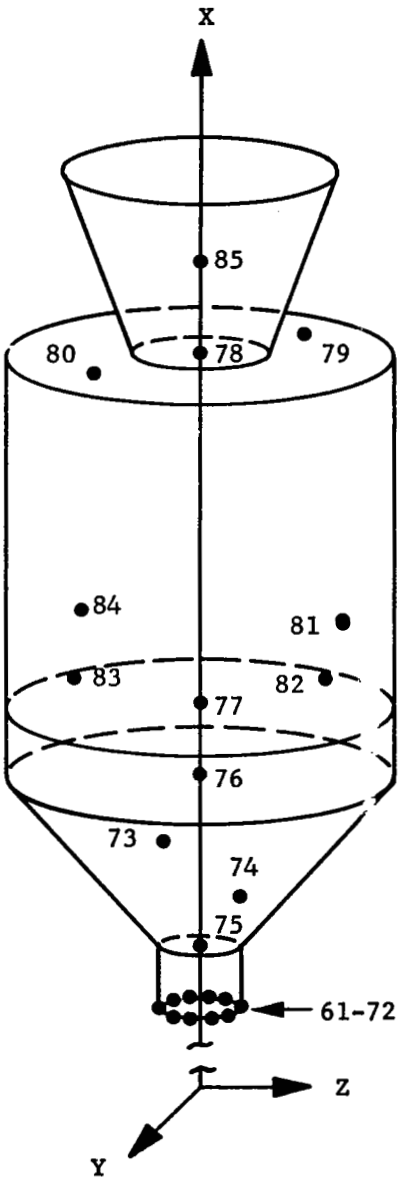

Figure 5.5 Axially Docked CSM

Table 5.1

IDENTIFICATION OF FIRST SIX NATURAL

FREQUENCIES FREE-FREE CSM ON DTA CSM SUSPENSION SYSTEM

Mode No.	Frequency, Hz	Comments
1	.1863	1st simple pendulum mode, mostly Y motion.
2	.1867	1st simple pendulum mode, mostly Z motion
3	.4363	θ_x rotation, mode, due to pair of lateral pendulum springs at outer skin.
4	.4997	Axial mode, on 0.5 Hz airspring
5	.6925	2nd pendulum mode, Y direction (primarily θ_z rotation about nearly stationary CG)
6	.7021	2nd pendulum mode, Z direction (primarily θ_y rotation about nearly stationary CG)

Table 5.2

IDENTIFICATION OF FIRST SIX NATURAL

FREQUENCIES FREE-FREE ATM ON DTA ATM SUSPENSION SYSTEM

Mode No.	Frequency, Hz	Comments
1	0.0000	θ_x rotation with no restraint
2	.1984	1st simple pendulum mode, primarily Y motion.
3	.2033	1st simple pendulum mode, primarily Z motion.
4	.5190	Axial mode, on 0.5 Hz air spring.*
5	.7546	2nd pendulum mode, Y direction (primarily θ_z rotation about nearly stationary CG)
6	.7749	2nd pendulum mode, Z direction (primarily θ_y rotation about nearly stationary CG)

*NOTE: This check run was made without any weight from the deployed DA. However the CSM Suspension System air spring is based on a suspended weight which includes 30 percent of the DA. Note that the 4th coupled mode for the total DTA is an axial suspension system mode at 0.489 Hz.

Table 5.3

ORBIT CONFIGURATION MODAL SURVEY
DEGREE OF FREEDOM TABLE FOR MODE SHAPES AND DISCRETE MASS MATRIX

NODE NO.	DEGREES OF FREEDOM DX	DY	DZ	TX	TY	TZ	LOCATION X	Y	Z	DESCRIPTION
1	1	2	3	4	5	6	3100.00	C.COC	0.00C	BASE RNG/CWS SKIRT
2	7	8	9	10	11	12	3223.000	0.000	0.000	CWS/IU INTERFACE
3	13	14	15	16	17	18	3258.555	C.COC	0.00C	IU/FAS INTERFACE
4	19	20	21				3316.555	81.473	46.683	FAS 02 BOTL1,+Y +Z
5	22	23	24				3316.555	46.683	81.473	FAS 02 BOTL2,+Y +Z
6	25	26	27				3316.555	-46.683	81.473	FAS 02 BOTL3,-Y +Z
7	28	29	30				3316.555	-81.473	46.683	FAS 02 BOTL4,-Y +Z
8	31	32	33				3316.555	-81.473	-46.683	FAS 02 BOTL5,-Y -Z
9	34	35	36				3316.555	-46.683	-81.473	FAS 02 BOTL6,-Y -Z
10	37	38	39				3341.615	116.050	0.000	FAS/AM/DA IF, +Y
11	40	41	42				3341.615	C.COC	116.060	FAS/AM/DA IF, +Z
12	43	44	45				3341.615	-116.060	0.000	FAS/AM/DA IF, -Y
13	46	47	48				3355.700	-82.346	-81.488	FAS/DA IF, -Y -Z
14	49	50	51				3341.615	0.000	-116.060	FAS/AM IF, -Z
15	52	53	54				3341.615	83.0143	-83.0143	FAS/DA IF, +Y -Z
16	55	56	57	58	59	60	3282.365	0.000	0.000	AM TUNNEL/SHEAR WB
17	61	62	63	64	65	66	3394.615	C.COC	0.000	AM TUNNEL/STS IF
18	67	68	69	70	71	72	3441.765	0.000	0.000	MDA/STS INTERFACE
19	73	74	75	76	77	78	3605.000	0.COC	0.000	MDA CONE/CYL ITRFC
20	79	80	81				3297.665	69.050	0.000	N2 TANK, +Y, LOWER
21	82	83	84				3348.365	69.050	0.000	N2 TANK, +Y, UPPER
22	85	86	87				3297.665	0.000	69.050	N2 TANK, +Z, LOWER
23	88	89	90				3348.365	C.COC	69.050	N2 TANK, +Z, UPPER
24	91	92	93				3297.665	0.000	-69.050	N2 TANK -Z, LOWER
25	94	95	96				3348.365	C.COC	-69.050	N2 TANK, -Z, UPPER
26	97	98	99	100	101	102	3678.000	0.000	0.000	CM, FWD BULKHEAD
27	103	104	105	106	107	108	3751.600	C.COC	0.00C	CM, AFT BULKHEAD
28	109	110	111	112	113	114	3766.500	0.000	0.000	SM, FWD BULKHEAD
29	115	116	117	118	119	120	3921.500	C.000	0.000	SM, AFT BULKHEAD
30	121	122	123				3454.765	0.000	-90.000	LOWER D LATCH, DA
31	124	125	126				3532.915	113.500	-11.850	LOWER +Y TRUNNION
32	127	128	129				3532.915	-113.500	-11.850	LOWER -Y TRUNNION
33	130	131	132				3418.765	0.00C	100.000	EREP PACKAGE C.G.
34	133	134	135				3479.094	27.299	-252.500	ATM PN 6,7 IF,OUTR
35	136	137	138				3517.701	-65.906	-252.500	ATM PN 4,5 IF,OUTR
36	139	140	141				3572.299	65.905	-252.500	ATM PN 8,1 IF,OUTR
37	142	143	144				3610.906	-27.299	-252.500	ATM PN 2,3 IF,OUTR
38	145	146	147				3479.094	27.299	-158.000	ATM PN 6,7 IF,INNR
39	148	149	150				3517.701	-65.906	-158.000	ATM PN 4,5 IF,INNR
40	151	152	153				3572.299	65.906	-158.000	ATM PN 8,1 IF,INNR
41	154	155	156				3610.906	-27.299	-158.00C	ATM PN 2,3 IF,INNR
42	157	158	159	160	161	162	3545.000	-65.906	-181.9925	CMG, -Y SIDE
43	163	164	165	166	167	168	3545.000	67.834	-181.995	CMG, +Y SIDE
44	169	170	171	172	173	174	3610.906	0.000	-182.000	CMG, +X SIDE
45	175	176					3599.9301	54.9301	-207.490	ATM SAS, PN 1
46	177	178					3599.9301	-54.9301	-207.490	ATM SAS, PN 3
47	179	180					3490.0699	-54.9301	-207.490	ATM SAS, PN 5
48	181	182					3490.0699	54.9301	-207.490	ATM SAS, PN 7
49	183	184	185	186	187	188	3545.000	C.00C	-240.709	SPAR CENTER
50	188	189	190	191	192	193	3545.000	0.000	-240.709	GRA/CAN CENTER

Table 5.4 Orbital Configuration (DTA) Coupled Analytical Modes

COUPLED MODE NO.	FREQUENCY, HZ.	GENERALIZED MASS	DESCRIPTION
1-6	0.28 - 0.51	1.0	Suspension System (rigid body) Modes.
7	1.37	1.0	First X-Z plane bending about MDA/CSM I/F, ATM rocking in X-Z plane out of phase with CSM.
8	1.57	.98	First X-Y plane bending about MDA/CSM I/F, ATM rocking in X-Y plane out of phase with CSM.
9	1.96	.95	First X-Y plane bending about MDA/CSM I/F, ATM rocking in X-Y plane in phase with CSM.
10	1.99	.99	First X-Z plane bending about MDA/CSM I/F,ATM rocking in X-Z plane in phase with CSM.
11	2.66	.99	Vehicle roll and first torsion coupled with X-Y plane first bending about MDA/CSM I/F, ATM X-Y plane rocking in phase with top of CSM.
12	3.25	.98	Vehicle first torsion with CSM, MDA/STS/AM out of phase with FAS/IU/OWS. Vehicle X-Y plane bending.
13	3.52	.99	First X-Z plane bending with ATM Z motion in phase with top of CSM.
14	4.93	.50	ATM rigid rotation about X-axis coupled with some vehicle X-Y plane second bending.
15	5.32	.26	ATM rigid rotation about X-axis coupled with vehicle X-Y plane second bending about CSM/MDA and STS/AM I/Fs.
16	5.76	.48	Vehicle X-Y plane second bending about CSM/MDA and STS/AM I/Fs, ATM X and Z rotations, GRA/Can Z rotation out of phase with ATM.
17	6.03	.95	ATM Rack rotation about Y axis with vehicle X-Z plane second bending.
18	6.79	.86	ATM Rack rotation about X axis with vehicle X-Y plane and some X-Z plane second bending.
19	7.04	.96	Vehicle X-Z plane second bending about CSM/MDA and STS/AM I/Fs. Significant DA-EREP Z motion.
20	7.70	.99	DA-EREP mode in Z direction with some X motion. Small vehicle second bending in both planes.
21	8.03	.31	GRA/Canister center torsion (rotation about Z).
22	8.51	.51	ATM Solar Arrays mode (out of plane motions of all four arrays).
23	8.62	.98	DA-EREP mode in Y direction coupled with Y and Z motions of FAS tanks.
24	8.69	.54	ATM Solar Arrays mode (out of plane motions of all four arrays).
25	8.89	.68	ATM Solar arrays out of plane motions coupled with DA-EREP Y motion and FAS Tanks Y and Z motions.
26	8.95	.57	ATM Solar Arrays mode (largely out of plane motions of panels 1 and 2 arrays).

Table 5.4 Orbital Configuration (DTA) Coupled Analytical Modes (Continued)

COUPLED MODE NO.	FREQUENCY, HZ.	GENERALIZED MASS	DESCRIPTION
27	9.03	.99	MDA/STS/AM and CSM rocking and translation (largely in X-Y) about AM trusses with CSM bending about MDA/CSM I/F.
28	9.10	.88	FAS Tanks Y and Z motions, DA-EREP Y motion with some out of plane motions of all four ATM Solar Arrays.
29	9.27	.97	FAS Tanks Y and Z motions (largely Tank 3 in Y and Tank 4 in Z).
30	9.38	.64	Vehicle first axial mode (largest motions in CSM).
31	9.40	.38	Similar to Mode 30 with slightly smaller axial responses.
32	9.59	.99	FAS Tanks Y and Z motions (largely Tanks 1, 3 and 4).
33	9.71	.99	FAS Tanks Y and Z motions (largely Tanks 2 and 6 in Y and Tanks 1 and 5 in Z).
34	9.90	.24	GRA/Canister Torsion (rotation about Z), some FAS Tanks motions in Y and Z.
35	9.95	.92	FAS Tanks Y and Z motions coupled with some rocking and translation of MDA/STS/AM about AM trusses in both planes.
36	10.28	.99	Vehicle second torsional mode with FAS tanks Y and Z motions (some X)
37	10.66	.01	Largely rigid translational motion of ATM in Z direction relative to I/F with DA.
38	12.63	.94	Rocking, translation, bending (X-Y plane) and torsion of CSM, MDA/STS/AM about AM trusses coupled AM Tanks Y motions and FAS Tanks Z, Y and X motions.
39	12.75	.89	Vehicle third torsional mode with some AM tanks Y motions and FAS tanks X, Y and Z motions.
40	12.91	.98	Largely AM Tanks (+Z upper and lower tanks) with some FAS tanks motions in all three directions. Some DA trunions Y and Z.
41	13.01	.19	Largely Y motions of AM Tanks (+Y upper and lower tanks), FAS tanks in all three directions with local deformations of ATM Rack. Out of phase rocking of GRA/Can and Spar about Y axis.
42	13.28	.20	AM Tanks Y and Z motions, Vehicle third bending in X-Z plane. Out of phase rocking of GRA/Can and Spar about Y axis.
43	13.40	.89	Vehicle X-Z plane third bending with large X-Z plane shear motion at CM/SM I/F.
44	13.52	.02	ATM rocking about Y axis with respect to DA interface, GRA/Can. and Spar out of phase X translation and Y axis rocking.

Table 5.4 Orbital Configuration (DTA) Coupled Analytical Modes (Continued)

COUPLED MODE NO.	FREQUENCY, HZ.	GENERALIZED MASS	DESCRIPTION
45	13.70	.06	ATM rocking about Y axis with respect to DA interface, GRA/Can. rocking about Z axis (torsion).
46	13.78	.14	ATM rocking about X and Y axes, AM Tanks Y motions, some vehicle X-Z plane third bending, GRA/Can rocking about Z.
47	13.97	.82	Vehicle third bending in both planes (largely X-Y), AM Tanks Y and Z motions (largely Y) complex torsion of entire vehicle, DA trunnions Y and Z motions.
48	14.08	.73	Largely DA trunnion Y and Z motions (mostly Z) with X-Y plane vehicle third bending, some AM Tanks Y and Z motions.
49	14.47	.99	Largely AM Tanks Z motions.
50	14.52	.30	ATM Solar Arrays out of plane motions of all four arrays.
51	14.61	.30	ATM Solar Arrays out of plane motions of all four arrays.
52	14.62	.31	ATM Solar Arrays out of plane motions of panels 1 and 5 arrays.
53	14.64	.32	ATM Solar Arrays out of plane motions of panels 3 and 7 arrays.
54	14.97	.98	AM Tanks Y motions (largely +Y upper and +Z lower tanks) with vehicle X-Y plane third bending.
55	15.56	.55	ATM rocking with respect to DA about Y axis with some ATM translation in X direction. GRA/Can and Spar out of phase Y axis rocking.
56	15.57	.99	AM Tanks Z motions (largely +Z upper and lower and -Z upper tanks).
57	15.64	.98	AM Tanks Y motions (largely +Y upper and lower tanks).
58	15.69	.98	AM Tanks Z motions (largely +Z and -Z upper and lower tanks).
59	16.15	.99	AM Tanks Z motions (largely +Y and -Z lower tanks).
60	16.57	.37	ATM rocking about X axis, translation in Y. GRA/Can and Spar rocking out of phase about X axis.
61	16.80	.14	ATM rocking about X and Y axes, GRA/Can. and Spar rocking out of phase about X axis.
62	16.95	.99	AM Tanks Y motions (largely +Z lower tank).
63	17.17	.17	ATM Solar Arrays out of plane motions of all four arrays.
64	17.20	.16	ATM Solar Arrays out of plane motions of panels 1 and 5 arrays.
65	17.27	.17	ATM Solar Arrays out of plane motions of all four arrays.
66	17.31	.25	ATM Solar Arrays out of phase motions of panels 3 and 7. Some GRA/Can. and Spar out of phase X and Y rotations.
67	17.54	.98	Largely AM Tanks Z motions (mostly +Y lower tank).
68	18.01	.95	FAS Tanks motions (mostly X), some AM Tanks Y motions.

Table 5.4 Orbital Configuration (DTA) Coupled Analytical Modes (Continued)

COUPLED MODE NO.	FREQUENCY, HZ.	GENERALIZED MASS	DESCRIPTION
69	18.32	.93	FAS Tanks X motions, AM Tanks Y motions (mostly -Z lower tank).
70	18.35	.20	GRA/Can. and Spar out of phase translations in X and rotations about Y. ATM Rack and CMGs X translation.
71	18.65	.96	FAS Tanks X motions coupled with AM Tanks Y motions (largely -Z lower tank).
72	18.75	.04	+Y and -Y CMGs Y motions, +X CMG X motion, -Y CMG rotation about X, FAS Tanks X motions, AM Tanks Y motions.
73	18.80	.01	GRA/Can. and Spar out of phase rotations about Y and translations in X and Y. -Y CMG Y motion, +X CMG rotation about Z.
74	18.82	.01	X motions of ATM Rack and CMGs, out of phase rotations about Y of GRA/Can. and Spar.
75	18.85	.00	ATM rack rotations about X and Z with translation in Z. GRA/Can. and Spar out of phase rotations about Y and Z.
76	18.88	.99	AM Tanks Y motions (almost all -Z upper tank).
77	19.51	.94	Vehicle second axial mode.
78	19.53	.30	ATM rack rotation about Y with Y deformations. GRA/Can and Spar out of phase Y translations and rotations about Y. Some vehicle second axial mode.

Table 5.5

ORBITAL CONFIGURATION ANALYTICAL MODES GMC SUMMARY

MODE NO.	FREQ, HZ.	GMC (DX)	GMC (DY)	GMC (DZ)	GMC (TX)	GMC (TY)	GMC (TZ)
1	.28	.0048	.9919	.0002	.0006	.0000	.0025
2	.29	.0055	.0021	.9887	.0015	.0021	.0000
3	.36	.0032	.5771	.1128	.3062	.0001	.0007
4	.48	.8773	.0334	.0811	.0001	.0053	.0028
5	.50	.0598	.6076	.2807	.0009	.0165	.0345
6	.51	.2126	.2849	.4598	.0000	.0271	.0156
7	1.37	.3078	.0020	.6548	.0019	.0335	.0000
8	1.57	.1170	.7103	.0309	.0761	.0000	.0657
9	1.96	.2668	.4774	.1136	.0794	.0034	.0594
10	1.99	.4857	.0569	.4053	.0078	.0385	.0059
11	2.66	.0118	.2920	.0265	.6490	.0002	.0205
12	3.25	.0048	.3387	.1054	.5412	.0000	.0099
13	3.52	.0135	.0200	.9190	.0042	.0431	.0001
14	4.93	.0508	.4831	.1396	.0830	.0006	.2430
15	5.32	.1210	.6200	.1121	.0581	.0045	.0843
16	5.76	.1185	.5725	.0077	.0116	.0003	.2895
17	6.03	.3245	.0541	.4456	.0011	.1740	.0006
18	6.79	.1435	.5559	.1390	.0911	.0065	.0640
19	7.04	.1175	.0639	.6948	.0053	.1167	.0017
20	7.70	.1286	.0191	.8331	.0013	.0178	.0001
21	8.03	.0527	.0529	.0013	.0045	.0009	.8878
22	8.51	.4984	.5012	.0002	.0001	.0000	.0092
23	8.62	.0293	.7239	.2074	.0387	.0003	.0004
24	8.69	.4612	.5004	.0377	.0005	.0002	.0000
25	8.89	.2604	.5858	.1219	.0263	.0028	.0028
26	8.95	.5106	.4234	.0324	.0036	.0290	.0011
27	9.03	.0194	.2259	.1620	.5923	.0003	.0002
28	9.10	.0865	.5011	.3482	.0454	.0121	.0067
29	9.27	.0243	.4857	.4782	.0014	.0078	.0026
30	9.38	.9286	.0297	.0320	.0002	.0043	.0053
31	9.40	.8793	.0402	.0346	.0000	.0043	.0415
32	9.59	.0590	.4410	.4807	.0167	.0020	.0006
33	9.71	.0319	.5053	.4602	.0019	.0003	.0004
34	9.90	.1157	.2329	.1993	.0108	.0006	.4407
35	9.95	.0646	.4980	.3705	.0522	.0021	.0126
36	10.28	.0721	.2458	.2473	.4332	.0013	.0003
37	10.66	.0387	.1059	.8491	.0033	.0028	.0001
38	12.63	.0550	.5142	.1274	.2793	.0062	.0178
39	12.75	.0520	.3825	.1231	.4164	.0130	.0131
40	12.91	.0707	.1815	.6398	.0784	.0278	.0018
41	13.01	.1315	.6245	.1475	.0166	.0556	.0242
42	13.28	.1126	.2655	.4298	.0212	.1376	.0333
43	13.40	.0173	.1296	.7433	.0434	.0574	.0091
44	13.52	.4343	.1821	.0936	.0532	.1350	.1018
45	13.70	.3048	.2764	.2319	.0312	.0459	.1099
46	13.78	.2541	.3779	.2477	.0154	.0179	.0870
47	13.97	.0108	.5582	.2820	.1315	.0037	.0144
48	14.08	.0329	.5079	.4104	.0294	.0028	.0166
49	14.47	.0270	.0559	.8911	.0031	.0226	.0002
50	14.52	.4989	.4973	.0022	.0008	.0003	.0006
51	14.61	.5001	.4999	-.0005	.0000	.0005	.0000
52	14.62	.5109	.4591	-.0002	.0006	.0285	.0010

Table 5.5 (CONTINUED)

ORBITAL CONFIGURATION ANALYTICAL MODES GMC SUMMARY

MODE NO.	FREQ, HZ.	GMC (DX)	GMC (DY)	GMC (DZ)	GMC (TX)	GMC (TY)	GMC (TZ)
53	14.64	.4795	.5158	.0008	.0014	.0023	.0002
54	14.97	.0348	.8703	.0395	.0148	.0052	.0354
55	15.56	.3457	.1372	.1141	.0079	.3925	.0027
56	15.57	.0090	.0015	.9815	.0005	.0074	.0001
57	15.64	.0096	.9246	.0567	.0007	.0059	.0024
58	15.69	.0117	.0440	.9345	.0006	.0091	.0002
59	16.15	.0155	.0169	.9587	.0034	.0054	.0000
60	16.57	.0499	.4226	.0417	.4187	.0579	.0092
61	16.80	.1571	.4574	.0315	.3053	.0453	.0034
62	16.95	.0251	.9211	.0247	.0205	.0002	.0084
63	17.17	.4974	.4998	.0004	.0006	.0000	.0017
64	17.20	.5001	.5001	-.0020	.0007	.0009	.0002
65	17.27	.4712	.4773	.0510	.0003	.0001	.0001
66	17.31	.3233	.4216	.0393	.1614	.0521	.0023
67	17.54	.0241	.0181	.9198	.0030	.0349	.0001
68	18.01	.5485	.2859	.1594	.0037	.0023	.0002
69	18.32	.3614	.5521	.0761	.0030	.0044	.0030
70	18.35	.3412	.2319	.0608	.0657	.2692	.0312
71	18.65	.3569	.5409	.0979	.0048	-.0015	.0010
72	18.75	.4512	.4217	.0725	.0444	.0088	.0013
73	18.80	.2167	.3307	.0360	.1014	.2856	.0297
74	18.82	.3766	.0407	.0208	.0098	.5355	.0166
75	18.85	.5164	.2746	.0112	.0629	.1000	.0349
76	18.88	.0114	.9506	.0153	.0204	.0001	.0021
77	19.51	.8851	.0347	.0702	.0034	.0062	.0004
78	19.53	.2600	.2667	.0395	.1390	.2912	.0036
79	20.07	.0724	.0931	.8106	.0139	.0082	.0018
80	20.19	.0117	.8638	.0863	.0256	.0008	.0116
81	20.46	.2507	.3762	.0836	.2265	.0438	.0192
82	20.57	.3175	.4221	.0203	.2289	.0055	.0057
83	20.58	.3738	.4254	.0441	.1220	.0332	.0015
84	20.61	.3582	.4156	.0781	.1317	.0160	.0004
85	20.65	.3655	.4123	.0592	.1494	.0105	.0031
86	21.25	.7431	.0892	.0657	.0990	.0004	.0026
87	21.47	.4724	.2038	.1017	.2133	.0063	.0025
88	21.68	.2485	.1948	.0463	.0837	.0723	.3545
89	21.78	.3218	.1547	.1190	.1510	.0209	.2331
90	22.06	.4305	.2477	.1009	.0728	.0357	.1124
91	22.22	.0573	.1747	.0138	.0799	.0422	.6322
92	22.35	.3732	.3150	.1810	.0892	.0352	.0065
93	22.65	.2957	.3032	.0331	.3065	.0548	.0067
94	23.09	.3976	.1329	.0761	.0899	.0841	.2193
95	23.19	.7053	.1414	.1334	.0043	.0126	.0031
96	23.41	.1286	.2615	.0956	.2697	.2004	.0443
97	23.63	.2485	.5337	.1523	.0567	.0031	.0056
98	24.02	.8577	.0200	.0873	.0174	.0169	.0008
99	24.27	.3978	.3210	.0188	.1030	.1524	.0071
100	24.29	.8659	.0761	.0082	.0253	.0197	.0049
101	24.82	.2772	.3519	.0675	.2363	.0152	.0519
102	25.15	.0575	.0897	.0266	.8200	.0019	.0043
103	25.60	.5044	.2117	.0561	.0248	.0032	.1998
104	25.67	.7959	.1060	.0409	.0111	.0055	.0036

5.2 Discussion of Test Modes

Thirty valid test modes were acquired during the Orbital Configuration modal survey. A list of these modes arranged in order of ascending frequencies is presented in Table 5.6. It will be noted that test run no. 400 has been deleted because it contained invalid data in the ATM area of the structure.

It can be seen in Table 5.6 that twenty-five unique modes were obtained ranging in frequency from 0.31 Hz through 17.01 Hz which represent all the major resonances which could be identified in the 0 to 20 Hz test range. The remaining five modes represent the results of efforts to retune some of the original modes to yield better orthogonality between modes. The reduction and normalization of data, modal characteristics and purity of the Table 5.6 modes are discussed below.

5.2.1 Reduction of Data - Reduction of data consisted of "translating" the acquired quadrature data for each test mode to specific collocation points using rigid body or "least square" mathematical transformations. The specific collocation points correspond to points selected from the pretest modal vibration analysis. The degrees of freedom corresponding to the reduced data and identical to the model DOF's are shown in Table 5.3. It will be noted that the Table 5.3 data define 193 reduced degrees of freedom but the original quadrature test data were for 200 degrees of freedom. This is explained as follows: The six accelerometers located on the outboard ends of the ATM outriggers were deleted for purposes of defining mode shapes. The primary purpose of these accelerometers were to provide reference accelerations for the six force shakers located on the outriggers. The outrigger accelerometers could not be utilized in a manner which would provide useful additional shape information. In addition, data from the five accelerometers located on the ATM Canister were deleted (three on the sun end, two on the MDA end). Instead of defining Canister motion separately, a new six degree of freedom collocation point was defined at the same geometrical location as the Spar Center. This point was defined as the GRA (Gimbal Ring Assembly)/Canister Center with motion given by the six accelerometers located on the GRA. The Spar Center point has five degrees of freedom defined by the five accelerometers located on the top and bottom of the Spar. The data deletions mentioned above total eleven resulting in 189 basic degrees of freedom. Since the ATM solar array uniaxial accelerometers were mounted in the plane of each folded array, transformation of each accelerometer to launch vehicle coordinates (X and Y) was necessary resulting in an additional four degrees of freedom bringing the total for reduced data to 193.

5.2.2 Normalization of Data - After reducing the data as described above, the results were normalized to a 193 by 193 discrete mass matrix. The normalization was performed in a manner which yielded unity generalized mass for each mode. This normalization technique is convenient for orthogonality calculations, determination of generalized mass contributions (GMCs) and comparison with analysis. The 193 by 193 mass matrix was derived from

analytical mass matrices which were available for each of the various structural components comprising the analytical model. The method for deriving the mass matrix consisted of static collapse of the component matrices to the 193 degrees of freedom contained in Table 5.3. The results were merged to form the final 193 by 193 matrix. Subsequent calculations involving this matrix and the mode shape data has shown it to have inadequate definition in the area of the ATM. This is attributed to a basic lack of definition of ATM motion caused by the limited number of accelerometers available for use on the ATM during testing. Since it is an extremely complex structure, the instrumentation required to define ATM motion adequately would have gone beyond practical limitations or resulted in sacrifices in other important areas of the structure.

5.2.3 Orthogonality of Test Modes - In order to determine the relative purity of each test mode and determine if a re-tuned mode yields a purer mode than the original tuned mode, orthogonality calculations were performed. The results represent the standard triple matrix product of normalized modes and the kernel mass matrix described above. This triple matrix product yields a 30 by 30 symmetrical orthogonality matrix containing a unity diagonal with the off-diagonal terms representing the amount of inertial coupling between modes as a fraction of the unity generalized masses. When multiplied by 100.0, the numbers in this matrix can be thought of as percentages. A summary of the data is shown in Table 5.7. The Table 5.7 data indicates generally excellent orthogonality between modes. Mode 15A exhibits excessive coupling with other modes (particularly Mode 14A) and is obviously not well isolated enough to be considered for use in correlation studies. Mode 02A (suspension system mode) contains apparent bad data at two accelerometers on the Base Ring/OWS interface (sequence nos. 1 and 3) causing apparent coupling with other modes. However, Mode 02A is a well-tuned mode. It should also be noted that mode 20A was not well isolated from mode 19A (32.4% coupling).

In the five cases of re-tuned modes, the orthogonality results show:

a. mode 06B is a purer mode than 06A,
b. mode 10A has slightly higher average coupling but slightly lower standard deviation than mode 10B, and is therefore slightly more well tuned,
c. mode 13B is purer than mode 13A,
d. mode 18A is purer than mode 18B,
e. mode 22B is purer than mode 22A.

Therefore, modes 06B, 10A, 13B, 18A and 22B will be used for correlation studies.

5.2.4 Characteristics of Test Modes - There are twenty-five unique modes contained in the thirty test runs given in Table .6. The unique modes are briefly described in Table 5.8. Most of the modes are highly

coupled modes involving motion throughout the structure while a few do have dominant local motions. GMCs based on the 193 by 193 discrete mass matrix were determined for each of the 193 degrees of freedom contained in Table 5.3 for every test mode. In addition, GMCs for the major components comprosing the configuration were calculated. The major components are considered to be the following:

a. Base Ring/OWS Skirt/IU/FAS,
b. 6-FAS O_2 Tanks,
c. MDA/STS/AM,
d. 6-AM N_2 Tanks,
e. Command/Service Module,
f. Deployment Assembly,
g. ATM Rack with CMGs and Solar Arrays,
h. ATM Spar,
i. ATM GRA with Canister.

Table 5.9 shows a summary of GMCs for each of the thirty test modes as an aid in determining the general nature of the test modes. It should be noted that the GMCs for Mode 02A are distributed improperly due to the bad accelerometer data previously noted. A redistribution would show most of the GMC concentrated in the X-Y Plane. Two-dimensional plots for each of the thirty mode shapes are presented in Volume II. The Volume II plots represent the translated and normalized test quadrature data.

As opposed to the Launch Configuration test modes, the Orbital Configuration test modes do not exhibit local motions relative to the various component centerlines. However, these modes do exhibit characteristic large relative deflections in most degrees of freedom in the CSM from the MDA interface forward through the CM/SM interface. These deflections occurred in the suspension system modes (Modes 01A and 02A) as well as the higher frequency modes.

5.3 Correlation of Test Modes with Analytically Predicted Modes

The following paragraphs present the methods, supporting data and the results of the study to correlate the test modes.

5.3.1 Methods of Correlation - Test and analytical GMCs and two-dimensional mode shape plots were compared. However, since the Orbital Configuration test modes did not indicate significant local deformation which were not measured (as was not the case for the Launch Configuration) two supporting correlation techniques became available: the first of these is the cross-orthogonality check in which a triple matrix product is formed using the transpose of the normalized test modes as the pre-multiplier and the reduced set of normalized analytical modes as the post-multiplier of the 193 x 193 mass matrix. The results of this triple product contains elements equal to or less than unity, indicating the degree of similarity between the analytical modes and the test modes. If a

given analytical mode tends to correlate with a given test mode, the cross-orthogonality check will indicate this by showing a cross GMC approaching unity. The second additional method consists of determining a best fit of analytical and test GMCs over the entire mode shape in a least-squares sense. This is done by finding, for a given test mode, the sum of the squares of the differences between the test and analytical GMCs for every degree of freedom. The analytical mode for which this sum is a minimum will be the mode which best fits the test mode GMC distribution. It should be noted that the latter methods are employed only as a guide to correlation and must be used in conjunction with direct shape comparisons and engineering judgement.

5.3.2 Correlation Results - Using the methods outlined above, twenty-four of the twenty-five unique test modes were correlated with analytical modes. Mode 15A is not correlated due to poor orthogonality characteristics discussed in Section 5.2. In general, the correlations are quite clear except for modes which contain significant FAS tanks responses which tend to make the correlation uncertain due to the known differences between the analytical and DTA FAS tanks. Table 5.10 shows a summary of the correlation results for the twenty-four unique test modes. Table 5.11 presents the cross-orthogonality and least-squares GMC fit results. The latter table shows both the "best" and "next best" correlations using these methods. It can be seen that the two methods agree in many cases.

5.3.3 Discussion of Correlation Results - In most cases, mode shape correlations are excellent. However, as Table 5.10 shows, the test and analytical frequencies vary in agreement. That is, in some cases, frequency differences are significant while in other cases they are not. For first vehicle bending modes, the analytical frequencies vary from 4.6 percent to 18.1 percent higher than test frequencies. The first vehicle axial mode analytical frequency is 6 percent higher than test while the second vehicle axial mode analytical frequency is 14.7 percent higher. The first vehicle torsional mode analytical frequency is almost 21 percent lower than test. All the modes mentioned above involve significant motions throughout the entire structure. Hence, it is difficult to determine with certainty at this point which individual components contain modeling deficiencies which would result in the above frequency differences. In most of the modes there are significant relative motions across the CSM axial port area and across the CM/SM interface. Hence, these areas are suspect.

The FAS oxygen tanks exhibit response characteristics similar to those observed during the Launch Configuration test. That is, the tanks respond analytically at frequencies higher than test frequencies (see Figures 5.6 through 5.8).

The ATM model appears to correlate well with test although there were not significant local deformations of the ATM in the test frequency range.

It can be seen in Table 5.10 that the vehicle second torsional mode obtained during test (Mode 18A) is correlated with analytical mode 39 which is actually a third torsional mode. The analytical second torsional mode is mode 36 which occurs at 10.28 Hz. However, the mode 39 correlation with mode 18A is the best correlation which could be found. The shape discrepancy leads one to suspect that the torsional stiffness across the CM/SM interface is modeled too softly. The correlation of the vehicle first torsional mode also indicates this apparent modeling deficiency.

5.3.4 Conclusions - As a result of evaluating the Orbital Configuration modal survey test data and correlating these data with the best available corresponding analytically derived data, the following conclusions were reached:

a. twenty-five unique test modes were acquired which represent all identifiable major structural resonances in the 0 to 20 Hz test frequency range;

b. the quality of the test modes is excellent with only one mode exhibiting poor orthogonality characteristics;

c. correlations of the test and analytical mode shapes are excellent. However, some significant differences in test and analytical frequencies were noted and required further, more detailed, studies in order to pinpoint the sources of these differences. Stiffness modeling in the areas of the CSM axial port and the CM/SM interface are suspected to be deficient, however, due to the nature of the test modes, other structural areas may be involved.

Table 5.6

SKYLAB ORBITAL CONFIGURATION MODAL SURVEY TEST

VALID TEST RUNS ARRANGED IN ASCENDING FREQUENCY ORDER

MODE NO.	MODE NAME	RUN NO.	FREQ., HZ.	COMMENTS
1	01A	333	0.31	
2	02A	336	0.31	
3	03B	614	1.31	
4	04A	378	1.43	
5	05A	386	1.66	
6	06A	434	1.72	
7	06B	610	1.74	RE-TUNE OF MODE 06A
8	07A	431	2.51	
9	08A	452	3.06	
10	09A	443	4.10	
11	10A	482	4.50	
12	10B	619	4.55	RE-TUNE OF MODE 10A
13	11A	536	5.03	
14	12A	574	5.86	
15	13A	491	6.25	
16	13B	667	6.36	RE-TUNE OF MODE 13A
17	14A	474	6.73	
18	15A	600	7.59	
19	16A	347	8.85	
20	17A	549	11.59	
21	18A	526	12.65	
22	18B	663	12.87	RE-TUNE OF MODE 18A
23	19A	586	13.30	
24	20A	627	13.68	
25	21A	633	14.55	
26	22B	654	15.40	RE-TUNE OF MODE 22A
27	22A	506	15.78	
28	23A	649	16.20	
29	24A	638	16.53	
30	25A	499	17.01	

Table 5.7 Summary of Test Modes Orthogonality Results

MODE NO.	MODE NAME	NO. OF MODES ≤ 10% COUPLING	NO. OF MODES >10% COUPLING	AVERAGE COUPLING PERCENT	STANDARD DEVIATION, PERCENT	RANGE OF COUPLING PERCENT/MODE	
						MAX.	MIN.
1	01A	25	4	3.95	3.78	12.6/22A	0.2/05A
2	02A	23	6	5.66	6.14	20.5/13A	0.2/18B
3	03B	29	0	2.05	2.61	9.4/13A	0.1/12A
4	04A	28	1	3.02	4.67	24.2/15A	0.1/17A
5	05A	26	3	4.24	7.09	35.8/06A	0.2/09A
6	06A	26	2	4.70	6.74	35.8/05A	0.0/12A
7	06B	26	2	3.10	4.15	19.6/02A	0.0/17A
8	07A	28	1	2.83	2.84	10.8/15A	0.1/17A
9	08A	28	1	2.77	2.55	11.5/13A	0.1/16A
10	09A	27	2	3.47	3.34	13.7/10A	0.2/05A
11	10A	26	2	4.29	8.61	45.5/15A	0.2/23A
12	10B	26	2	4.43	8.49	45.2/15A	0.2/05A
13	11A	29	0	1.97	1.77	6.4/06B	0.0/22A
14	12A	26	3	3.64	5.14	24.2/15A	0.0/23A
15	13A	24	4	4.48	4.75	20.5/02A	0.3/06A
16	13B	27	1	2.69	3.68	17.5/02A	0.0/15A
17	14A	27	2	5.72	11.53	63.8/15A	0.1/24A
18	15A	22	7	10.38	15.83	63.8/14A	0.0/13B
19	16A	28	1	2.49	3.27	15.9/02A	0.1/08A
20	17A	28	1	3.56	3.52	15.1/22A	0.0/06B
21	18A	25	3	4.21	5.80	27.5/22B	0.1/11A
22	18B	25	3	5.32	9.12	48.1/19A	0.2/02A
23	19A	25	4	7.37	11.06	32.4/20A	0.5/10B
24	20A	25	4	5.68	6.79	20.3/21A	0.2/03B
25	21A	24	5	5.26	7.79	32.5/22A	0.3/03B
26	22B	22	6	6.10	8.57	32.0/23A	0.3/13B
27	22A	21	7	8.13	9.86	37.1/23A	0.0/11A
28	23A	25	4	6.31	8.49	37.1/22A	0.0/12A
29	24A	26	3	4.95	4.11	16.6/25A	0.1/14A
30	25A	27	2	3.63	3.83	16.6/24A	0.2/10A

Table 5.8 Descriptions of Test Modes

MODE NO.	NAME	FREQUENCY HZ.	DOMINANT CHARACTERISTICS
1	01A	0.31	Suspension system mode - largely X-Z plane translation of the vehicle.
2	02A	0.31	Suspension system mode - largely translation and rotation of the vehicle in the X-Y plane.
3	03B	1.31	First vehicle X-Z plane bending about the MDA/CSM interface with ATM X-Z plane rocking out of phase with CSM.
4	04A	1.43	First vehicle X-Y plane bending about the MDA/CSM interface with ATM X-Y plane rocking out of phase with CSM.
5	05A	1.66	First vehicle X-Y plane bending about the MDA/CSM interface with ATM X-Y plane rocking in phase with CSM.
7	06B	1.74	First vehicle X-Z plane bending about the MDA/CSM interface with ATM X-Y plane rocking in phase with CSM.
8	07A	2.51	Vehicle roll and first torsion coupled with X-Y plane first bending about MDA/CSM interface and ATM X-Y plane rocking in phase with top of CSM.
9	08A	3.06	First vehicle X-Z plane bending about the MDA/CSM interface with ATM Z motion in phase with top of CSM.
10	09A	4.10	First vehicle torsional mode with CSM and MDA/STS/AM out of phase with OWS/IU/FAS. Large torsional motion of CSM relative to MDA.
11	10A	4.50	ATM rotation about X axis with vehicle X-Y plane second bending about the MDA/CSM and STS/AM interfaces.
13	11A	5.03	ATM rotation about Y axis.
14	12A	5.86	Vehicle second X-Y plane bending about MDA/CSM and STS/AM interfaces with some FAS tanks motions in Y and Z directions.
16	13B	6.36	Vehicle second X-Z plane bending about the MDA/CSM and STS/AM interfaces.
17	14A	6.73	FAS Tanks Y and Z motions coupled with OWS/IU/FAS rocking about the Base Ring in the X-Z plane.
19	16A	8.85	Vehicle first axial mode.
20	17A	11.59	FAS tanks Y and Z motions, MDA/STS/AM X-Y plane motion. Some Y motions of both +Y AM tanks.
21	18A	12.65	Vehicle second torsional mode.
23	19A	13.30	Large Y motion of one AM tank (+Y, lower tank) with vehicle X-Y plane third bending.
24	20A	13.68	Large Y motion of +Y, upper AM tank and some Z motion of -Z, lower AM tank coupled with vehicle X-Z plane third bending.

Table 5.8 Descriptions of Test Modes (Continued)

MODE NO.	NAME	FREQUENCY HZ.	DOMINANT CHARACTERISTICS
25	21A	14.55	Large Y motion of +Y, upper AM tank coupled with vehicle X-Y plane third bending.
26	22B	15.40	FAS tanks motions in all three directions, AM tanks motions in Y coupled with vehicle third bending in the X-Y plane.
28	23A	16.20	FAS tanks motions in all three directions (mostly X) AM tanks Z motions, fourth vehicle X-Z plane bending.
29	24A	16.53	FAS tanks X motions with AM tanks Y motions.
30	25A	17.01	Vehicle second axial mode.

Table 5.9

ORBITAL CONFIGURATION TEST MODES GMC SUMMARY

MODE NO.	FREQ, HZ.	GMC (DX)	GMC (DY)	GMC (DZ)	GMC (TX)	GMC (TY)	GMC (TZ)
01A	.31	.0106	.0171	.9559	.0009	.0062	.0092
02A	.31	.2027	.2219	.3995	.0018	.0702	.1040
03B	1.31	.3567	.0026	.6142	.0004	.0247	.0013
04A	1.43	.2205	.6185	.0641	.0524	.0010	.0434
05A	1.66	.1138	.6374	.0946	.1222	.0015	.0605
06A	1.72	.3625	.1600	.3210	.0299	.0292	.0974
06B	1.74	.4395	.0245	.4927	.0011	.0384	.0038
07A	2.51	.0331	.5621	.0983	.2573	.0001	.0493
08A	3.06	.0596	.0182	.8630	.0003	.0562	.0026
09A	4.10	.0215	.0534	.0401	.8755	.0001	.0094
10A	4.50	.1528	.4752	.1840	.1449	.0010	.0420
10B	4.55	.1528	.4772	.1870	.1394	.0006	.0430
11A	5.03	.3596	.0176	.4199	.0002	.2007	.0021
12A	5.86	.0509	.6246	.2016	.0254	.0006	.0969
13A	6.25	.0737	.0510	.6970	.0137	.1630	.0017
13B	6.36	.0563	.0415	.7615	.0096	.1307	.0007
14A	6.73	.0341	.4890	.3666	.0457	.0035	.0611
15A	7.59	.0315	.4499	.3304	.1712	.0023	.0147
16A	8.85	.8781	.0139	.0427	.0012	.0029	.0613
17A	11.59	.0033	.5830	.3838	.0195	.0050	.0055
18A	12.65	.0320	.0723	.0739	.8192	.0013	.0013
18B	12.87	.0276	.2459	.0812	.6278	.0029	.0147
19A	13.30	.0075	.7573	.1902	.0081	.0107	.0262
20A	13.68	.0148	.4335	.4936	.0049	.0475	.0056
21A	14.55	.0079	.8269	.1080	.0273	.0061	.0239
22B	15.40	.1503	.4681	.2327	.0957	.0088	.0445
22A	15.78	.2703	.3849	.2322	.0352	.0395	.0379
23A	16.20	.1946	.0932	.6228	.0239	.0591	.0065
24A	16.53	.2824	.5888	.0792	.0119	.0210	.0166
25A	17.01	.8257	.0568	.0952	.0032	.0044	.0148

Table 5.10 Summary of Test and Analytical Modes Correlation

TEST MODE			CORRELATING ANALYTICAL MODE		
NO.	FREQ. HZ.	DOMINANT MOTION	NO.	FREQ. HZ.	DOMINANT MOTION
1(1A)	.31	Suspension system mode. Rigid body translation in the X-Z plane.	2	0.28	Suspension system mode. Rigid body translation in the X-Z plane.
2(2A)	.31	Suspension system mode. Rigid body translation in the X-Y plane.	1	0.28	Suspension system mode. Rigid body translation in the X-Y plane.
3(3B)	1.31	First bending about the MDA/CSM interface in X-Z plane with ATM rocking in X-Z plane out of phase with CSM.	7	1.37	First bending about the MDA/CSM interface in X-Z plane with ATM rocking in X-Z plane out of phase with CSM.
4(4A)	1.43	First bending about the MDA/CSM interface in X-Y plane with ATM rocking in X-Y plane out of phase with CSM.	8	1.57	First bending about the MDA/CSM interface in X-Y plane with ATM rocking in X-Y plane out of phase with CSM.
5(5A)	1.66	First bending about the MDA/CSM interface in X-Y plane with ATM rocking in X-Y plane in phase with CSM.	9	1.96	First bending about the MDA/CSM interface in X-Y plane with ATM rocking in X-Y plane in phase with CSM.
7(6B)	1.74	First bending about the MDA/CSM interface in X-Z plane with ATM rocking in X-Z plane in phase with CSM.	10	1.99	First bending about the MDA/CSM interface in X-Z plane with ATM rocking in X-Z plane in phase with CSM.
8(7A)	2.51	Vehicle roll and first torsion coupled with X-Y plane first bending about MDA/CSM interface and ATM rocking in Y-Z plane in phase with the top of CSM.	11	2.66	Vehicle roll and first torsion coupled with X-Y plane first bending about MDA/CSM interface and ATM rocking in Y-Z plane in phase with the top of CSM.
9(8A)	3.06	First bending about theMDA/CSM interface in X-Z plane with ATM Z motion in phase with the top of CSM.	13	3.52	First bending about the MDA/CSM interface in X-Z plane with ATM Z motion in phase with the top CSM.
10(9A)	4.10	Vehicle first torsional mode with CSM, MDA/STS/AM out of phase with FAS/IU/OWS. Large torsional motion of CSM relative to MDA.	12	3.25	Vehicle first torsional mode with CSM out of phase with MDA/STS/AM and FAS/IU/OWS. Large torsional motion of CSM relative to MDA.

Table 5.10 Summary of Test and Analytical Modes Correlation (Cont'd)

TEST MODE			CORRELATING ANALYTCAL MODE		
NO.	FREQ. HZ.	DOMINANT MOTION	NO.	FREQ. HZ.	DOMINANT MOTION
11(10A)	4.50	ATM rotation mostly about X axis with vehicle second bending about the MDA/CSM and STS/AM interfaces in X-Y plane.	15	5.32	ATM rotation mostly about X axis with vehicle second bending about the MDA/CSM and STS/AM interfaces in X-Y plane.
13(11A)	5.03	ATM rotation about Y axis.	17	6.03	ATM rotation about Y axis.
14(12A)	5.86	Vehicle second bending about the MDA/CSM and STS/AM interfaces in X-Y plane with some FAS tank motion in Y-Z plane.	16	5.76	Vehicle second bending about the MDA/CSM and STS/AM interfaces in X-Y plane coupled with ATM rotations about X and Z axes, GRA/CAN center rotation about Z axis out of phase with ATM rack.
16(13B)	6.36	Vehicle second bending about the MDA/CSM and STS/AM interfaces in the X-Z plane.	19	7.04	Vehicle second bending about the MDA/CSM and STS/AM interfaces in the X-Z plane.
17(14A)	6.73	FAS O_2 tanks motion in Y-Z plane coupled with OWS Skirt/IU/FAS rocking about the base ring in X-Z plane.	28*	9.10	FAS O_2 tanks' motion in Y-Z plane, Y motion of EREP.
19(16A)	8.85	Vehicle first axial mode.	30	9.38	Vehicle first axial mode.
20(17A)	11.59	FAS O_2 bottle Y and Z motion, MDA/AM Y motion, AM N_2 tanks mathematical model point 20 and 21 motion in Y direction.	38	12.64	MDA/AM Y motion, AM N_2 tanks-mathematical model point 20 and 21 motion in Y direction. FAS bottle motion does not correlate with test mode 17A. FAS O_2 tank motion in test mode 17A has elements of analytical modes 29(9.266 Hz.), 32 (9.593 Hz.), 33(9.710 Hz.), and 35 (9.95 Hz.) all being predominately FAS tank modes.
21(18A)	12.65	Vehicle second torsional mode	39	12.75	Vehicle third torsional mode.**

*Correlation not clear.
**Identical in shape as test mode except for CSM phase.

Table 5.10 Summary of Test and Analytical Modes Correlation (Cont'd)

TEST MODE			CORRELATING ANALYTICAL MODE		
NO.	FREQ. HZ.	DOMINANT MOTION	NO.	FREQ. HZ.	DOMINANT MOTION
23(19A)	13.3	Y motion of AM N_2 tank math. model point No 20, vehicle third bending predominately in X-Y plane.	41	13.01	Y motion of AM N_2 tank math. model point No 20, vehicle third bending does not correlate well. Vehicle bending correlates closer with analytical modes 47(13.970) and 48 (14.084).
24(20A)	13.68	AM N_2 tanks Y and Z motion, vehicle third bendings predominately in X-Z plane. This mode was not well separated from test mode 19A(13.3 Hz) as shown by large coupling in orthogonality check.	42	13.28	AM N_2 Tanks Y and Z motions, vehicle third bending predominately in X-Z plane.
25(21A)	14.55	AM N_2 tanks Y motion and vehicle third bending in X-Y plane.	47	13.97	Vehicle third bending in X-Y plane, AM tanks motions do not correlate well.
			54	14.97	AM N_2 tanks Y motion, vehicle bending does not correlate.
26(22B)	15.40	Vehicle third bending predominately in X-Y plane, AM N_2 tanks Y and Z motions, FAS O_2 tanks X, Y and Z motions.	47	13.97	Vehicle third bending predominately in X-Y plane, AM N_2 tanks and DA trunions Y and Z motion.
28(23A)	16.20	Z motion of AM N_2 tanks coupled with X, Y, Z motions of FAS O_2 tanks (X motion is largest), fourth bending of total vehicle in X-Z plane.			No single mode correlates well. Analytical modes in the 18-19 Hz range resemble FAS tanks motions but the FAS tanks motions are coupled with Y motions of AM tanks and not Z motion as it occurs in test mode 23A.
			67	17.54	AM N_2 tanks Z motion. Note: Analytical mode 67 only approximates correlation.

Table 5.10 Summary of Test and Analytical Modes Correlation (Cont'd)

TEST MODE			CORRELATING ANALYTICAL MODE		
NO.	FREQ. HZ.	DOMINANT MOTION	NO.	FREQ. HZ.	DOMINANT MOTION
29(24A)	16.53	FAS O_2 tanks X motion coupled with AM N_2 tanks Y motion.	69	18.32	FAS O_2 tanks X motions and AM N_2 tanks Y motion.
30(25A)	17.01	Vehicle second axial mode.	77	19.51	Vehicle second axial mode.

Table 5.11 Cross-Orthogonality and GMC Least-Squares Fit Results

TEST MODE	TEST FREQ., HZ.	CORRELATING ANALYTICAL MODES BASED ON CROSS-ORTHOGONALITY						CORRELATING ANALYTICAL MODES BASED ON GMC LEAST-SQUARES FIT			
		BEST			NEXT BEST			BEST		NEXT BEST	
		MODE NO.	COUPLING	FREQ., HZ.	MODE NO.	COUPLING	FREQ., HZ.	MODE NO.	FREQ., HZ.	MODE NO.	FREQ., HZ.
1(01A)	0.31	2	.964	0.29	37	.366	10.66	2	0.29	*	-----
2(02A)	0.31	1	.445	0.28	6	.245	0.51	1	0.28	*	-----
3(03B)	1.31	7	.894	1.37	37	.310	10.66	7	1.37	*	-----
4(04A)	1.43	8	.876	1.57	75	.405	18.85	9	1.96	8	1.57
5(05A)	1.66	9	.809	1.96	8	.468	1.57	8	1.57	9	1.96
6(06A)	1.72	10	.766	1.99	37	.326	10.66	10	1.99	9	1.96
7(06B)	1.74	10	.831	1.99	37	.403	10.66	10	1.99	*	-----
8(07A)	2.51	11	.704	2.66	12	.490	3.25	15	5.32	12	3.25
9(08A)	3.06	13	.959	3.52	37	.502	10.66	13	3.52	*	-----
10(09A)	4.10	12	.740	3.25	11	.601	2.66	11	2.66	12	3.25
11(10A)	4.50	14	.756	4.93	15	.738	5.32	18	6.79	15	5.32
12(10B)	4.55	14	.764	4.93	15	.744	5.32	18	6.79	15	5.32
13(11A)	5.03	17	.709	6.03	45	.416	13.70	17	6.03	*	-----
14(12A)	5.86	18	.650	6.79	16	.635	5.76	15	5.32	18	6.79
15(13A)	6.25	19	.820	7.04	17	.324	6.03	19	7.04	*	-----
16(13B)	6.36	19	.833	7.04	17	.377	6.03	19	7.04	*	-----
17(14A)	6.73	18	.441	6.79	16	.343	5.76	35	9.95	18	6.79
18(15A)	7.59	18	.636	6.79	60	.246	16.57	18	6.79	15	5.32
19(16A)	8.85	30	.899	9.38	31	.874	9.40	30	9.38	31	9.40
20(17A)	11.59	38	.606	12.63	41	.525	13.01	32	9.59	38	12.63
21(18A)	12.65	39	.508	12.75	27	.404	9.03	39	12.75	*	-----
22(18B)	12.87	39	.631	12.75	38	.429	12.63	39	12.75	38	12.63
23(19A)	13.30	43	.491	13.40	42	.476	13.28	41	13.01	38	12.63
24(20A)	13.68	47	.465	13.97	49	.455	14.47	41	13.01	42	13.28
25(21A)	14.55	57	.552	15.64	47	.525	13.97	54	14.97	57	15.64
26(22B)	15.40	43	.297	13.40	67	.292	17.54	38	12.64	47	13.97
27(22A)	15.78	43	.363	13.40	48	.299	14.08	47	13.97	15	5.32
28(23A)	16.20	67	.569	17.54	87	.251	21.47	18	6.79	46	13.78
29(24A)	16.53	54	.403	14.97	69	.384	18.32	90	22.06	72	18.75
30(25A)	17.01	77	.777	19.51	78	.345	19.53	77	19.51	92	22.35

*An asterisk (*) indicates the second best fit was too poor to consider.

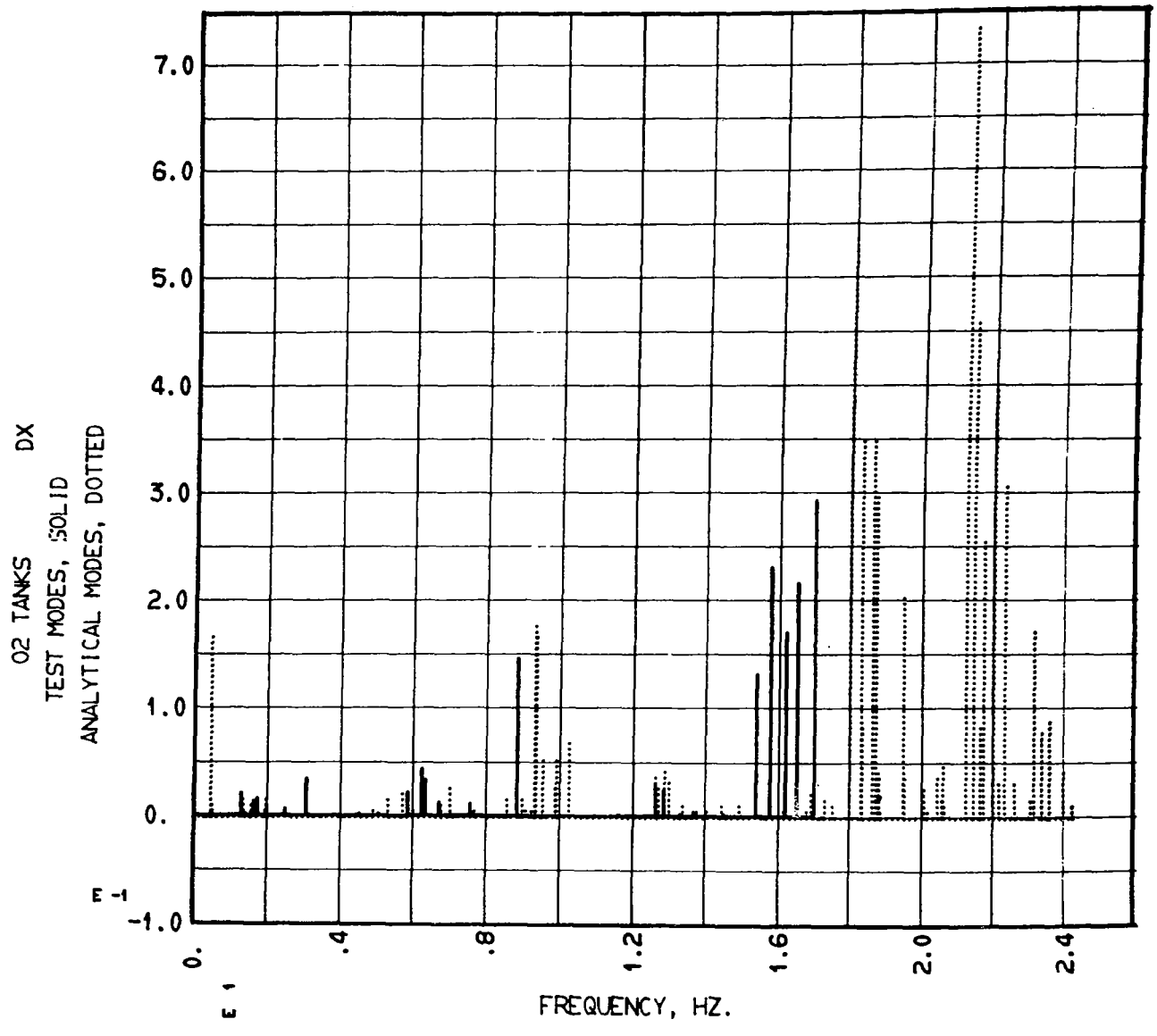

Figure 5.6 COMPONENT GMC SUMMARIES VS. FREQUENCY

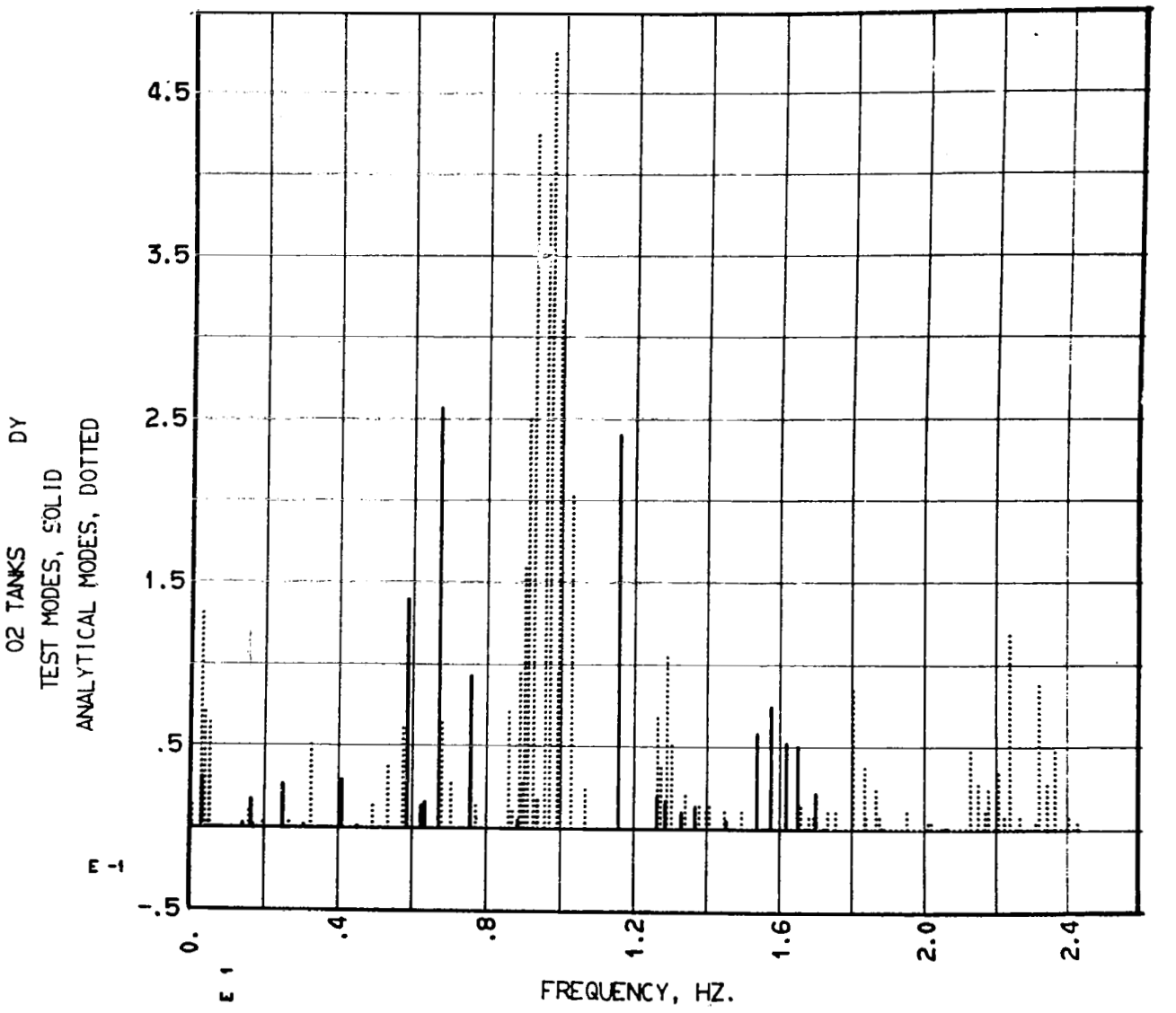

Figure 5.7 COMPONENT GMC SUMMARIES VS. FREQUENCY

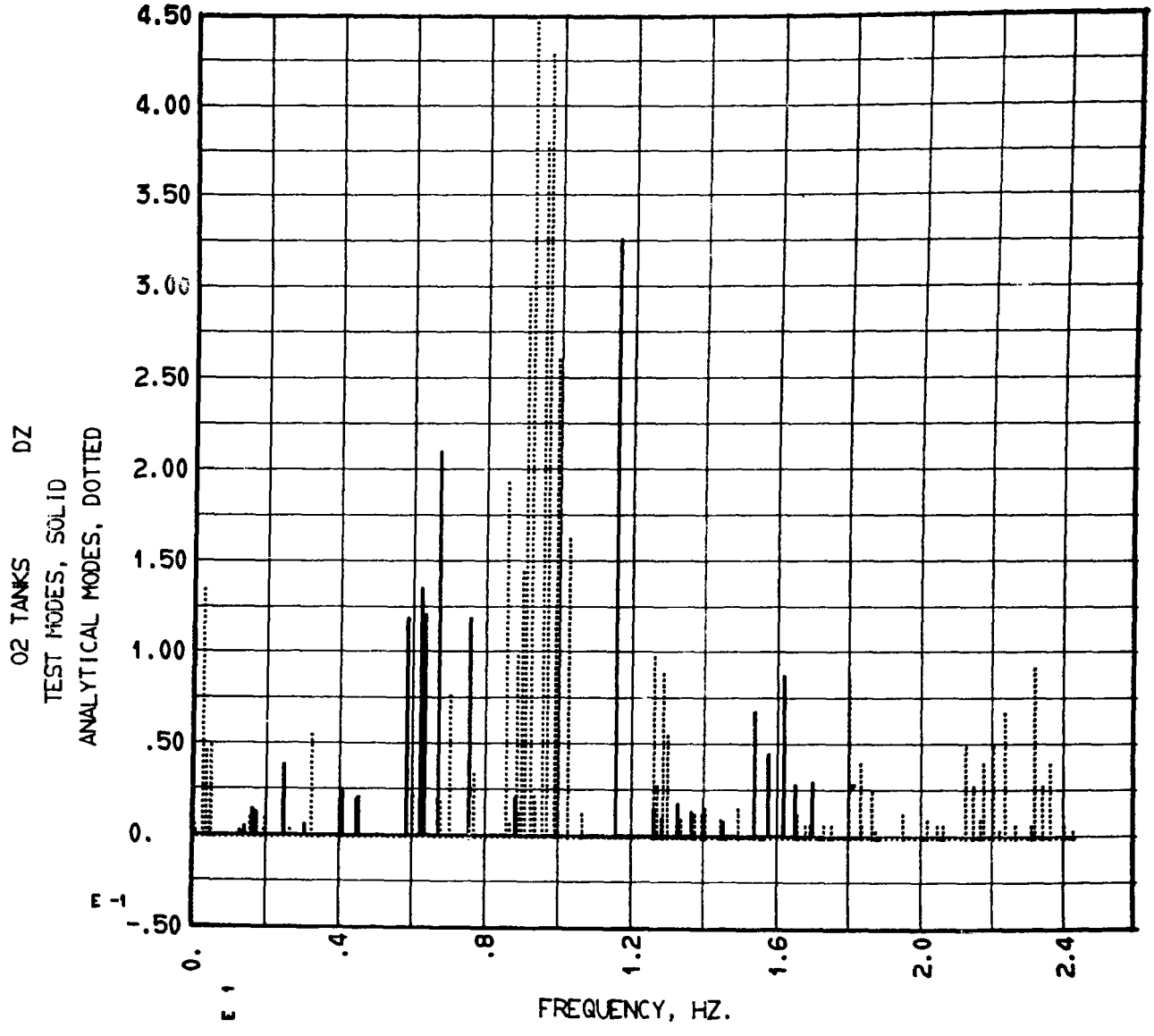

Figure 5.8 COMPONENT GMC SUMMARIES VS. FREQUENCY

5.4 Correlation Improvement Methodology

5.4.1 General Approach - A list of the literature reviewed in search of a suitable method to improve correlation between experimental and theoretical results is presented in the Reference Section of this report. Most of the referenced methods involve computations using measured amplitude data and result in a model limited in size to the number of degrees of freedom measured in test. They also require the existence of a compatable mass matrix that is orthogonal to the measured data. Hall* proposed a method of modifying existing detailed analytical models to achieve the desired correlation, but his approach also requires direct computations using measured amplitude data. It was felt that valid Skylab modeling results could not be obtained using any method which depends on measured modal amplitude for the following reasons:

a. 630 degrees of freedom (DOF) in the analytical model were judged necessary for good fidelity in loads calculations. Only 200 DOF were measured;

b. it was not possible to derive a test compatable mass matrix that adequately represented the Skylab Launch Configuration kinetic energy distribution in all areas of the analytical model;

c. much of the measured amplitude data contained local effects which could not be properly accounted for.

In order to minimize these shortcomings, a method to improve correlation between the Skylab experimental results and the theoretical model was developed which relies heavily on measured frequency data. A detailed description of this method is presented in "Dynamic Test Reflected Structural Model Methodology Report", published in December 1972. The methodology presented in this section is limited to a brief discussion of the frequency algorithm that has been developed and to discussion of its application to the Skylab Orbit Configuration test results.

5.4.2 The Frequency Algorithm - Theoretical mode shapes and frequencies of the pretest model were obtained from the solution of the general eigenproblem,

$$\left(-\omega_i^2 [M] + [K]\right) \{\phi_i\} = \{0\} \qquad (1)$$

where subscript i refers to the ith mode.

---

* Linear Estimation of Structural Parameters from Dynamic Test Data

It is assumed that theoretical mode shapes and frequencies of a model that correlates with test results can be obtained from the solution of the eigenproblem,

$$\left[-\Omega_i^2\left(\left[M\right]+\Sigma\delta_m\left[m\right]\right)+\left(\left[K\right]+\Sigma\delta_k\left[k\right]\right)\right]\left\{\psi_i\right\}=\left\{0\right\} \quad (2)$$

where the matrices [m] and [k] are the mass and stiffness of subcomponent elements whose respective sums produce [M] and [K]. $\{\delta\}$ are scaling factors which must be determined in order to obtain both eigenvector and eigenvalue correlation with test results. It was shown in the Dynamic Test Reflected Structural Model Methodology Report that scaling factors which produce eigenvalue correlation in all modes would also produce eigenvector correlation. This phenomenon led to the development of a Taylor's series expansion of the theoretical eigenvalues about the pre-test values as a function of the scaling factors to obtain an expression from which those factors can be determined. The first order approximation of this expansion is,

$$\left\{\omega_e^2\right\} = \left\{\omega_o^2\right\} + \left[\frac{\partial\,\omega_o^2}{\partial\,\delta}\right]\left\{\delta\right\} \quad (3)$$

where subscript (e) refers to experimental data and subscript (o) refers to the initial, or pre-test, data. Each row of the matrix of equations represents a theoretical mode for which is assumed that corresponding experimental data is available and the derivative with respect to each required scaling parameter may be determined. Ideally, when subcomponent detail is sufficient to produce as many scaling factors as there are modes, the solution from Equation (3) is

$$\left\{\delta\right\} = \left[\frac{\partial\,\omega_o^2}{\partial\,\delta}\right]^{-1}\left(\left\{\omega_e^2\right\} - \left\{\omega_o^2\right\}\right) \quad (4)$$

In practice, this requirement will not be satisfied, nor will experimental data be determined for all modes. However, a least-squares solution for $\{\delta\}$ is possible when Equation (3) contains more modes than scaling factors. Or, if the Taylor's series expansion of the ith theoretical eigenvalue is dominated by a single scaling factor, δ_j, an approximation of that factor may be obtained from,

$$\delta_j = \left(\omega_{ei}^2 - \omega_{oi}^2\right) \Big/ \left(\frac{\partial\,\omega_{oi}^2}{\partial\,\delta_j}\right) \quad (5)$$

Because of the first order approximation of the Taylor's series expansion, an iterative application of the algorithm is required whereby each set of parameters is used to calculate an updated model whose eigenvalue and eigenvalue derivatives are used to calculate new parameters until the difference in successive parameters is arbitrarily small.

5.4.3 Calculation of Eigenvalue Derivatives - Fox and Kapoor* provided an expression for the partial derivatives of an eigenvalue with respect to a structural parameter. The general expression is stated as a function of the derivatives of the mass and stiffness of the eigenproblem with respect to that parameter as

$$\frac{\partial \omega_i^2}{\partial \delta} = \{\phi_i\}^T \left(-\omega_i^2 \frac{\partial}{\partial \delta}[M] + \frac{\partial}{\partial \delta}[K] \right) \{\phi_i\} \qquad (6)$$

If the mass and stiffness matrices are defined as linear functions of their subcomponent elements, as in Equation (2), where the structural parameters are regarded scaling factors on the original modeling, as opposed to real hardware changes that would alter both mass and stiffness, Equation (6) produces two derivative terms of the form,

$$\frac{\partial \omega_i^2}{\partial \delta_m} = -\omega_i^2 \{\phi_i\}^T [m] \{\phi_i\} \qquad (7)$$

and,

$$\frac{\partial \omega_i^2}{\partial \delta_k} = \{\phi_i\}^T [k] \{\phi_i\} \qquad (8)$$

Equations (7) and (8) may be recognized as expressions for the kinetic and potential energy of the ith mode contained in the subcomponent elements defined by [m] and [k] respectively. Since the sum of the subcomponents equals the total system, the sum of the eigenvalue derivatives with respect to the mass scaling factors equals the total kinetic energy of the system, and the sum of the eigenvalue derivatives with respect to the stiffness scaling factors equals the total potential energy of the system. Thus, dividing both sides of Equations (7) and (8) by the eigenvalue, ω_i^2, yields the fractional parts of the respective total energies contained in a particular subcomponent. This observation allows Equation (3) to take the form,

---

* R. L. Fox and M. P. Kapoor, "Rates of Change of Eigenvalues and Eigenvectors", AIAA Journal, Vol. 6, No. 12, December 1968, pp. 2426-2429.

$$\left\{\frac{f_e^2}{f_o^2}\right\} - \{1.\} = \left[\omega_o^2\right]^{-1}\left[\frac{\partial \omega_o^2}{\partial \delta}\right]\{\delta\} \equiv [\Gamma]\{\delta\} \qquad (9)$$

Where element Γ_{ij} of matrix $[\Gamma]$ is the fractional part of the total kinetic or potential energy contained in the ith test correlated analytical mode that is contributed by the jth subcomponent.

5.5 Correlation Improvement Procedure

Prior to the initiation of this study, the Skylab Orbit Configuration Dynamic Test Article (DTA) vibration analysis model had been constructed. Each component of this model consisted of mass and stiffness data representing the combination of many subcomponents. Information concerning the details of these subcomponents was not available for use in this study. This condition limited the scope of the effort to the determination of component, rather than subcomponent, scaling factors that would improve the correlation between experimental and theoretical results. Also, it was assumed at the outset of the study that the mass of all components was adequately represented in the pre-test model so that the determination of mass scaling factors was not required.

5.5.1 The Pre-Test Model Strain Energy Distribution - The strain energy distribution in the components of the Orbit DTA pre-test model was calculated for each of the analytical modes by the method defined in paragraph 5.4.3. The results of these calculations in the modes that are correlatable with test results are presented in Table 5.12. A review of the correlation revealed that analytical mode 14 correlated with test mode 10A as well as analytical mode 15 did. Also, analytical mode 18 correlated with test mode 12A as well as analytical mode 16 did. These two additional modes are also included in Table 5.12 with an asterisk. Although GMC data indicated apparent correlation between test mode 18A and analytical mode 39, the actual vehicle second torsional mode occurred analytically as mode 36 at 10.285 Hz. Strain energy for both mode 36 and 39 are included in the table, but the correlation is shown as existing between analytical mode 36 and test mode 18A. Analytical mode 47 appears twice in Table 5.12; once with each of the test modes with which it was correlated.

The strain energy in analytical modes 41 and 42 is contained primarily in the Solar Arrays. Frequency correlation of the pre-test model with test results is very good in these modes and would not be affected by changes to other components due to the lack of strain energy in other components in these modes. Similarly, all other analytical modes listed in Table 5.12 have very little strain energy in the Solar Arrays and would not be affected by changes to Solar Array components. Since no changes to the Solar Array components can be made in this study, strain energy contribution for these components is not included in Table 5.12.

For convenient reference, the experimental and analytical modal frequencies are repeated in Table 5.12 as are the frequency differences expressed as a fraction of the experimental frequencies. The square of the frequency ratios minus one that are required for the solution of the frequency algorithm defined by Equation (9) in paragraph 5.4.3 also are presented in Table 5.12.

In general, the tabulated strain energy values reflect six degree of freedom motion of an entire component so that it is not possible, by review of Table 5.12 alone, to determine the specific locations, if any, in a particular component where the strain energy is concentrated nor the direction of motion with which it is associated. Motion in many of the test modes is dominated by the FAS Oxygen Tanks or the AM Nitrogen Tanks. Determination of scaling factor for local support structure for these tanks is required for improvement of correlation in those modes. Examination of Table 5.12 shows that a CSM component scaling factor large enough to improve correlation with the first torsional mode, test mode 09A, would have a large detrimental effect on the existing good correlation between analytical mode 11 and test mode 07A due to the very large CSM strain energy contribution in analytical mode 11. Many other examples can be cited from Table 5.12 to show that the lack of subcomponent detail disallows application of the idealized methodology for correlation improvement. However, the essence of the methodology was applied within the limits of the available data to determine required changes to the deployed DA and the CSM by the rationale discussed in the following paragraphs.

5.5.2 The Deployed DA Component Model - Analytical mode 9 has 70.8 percent of the total strain energy concentrated in the DA (see Table 5.12). The generalized mass contributions (GMC) of its corresponding test mode, Table 5.13, were in the ATM Rack in the X, Y, and Z directions. Review of the plotted data in Volume II for this mode shows very little relative motion in the lower DA between the trunnions and the FAS interface. This type of motion suggests that the upper DA, between the trunnions and the ATM interface, contains the full 70.8 percent of strain energy with a fairly uniform distribution. The data in Table .12 shows that an increase in DA stiffness is required to improve frequency correlation between analytical mode 9 and test mode 05A. It was concluded that, since part of the DA was already too stiff to be involved in the motion of analytical mode 9 and the remaining parts contributed equally, a scaling factor applied to the entire DA component should result in a stiffness matrix that approximates one which would result from adjustment of individual DA truss members had the data required to do so been available. An estimate of such a scaling factor was calculated using Equation (9) in paragraph 5.3.3 and the data of analytical mode 9 and experimental mode 05A in Table 5.12 by,

$$\delta_{DA} = -.282/.70774 = -.398$$

the McDonnell Douglas Corporation model with a Deployed DA stiffness model developed by Martin Marietta Corporation (MMC) for use in stress analyses. Frequency data from a Skylab Orbital Configuration DTA coupled system vibration analysis using the MMC DA component stiffness model and the revised CSM component model discussed below in paragraph .5.3 is presented in Table .14 as "MMC DA + CSM Eigensolution". Only data for the first few modes is presented to support credibility of the least squares scaling factor and no attempt was made to correlate the modes that are not presented. A comparison of the flexibility influence coefficient data for both DA models showed that the MMC model is only 85 percent as stiff as the McDonnell Douglas model overall and only 58 percent as stiff in the Z direction at the upper rigidizing arms and 58 percent as stiff in the X direction at the lower rigidizing arms.

This concluded the procedure for improvement of correlation between theoretical and experimental results by perturbation of the theoretical DA component model.

.5.3 The CSM Component Model - Experimental modes 09A and 18A were identified respectively as the first and second torsional modes of the Skylab Orbit Configuration DTA. The correlating analytical modes, are listed in Table .12. The data of Table .12 shows that an increase in stiffness somewhere in the DTA was required to improve frequency correlation with test results. The first analytical torsion mode, mode 12 in Table .12 has 36.2 percent of the strain energy in the CSM component and 43.7 percent in the DA component. The remaining energy is contained in insignificant amounts in the other components. Although a DA change produces the largest frequency change in this mode, the DA change calculated in paragraph .5.2 to improve correlation in other modes is in the wrong direction. Table .14 shows the first analytical torsion mode frequency decreased to 2.995 Hz as a result of the least squares DA component scaling factor. The second analytical torsion mode, mode 36 in Table .12 has 59.4 percent of the strain energy in the FAS/IU/OWS component, 28.2 percent in the CSM component, and the remainder spread in insignificant amounts in the other components. Although GMC data for analytical mode 36 was not reported because it was not correlated with test data, GMC data for that mode was calculated and it showed large FAS Oxygen Tanks motion. Due to the lack of FAS subcomponent stiffness data the strain energy associated with Oxygen Tanks motion could not be separated from the total FAS/IU/OWS component contribution. A total FAS/IU/OWS component scaling factor calculated to improve correlation in the second torsional mode would produce a comparable decrease in correlation between experimental mode 24A and analytical mode 69 which, as Table .12 shows, has 50.8 percent of the strain energy in the FAS/IU/OWS component and requires scaling in the opposite direction. A total CSM component scaling factor to improve correlation in either torsion mode was also disallowed by the detrimental effects it would have on existing good correlation in other modes. However, examination of the first and second analytical torsion modes as plotted data suggested that the addition of torsion springs between the Command Module forward and aft bulkheads and

The effect of this scaling factor on all other analytical modes listed in Table 5.12 was determined by using Equation (3) of paragraph 5.4.2 to solve for the new eigenvalues, $\{\omega_e^2\}$, that are produced by the above value of $_{DA}$ when the scaling parameters for all other components are set equal to zero. The results of these calculations are presented in Table 5.14 as "Mode 9 Estimation" data. The differences between these frequencies and experimental results, expressed as a fraction of the experimental frequencies, also are included in Table 5.14. Experimental and pre-test model analytical data are repeated in Table 5.14 for convenient comparison. A comparison shows significant improvement or no effect in all modes except the first torsional mode, correlated with experimental mode 09A, and analytical mode 47 which correlates with experimental modes 21A and 22B, both of which are strongly tank modes. This result led to the examination of those analytical modes which showed the greatest improvement from application of the DA scaling factor. The examination revealed that the same type of motion occurs in those modes as in analytical mode 9; that is, multi-directional ATM activity on the upper DA and relatively stiff lower DA. It was then decided that a DA scaling factor, that satisfies the frequency algorithm (Equation (9) of paragraph 5.3.3) in a least squares sense, for all test correlated modes which are clearly associated with uniform strain in the upper DA, would produce the best correlation improvement possible within the limits of available data. All data involved in the determination of the least squares scaling factor are presented in Table 5.15. A question regarding which analytical modes best correlated with test modes 10A and 12A was raised previously. Analytical modes 14 and 18 were chosen for this calculation because of their higher DA strain energy contributions. Correlation in these modes is not too important since calculation of the least squares scaling factor was dominated by analytical modes 9 and 17.

The effect of the least squares scaling factor on all other analytical modes listed in Table 5.12 was determined by using Equation (3) in the same manner as was done for "Mode 9 Estimation". The results of these calculations are presented in Table 5.14 as "Least Squares Estimation". The corresponding frequency ratio data also are included. Figures 5.9 and 5.10 compare pre-test and perturbated analytical mode shapes to test mode shapes in the X-Y and X-Z planes. Improved correlation between tests mode shapes and analytical mode shapes was obtained from the least square DA scaling factor.

Comparison of these results with test and the "Mode 9 Estimation" data led to the decision to calculate the coupled modes of the system using the least squares scaling factor on the DA component stiffness matrix. The frequency data for the first few modes from this vibration analysis is presented in Table 5.14 as "Least Squares Eigensolution". No attempt was made to correlate the modes not shown.

Although the results obtained by scaling the Deployed DA component stiffness lend confidence in the methodology by which the scaling was determined, an independent check on these results was made by replacing

between the Command Module aft bulkhead and Service Module forward bulkhead would improve torsional correlation without disturbing motion in non-torsion modes if springs of the proper magnitude could be determined. An estimate of the proper torsional spring magnitude was made using the data of analytical mode 12 in Table 5.12 and the least squares DA component scaling factor determined in paragraph 5.5.2 in Equation (9) from paragraph 5.3.3 by,

$$.36221\ \delta_{CSM} + .43725\ (-.4664) = +\ .591$$

$$\delta_{CSM} = 2.19$$

This meant that torsional springs 2.19 times the magnitude of those in the CSM Component model should be added to the existing springs to improve correlation. Such a large change questioned the credibility of the estimate. At this point, flexibility influence coefficient data for the Apollo CSM was obtained by telecon from Jack Nichols of NASA, Huntsville. Table .16 presents this data and the corresponding Skylab CSM component flexibility influence coefficient data. The ratios of relative deflection across the ports in question, also presented in Table 5.16 shows the difference in these models is greater than indicated by the scaling factor estimated above. This result is consistent with the methodology since the calculation of the scaling factor involves division by the total CSM component strain energy which is larger than that undeterminable portion associated with torsion alone.

With the Apollo CSM data in hand, it was decided that the best Skylab CSM component model improvement would result from the addition of torsional springs that reflected the flexibility influence coefficient ratios shown in Table 5.16. Calculations of these springs are included in Table 5.16. The coupled modes of the Skylab Orbit Configuration DTA were then calculated using the CSM component with the alterations discussed above the the Deployed DA component with stiffness increased by the least squares scaling factor determined in paragraph 5.5.2. The frequency data from this vibration analysis is presented in Table 5.14 as "Test Verified Eigensolution" data. Figures 5.11 and 5.12 show the improvements obtained over the pretest analytical modes by the inclusion of torsional springs and DA scaling factors.

This concluded the procedure for improvement of correlation between theoretical and experimental results by perturbation of the theoretical CSM component model.

No other component changes were made in this study.

5.5.4 Results - Table 5.17 presents a summary of the correlation results. This table provides the basis for acceptance of the modeling changes discussed in the previous paragraphs. Supporting data for the statements made in Table 5.17 are provided in Volume II. Volume II

contain plots for both test and analytical results. The analytical modes were calculated using 198 component (uncoupled) modes. It was observed that many of those component modes had no effect on the coupled modes of interest in this study. To improve efficiency in conducting the analysis, those ineffective component modes were deleted.

5.5.4.1 The DA Component Scaling Factor Results - The primary effect of scaling the DA component stiffness matrix was to improve the correlation of experimental and theoretical frequency data. The mode shape correlation between the experimental results and the pre-test theoretical model results was satisfactory in those modes which may be categorized as coupled main beam bending and ATM activity. This good correlation was essentially unchanged by the DA scaling factor. The pre-test model exhibited strong coupling between the first torsional mode and an X-Y plane first bending mode. This motion was not observed in test. The application of the DA component scaling factor eliminated this coupling in the analytical model. However, it also decreased the torsional mode frequency to 2.995 Hz prior to the CSM component model alterations. Correlation of FAS Oxygen and AM Nitrogen tank modes and of longitudinal modes was unaffected by the DA component scaling factor.

5.5.4.2 The CSM Component Torsional Springs Results - The effect of the addition of the two torsional springs to the CSM component model was improvement of mode shape and frequency correlation between experimental and theoretical results in the first two torsional modes.

Inclusion of the springs decreased the difference between experimental and analytical frequencies of the first torsional mode from 20.7 percent of the experimental frequency to 13.9 percent. The pre-test analytical model produced a large relative torsional deflection between the command and service module bulkheads which resulted in the node of the first torsional mode being located in the MDA cone structure whereas the node was observed to be at the AM trusses in the test results. As a result of the CSM component changes the analytical node was shifted aft to the STS/AM component. The difference between experimental and analytical frequencies of the second torsional mode decreased from 18.7 percent of the experimental frequency to 4.6 percent as a result of the CSM component changes. A significant improvement in the second torsional mode shape correlation in the CSM component also was produced by these changes.

Correlation of FAS Oxygen and AM Nitrogen tank modes and of longitudinal modes was unaffected by the CSM component changes.

5.5.5 Conclusions -

a. A valid methodology for perturbating a theoretical dynamic model to improve correlation with experimental results has been developed as part of this study.

b. The changes incorporated into the Skylab Orbit Configuration DTA model produce acceptable primary modal characteristics correlation of that model with test results in all planes of motion.

c. While complete correlation of all test data with analytical results was not achieved, further effort to produce total agreement is unwarranted because DTA model changes required to do so would not necessarily be applicable to the flight article.

d. Component models resulting from this study are technically acceptable for use in the test verified dynamic model.

Table 5.12

Pre-Test Model Strain Energy Distribution

EXPERIMENTAL		ANALYTICAL		$\frac{F_a-F_e}{F_e}$	COMPONENT STRAIN ENERGY FRACTIONAL CONTRIBUTION							$\left(\frac{F_e}{F_a}\right)^2-1$
MODE	F_e	MODE	F_a		FAS/IU/ OWS	MDA/STS/ AM	MDA PORT	CSM	DA	ATM RACK	SPAR/CAN	
03B	1.31	7	1.372	.047	.02702	.18745	.26758	.20826	.13026	.00448	.00021	-.008
04A	1.43	8	1.566	.095	.00548	.12829	.26984	.21496	.21567	.00508	.00023	-.166
05A	1.66	9	1.959	.180	.02482	.01484	.07753	.07425	.70774	.01064	.00100	-.282
06B	1.74	10	1.994	.146	.13517	.01564	.06044	.05708	.64632	.01258	.00088	-.239
07A	2.51	11	2.663	.061	.02514	.08675	.08761	.47598	.28279	.00601	.00044	-.112
08A	3.06	13	3.519	.150	.14959	.28163	.08181	.18949	.27271	.00720	.00037	-.244
09A	4.10	12	3.251	.207	.03898	.06468	.05558	.36221	.43725	.00841	.00090	+.590
10A	4.50	14*	4.933	.096	.02038	.14496	.00641	.03776	.23315	.23250	.30389	-.168
		15	5.319	.182	.01378	.11146	.00387	.02766	.09902	.00808	.72599	-.284
11A	5.03	17	6.029	.199	.05687	.12028	.00490	.02923	.61267	.09363	.00797	-.304
12A	5.86	16	5.757	.018	.02587	.19523	.00579	.04979	.05104	.26714	.39074	+.018
		18*	6.791	.159	.08704	.14616	.00446	.05054	.43898	.08520	.07523	-.255
13A	6.36	19	7.043	.107	.20097	.15848	.00457	.05046	.43079	.06846	.00449	-.185
14A	6.73	28	9.101	.352	.49526	.02542	.00087	.01829	.18583	.01697	.01193	-.453
16A	8.85	30	9.381	.060	.07336	.25603	.14732	.13667	.01091	.00597	.35817	-.110
17A	11.59	38	12.635	.090	.27705	.25149	.03032	.16828	.03737	.01739	.00471	-.159
18A	12.65	36	10.285	.187	.59394	.03747	.02377	.28230	.03436	.00172	.00027	+.513
NONE	-----	39	12.746	----	.16536	.46854	.03473	.17765	.01982	.03057	.00729	-----
19A	13.3	41	13.007	.022	.04304	.08742	.00100	.00325	.02189	.09288	.03606	+.046
20A	13.68	42	13.282	.029	.00777	.06620	.01246	.05193	.01006	.08249	.15686	+.061
21A	14.55	47	13.970	.040	.05453	.28277	.05235	.23121	.31787	.00313	.00046	-.085
		54	14.966	.029	.10289	.68815	.03927	.13489	.01154	.01055	.00357	-.055
22B	15.40	47	13.970	.093	.05453	.28277	.05235	.23121	.31787	.00313	.00046	+.215
23A	16.20	67	17.541	.083	.07183	.84068	.01306	.06179	.00248	.00454	.00221	-.147
24A	16.53	69	18.319	.108	.50765	.39711	.00302	.01844	.01288	.00893	.04595	-.186
25A	17.01	77	19.508	.147	.27097	.36148	.14509	.16776	.00205	.00971	.04104	-.240

Table 5.13 ORBITAL CONFIGURATION MODAL SURVEY

TEST MODES GENERALIZED MASS CONTRIBUTION SUMMARY

TEST MODE NO. 05A TEST FREQUENCY = 1.66 HZ.

COMPONENT NAME	GMC (DX)	GMC (DY)	GMC (DZ)	GMC (TX)	GMC (TY)	GMC (TZ)
BR/OWS SKIRT/IU/FAS	.0084	.0888	.0162	.0671	.0005	.0333
6-FAS 02 TANKS	.0141	.0174	.0149	0.	0.	0.
MDA/STS/AM	.0002	.0528	.0004	.0128	.0001	.0057
6-AM N2 TANKS	.0007	.0036	.0016	0.	0.	0.
COMMAND/SERVICE MOD.	.0004	.2882	.0021	.0187	-.0001	.0125
DEPLOYMENT ASSEMBLY	.0078	.0041	.0018	0.	0.	0.
ATM-RACK,CMGS,4-SAS	.0773	.1172	.0561	.0303	.0000	.0004
ATM-SPAR CENTER	.0030	.0184	.0009	.0075	.0005	0.
ATM-GRA/CAN CENTER	.0018	.0168	.0009	.0159	.0005	.0087
SUM	.1138	.6074	.0946	.1222	.0015	.0605

TOTAL GM CONTRIBUTION FOR EACH COMPONENT

BR/OWS SKIRT/IU/FAS	.2142
6-FAS 02 TANKS	.0465
MDA/STS/AM	.0718
6-AM N2 TANKS	.0059
COMMAND/SERVICE MOD.	.3219
DEPLOYMENT ASSEMBLY	.0137
ATM-RACK,CMGS,4-SAS	.2513
ATM-SPAR CENTER	.0333
ATM-GRA/CAN CENTER	.0445

Table 5.14
Frequency Correlation Summary

EXPERIMENTAL MODE	F_e	F_a	$\frac{\lvert F_a-F_e\rvert}{F_e}$	F_a	$\frac{\lvert F_a-F_e\rvert}{F_e}$	F_a	$\frac{\lvert F_a-F_e\rvert}{F_e}$	F_a	$\frac{\lvert F_a-F_e\rvert}{F_e}$	F_a	$\frac{\lvert F_a-F_e\rvert}{F_e}$	F_a	$\frac{\lvert F_a-F_e\rvert}{F_e}$
03B	1.31	1.372	.047	1.336	.020	1.330	.015	1.278	.024	1.279	.024	1.348	.029
04A	1.43	1.566	.095	1.497	.047	1.485	.038	1.377	.037	1.377	.037	2.053	.436
05A	1.66	1.959	.180	1.660	.0	1.603	.034	1.667	.004	1.670	.006	1.554	.064
06B	1.74	1.994	.146	1.719	.012	1.667	.042	1.643	.056	1.643	.056	1.868	.074
07A	2.51	2.663	.061	2.509	.0	2.481	.012	2.310	.080	2.338	.069	2.435	.030
08A	3.06	3.519	.150	3.323	.086	3.288	.075	3.164	.034	3.151	.030	3.281	.072
09A	4.10	3.251	.207	2.955	.279	2.901	.292	2.995	.270	3.532	.139	3.546	.135
10A	4.50	4.933 5.319	.096 .182	4.699 5.213	.044 .158	4.657 5.195	.035 .154	4.313	.042	4.323	.039	5.293	.176
11A	5.03	6.029	.199	5.243	.042	5.095	.013	4.858	.034	4.868	.032	5.861	.165
12A	5.86	5.757 6.791	.018 .159	5.698 6.169	.028 .053	5.688 6.056	.029 .033	5.698	.028	5.706	.026	5.739	.021
13A	6.36	7.043	.107	6.411	.008	6.296	.010	6.544	.029	6.552	.030	6.602	.038
14A	6.73	9.101	.352	8.758	.301	8.698	.292			9.192	.366		
16A	8.85	9.381	.060	9.361	.058	9.357	.057			9.405	.063		
17A	11.59	12.635	.090	12.541	.082	12.524	.081						
18A	12.65	10.285	.187	10.214	.193	10.202	.194	12.072	.046	12.072	.046	12.029	.049
NONE		12.746		12.696		12.687							
19A	13.3	13.007	.022	12.950	.026	12.940	.027			12.568	.055		
20A	13.68	13.282	.029	13.255	.031	13.251	.031			13.323	.026		
21A	14.55	13.970 14.966	.040 .029	13.056 14.931	.103 .026	12.893 14.926	.114 .026			13.323 14.855	.084 .021		
22B	15.40	13.970	.093	13.056	.152	12.893	.163			14.855	.035		
23A	16.20	17.541	.083	17.532	.083	17.531	.082			17.552	.083		
24A	16.53	18.319	.108	18.272	.105	18.264	.105			18.361	.111		
25A	17.01	19.508	.147	19.500	.146	19.499	.146			19.644	.155		
		Pre-Test Model		Mode 9 Estimation		Least Squares Estimation		Least Squares Eigensolution		Test Verified Eigensolution		MMC DA + CSM Eigensolution	

Table 5.15

Calculation of Least Squares DA Scaling Factor

EXPERIMENTAL MODE	EXPERIMENTAL F_e	ANALYTICAL MODE	ANALYTICAL F_a	DA STRAIN ENERGY	$\left(\frac{F_e}{F_a}\right)^2-1$	$\left(\text{DA STRAIN ENERGY}\right)^2$	COLUMN 5 X COLUMN 6
03B	1.31	7	1.372	.13025	-.088	-.0115	.0170
04A	1.43	8	1.566	.21567	-.166	-.0358	.0465
05A	1.66	9	1.953	.70774	-.282	-.1996	.5009
06B	1.74	10	1.994	.64632	-.239	-.1525	.4177
07A	2.51	11	2.663	.28279	-.112	-.0317	.0800
08A	3.06	13	3.519	.27271	-.244	-.0665	.0744
09A	4.10	12	3.251	1st Torsion	mode		
10A	4.50	14*	4.933	.23315	-.168	-.0392	.0544
		15	5.319	.09902	-.284	+.0281	.0098
11A	5.03	17	6.029	.61267	-.304	-.1863	.3754
12A	5.86	16	5.757	.05104	+.018	+.0009	.0026
		18*	6.791	.43898	-.255	-.1119	.1927
13B	6.36	19	7.043	.43079	-.185	-.0797	.1856
14A	6.73	28	9.101	Oxygen tanks	mode		
16A	8.85	30	9.381	1st Axial	mode		
17A	11.59	38	12.635	Nitrogen tanks	mode		
18A	12.65	36	10.285	2nd Torsion	mode		
None		39	12.746	3rd Torsion	mode		
19A	13.3	41	13.007	Nitrogen tanks	mode		
20A	13.68	42	13.282	Nitrogen tanks	mode		
21A	14.55	47	13.970				
		54	14.966	Nitrogen tanks	mode		
22B	15.40	47	13.970	Repeated	data		
23A	16.20	67	17.541	Nitrogen tanks	mode		
24A	16.53	69	18.319	Oxygen and	Nitrogen	tanks mode	
25A	17.01	77	19.508	2nd Axial	mode		
						Σ = .9127	Σ = 1.957

Notes:

Least squares equation is,

$$\left\{\left(\frac{f_e}{f_a}\right)^2-1\right\} = \left\{\Gamma_{i_{DA}}\right\} \delta_{DA}$$

or briefly,

$$R = \Gamma\delta,$$

$$\therefore \delta = (\Gamma^T\Gamma)^{-1}\Gamma^T R$$

$$= \frac{\Sigma \text{Column 8}}{\Sigma \text{Column 7}}$$

$$= -.4664$$

Table 5.16

CSM Flexibility Influence Coefficient Data
(Angular deflections due to applied unit moments)

DEFLECTION AT	APOLLO MODEL		SKYLAB MODEL		SKYLAB RELATIVE / APOLLO RELATIVE
	ABSOLUTE	RELATIVE	ABSOLUTE	RELATIVE	
CM Forward Bulkhead	$.307(10)^{-8}$		$1.03(10)^{-8}$		
		$.057(10)^{-8}$		$.253(10)^{-8}$	4.44
CM Aft Bulkhead	$.250(10)^{-8}$		$.777(10)^{-8}$		
		$.2086(10)^{-8}$		$.7332(10)^{-8}$	3.52
SM Forward Bulkhead	$.0414(10)^{-8}$		$.0438(10)^{-8}$		

Note: Models are constrained at the aft end of the SM and unit moment is applied at the docking port.

Calculation of incremental torsional springs:

1. Between CM forward and aft bulkheads,

$$K^1_{Apollo} = K^1_{Skylab} + \quad K^1 = K^1_{Skylab} + 3.44\, K^1_{Skylab}$$

$$\therefore \quad K^1 = 3.44 \left(\frac{1}{.253(10)^{-8}} \right) = 1.36(10)^9$$

2. Between CM aft bulkhead and SM forward bulkhead,

$$K^2_{Apollo} = K^2_{Skylab} + \quad K^2 = K^2_{Skylab} + 2.52\, K^2_{Skylab}$$

$$\therefore \quad K^2 = 2.52 \left(\frac{1}{.7332(10)^{-8}} \right) = 3.42(10)^8$$

Figure 5.9 Test/Analytical Mode Comparisons

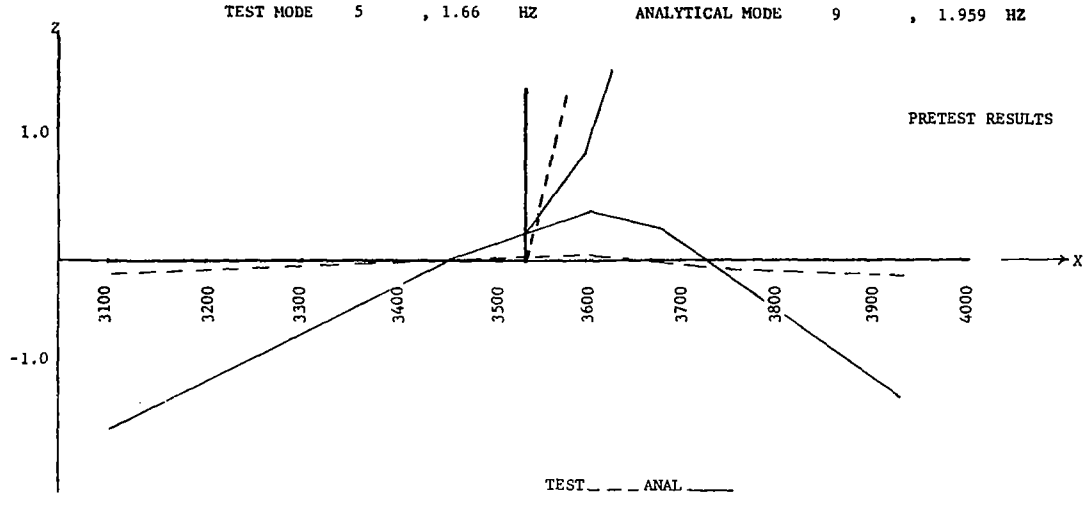

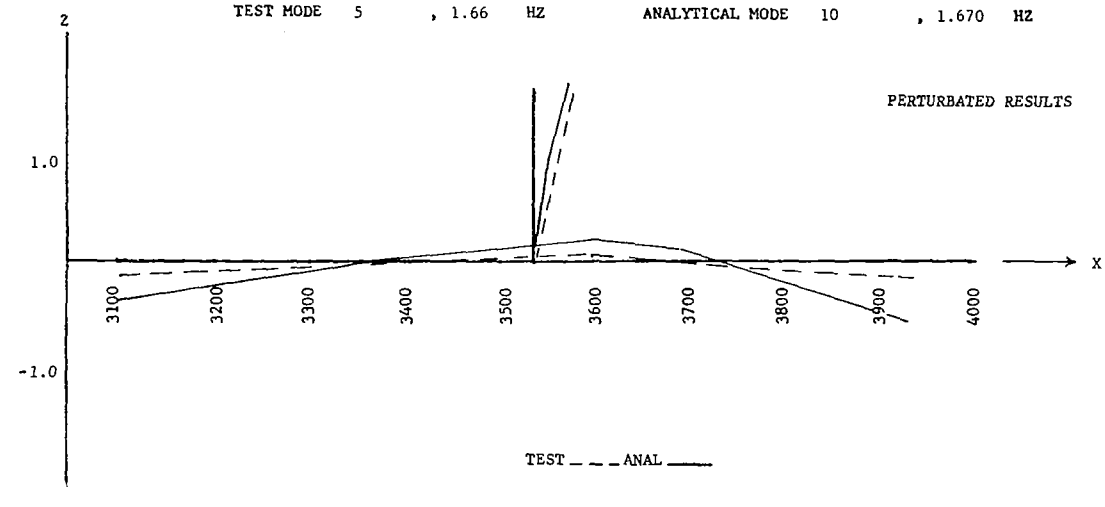

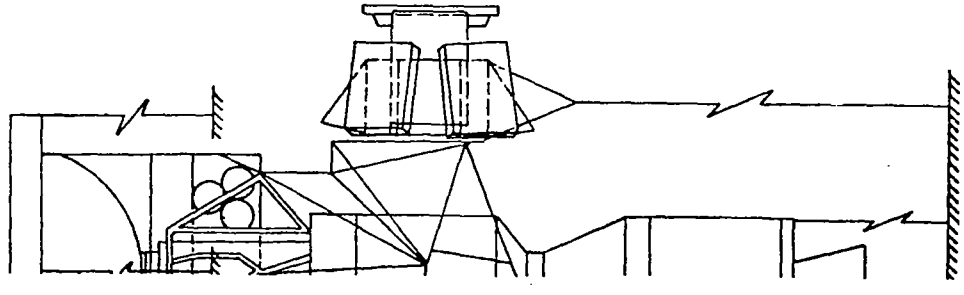

Figure 5.10 Test/Analytical Mode Comparisons

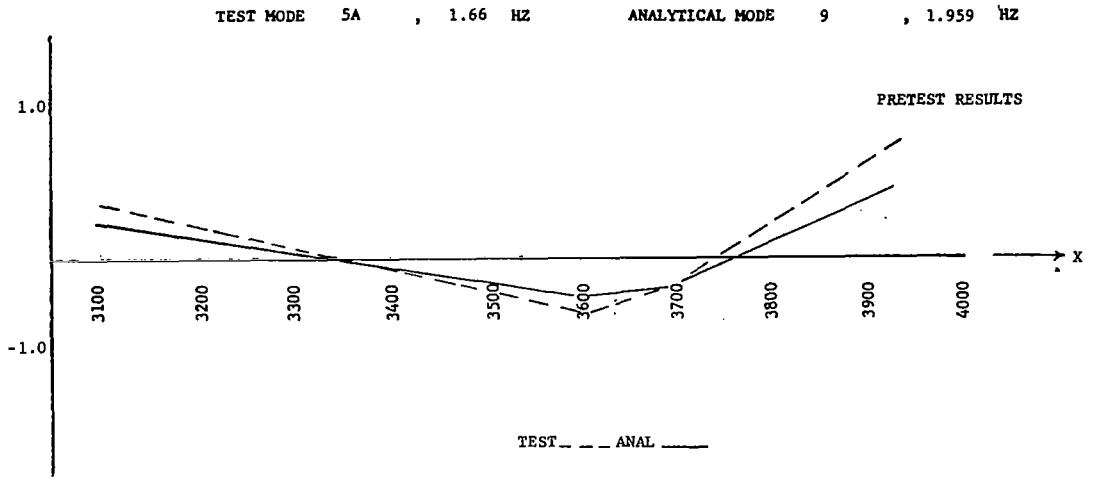

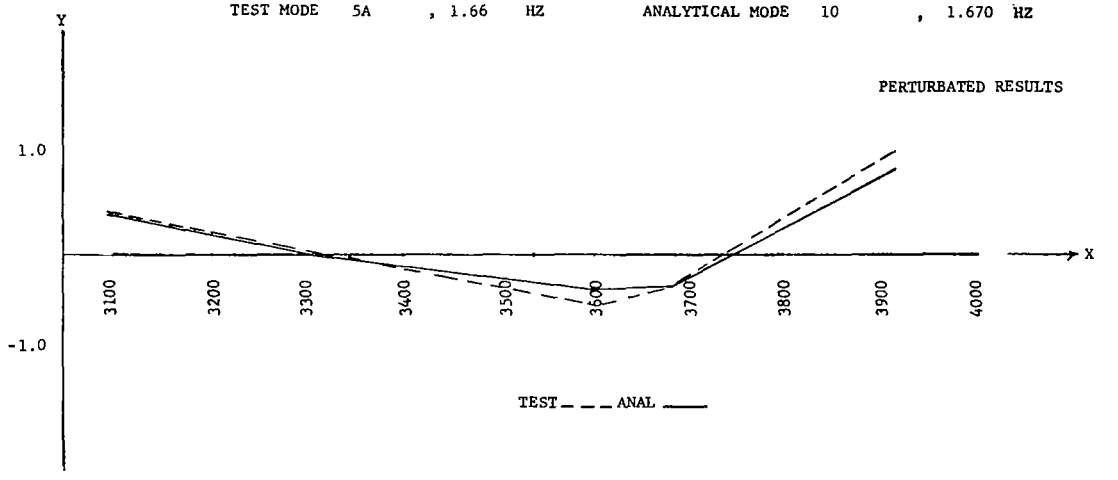

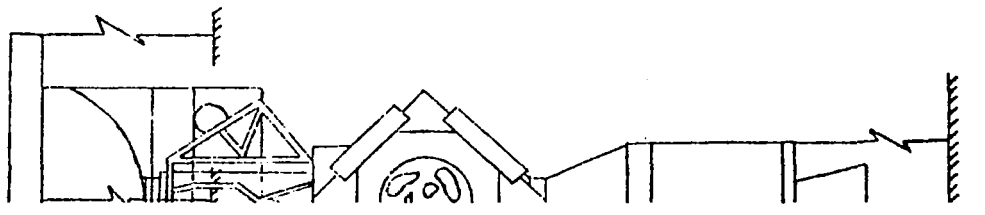

Figure 5.11 Test/Analytical Mode Comparisons

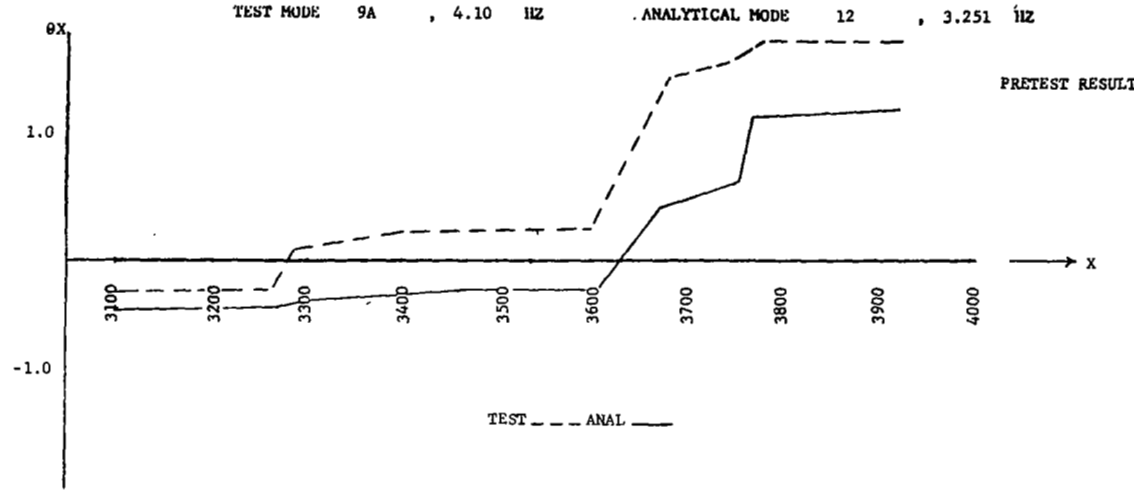

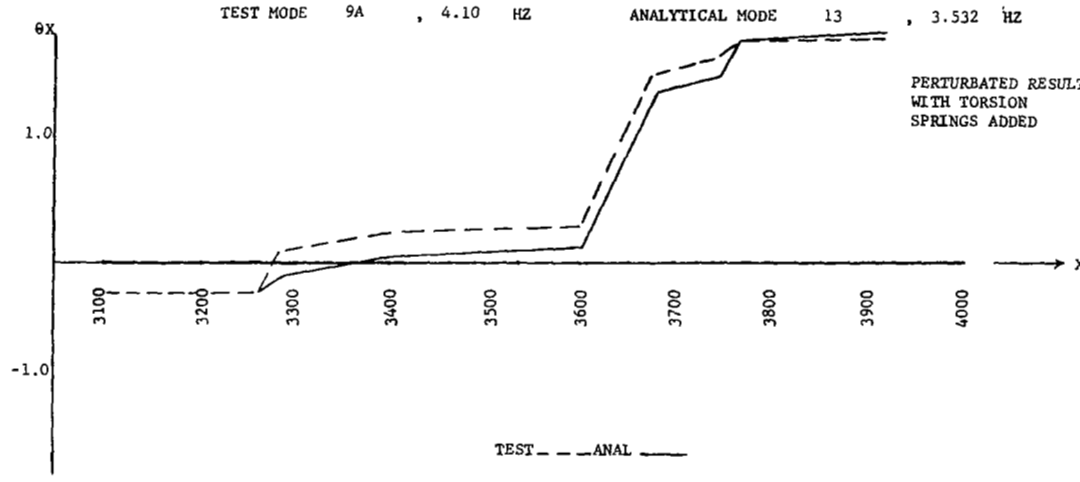

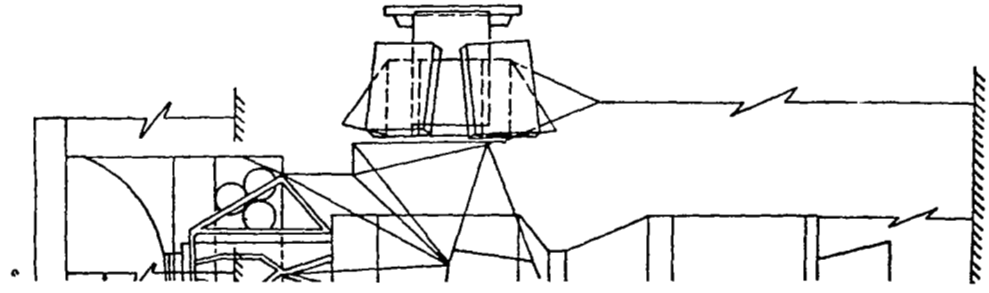

Figure 5.12 Test/Analytical Mode Comparisons

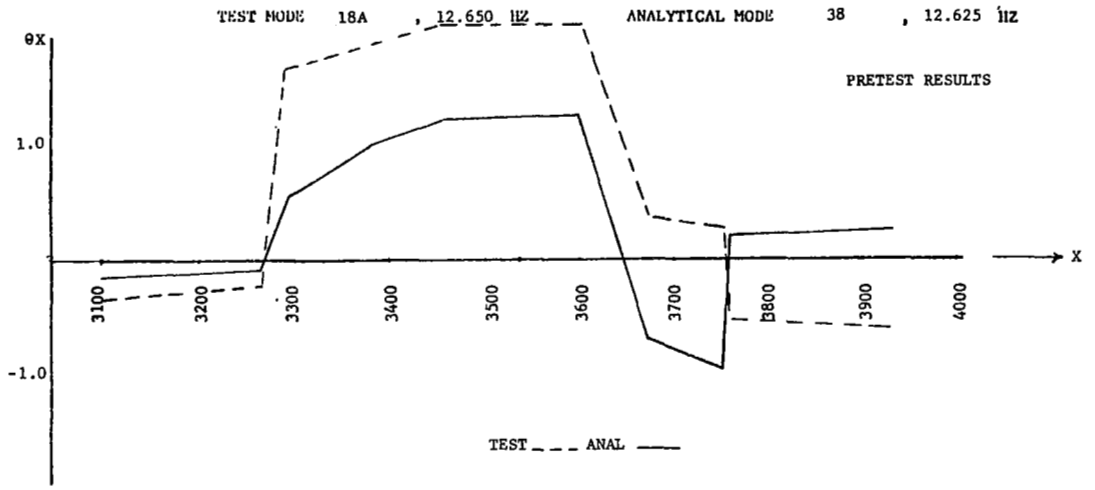

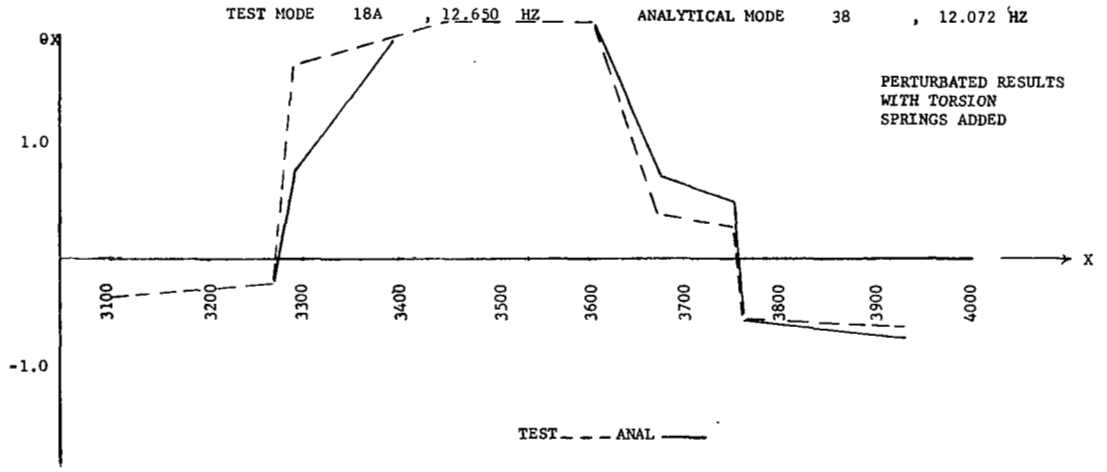

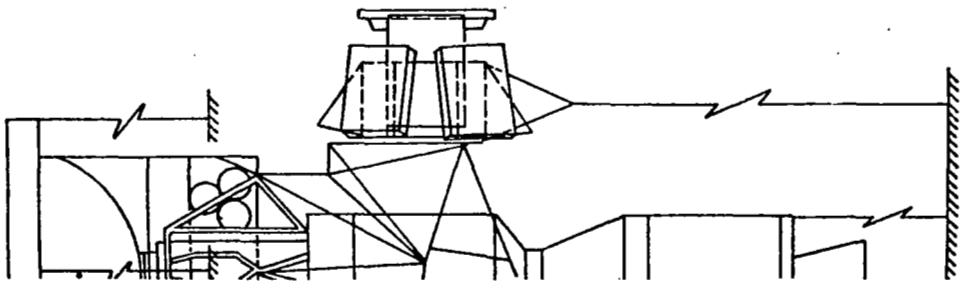

Table 5.17

Summary of Test and Analytical Modes Correlation

TEST MODE					ANALYTICAL MODE				
MODE NO.	FREQ. HZ.	GMC TABLES	PLOT NO.	DESCRIPTION/COMMENTS	MODE NO.	FREQ. HZ.	GMC TABLES	PLOT NO.	DESCRIPTION/COMMENTS
03B	1.31	A-5 A-6	B-1	X-Z plane 1st bending in MDA cone with ATM Y axis rotation on upper DA truss out of phase with CSM. (Spurious TH Z motion at Node 28. suspected).	7	1.279	C-1 C-2	D-1	Good agreement with test, GMC and plotted data in all planes.
04A	1.43	A-7 A-8	B-2	X-Y plane 1st bending in MDA cone with ATM X axis rotation on upper DA truss in phase with main beam, outer ATM Y motion in phase with CSM.	8	1.377	C-3 C-4	D-2	Good agreement with test, GMC and plotted data in all planes.
05A	1.66	A-9 A-10	B-3	X-Y plane 1st bending in MDA cone with ATM X axis rotation on upper DA truss out of phase with main beam, outer ATM Y motion out of phase with CSM. (Spurious TH Z motion at node 28 suspected.).	10	1.670	C-7 C-8	D-4	Combination of 05A and 06B motion, predominately 05A.
06B	1.74	A-13 A-14	B-5	X-Z plane 1st bending in MDA cone with ATM Y axis rotation on upper DA truss in phase with CSM.	9	1.643	C-5 C-6	D-3	Combination of 05A and 06B motion, predominately 06B.

Table 5.17 Continued

Summary of Test and Analytical Modes Correlation

TEST MODE					ANALYTICAL MODE				
MODE NO.	FREQ. HZ.	GMC TABLES	PLOT NO.	DESCRIPTION/COMMENTS	MODE NO.	FREQ. HZ.	GMC TABLES	PLOT NO.	DESCRIPTION/COMMENTS
07A	2.51	A-15 A-16	B-6	X-Y plane 1st bending in MDA cone with ATM X axis rotation on upper DA truss out of phase with main beam, outter ATM Y motion in phase with CSM. (TH Y and TH Z data inconsistent with Y and Z results.)	11	2.338	C-9 C-10	D-4	Good agreement with test GMC data in all planes and with plotted data in X, Y, Z and TH X.
08A	3.06	A-17 A-18	B-7	X-Z plane 1st bending in MDA cone with ATM Y axis rotation on upper DA truss out of phase with CSM, and ATM Z axis translation on upper DA truss in phase with CSM.	12	3.151	C-11 C-12	D-5	Good agreement with test GMC data in all planes and with plotted data in X, Y, Z and TH Y.
09A	4.10	A-19 A-20	B-8	1st torsional mode with CSM. MDA/STS/AM out of phase with FAS/IU/OWS. Large torsional deflection across MDA cone.	13	3.531	C-13 C-14	D-6	Good agreement with test GMC data in all planes and with plotted data in Y and TH X.
10A	4.50	A-21 A-22	B-9	X-Y plane 2nd bending in MDA cone and STS/AM coupled with 1st torsional mode, and ATM X axis rotation on upper DA out of phase with CSM.	14	4.323	C-15 C-16	D-7	Good agreement with test GMC data in all planes and with plotted data in X, Y, Z and TH X.

Table 5.17 Continued

Summary of Test and Analytical Modes Correlation

TEST MODE					ANALYTICAL MODE				
MODE NO.	FREQ. HZ.	GMC TABLES	PLOT NO.	DESCRIPTION/COMMENTS	MODE NO.	FREQ. HZ.	GMC TABLES	PLOT NO.	DESCRIPTION/COMMENTS
11A	5.03	A-25 A-26	B-11	X-Z plane 2nd bending in MDA cone and STS/AM with large ATM Y axis rotation on upper DA truss in phase with CSM. (Spurious TH Z data at Node 28 suspected)	15	4.868	C-17 C-18	D-8	Good agreement with test GMC and plotted data in all planes (when spurious test TH Z is ignored).
12A	5.86	A-27 A-28	B-12	X-Y plane 2nd bending in MDA cone and STS/AM coupled with 1st torsional mode and ATM X axis rotation on upper DA out of phase with CSM (Similar to 10A except TH X and Y motion phase reversed). Also FAS Oxygen tanks Y and Z motion.	18	5.706	C-19 C-20	D-9	Good agreement with test GMC data except for Oxygen tanks motion and with plotted data in X, Y and TH Z.
13B	6.36	A-31 A-32	B-14	X-Z plane 2nd bending in MDA cone and STS/AM with ATM Y axis rotation on upper DA truss out of phase with CSM.	21	6.552	C-21 C-22	D-10	Good agreement with test GMC and plotted data in all planes.
14A	6.73	A-33 A-34	B-15	FAS Oxygen tanks Y and Z motion.	28	9.192	C-23 C-24	---	FAS Oxygen tanks Y and Z motion, no shape correlation.

Table 5.17 Continued

Summary of Test and Analytical Modes Correlation

TEST MODE					ANALYTICAL MODE				
MODE NO.	FREQ. HZ.	GMC TABLES	PLOT NO.	DESCRIPTION/COMMENTS	MODE NO.	FREQ. HZ.	GMC TABLES	PLOT NO.	DESCRIPTION
16A	8.85	A-37 A-38	B-17	1st axial mode with node point in AM.	30	9.405	C-25 C-26	D-11	Good agreement with test GMC data in all planes and with plotted data in axial plane (except CSM X deflection is larger in test than analysis.)
17A	11.59	A-39 A-40	B-18	FAS Oxygen tanks Y and Z motion.	--	-----	----	----	No true correlation.
18A	12.65	A-41 A-42	B-19	2nd torsional mode with nodes between CM and SM bulkheads and across AM trusses.	38	12.072	C-28 C-29	D-12	Good agreement with test GMC data in all planes and with plotted data in torsional plane.
19A	13.30	A-45 A-46	B-21	AM Nitrogen tank Y motion (model point 20) and vehicle 3rd bending predominately in X-Y plane.	39	12.568	C-29 C-30	----	AM Nitrogen tanks Y motion (Model points 20 and 21) no shape correlation.
20A	13.68	A-47 A-48	B-22	AM Nitrogen tanks Y and Z motion with vehicle 3rd bending predominately in X-Z plane. This mode was not well separated from test mode 19A as shown by large coupling in orthogonality check. (Ref. ED-2002-1522).	41	13.323	C-31 C-32	D-13	Good agreement with test mode 19A plotted data in Y and TH Z. Good agreement with test mode 20A plotted data in Z and TH Y.

Table 5.17 (Concluded)

Summary of Test and Analytical Modes Correlation

TEST MODE					ANALYTICAL MODE				
MODE NO.	FREQ. HZ.	GMC TABLES	PLOT NO.	DESCRIPTION/COMMENTS	MODE NO.	FREQ. HZ.	GMC TABLES	PLOT NO.	DESCRIPTION/COMMENTS
21A	14.55	A-49 A-50	B-23	AM Nitrogen tanks Y motion and vehicle 3rd bending in X-Y plane	45	14.855	C-33 C-34	D-14	Good agreement with test mode 21A GMC data in Y plane. Shape correlation is only fair. (Shape of analytical mode 41 correlates better with test mode 21A). Poor agreement with test mode 22B GMC data but shape correlation is fair.
22B	15.4	A-51 A-52	B-24	Predominately vehicle 3rd bending in X-Y plane. AM Nitrogen tanks Y and Z motions, FAS Oxygen tanks X, Y, and Z motions.					
23A	16.20	A-55 A-56	B-26	AM Nitrogen tanks Z motion with FAS Oxygen tanks X, Y, and Z motion 4th vehicle bending in X-Z plane.	56	17.553	C-35 C-36	----	Large AM Nitrogen tanks Z motions. No shape correlation.
24A	16.53	A-57 A-58	B-27	AM Nitrogen tanks Y motion with FAS Oxygen tanks X motion.	58	18.361	C-37 C-38	----	Fair agreement with test GMC data in all planes. No shape correlation.
25A	17.01	A-59	B-28	2nd Axial mode with node points between SM and CM bulkheads and across AM trusses.	65	19.644	C-39 C-40	D-15	2nd axial mode with node points at port and across AM trusses (CSM X deflection is larger than analysis).

5.6 Postflight Model Verification

This is a good time to show how the analyst can be trapped into altering a component stiffness properties without sufficient knowledge of the components structural detail. A fourier analysis of the ATM rack rate gyro flight measurements provides frequency data representing the ATM supported by the DA.

5.6.1 Flight Results - During maneuvers performed at 149:10:25:10 in SL-2 flight, the rate gyros displayed the data presented in Figure 5.13 for the x, y and z axes. The sampling rate of the gyro data is 12 samples per second. A Fourier analysis was performed to identify the frequency of the recorded signal. The period analyzed was 512 samples which corresponds to 42.66 seconds. The frequency content is plotted also in Figure 5.13 with a frequency resolution of 0.0234 (12/512) Hz. The dominant frequencies are listed by axis in the following table.

	Dominant Frequency - Hz		
Axis	1	2	3
X	0.8767	1.027	--
Y	1.60	1.35	1.80
Z	0.876	1.027	--

The principal frequency content is 0.88 Hz about the x and z axes and 1.6 Hz about the y axis. Review of vibration analyses of the Skylab configuration indicates the following correlation with orbital data.

Flight Data	Pre-GVS Analysis Config. 1.2 (Ref. ED-2002-790-4, January 1971)	Post-GVS Analysis Config. 1.2 (Ref. ED-2002-1562-2, November 1972)
.88 Hz	.888 Hz ATM/DA1 (81%)	.594 Hz DA (DEPL)1 (77%)
1.60 Hz	1.655 Hz ATM/DA4 (72%)	1.275 Hz DA (DEPL)2 (25%)

The low frequency analytical modes were selected on the basis of their correlation of ATM slopes in the x and z axis with θ_x and θ_z flight rate gyro data at .88 Hz. Similarly, the high frequency analytical modes exhibited ATM θ_y correlation with the 1.60 Hz rate gyro data. ATM/DA4 is the essentially same mode as DA(DEPL)2. The names and uncoupled mode numbers differ due to a change in component definitions between the two analyses.

The differences in the pre and post-GVS results reflect the DA stiffness scaling factor. A scaling factor to decrease the DA stiffness was determined which improved correlation between experimental and analytical frequency data in a least squares sense. Unfortunately this scaling factor decreased correlation with flight results. A rigorous explanation for these conflicting results would require extensive reanalysis. However, it is theorized that the source of the discrepancy arises from the fact that individual DA truss member adjustments required to improve experimental/theoretical correlation could not be made due to lack of component modeling detail information at MMC. A review of the type of motion in the modes of concern and comparison of MDAC and MMC flexibility definition of the DA truss were made to support this theory as follows.

The on-orbit configuration vibration analysis was rerun using the original (unscaled) MDAC DA truss stiffness model. This analysis produced a .785 Hz and a 1.497 Hz mode which correlate respectively with the .88 Hz and 1.6 Hz flight data. Examination of the mode shapes of the modes of interest (Table 5.18) shows the relative deflection across the DA rigidizing arms is very large in the directions associated with the primary motion of the overall mode shape. That is, large Δ X and Δ Y motions occur in the .784 Hz mode which is primarily θ_z of the ATM, and large Δ X motions occur in the 1.497 Hz mode which is primarily X, θ_y of the ATM. This observation suggests that increasing the stiffness modeling of the DA rigidizing arms alone would improve correlation of these modes with flight data. It also suggests that the stiffness of the DA between the ATM support frame (excluding rigidizing arms) and the trunnions could be decreased as required to improve correlation with GVS results without greatly affecting the frequency of the modes observed from flight data.

A comparison of MDAC and MMC DA truss flexibility influence coefficient data (Table 5.19) shows that the MMC model is considerably softer than MDACs between the ATM support frame and the FAS interface. The fact that the MMC model produced lower frequency GVS correlatable modes than the MDAC model was pointed out and supported the DA scaling factor that was defined. Table 5.19 also shows that MMC model represents the rigidizing arms to be stiffer than the MDAC model by a factor of 2 at DOF 13 and 19 and a factor of 1.5 at DOF 14 and 20. Although the MMC DA model has not been used in an on-orbit configuration vibration analyses with which to compare the modes of interest, these differences in DA modeling in an area that strongly affects the flight data modes indicates that local DA truss member modeling adjustments are required for theoretical correlation with both flight and GVS results.

Since the only significant structural response observed from on-orbit flight data was contained primarily in the .88 hz and 1.6 Hz modes, the DA scaling factor was abandoned.

Configuration 1.3N1/ was revised to incorporate the unscaled MDAC truss stiffness model.

.6.2 Recommendations -

a. In future applications of the methodology developed under this task to other vehicles, assure the availability of subcomponent modeling detail.

b. Develop a method to determine the type of test results that will be most suitable for theoretical/experimental correlation studies on a particular vehicle, and improve testing techniques to assure that such data will be obtained.

Table 5.18 Modal Deflections Across DA Rigidizing Arms

	25th Mode .784 Hz DA(DEPL)1					40th Mode 1.497 Hz, DA(DEPL)2				
Direction	DOF	ATM Attach Point	DOF	ATM Support Frame	Attach Point/ Support Frame	DOF	ATM Attach Point	DOF	ATM Support Frame	Attach Point/ Support Frame
X	1	$-4.587(10)^{-2}$	31	$-2.546(10)^{-2}$	1.81	1	$5.318(10)^{-2}$	31	$1.646(10)^{-2}$	3.25
Y	2	$5.101(10)^{-2}$	32	$3.584(10)^{-2}$	1.42	2	$-3.958(10)^{-3}$	32	$-3.045(10)^{-3}$	small ampl.
Z	3	$-2.422(10)^{-2}$	33	$-2.629(10)^{-2}$	.92	3	$-1.989(10)^{-2}$	33	$-2.082(10)^{-2}$	.95
X	7	$4.644(10)^{-2}$	34	$2.581(10)^{-2}$	1.80	7	$4.627(10)^{-2}$	34	$1.064(10)^{-2}$	4.34
Y	8	$5.097(10)^{-2}$	35	$3.585(10)^{-2}$	1.42	8	$-4.698(10)^{-3}$	35	$-9.236(10)^{-4}$	small ampl.
Z	9	$2.427(10)^{-2}$	36	$2.630(10)^{-2}$	.93	9	$-2.573(10)^{-2}$	36	$-2.733(10)^{-2}$	.94
X	13	$1.952(10)^{-2}$	28	$1.059(10)^{-2}$	1.85	13	$4.872(10)^{-2}$	28	$1.230(10)^{-2}$	3.96
Y	14	$-1.430(10)^{-2}$	29	$4.394(10)^{-3}$	-3.25	14	$1.351(10)^{-4}$	29	$2.293(10)^{-4}$	small ampl.
Z	15	$1.004(10)^{-2}$	30	$5.960(10)^{-3}$	1.68	15	$-6.110(10)^{-2}$	30	$-5.956(10)^{-2}$	1.03
X	19	$-1.888(10)^{-2}$	25	$-1.024(10)^{-2}$	1.84	19	$5.170(10)^{-2}$	25	$1.554(10)^{-2}$	3.33
Y	20	$-1.432(10)^{-2}$	26	$4.395(10)^{-3}$	-3.26	20	$-1.685(10)^{-5}$	26	$2.633(10)^{-4}$	small ampl.
Z	21	$-1.058(10)^{-2}$	27	$-6.461(10)^{-3}$	1.63	21	$-6.216(10)^{-2}$	27	$-6.024(10)^{-2}$	1.03

DOF Locations:

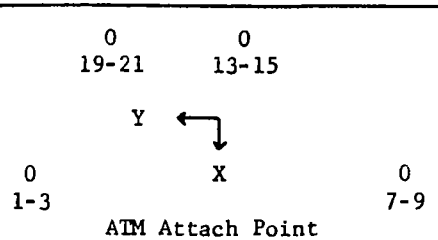

ATM Attach Point

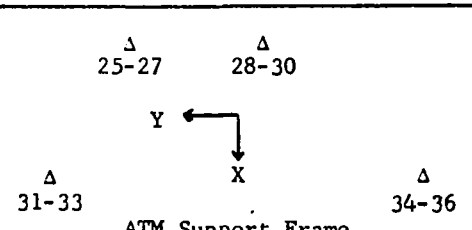

ATM Support Frame

Table 5.19 Flexibility Influence Coefficients Across Rigidizing Arms

	MDAC DA Model					MMC DA Model				
Direction	i/j	ATM Attach Point Defl i/Load j	i/j	ATM Support Frame Defl i/Load j	Attach Point/ Support Frame	i/j	ATM Attach Point Defl i/Load j	i/j	ATM Support Frame Defl i/Load j	Attach Point/ Support Frame
X	1/1	$3.340(10)^{-4}$	31/1	$1.322(10)^{-4}$	2.53	1/1	$4.378(10)^{-4}$	31/1	$1.605(10)^{-4}$	2.72
Y	2/2	$3.707(10)^{-4}$	32/2	$1.840(10)^{-4}$	2.02	2/2	$4.818(10)^{-4}$	32/2	$2.126(10)^{-4}$	2.27
Z	3/3	$1.175(10)^{-4}$	33/3	$1.091(10)^{-4}$	1.075	3/3	$1.877(10)^{-4}$	33/3	$1.874(10)^{-4}$	1.0
X	7/7	$3.333(10)^{-4}$	34/7	$1.321(10)^{-4}$	2.52	7/7	$4.385(10)^{-4}$	34/7	$1.610(10)^{-4}$	2.72
Y	8/8	$3.715(10)^{-4}$	35/8	$1.843(10)^{-4}$	2.01	8/8	$4.823(10)^{-4}$	35/8	$2.128(10)^{-4}$	2.26
Z	9/9	$1.155(10)^{-4}$	36/9	$1.071(10)^{-4}$	1.07	9/9	$1.838(10)^{-4}$	36/9	$1.836(10)^{-4}$	1.0
X	13/13	$3.659(10)^{-4}$	28/13	$1.136(10)^{-4}$	3.22	13/13	$3.211(10)^{-4}$	28/13	$1.937(10)^{-4}$	1.66
Y	14/14	$3.707(10)^{-4}$	29/14	$1.607(10)^{-4}$	2.31	14/14	$3.516(10)^{-4}$	29/14	$2.297(10)^{-4}$	1.53
Z	15/15	$7.127(10)^{-5}$	30/15	$5.823(10)^{-5}$	1.22	15/15	$7.362(10)^{-5}$	30/15	$7.337(10)^{-5}$	1.0
X	19/19	$3.654(10)^{-4}$	25/19	$1.137(10)^{-4}$	3.21	19/19	$3.213(10)^{-4}$	25/19	$1.938(10)^{-4}$	1.66
Y	20/20	$3.706(10)^{-4}$	26/20	$1.606(10)^{-4}$	2.31	20/20	$3.516(10)^{-4}$	26/20	$2.298(10)^{-4}$	1.53
Z	21/21	$7.277(10)^{-5}$	27/21	$5.956(10)^{-5}$	1.22	21/21	$7.073(10)^{-5}$	27/21	$7.049(10)^{-5}$	1.0

DOF Locations:

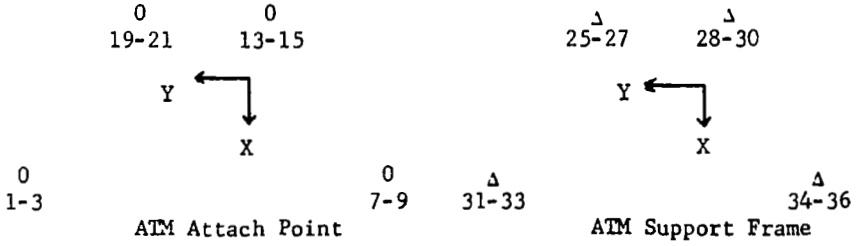

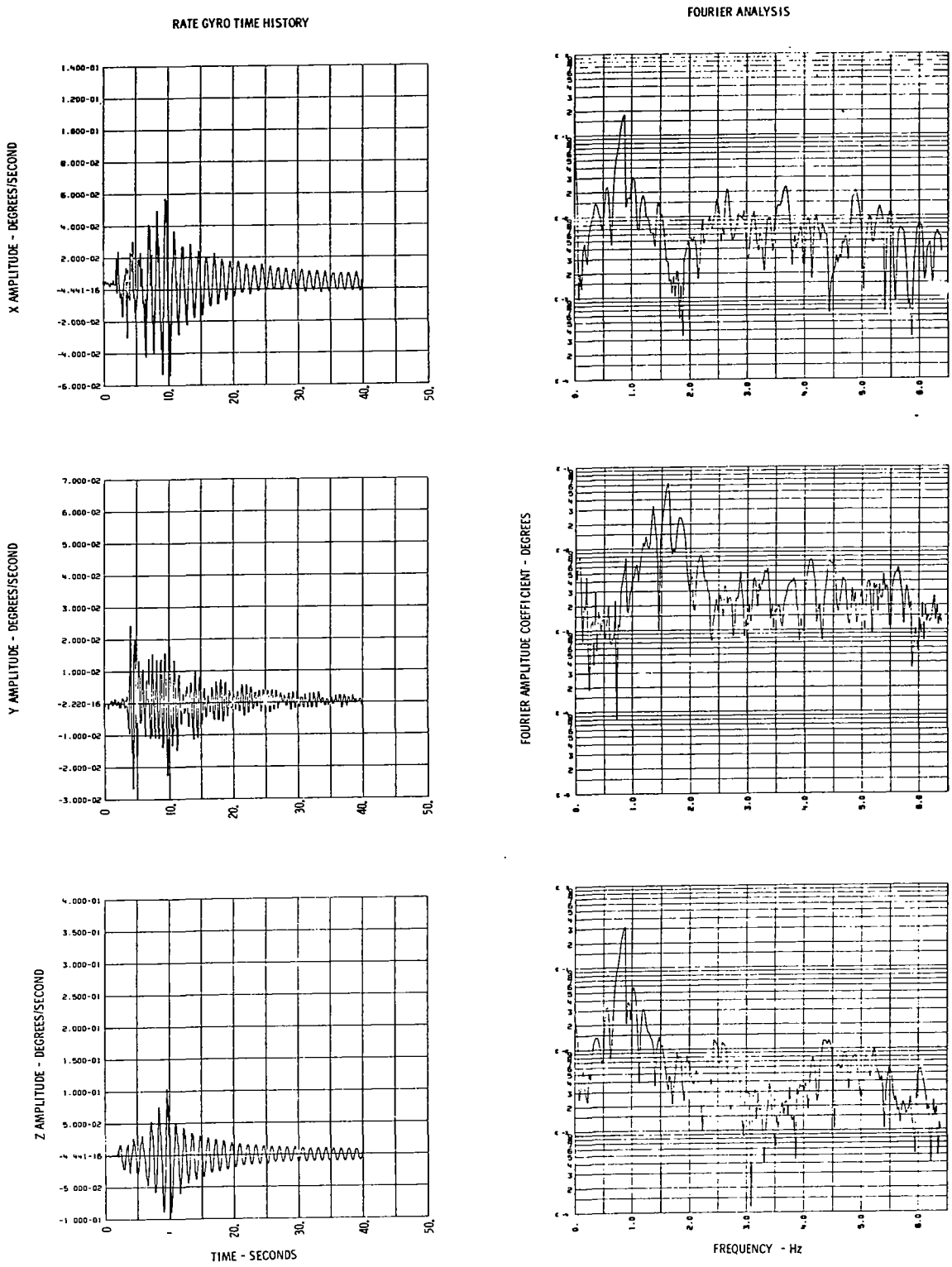

Figure 5.13 RATE GYRO TIME HISTORY AND FOURIER ANALYSIS

6.0 CONCLUSIONS

Detailed conclusions and subsequent recommendations are included within each section. However, on an overview of the Skylab program, several distinct points are obvious. In the process of completing a particular difficult project both on a logistics and a technical basis short cuts are taken, baseline costs are trimmed, programs are delayed or ignored, all of which normally have to be repeated at a much larger cost. These items are particularly true in structural analyses.

As a result of this summary of the Skylab project, the following recommendations are presented for evaluation in the areas of importance and on a chronological basis.

6.1 Structural Models

It is imperative that detailed plans be established initially in the program to define sensitive structural areas. These areas refer to either response, which affects modal characteristics and resultant stability studies, or load which affects structural design, material properties and sizing.

Since the problem is one of integration in a design beam or stick models will always be required, initially. However, even with beam models care should be exercised with modeling, in some detail, "all" structural system interfaces. "All" should be literally interpretated if possible and at a minimum should include any interface between separate system modeling, contractors or centers.

After completion of detailed analytical studies, using the derived beam models, resulting load and response data should be integrated in the structural design. This should culminate in finite element models of all sensitive structures and will remain "frozen" until completion of the subject dynamic test. Obviously, all sensitive structure will complete, at a minimum, static influence coefficient tests.

6.2 System Modal Characteristics

Accurate vibration analyses must be completed for both load, response and control stability studies. However, these studies should be completed in an orderly manner and in sufficient detail so as to satisfy modal fidelity, and modal characteristics for the data users.

Initial studies should be limited to the structural beam models. There is a strong tendency in projects and the customer to require instantaneous vibration analysis. This results in a continued update of the data at great expense. In reality, programs should be planned to

follow four periods of structural modeling and derivation of modal characteristics of the Structural System. These are:

a. initial beam models,
b. preliminary finite element models,
c. models generated at completion of static test and initial design reviews,
d. models generated at completion of dynamic test and system design reviews.

6.3 Structural Testing

Static, dynamic and acoustic test seems to always be completely planned on a project then revised continually throughout the program. Initially, in the program a strong committment should be made on structural testing and what areas are to be completed. This includes preliminary instrumentation, support system and data retrieval programs.

If a test is worth completing, and considering the associated cost of just initiating any structural test, it must have a strong committment from the project. It should be planned and frozen well in advance of scheduled testing and completed in a timely manner so as to affect design and reduce costly analysis requirement.

Structural testing should not be considered only as ground tests. As a post mortem on the Skylab program, it seems ridiculous that such limited structural data was retrieved from flight. Mega dollars were spent during the study to resolve array response, gimbal ring response, docking loads and beam fairing loads yet limited if any flight data was retrieved to verify design decisions, load/response criteria, or as a guide to future projects. Additionally, dynamic test data relating to acoustic environment (a noted problem in orbit) and structural damping data (a significant problem in structural design) remains to be analyzed.

Specifically, the following recommendations are made for structural testing:

a. influence coefficient test should be completed for all interface structural systems;

b. automatic modal tuning programs should be devised to speed up testing and assure accurate and timely results;

c. detailed pretest analyses should be completed;

d. adequate instrumentation must be provided to assure accurate results especially in resolving structural damping;

e. detailed correlation studies should be planned and completed in a timely manner;

f. results of all tests should be implemented in the analysis schedule.

6.4 General

Control and loads studies are generally analyzed in sufficient detail. However, emphasis should be placed on limiting these studies to the four periods of structural modeling and in completing the final response and load studies with test verified models.

The abandoned child in most major projects is the adequate mission evaluation studies for structural systems. Therefore, it is imperative that project directors assure there is adequate flight evaluation and correlation of structural design decisions and models, based on sufficient flight instrumentation.

7.0 NOTES

7.1 Abbreviations

$\bar{\alpha}$	Average Absorption Coefficient
AM	Airlock Module
ATM	Apollo Telescope Mount
CDR	Commander
CG	Center of Gravity
CMG	Control Moment Gyro
CSM	Command and Service Module
DA	Deployment Assembly
dB	Decibels
dBA	Sound level measured with A-weighting network
DC	Direct Current
DTA	Dynamic Test Article
FAS	Fixed Airlock Shroud
FCC	IU Flight Control Computer
FS	S-IVB Forward Skirt
ft	Feet
GRA	Gimbal Ring Assembly
GMC	Generalized Mass Contribution
Hz	Hertz (cycles per second)
IMC	IMC Magnetics Corporation
in	Inches
IU	Instrumentation Unit
Log_{10}	Logarithm to the base 10
MDA	Multiple Docking Adapter
MDAC-E	McDonnell Douglas Astronautics Company - Eastern Division
MDAC-W	McDonnell Douglas Astronautics Company - Western Division
Microbar	A pressure of one dyne per square centimeter
MMC	Martin Marietta Corporation
MSC	Manned Spacecraft Center

MSFC	Marshall Space Flight Center
MST	Modal Survey Test(s)
MSIL	Modified Speech Interference Level
N_2	Gaseous Nitrogen
NAR	North American Rockwell Corporation
NASA	National Aeronautics and Space Administration
O_2	Gaseous Oxygen
OB	Octave Band
OWS	Orbital Workshop
P	Pressure
PA	Payload Assembly
PLT	Pilot
PLV	Post Landing Ventilation
PSI	Pounds Per Square Inch
PSIA	Pounds Per Square Inch, Absolute
PSIL	Preferred Speech Interference Level
PRI	Primary Mole Sieve Fans
PS	Payload Shroud
PWL	Acoustic Power Level, dB
R	Room Constant
Ref.	Reference
S	Area of Room
SAS	Solar Array System
SAT	Systems Assurance Test
Sec	Secondary Mole Sieve Fans
SIA	Speaker Intercom Assembly
SIL	Speech Interference Level
SMEAT	Skylab Medical Experiment Altitude Test
SPL	Sound Pressure Level, dB
SPT	Science Pilot
STS	Structural Transition Section
SWS	Saturn Workshop
T60	Reverberation Time, Seconds
TCBD	Test Control Board Directive

TL	Transmission Loss, dB
TVIS	TV Input Station
V	Volume
VCS	Ventilation Control System
WMC	Waste Management Compartment
WOB	Weighted Octave Band

7.2 References

The following documents are referenced in the foregoing sections by numbers only.

1. W. A. Benfield and R. F. Hruda: Vibration Analysis of Structures by Component Mode Substitution, AIAA/ASME 11th Structural Dynamics and Material Conference, Denver, Colorado, April 22 - 24, 1970.

2. W. D. Brayton, "Dynamic Analysis of the Probe and Drogue Docking Mechanism", Journal of Spacecraft and Rockets, May 1966.

3. David W. Malone: A Program to Derive Analytical Model Representations of the Apollo Spacecraft and ITS Launch Vehicles, Docking Analysis Final Report. D2-84124-3. The Boeing Company, Space Division, Seattle, Washington, May 1967.

4. R. J. Ravera: Docking Dynamics Simulation for AAP. Technical Memorandum TM-69-1022-6. Bellcomm, Inc., Washington, D.C., July 1969.

5. C. Lanczos: The Variational Principles of Mechanics. University of Toronoto Press, 1966.

6. C. S. Bodley and A. C. Park: Skylab Docking Response Program. ED-2002-770. Martin Marietta Corporation, Denver, Colorado, April 1970.

7. J. Gremel (Personal Communication), McDonnell Douglas Astronautics Company-East: 1972.

8. Caldwell C. Johnson: TM-X-58163, Skylab M487 Habitability/Crew Quarters, dated October 1975

9. AFSC Design Handbook, Series 1-0, Personnel Subsystems, DH 1-3, January 1969.

10. Acoustic Absorption Data Internal to Shroud, MSC TCBD No. OWS/PA-52, Houston, Texas, 26 August 1971.

11. Additional Acoustic Test for IU Anomaly Investigation, MSC, TCBD No. OWS/PA-57, Houston, Texas, 6 October 1971.

12. Vibration Acoustic Data from the Skylab Phase IIA Payload Assembly Vibroacoustic Test for the Liftoff Condition, Data Book for:

Runs	Enclosure
PA-A-008 & 009	3
PA-A-040	5
PA-A-043	7
PA-A-044	8

MSFC Document No. S&A-ASTN-ADD-72- , Huntsville, Alabama, Release Date Pending.

13. Vibration Acoustic Data from the Skylab Phase IIA Payload Assembly Vibroacoustic Test for Boundary Layer Condition, Data Book for:

Runs	Enclosure
PA-A-011 & 012	4
PA-A-041	6
PA-A-045	9

MSFC Document No. S&E-ASTN-ADD-72- , Huntsville, Alabama, Release Date Pending.

14. Phase and Amplitude Data from the Skylab Phase IIA Payload Assembly Special Modal Survey Test Performed on the Instrument Unit, Data Book for:

Runs	Enclosure
PA-V-012, 014, 015, 019, 021, 026, 027, 029, 031, 033, 034, 036, 038, 040, 041 and 044	10

MSFC Document No. S&E-ASTN-ADD-72- , Huntsville, Alabama, Release Date Pending.

15. W. P. Rodden, "A Method for Deriving Structural Influence Coefficients from Ground Vibration Tests", AIAA Journal, Vol. 5, No. 5, May 1967, pp. 991-1000.

16. A. Breman and W. C. Flannelly, "Theory of Incomplete Models of Dynamic Structures", AIAA Journal, Vol. 9, No. 8, August 1971, pp. 1481-1487.

17. R. G. Ross Jr., "Synthesis of Stiffness and Mass Matrices from Experiments Vibration Modes", SAE Preprint 710787, pp. 1-9.

18. A. E. Galef and D. L. Cronin, "Determination of Structural Properties from Test Data", The Shock and Vibration Bulletin, Bulletin 41, Part 7, December 1970, pp. 9-18.

19. B. M. Hall and E. D. Calkin, "Linear Estimation of Structural Parameters from Dynamic Test Data", AIAA/ASME 11th Structures, Structural Dynamics, and Materials Conference, Denver, Colorado, April 22-24, 1970.

20. R. L. Fox and M. P. Kapoor, "Rates of Change of Eigenvalues and Eigenvectors", AIAA Journal, Vol. 6, No. 12, December 1968, pp. 2426-2429.

7.3 Additional Reference Material

This section provides a listing of the date, report number and title of Skylab documents that are applicable to the dynamics effort. Much of the information in this report was developed from these documents, therefore, persons requiring additional information or specific data may find this reference section useful.

Date	Report No. ED-2002-	Title
10/27/67	181	AAP Docking Loads Analysis
04/15/68	445-1	Docking Loads Report
06/15/68	445-2	Docking Loads Report
08/01/68	580-1	Cluster Docking Report
08/15/68	445-3	Docking Loads Report
05/30/69	827-1	AAP Cluster Docking Response Report
06/30/69	847	Control Impulse Methodology Report
08/23/69	595	Methodology Report for Docking Loads
09/25/69	908	CSM/MDP (Axial) Latch Loads
10/20/69	924	Latch Loads Evaluation Report
04/06/70	770	Docking Probe Analytical Model
09/23/70	1190	ATM Deployment Loads Report
09/23/70	1197	Evaluation of Solar Array Deflection Model
10/15/70	1201	Pre-Test Static Influence Coefficients
11/02/70	1136-1	Latch Load Evaluation Report
11/16/70	827-2	Skylab Cluster Docking Loads Report
03/29/71	1279	Orbital Workshop Solar Array System Sensitivity Analysis

Vibration Modal Analysis

Date	Report No. ED-2002-	Title
06/30/67	137	Vibration Analysis of the AAP Orbital Workshop
07/01/67	141	Vibration and Acoustic Analysis for AAP Flight Configuration 4.
12/18/67	300	Vibration Analysis of the AAP Orbital Workshop
03/15/68	384-1	Cluster Modal Vibration Report
04/01/68	414	Vibration Report for AAP Beamology Model
04/15/68	384-2	Cluster Modal Vibration Report
05/15/68	384-3	Cluster Modal Vibration Report
06/15/68	384-4	Cluster Modal Vibration Report
06/18/68	539-1	AAP Vibration Analysis Report
07/22/68	384-5	Cluster Modal Vibration Report
08/15/68	539-2	AAP Vibration Analysis Report
12/15/69	960	Cluster Vibration Analysis Mass Properties
07/24/70	790-2	Vibration Modal Analysis Report
09/23/70	790-3	Vibration Modal Analysis Report
01/14/71	790-4	Vibration Modal Analysis Report
02/10/71	1256	Modal Coupling Program and Report
04/12/71	790-5	Vibration Modal Analysis Report
06/30/71	1325	Pre-Test Vibration Analysis Report
07/16/71	790-6	Vibration Modal Analysis Report
07/19/71	1355	Modal Tolerance Report
09/01/71	1326	Vibration Modal Analysis Mass Properties
09/23/71	1355	Modal Tolerance Report
09/30/71	1338	Vehicle Dynamics Mechanical Vibration Modal Survey Test Plan
01/31/72	1433	Modal Property Data Report, Configuration 7
02/15/72	790-7	Vibration Modal Analysis Report
02/26/72	1446	Modal Property Data Report, Configurations 9 & 10
03/31/72	1459	Modal Property Data Report, Configuration 6
04/20/72	1433 Rev. A	Modal Property Data Report, Configuration 7

Date	Report No. ED-2002-	Title
04/15/71	1263	MDA Influence Coefficient Test Evaluation Report
04/19/71	827-3	Skylab Cluster Docking Loads Report
04/19/71	1281-1	Orbital Maneuver Loads Report
05/21/71	1136-2	Latch Load Evaluation Report
05/15/71	1309-1	ATM/SA Deployment Loads Report
06/30/71	1324	Pre-Test Structural Response Report
07/30/71	1350-1	Control Impulse Response Report (Preliminary)
08/09/71	1339-2	Apollo Telescope Mount Solar Array System Sensitivity Analysis
08/23/71	1333-1	Skylab Cluster Docking/Latching Loads Report (Preliminary)
11/22/71	1350-2	Control Impulse Response Report (Preliminary)
11/22/71	1395	Skylab Docking Maneuver Simulation Mathematical Model Report (Final)
02/23/72	1350-3	Control Impulse Response Report (Final)
02/23/72	1403	Skylab Control System Simulation Report
02/23/72	1309-2	Deployment Loads Report
05/22/72	1480	Skylab Cluster Radial Docking/Latching Loads Report
06/23/72	1309-3	Deployment Loads Report
06/23/72	1487	OWS-SAS Loads Evaluation Report
03/19/73	1333-3	Skylab Cluster Docking/Latching Loads Report (Final)
06/18/73	1689	Docking/Latching Loads ATM Undeployed Orbital Configuration Report
07/23/73	1333-2	Skylab Cluster Docking/Latch Loads Report (Final)
08/23/73	1695	Skylab Premission Support of SL-2 Orbital Loads
08/27/73	1704	Skylab Rescue Mission Latching Loads Report
09/20/73	1706	SL-2 Mission Evaluation Report
11/16/73	1714	SL-3 Mission Evaluation Report
03/15/74	1720	SL-4 Mission Evaluation Inputs

Date	Report No. ED-2002-	Title
06/21/72	1494	Vibro-Acoustic Modal Survey Test Evaluation Report (Launch Configuration)
09/15/72	1544	Modal Property Data Report, Configuration 7
09/15/72	1522	Vibro-Acoustic Modal Survey Test Evaluation Report (Orbital Configuration)
09/29/72	1525	Cluster Modal Properties for Control Analysis Interim Report
10/16/72	1546	Dynamics Modal Verification Report (Launch Configuration)
10/27/72	1551	Dynamics Model Verification Report (Orbit Configuration)
10/31/72	1554	Modal Property Data Report, Configuration 6
11/14/72	1562-1	Modal Property Data Report, Configuration 3.2
11/14/72	1562-2	Modal Property Data Report, Configuration 1.2
11/14/72	1562-3	Modal Property Data Report, Configuration 2.1
11/21/72	1563-1	Cluster Modal Properties for Control Analysis, Configuration 1.3/Nom
11/21/72	1563-2	Cluster Modal Properties for Control Analysis, Configuration 1.3/-67.5^{o}
11/21/72	1563-3	Cluster Modal Properties for Control Analysis, Configuration 1.3/112.5^{o}
12/19/72	1577	Dynamic Test Reflected Structural Model Methodology Report
12/20/72	1564	Final Vibration Modal Analysis Report
		ATM System and Subsystem Dynamic Analysis
04/01/70	948-1	Interim Report, Spar Canister Modal Data for Control Loop Analysis
10/15/70	1168	Interim Report, Spar Canister Modal Data for Control Loop Analysis
04/01/71	1265	Interim Report, Spar Canister Modal Data for Control Loop Analysis
05/15/71	1303	ATM Rack and Spar/Canister Boost Condition Vibrational Transfer Function
09/15/71	1303 Rev. A	ATM Rack and Spar/Canister Boost Condition Vibrational Transfer Function
10/20/71	1380	Spar/Canister Modal Data for Control Loop Analysis

Date	Report No. ED-2002-	Title
03/31/72	1280-1	Spar/Canister Modal Data for Control Loop Analysis
		SWS Subsystem Interior Acoustic Levels - Orbital Conditions
10/30/70	1200-1	Skylab Interior Acoustic Environment Report
01/31/71	1200-2	Skylab Interior Acoustic Environment Report
04/30/71	1200-3	Skylab Interior Acoustic Environment Report
07/31/71	1200-4	Skylab Interior Acoustic Environment Report
11/30/71	1200-5	Skylab Interior Acoustic Environment Report
02/29/72	1200-6	Skylab Interior Acoustic Environment Report
06/30/72	1200-7	Skylab Interior Acoustic Environment Report
12/31/72	1200-8	Skylab Interior Acoustic Environment Report
08/31/73	1200-9	Skylab Interior Acoustic Environment Report
03/31/74	1200-10	Skylab Interior Acoustic Environment Report
		Vibro-Acoustic Test
03/31/71	1255	Dynamic Instrumentation Plan Volume I Acoustic Test
06/30/71	1255 Chg. 1	
09/30/71	1338	Vehicle Dynamic Mechanical Vibration/Modal Survey Plan
12/31/71	1255 Rev. A	
05/31/72	1255 Rev. B	
01/31/72	1409	Acoustic Test Summary Report
05/31/72	1479	Acoustic Test Summary Report Volume I
05/31/72	1479	Acoustic Test Summary Report Volume II
09/30/72	1516	Modal Survey Test Summary Report
09/30/72	1532	Dynamic Instrumentation Plan
		Skylab Payload Boost Flight Analysis
09/15/71	1366	Skylab Boost Flight Phase Modal Properties
10/31/71	1396	Modal Property Data Configuration 8
11/21/71	1388	Skylab Payload Base Motion Analysis Report

Date	Report No. ED-2002-	Title
12/17/71	1417	Modal Property Data Report S-IC Flight Configuration 1, Part 2
12/17/71	1418	Modal Property Data Report S-IC Flight Configuration 2
12/19/71	1424	Skylab Boost Flight Phase Model Properties Report
01/10/72	1420	Modal Property Data Report, S-IC Flight Configuration 4
01/10/72	1421	Modal Property Data Report, S-II Flight Configuration 1
01/10/72	1422	Modal Property Data Report, S-II Flight Configuration 2
01/10/72	1423	Modal Property Data Report, OWS Flight Configuration 1
01/10/72	1419	Modal Property Data Report, S-IC Flight Configuration, Part 2
01/15/72	1431	Skylab Boost Flight Loads Analysis Report
02/18/72	1435	Skylab Boost Flight Loads Methodology Report
03/31/72	1459	Modal Property Data Report Configuration 6
05/19/72	1431-2	Skylab Boost Flight Loads Analysis Report
04/20/72	1433 Rev. A	Modal Property Data Report Configuration 7
10/20/72	1555	Skylab Payload Base Motion Vibration Analysis Report
10/23/72	1556	Modal Property Data Report, Base Motion Configuration
11/06/72	1421-2	Modal Property Data Report, S-II Flight Configuration 1
11/13/72	1420-2	Modal Property Data Report, S-IC Flight Configuration 4
11/15/72	1422-2	Modal Property Data Report, S-II Flight Configuration 2
11/20/72	1424-2	Skylab Boost Flight Phase Modal Properties Report
12/18/72	1431-3	Skylab Boost Flight Loads Analysis Report
12/18/72	1388-2	Skylab Payload Base Motion Analysis Report
03/19/73	1388-3	Skylab Payload Base Motion Analysis Report
09/20/73	1700	Informal Flight Loads Data for Inclusion to Skylab Mission Support

SPS Cluster Reorientation Studies

Date	Report No. ED-2002-	Title
03/26/73	1658	Informal Loads/Response Data SWS Deorbit Feasibility Study
06/29/73	1694	SPS Cluster Reorientation Loads - Preliminary
08/15/73	1694	SPS Cluster Reorientation Loads - Final Volume I
08/15/73	1694	SPS Cluster Reorientation Loads - Final Volume II
08/15/73	1694	SPS Cluster Reorientation Loads - Final Volume III
08/15/73	1694	SPS Cluster Reorientation Loads - Final Volume IV
		Task Miscellaneous Special Studies
10/04/68	643	Acoustic Test of Multiple Docking Adapter (MDA) Panel
07/01/70	1055	Preliminary Saturn Workshop Acoustical Environmental Mapping
04/19/71	1281-1	Orbital Maneuver Loads Report
06/15/71	1131	Subsystem Design Load Factors Due to Shock, Acoustic and Vibration
08/09/71	1339-2	Apollo Telescope Mount Solar Array System Sensitivity Analysis
08/31/71	1356	CSM/MDA Docking Shock Final Test Report
08/31/71	1357	EPCS Orbital Cluster Modal Properties and ATM Boost
09/14/71	1365	ATM Alignment Modeling
11/19/71	1281-2	Orbital Maneuver Loads Report (Final)
01/31/72	1432	Recommended Specification Revisions and Equipment Exceedance Study for MDA
02/15/72	1444	Skylab RCS-DAP Vibration Analysis
05/22/72	1444 Sup. 1	Skylab RCS-DAP Vibration Analysis for Configurations 1.3 and 3.2
05/07/73	1687	Reduced Dynamic Test Damping Data Analysis Report
08/23/73	1695	Skylab Premission Support of SL-2 Orbital Loads